The Late Quaternary evolution of subsurface water masses in the Gulf of Guinea: High-latitude versus monsoonal control

Dissertation

zur Erlangung des Doktorgrades

Dr. rer. nat.

der Mathematisch-Naturwissenschaftlichen Fakultät

der Christian-Albrechts-Universität zu Kiel

vorgelegt von

Steffanie Kraft

Kiel, 2013

1. Gutachter und Betreuer:	Prof. Dr. Martin Frank
2. Gutachter:	Prof. Dr. Dirk Nürnberg
Tag der Disputation:	03. Dezember 2013
Zum Druck genehmigt:	03. Dezember 2013

gez. Prof. Dr. Wolfgang J. Duschl, Dekan

Erklärung

Hiermit erkläre ich, dass ich die vorliegende Abhandlung, abgesehen von der Beratung durch meinen Betreuer, nach Inhalt und Form selbst erarbeitet habe und dabei keine anderen als die angegebenen Quellen und Hilfsmittel verwendet wurden. Diese Arbeit ist unter Einhaltung der Regeln guter wissenschaftlicher Praxis der Deutschen Forschungsgemeinschaft entstanden und hat weder in Auszügen noch in ganzer Form einer anderen Stelle im Rahmen eines Promotionsverfahrens vorgelegen. Sie wurde in ihrer Gesamtheit nicht veröffentlicht.
Teile dieser Arbeit wurden bereits in Fachzeitschriften veröffentlicht oder sind in Vorbereitung eingereicht zu werden.

Kiel, den 03.12.2013

Steffanie Kraft

Contents

Abstract

The area of this study has been under the influence of a monsoon-driven tropical climate and has experienced variable contributions from river systems in a near shelf area characterized by a complex hydrography. The goal of this study is to improve the understanding of the coupling mechanisms between high latitudes and the tropics via atmospheric and oceanic circulation. The study investigates subsurface tropical water masses and their role in hydrographic changes in response to bipolar climatic oscillations and in modulating the interhemispheric heat exchange, focussing on glacial-interglacial cycles and shorter term millennial scale variability, in particular during Marine Isotope Stage 3 (MIS 3). MIS 3 was characterized by millennial-scale temperature oscillations, which were essentially in opposite phase in the northern and southern hemisphere. Various geochemical proxies are investigated and tested for their reliability for distinct applications, such as reconstructing past riverine input, water mass mixing and boundary exchange.

The radiogenic neodymium (Nd) isotope composition is a widely used proxy to investigate past changes in sources and mixing of water masses, in particular that extracted from foraminiferal shells. However, the extracted seawater Nd isotope ratios can be biased by contaminant phases such as organic matter, detrital silicates, and early diagenetic ferromanganese coatings. We tested different cleaning methods (Flow Through and batch cleaning) of planktonic foraminifera in order to obtain seawater εNd signatures to distinguish surface water mass mixing from riverine inputs and deep water signatures. Both methods reveal indistinguishable levels of cleaning efficiency and identical Nd isotope compositions. Element/calcium ratios and rare earth element (REE) concentration patterns, as well as similar εNd ratios for cleaned and uncleaned foraminiferal samples, suggest that the planktonic foraminiferal Nd isotope signatures reflect bottom water or sedimentary pore water signatures. The results of planktonic foraminiferal analyses were complemented by analyses of Fe-Mn coatings of de-carbonated bulk sediment leachates and the residual detrital fractions of the same sediment samples. Close to the Niger River mouth, the sediment leachates differ significantly from the foraminiferal data, but agree well with the Niger River signature, suggesting contributions of pre-formed coatings originating from the river. The riverine input influences the geochemistry of seawater and deposited authigenic phases. The riverine inputs in the study area have been strongly influenced by the West African Monsoon (WAM) system, which itself has been closely linked to location and movement of the Intertropical

Convergence Zone (ITCZ) and the related rain belt, resulting in changes of their discharge into the Gulf of Guinea. The evolution of the riverine inputs of two large river systems (Sanaga/Nyong and Ntem Rivers) during the past 135 kyr was reconstructed using different sedimentary phases (foraminiferal shells, bulk sediment leachates, residual detrital fraction) of core MD03-2707 which were analyzed for Nd isotope compositions, element/calcium ratios and REE concentrations. The isotopic signature of the residual detrital fraction directly reflects changes in local riverine input, whereas the sediment coatings and foraminiferal shells represent past bottom water signatures, as well as exchange processes between bottom water and the shelf and/or continental material. All phases show similar trends with markedly less radiogenic values during glacial phases as a consequence of the glacial southward migration of the ITCZ and the related rain belt resulting in enhanced runoff of more southerly located rivers draining Precambrian basement with characteristically unradiogenic Nd isotope signatures during sea level low stands.

Combined measurements of trace element contents (Mg/Ca, Ba/Ca) and stable isotopes ($\delta^{18}O$, $\delta^{13}C$) of foraminiferal samples are applied to obtain a detailed record of the evolution of subsurface water masses (< 500 m) and their relationship to climate changes in high latitudes during the last glacial period (5 to 60 kyr). For this purpose, a core top-based multi-species Mg/Ca-temperature calibration of foraminiferal Mg/Ca and oxygen isotopes ($\delta^{18}O$) was established. Shells of two planktonic foraminiferal species *N. dutertrei* and *G. crassaformis* inhabiting different subsurface water masses the Subtropical Underwater (STUW) and South Atlantic Central Water (SACW), respectively, were investigated in detail. *N. dutertrei* represents the lower thermocline and the variability of its proxy data shows clear influence of northern hemisphere climate changes but was also affected by changes in the southern hemisphere due to enhanced admixture of water masses during the last glacial period. *G. crassaformis* inhabits a deeper water mass (SACW), which has mainly been affected by climate changes in the southern hemisphere. The similarity of the records of *N. dutertrei* and *G. crassaformis*, particularly between 55 and 32 kyr, suggests that the SACW strongly influenced the thermocline waters. Furthermore, vertical mixing most likely driven by stronger trade winds resulted in a decrease of thermocline depth during this period of time. Since 32 kyr the trends in the records of *N. dutertrei* and *G. crassaformis* have diverged, suggesting a decrease of the influence of southern water masses and an attenuation of the mixing of the thermocline and SACW water masses.

Kurzfassung

Das Untersuchungsgebiet unterliegt einem monsungesteuerten tropischen Klima und ist durch hohe Einträge der Flusssysteme in einem schelfnahen Gebiet beeinflusst, was in einer komplexen Hydrographie resultiert. Ziel dieser Studie ist es, das Verständnis der Kopplungsmechanismen zwischen hohen Breiten und den Tropen über atmosphärische und ozeanische Zirkulation zu verbessern. Sie befasst sich mit den Wassermassen oberhalb von 500 m, den hydrographischen Veränderungen als Reaktion auf die bipolaren Klimaschwankungen, sowie deren regulierende Rolle für den inter-hemisphärischen Wärmeaustausch. Der Fokus liegt hierbei auf dem Marinen Isotopenstadium 3, das durch Klima-Zyklen auf Zeitskalen von Tausenden von Jahren geprägt war, die sich in der Nord- und Südhemisphäre gegenläufig verhielten. Verschiedene geochemische Proxy-Indikatoren wurden untersucht und auf ihre Verlässlichkeit für Anwendungen, wie der Rekonstruktion von Flusseinträgen, Wassermassenmischung und von Austauschprozessen mit den Schelfsedimenten getestet.

Ein häufig verwendeter Proxy um Veränderungen des Ursprungs und in der Mischung von Wassermassen zu rekonstruieren sind die radiogenen Nd-Isotopen-Verhältnisse (εNd). Die aus den Foraminiferen extrahierten Meerwasser-εNd-Signaturen können durch organisches Material, detritische Silikate und frühdiagenetische Eisen-Mangan-Oxide überprägt worden sein. Zwei Reinigungsmethoden ("Flow Through" und "batch cleaning") wurden untersucht und verglichen, um die Effektivität der Methoden und die Verlässlichkeit der extrahierten εNd-Verhältnisse zu bewerten. Elementverhältnisse (Al/Ca, Mn/Ca) und identische εNd-Werte (der gleichen Probe) implizieren, dass die Effektivität beider Reinigungsmethoden gleichwertig ist. Die Elementverhältnisse und die Verteilungsmuster der Seltenen Erdelemente (REE), sowie identische Nd-Isotopensignaturen gereinigter und ungereinigter Foraminiferen, weisen darauf hin, dass die εNd-Signaturen der planktonischen Foraminiferen Boden- oder Porenwässer repräsentieren. Die Ergebnisse der Foraminiferen-Analysen wurden mit Messungen von Eisen-Mangan-Oxiden von entkarbonatisierten Sedimentproben und der detritischen Fraktion des selben Sediments ergänzt. Nahe der Nigermündung, weichen die Nd-Ergebnisse der Fe-Mn-Oxide signifikant von den Foraminiferen-Daten ab, sie stimmen jedoch mit den Niger-Signaturen überein, was auf einen signifikanten Beitrag von im Fluss vorgeformten Fe-Mn-Oxiden schließen lässt. Flusseinträge können die Geochemie des Meerwassers sowie der authigenen Ablagerungen beeinflussen. Der Flusseintrag im Untersu-

chungsgebiet wird stark vom Westafrikanischen Monsunsystem beeinflusst, das eng mit der Lokation und der Oszillation der Intertropischen-Konvergenz-Zone (ITCZ) über die verschiedenen Breitengrade und dem damit verbundenen Regenband gekoppelt ist. Diese Migration über die Einzugsgebiete der Hauptflüsse führt folglich zu Variationen im Einstrom in den Golf von Guinea. Der Flusseintrag der zwei großen Flusssysteme (Sanaga/Nyong und Ntem) während der letzten 135 ka wurde mit Hilfe verschiedener Sedimentphasen (Foraminiferen, Sediment-Coatings, detritische Sedimentfraktion) aus dem Kern MD03-2707 rekonstruiert. Es wurden dazu Nd-Isotope, Elementverhältnisse und REE-Konzentrationen untersucht. Die detritische Fraktion zeigt direkt Veränderungen im lokalen Flusseintrag an, wohingegen die Fe-Mn-Oxide des Sediments und die Foraminiferen Paläo-Bodenwasser-Signaturen und Austauschprozesse zwischen Bodenwasser und Schelf-Material und/oder kontinentalem Material repräsentieren. Alle analysierten Phasen zeigen ähnliche Trends mit markant unradiogenen Nd-Isotopenwerten während der glazialen Perioden als Konsequenz der südwärts Migration der ITCZ und dem Regenband, was in einem erhöhten Abfluss aus südlicheren Gebieten mit präkambrischem Untergrund (unradiogene εNd-Signaturen) resultierte.

Mit Hilfe kombinierter Messungen von Spurenelementverhältnissen (Mg/Ca, Ba/Ca) und stabilen Isotopen ($\delta^{18}O$, $\delta^{13}C$) an Foraminiferen wurde die Entwicklung der Wassermassen oberhalb von 500 m Wassertiefe, ebenso wie deren Beziehung zu Klimaveränderungen in hohen Breiten mit Fokus auf dem letzten Glazial (5 bis 60 ka) untersucht. Hierfür wurde eine oberflächenbasierte Multispezies-Mg/Ca-Temperatur-Kalibration mit Hilfe von Mg/Ca-Verhältnissen und Sauerstoffisotopen ($\delta^{18}O$) erstellt. Zwei Spezies aus verschiedenen Habitat-Tiefen wurden für die Analysen ausgewählt. *N. dutertrei* kommt im Subtropischen Unterwasser (STUW) vor und repräsentiert die untere Thermokline, welche sowohl Einflüsse aus der Nordhemisphäre, als auch aus der Südhemisphäre während des letzten Glazials wiederspiegelt. *G. crassaformis* bewohnt dagegen tiefere Wasserschichten und repräsentiert hauptsächlich den Einfluss des Südatlantische Zwischenwassers (SACW), das durch Klimaschwankungen der Südhemisphäre geprägt ist. Die signifikante Korrelation der Ergebnisse beider Spezies, besonders zwischen 55 und 32 ka, legt nahe, dass das SACW die Thermokline wahrscheinlich durch Mischungsprozesse stark beeinflusst, die außerdem eine Verflachung der Thermokline verursachten und durch starke Passatwinde ausgelöst worden sein können. Seit 32 ka laufen die Kurven von *N. dutertrei* und *G. crassaformis* auseinander, was für eine Abschwächung des Einflusses der südlichen Wassermassen auf die Thermokline und eine Abschwächung der Mischungsprozesse der Wassermassen spricht.

Chapter 1

Introduction

1.1 Atmospheric circulation

The West African Monsoon (WAM) has been one of the major components of the global monsoon system. It has played an important role for the global climate system through its impact on the moisture and heat budgets, which in turn have strongly influenced regional agriculture and economy in western Africa.

Today shifts of the Intertropical Convergence Zone (ITCZ) are caused by seasonal changes in insolation, which result in different patterns of monsoonal circulation dominated by the contrast between land surface temperature and sea surface temperature (SST). The study area is particular affected because of the strong seasonal temperature and humidity differences between the Sahara and the equatorial Atlantic Ocean. The associated changes in precipitation and atmospheric circulation are defined as monsoon. The position of the African rain belt, as well as the associated convergence of the trade winds at the ITCZ oscillates seasonally between 17°N and 21°S and controls the distribution of rainfall over tropical Africa (Nicholson, 2000; Nicholson and Grist, 2003). Recent studies have shown variations in rainfall linked to large-scale processes, such as atmospheric and ocean circulation in the tropical eastern Atlantic, on seasonal and intra-seasonal time scales (Gu and Adler, 2004; Maloney and Shaman, 2008).

The ITCZ and the related rain belt (dashed red line and green areas in Figure 1.1 A) move seasonally across the study area the Gulf of Guinea in the easternmost equatorial Atlantic and West Africa. The ITCZ has moved across the equator seasonally, as well as on longer time scales (reconstructed positions depicted in Figure 4.1 A: Leroux et al., 1993; Gasse et al., 2000; Talbot et al., 2007; Nicholson et al., 2009; Kim et al., 2010).

The amount and timing of the precipitation coupled with the migration of the ITCZ has an important effect on the hydrography and seawater chemistry in the Gulf of Guinea (Zabel et al., 2001; Weldeab et al., 2007a, 2007b) given that the latitudinal movement of the ITCZ also influences the riverine runoff and inputs into the Gulf of Guinea.

Large rivers such as Niger, Nyong/Sanaga, Ntem and Congo are draining the West African continent and supply dissolved and particulate matter into the Gulf of Guinea (Figure 1.1 B). Consequently, the riverine inputs have varied with the migration of the rain belt across the river catchment areas and with the intensity of the WAM on millennial time scales during the Quaternary resulting in changes in salinity and trace element composition of the surface waters, as well as in the composition of terrigenous sediments in the eastern equatorial Atlantic and the Gulf of Guinea (e.g. Schneider et al., 1997; Zabel et al., 2001; Adegbie et al., 2003; Lezine et al., 2005; Weldeab et al., 2005; 2007a; 2007b; Weldeab, 2012a; 2012b).

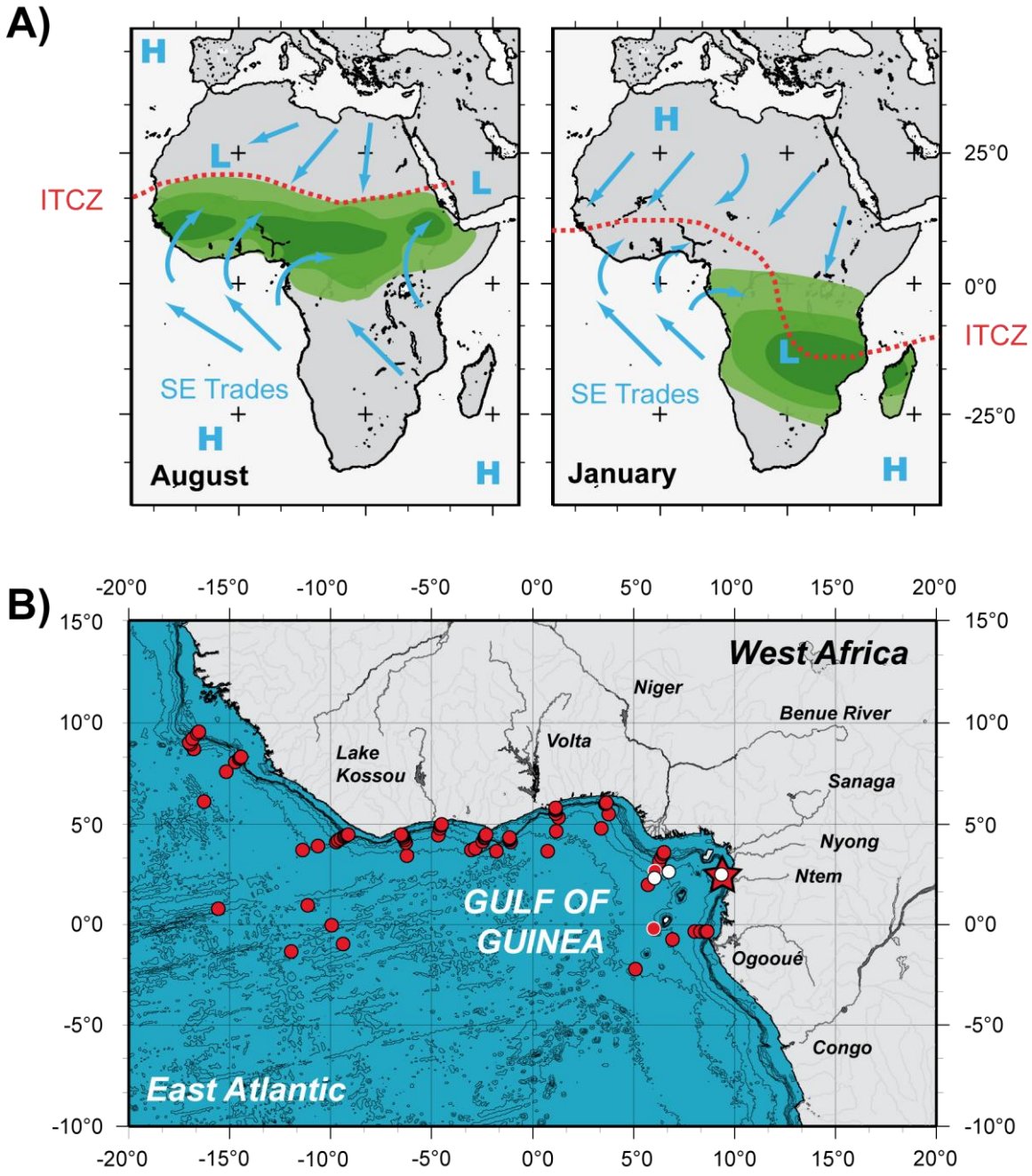

Figure 1.1: A) *Simplified seasonal changes: Left: Monsoon circulation under wet summer monsoon conditions with a low pressure cell over western North Africa (August) and Right: Dry winter monsoon conditions with high pressure cell over western North Africa (January) (redrawn after Nicholson, 1996; Ruddiman, 2008 and references therein; Griffith, 1972; Nicholson et al., 2009; Gasse et al., 2000; NOAA-NCEP Climate Prediction Center), green areas mark the regions with most intense monthly precipitation, dashed red line = ITCZ, blue arrows = general patterns of winds trajectories (H: high pressure cell, L: low pressure cell);* ***B)*** *Study area in the eastern equatorial Atlantic and the Gulf of Guinea with core top samples (red circles = GIK samples, white circles = GeoB-samples) and core MD03-2707 (red star)*

1.2 Linkage between tropics and high latitude climate oscillation

Ice core records from Greenland and Antarctica display rapid and recurring oscillations of temperature and atmospheric greenhouse gases on centennial time scales (Blunier and Brook, 2001; Flückiger et al., 2004; NGRIP, 2004; EPICA, 2006, Ahn and Brook, 2008). Those atmospheric fluctuations have been accompanied by ice sheet instabilities (Kanfoush et al., 2000; Bond et al., 2001; Anderson et al., 2009; Barker et al., 2009) and changes or even interruptions of the thermohaline circulation (McManus et al., 2004; Negre et al., 2010). The ice core records suggest that Greenland cold events coincided with southern high latitude warming (e.g. EPICA, 2006).

Previous studies on sediments from the Gulf of Guinea (MD03-2707, red star in Figure 1.1 B) (Weldeab et al., 2007a, 2007b; 2011; Weldeab, 2012a) have revealed the linkage between the evolution and variation of the West African Monsoon (WAM) system and northern and southern hemispheric climate oscillations in the past. These studies proposed a tight coupling of the WAM variability with northern high latitude ice sheet instabilities and cold and warm events in Greenland ice core records.

Furthermore, modeling studies (e.g. Broccoli et al., 2006) suggested a linkage between climate oscillations in the high latitudes and changes in atmospheric heat exchange, as well as displacements of the ITCZ on decadal to glacial-interglacial time scales. Close relationships between changes of the global thermohaline circulation and variations of the West African monsoon system have also been identified (e.g. Chang et al., 2008).

Modeling studies predicted an increase in sea surface temperature in the tropical Atlantic (e.g. Chang et al., 2008) during Heinrich Events, when increasing meltwater influx into the North Atlantic occurred and thermohaline circulation slowed down caused by reduced deep water formation resulting in a reduction of northward heat transport and the Atlantic Meridional Overturning Circulation (AMOC). This modeling study (Chang et al., 2008) also emphasized the importance of subsurface water masses for inter-hemispheric heat exchange. Most subsurface water studies have been focused on the last de-glacial phase (Rühlemann et al., 2004; Schmidt et al., 2012). The studies of Rühlemann et al. (2004) and Schmidt et al. (2012) combined both modeling results and foraminiferal proxy records from the western and eastern tropical Atlantic (Cariaco Basin, Tobago Basin and off the coast of Angola) covering the last 22 kyr. Both studies revealed that a slowdown in thermohaline circulation (THC) was accompanied by a warming at intermediate depths in the tropical Atlantic. This relationship

between the strength of the THC and the subsurface tropical Atlantic might be relevant for tracing past, present and future changes in the THC associated with climate shifts, providing that anthropogenic signals can be separated (Rühlemann et al., 2004).

The atmospheric circulation cells have shifted with the changes of the wind systems (Figure 1.1 A) and have influenced the oceanic circulation patterns. For example during warm climate phases of the past over Antarctica and the Southern Ocean the westerlies shifted southward together with the Subtropical Front (STF). This caused an increase of the Agulhas leakage with increasing influx from the Indian Ocean (Biastoch et al., 2009) due to an enlargement of the distance between the South African tip and the STF.

The important role of Atlantic water masses (TSW = Tropical Surface Water, AAIW = Antarctic Intermediate Water, NADW = North Atlantic Deep Water, AABW = Antarctic Bottom Water) and the associated heat flow for the linkage of northern and southern latitudes has for example been revealed by studies of Ganachaud and Wunsch (2000) and Knorr and Lohmann (2007). For instance, higher quantities of southern sourced waters entered the deep North Atlantic basin whereas NADW was most likely weaker and its main southward flow occurred at significantly shallower depth during the last glacial compared to the present day (e.g. Marchitto et al., 2002; Hall and Chan, 2004; Gutjahr et al., 2008).

1.3 Ocean circulation and hydrographic setting

The oceanic circulation in the study area the Gulf of Guinea is complex. In the modern water column five water masses can be distinguished: Tropical Surface Water (TSW), Subtropical Underwater (STUW), South Atlantic Central Water (SACW), Antarctic Intermediate Water (AAIW), and North Atlantic Deep Water (NADW) (Figure 1.2).

The mixed layer in the easternmost tropical Atlantic and the Gulf of Guinea is formed by the Tropical Surface Water (TSW) and the Subtropical Underwater (STUW) and covers an annual temperature range between 20 and 30°C and an annual salinity range between 33 and 36 (psu) (Figure 1.2). The TSW is characterized by low salinity and high temperature (Figure 1.2), whereas the STUW is marked by high salinity. The reason for the low sea surface salinity is on the one hand the high precipitation and on the other hand the high riverine supply of fresh water.

The TSW with temperatures up to 30°C and salinities down to 33 (psu) in the easternmost Gulf of Guinea (Figure 1.2) is receives contributions by the Guinea Current (GC) from the

northwest and by the South Equatorial Current (SEC) from the south (Figure 1.3 A). Below the TSW, the STUW is characterized by pronouncedly higher salinities up to 36 (psu) (Figure 1.2) and is advected by the Equatorial Undercurrent (EUC) and the northern South Equatorial Current (nSEC) (Stramma and Schott, 1999; Bayon et al., 2011). The STUW is formed south of 12°S (Figure 1.3 A) by subduction of high salinity surface water, which spreads northward below the surface (Sprintall and Tomczak, 1992). The thermocline marks the lower boundary of the mixed layer at about 75 m water depth (Chapter 5).

South of 15°N the northern boundary the SACW is found between 100 and 500 m water depth with temperatures and salinities plotting on the straight line between 5°C and 34.3 (psu) and 20°C and 36.0 (psu) (Stramma and England, 1999). The SACW is formed in the southern hemisphere subtropical convergence (Figure 1.3 B; Stramma and Peterson, 1990; Stramma and England, 1999; Stramma and Schott, 1999) within the confluence of the Brazil and the Falkland Currents. Together with the South Atlantic Currents the SACW flows eastward. Before flowing westward with the Benguela Current and turning northward as a part of the North Brazil Undercurrent, warm and saline waters from the southern Indian Ocean are entrained in the SACW via the Agulhas Current eddies (Sprintall and Tomczak, 1993; Tomczak and Godfrey, 1994; Stramma and Schott, 1999; Biastoch et al., 2008). At the equator the SACW is reflected towards the Gulf of Guinea (Stramma and England, 1999; Stramma and Schott, 1999). In the Gulf of Guinea the SACW is influenced by contributions of the EUC and the nSEC (Stramma and Schott, 1999). At intermediate water depth between 500 and 1200 m the Northern Intermediate Countercurrent (NICC) transports AAIW with temperatures around 4 to 5°C and salinities around 34.5 (Figure 1.2). The deep water column between 1200 and 4000 m water depth in the Gulf of Guinea is dominated by North Atlantic Deep Water (NADW) with temperatures below 4°C and salinities up to 35 (psu) (Figure 1.2). All water masses flow northward in the eastern tropical Atlantic except NADW, which flows southward (Stramma and Schott, 1999; Stramma and England, 1999).

Today the water depth of core MD03-2707 at 1294 m is located at the top of the NADW close to the lower boundary of AAIW. Thus, the location has been sensitive to vertical shifts of NADW and AAIW.

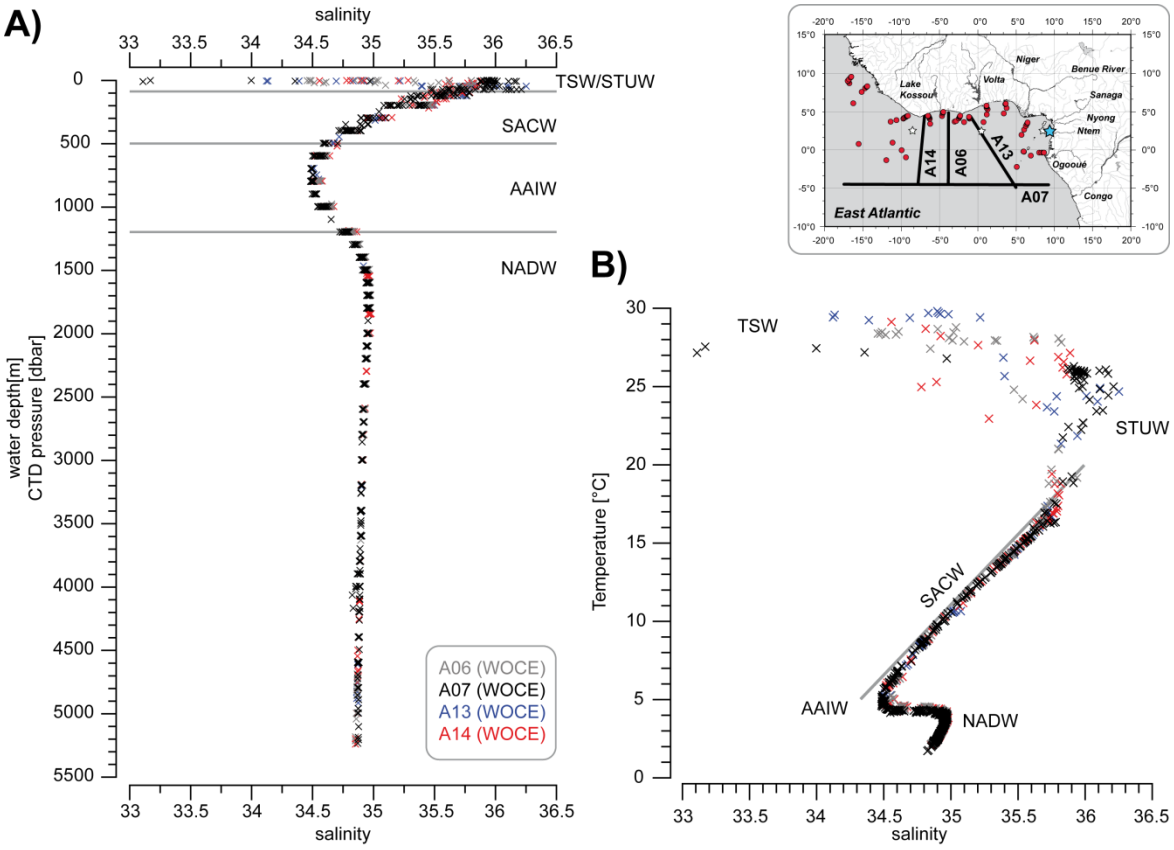

Figure 1.2: A) *Salinity in the water column of different WOCE sections in the study area (World Ocean Circulation Experiment Data: Schlitzer, 2000) which are depicted in the upper right inset;* ***B)*** *Temperature-Salinity Plots of the same WOCE sections as in A) for identification of the different water masses in the study area (TSW = Tropical Surface Water, STUW = Subtropical Underwater, SACW = South Atlantic Central Water, AAIW = Antarctic Intermediate Water, NADW = North Atlantic Deep Water), the gray line marks the typical properties of SACW (Stramma and England, 1999).*

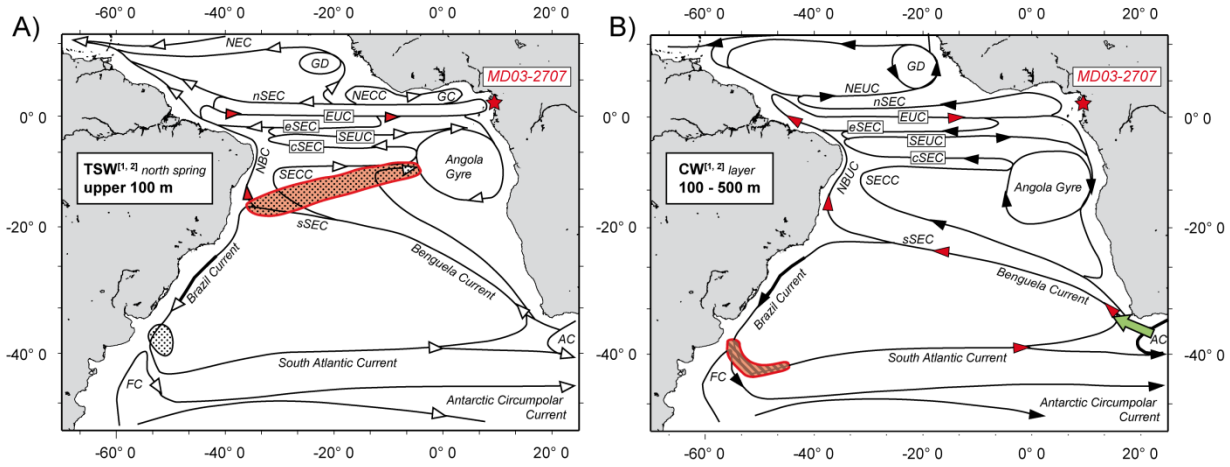

Figure 1.3: *Simplified circulation of the surface and subsurface current systems after Stramma and England (1999) and Stramma and Schott (1999)* ***A)*** *in the depth of the Tropical Surface Layer (TSW) within the upper 100 m, the formation region (encircled areas) of high salinity waters of the Subtropical Underwater (STUW) in the tropics (marked in red) and mode waters in the subtropics;* ***B)*** *in the Central Water (CW) layer between 100 and 500 m water depth with the main formation region marked by red hatched area. This water mass is also fed by waters from the Indian Ocean via the Agulhas Leakage (green arrow) (e.g. Tomczak and Godfrey, 1994). Red arrows mark the respective path-ways of the different water masses to core site MD03-2707 (red star).*
AC = Agulhas Current, GC = Guinea Current, GD = Guinea Dome, FC = Falkland Current, NBC = North Brazil Current, NBUC = North Brazil Undercurrent, NEC = North Equatorial Current, NECC = North Equatorial Countercurrent, NEUC = North Equatorial Undercurrent, SEC = South Equatorial Current with the northern (nSEC), equatorial (eSEC), central (cSEC) and the southern (sSEC) branch, SECC = South Equatorial Countercurrent, SEUC = South Equatorial Undercurrent.

1.4 Motivation and objectives

The study area of this thesis the Gulf of Guinea has been under monsoon-driven influence of changes in tropical climate and atmospheric conditions as well as high influence of river systems in a near shelf area setting and complex hydrology.

The main goal was to improve our understanding of coupling mechanisms between the northern and southern high latitudes and the tropics via atmospheric and oceanic processes. This is achieved based on an improved knowledge of the past subsurface tropical Atlantic Ocean and of the role of hydrographic changes in response to climate changes focussing on the last glacial-interglacial cycles.

The influence of the riverine input on the geochemistry of the sea water and on the deposited authigenic phases to reconstruct atmospheric circulations over land is investigated with a focus on the monsoon cycle and its associated precipitation changes. For these investigations

we used various geochemical proxies (detailed in the following section) and tested their reliability for distinct applications, in particular for riverine input, water mass mixing and boundary exchange.

One prominent objective in this regard was to test different cleaning methods of planktonic foraminifera in order to obtain seawater εNd signatures to distinguish surface water mass mixing from riverine inputs and deep water signatures (Chapter 3). A second objective was the development of a temperature-Mg/Ca calibration for the study area using core top samples from the entire Gulf of Guinea to obtain a reliable tool for temperature reconstructions of the past (Chapter 5).

Following the achievement of those objectives the proxies are applied for paleo-reconstructions of changes in water mass mixing and circulation in the easternmost equatorial Atlantic over the past 135,000 years (Chapter 4) and over the past 60,000 years as a part of a high resolution record of temperature and salinity changes (Chapter 5) under changing glacial and interglacial boundary conditions.

We focus on Marine Isotope Stage (MIS) 3, as well as the Last Glacial Maximum (LGM) and the Early Holocene. MIS 3 was characterized by millennial-scale temperature oscillations. Those oscillations marked by abrupt warming and gradually cooling (Dansgaard-Oeschger Events) in the northern latitudes and gradual temperature fluctuations in the southern hemisphere occurred essentially in opposite phase (Blunier and Brook, 2001). The direct relationship between warm phases in the south (Antarctica) and cold phases in the north (Greenland) is shown in the study of EPICA (2006). In particular during MIS 3 the most pronounced warming over Antarctica (A1 to A4 events) occurred contemporaneously with cold Heinrich and D/O events in the northern hemisphere (Blunier and Brook, 2001; EPICA, 2006).

1.5 Outline and research questions

This thesis is separated into two parts. In the **first part** we focus on determination of the origin of water masses, mixing processes between the different water masses and riverine waters, as well as the influence of the monsoon system, the related rainfall, and the riverine inflow in the river influenced shelf setting of the Gulf of Guinea (Chapters 3 and 4). The main proxy of this part of the thesis is the radiogenic neodymium isotope composition, which has been widely used to trace changes in sources of water masses and their mixing, in the

northern and tropical Atlantic Ocean (e.g. Piepgras and Wasserburg, 1980, 1982; Goldstein et al., 1984; Goldstein and Jacobsen, 1987; Tachikawa et al., 1999; Rickli et al., 2009; Bayon et al., 2011).

We analyzed neodymium isotope compositions (εNd) and rare earth element (REE) concentrations of foraminiferal shells and complemented these analyses by measurement of uncleaned planktonic foraminifera, benthic foraminifera, bulk sediment leachates, and the residual detrital fraction of the same sediment (silicates) from several core top samples and from sediment core MD03-2707. Reductively cleaned planktonic foraminifera have been supposed to be reliable archives for seawater Nd isotope signatures (surface and subsurface) (Vance and Burton, 1999; Burton and Vance, 2000; Scrivner et al., 2004; Vance et al., 2004; Stoll et al., 2007; Osborne et al., 2008, 2010; Pena et al., 2013), whereas ferromanganese coatings from bulk sediments and from un-cleaned planktonic foraminifera are supposed to reflect bottom water signatures (Rutberg et al., 2000; Bayon et al., 2002; Piotrowski et al., 2005; Gutjahr et al., 2007, 2008; Pahnke et al., 2008; Roberts et al., 2010; Piotrowski et al., 2012).

Two cleaning methods (Chapter 2), the Flow Through (Haley and Klinkhammer, 2002) and batch cleaning methods (Boyle, 1981; Vance and Burton, 1999; Vance et al., 2004), were compared to evaluate the cleaning efficiency (Chapter 3) to extract Nd isotope compositions from planktonic foraminifera in a river dominated shelf setting and the applicability for the paleo-record to determine contaminations of the foraminiferal carbonates, because only fully cleaned carbonates can provide reliable seawater signatures originating from the habitat depth of the planktonic foraminiferal species. The core top samples used for analyses of element/calcium ratios were taken from different water depth and different hydrographic conditions (White framed and white circles in Figure 1.1 B).

The analyses of changes in Nd isotope composition of the different sedimentary phases (sediment leach, residual sediment, foraminifera) and element/Ca ratios plus REE concentration patterns of foraminiferal samples provide insights into changes in the origin of the water masses, riverine influence, redox-conditions, oxygenation conditions and export productivity during glacial-interglacial cycles over the past 135,000 years (Chapter 4), during which changes in the riverine influence have been related to the migration of the ITCZ and the associated rain belt. We extended the detrital εNd paleo-record of core MD03-2707 (Weldeab et al., 2011) to 135 kyr to cover the same period of time. Element/calcium ratios and REE concentration patterns obtained from foraminiferal samples are used to evaluate the

completeness of the applied cleaning procedures (mechanical, oxidative and reductive cleaning) and thus the origin of the neodymium isotope signature.
The summarized main research questions for the first part of the thesis are:

- → How efficient is the cleaning of planktonic foraminiferal carbonates from contaminant phases with regard to extraction of the water mass Nd isotope signature inhabited by the foraminifera and can reliable surface and subsurface water mass neodymium isotope compositions be extracted?
- → How do the cleaning methods differ?
- → How does the input of the different rivers influence the neodymium isotope compositions of bottom waters and of the authigenic phases of sediments?
- → How reliable are sediment leachates as recorders of bottom water signatures in river influenced shelf settings? What does the sediment leachate record tell us?
- → What are the factors influencing the detrital sediment record?
- → What is the information potential of foraminiferal records?

In the **second part** of this thesis, combined measurements of trace element contents (Mg/Ca, Ba/Ca) and stable isotopes ($\delta^{18}O$, $\delta^{13}C$) of foraminiferal samples are applied to determine thermal, salinity and source changes of subsurface water masses (< 500 m) in the easternmost equatorial Atlantic and their connection to climate changes in high latitudes during the last glacial period (Chapter 5). The used preparation, cleaning and analyses methods are detailed in Chapter 2. The analysed foraminifera *N. dutertrei* and *G. crassaformis* represent thermocline waters (75 - 150 m) of the Subtropical Underwater (STUW) and deeper subsurface waters (300 - 400 m) of the South Atlantic Central Water (SACW), respectively.
Magnesium uptake into foraminiferal calcite is mainly controlled thermodynamically. Several core top sample analyses and culture experiments reveal an exponential relationship between planktonic foraminiferal Mg/Ca ratios and temperature of the inhabited water, in which the foraminifera calcify (Nürnberg, 1995; Nürnberg et al., 1996; Lea et al., 1999; Elderfield and Ganssen, 2000, Dekens et al., 2002). Thus, Mg/Ca ratios of planktonic foraminiferal tests are widely used for reconstructions of past ocean temperatures (e.g. Nürnberg et al., 1996; 2000;

Elderfield and Ganssen, 2000; Barker et al., 2003; Lea, 2003; Weldeab et al. 2007a; 2007b; Dürkop et al., 2008; Weldeab, 2012a; 2012b).

A regional calibration for Mg/Ca-thermometry with data from 83 core top samples distributed over the entire Gulf of Guinea (Figure 1.1 B) was established, which is used for the reconstruction of temperature changes during the past 60,000 years (BP) and changes in thermocline depth via comparison with surface data (Weldeab, 2012b).

Barium is incorporated into the foraminiferal shells depending on the barium concentration of the surrounding seawater, independent on temperature, salinity, pH or symbiotic photosynthesis (e.g. Lea and Boyle, 1991; Lea and Spero, 1992, 1994; Hönisch et al., 2011). Thus, foraminiferal Ba/Ca ratios can be used to reconstruct Ba concentrations of the water mass inhabited by the foraminifera and to trace change in source of the water mass, but authigenic barite can potentially contaminate the carbonate Ba/Ca and complicate paleo-reconstructions. Ba/Ca combined with $\delta^{18}O$ records of foraminiferal tests from surface dwelling species were used in previous studies to reconstruct changes in riverine runoff and monsoon precipitation (Weldeab et al., 2007a; Weldeab 2012a).

The changes for example in temperature, depth and salinity of the subsurface water masses, in particular those of the thermocline are influencing the surface waters as well and are indicative for changes in the stratification, wind stress and upwelling processes.

The main research questions for the second part of the thesis are:

- → How did temperature and salinity in subsurface waters in the tropics vary between 60,000 and 5,000 years BP? How were those changes in water mass parameters linked to high latitude climate oscillations?
- → What caused the changes in depth and temperature of the thermocline during the past 60,000 years?
- → What was the consequence of increasing influence of southern sourced waters in the tropical Atlantic during the last glacial?

1.6 Manuscripts

Declaration of my contribution to the following chapters:

Chapter 3:

Assessment of seawater Nd isotope signatures extracted from foraminiferal shells and authigenic phases of Gulf of Guinea sediments

Statement:
The experiments of the Flow Through cleaning were planned and arranged together with Brian Haley and Edmund Hathorne. I re-sampled the core MD03-2707 and prepared the samples and the GeoB samples for sedimental analyses, performed the chemical preparation and measured the Nd isotope concentration, furthermore I picked the foraminifera. From the other samples (GIK sites) I picked the foraminifera, performed the cleaning and chemical preparation of the samples and measured the Nd isotope compositions. The REE concentrations were measured by Edmund Hathorne. I wrote the manuscript. All co-authors and 4 external reviewers helped improving and revising the manuscript.

Chapter 4:

Migration of the West African Monsoon over the past 135,000 years: Evidence from sedimentary Nd isotope composition in the Gulf of Guinea

Statement:
The foraminiferal samples were picked by myself and a student assistant. A picked sample set of 19 benthic foraminiferal shells was already available. I cleaned the foraminiferal samples and carried out the measurements. The core MD03-2707 was re-sampled and the sediment samples were prepared by myself, as well as the measurements of the Nd isotope composition. The REE concentrations were measured by Edmund Hathorne. I interpreted the data and wrote the chapter and Martin Frank and Edmund Hathorne helped to discuss the data.

Chapter 5:

Changes of temperature and sources of tropical Atlantic subsurface water in response to the last glacial bipolar oscillation (5 - 60 kyr BP)

Statement:
The foraminiferal samples were picked by myself and the complete sample preparation was performed by myself. The measurements of Mg/Ca and Ba/Ca were performed at the UCSB and the measurements of $\delta^{18}O$, $\delta^{13}C$ were carried out at the Leibniz-Laboratory.
At the initial stage of the data analyses I was supported by Dirk Nürnberg. I discussed the core top calibration and the related data analysis with Syee Weldeab. I then wrote the chapter and Edmund Hathorne supported the paleo-discussion and helped improving the first draft of the chapter.

Chapter 2

Material and Methods

2.1 Material

In this study core top samples were used for method tests (Chapter 3) and calibration studies (Chapter 5). Down core samples from core MD03-2707 (1294 m water depth, 2°30'07 N, 9°23'41 E) were used for paleoceanographic reconstructions (Chapters 4 and 5). The core top sediment samples were recovered from 83 different sites distributed over the Gulf of Guinea in the eastern equatorial Atlantic from water depths ranging from 390 m to 4970 m (Figure 1.1, Appendix Tables A3.1, A5.1 and A5.2). In total 83 core top sites (GIK) sampled with a giant box corer during Meteor cruise M6-5 in 1988 (Lutze et al., 1988) and 3 sites (GeoB) sampled with a multicorer during Meteor cruise M41-1 (1986) were analyzed.

2.1.1 Foraminiferal samples

For the analyses of Nd isotope compositions, oxygen and carbon isotope analyses, and trace element analyses different amounts of foraminiferal shells were needed.

For the extraction of Nd isotope compositions, analyses of element/calcium ratios and rare earth element (REE) concentration between 9 and 35 mg of foraminiferal tests were used. For the core top analyses and method tests with foraminiferal shells (size fraction > 250 µm) mainly mono-specific planktonic samples (*Globigerinoides ruber* pink, *Globorotalia menardii, Neogloboquadrina dutertrei* and *Globorotalia tumida*) and mixed benthic foraminiferal samples were used (Chapter 3, Appendix Table A3.1). Because of the lower abundance of foraminiferal shells in the down core samples bulk planktonic samples (test size > 150 µm) were used for Nd isotope analyses (Chapter 4, Appendix Table A4.1). The mixed benthic samples of both, core top and down core samples consisted of about 20 mg epibenthic and shallow endobenthic species (e.g. *Oridorsalis umbonata*, *Uvigerina spp*., *Bulimina spp*., *Cibicidoides spp*., *Hoeglundina elegans*).

The trace element analyses (Mg/Ca, Ba/Ca) and stable oxygen and carbon isotope analyses ($\delta^{18}O$, $\delta^{13}C$) were performed each with on average 5 to 6 foraminiferal shells (*N. dutertrei*, *G. crassaformis*; mainly in the size fraction 300 - 400 µm) (Chapter 5).

2.1.2 Sediment samples

In this study about 2.5 g bulk sediment samples were used for the extraction of Nd isotope compositions from Fe-Mn coatings. About 50 mg of dried previously leached samples were subsequently used for detrital sediment analyses.

2.2 Methods

2.2.1 Sample preparation

2.2.1.1 Foraminiferal samples

The foraminiferal tests used for all analyses were handpicked under a binocular microscope and gently cracked between two glass plates to open the chambers and to ensure effective cleaning. Any visible contaminants were manually removed. The foraminiferal samples for the stable oxygen and carbon isotope analyses were not cracked and further treated.

A) Cleaning for extraction of neodymium isotope compositions

The foraminiferal samples were cleaned with two different methods to evaluate the cleaning efficiency, which were tested in the course of the study and are detailed in Chapter 3. A modified version of the Flow Through (FT) cleaning method of Haley and Klinkhammer (2002) and batch cleaning method originally developed by Boyle (1981) and modified (scaled up for larger samples) by Vance and Burton (1999) and Vance et al. (2004) were applied to obtain seawater neodymium isotope compositions (Chapter 3). Both methods consist of rinsing, oxidative and reductive cleaning steps to remove contaminant phases, such as silicate phases, organic matter, ferromanganese oxides and early diagenetic oxyhydroxide coatings. After cleaning, the samples were dissolved in HNO_3 and aliquots were separated for element (particularly Al/Ca, Mn/Ca, Fe/Ca), rare earth element (REE) and Nd isotope analyses (Chapters 3 and 4). The measurements of the elements and REE were performed with a Agilent 7500-CX ICP-MS and the Nd isotope compositions were analyzed with a Nu instruments multicollector ICP-MS (detailed in Section 2.3).

Modification of the Flow Through cleaning method

The FT method of Haley and Kinkhammer (2002) was modified after performing systematic tests. The general setup of the manually performed FT cleaning method is shown in Figure 2.1, and consists of a Teflon tube, a peristaltic pump, a water bath to heat the reagents, and a sampling rack that was moved beneath the syringe filter with the sample to collect the solutions of the different cleaning steps. For the FT cleaning method the cracked foraminiferal samples were placed in the centre of the filter membrane inside a syringe filter.

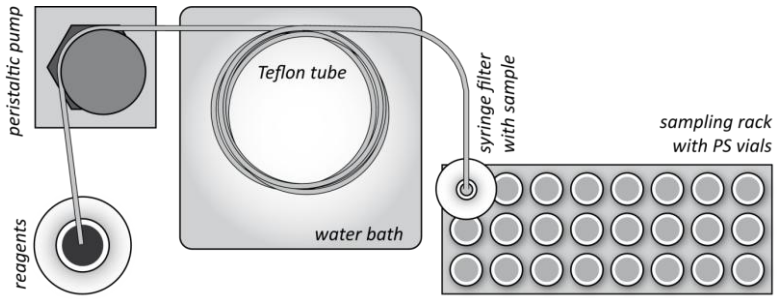

Figure 2.1: *Simplified setup of the Flow Through cleaning method*

The FT method was performed with different filters and different reagents to optimize cleaning efficiency. The two different filters which were tested are syringe filters with 0.45 µm PTFE-membranes and PP-housings with different diameters. The larger filter (diameter 25 mm, Minisart SRP 25) can take a larger sample volume but is also coupled with a larger dead volume than the small filter (diameter 13 mm, Puradisc™ 13, Whatman). The large dead volume can host a significant amount of gas bubbles, which inhibit the contact of the reagents with the sample and lead to incomplete cleaning and incomplete dissolution. The different effects on the element concentrations within the cuts of the FT methods are shown in Figures 2.2 A and B. The smaller filters clearly allow more effective cleaning due to the smaller amount of gas bubbles within the filter dead volume.

Furthermore, we tested different concentrations of the reductive solution. A higher concentration (0.5 M hydroxylamine solution) causes a much higher carbonate loss during the reductive cleaning than the 0.1 M hydroxylamine solution (Figures 3.2, A3.1), but both concentrations result in a comparable efficiency of manganese removal (Figures 2.2 B and C). A modified extended cleaning procedure introducing an extended sample rinsing step between the reductive cleaning and the dissolution of the carbonates (Figure 2.2 C, Table 3.2) results in a more defined concentration peak of Ca, Mg and Sr within the dissolution steps than the previously used procedure (Figures 2.2 A and B, Table 3.1).

A high temperature of the cleaning solution supports the reaction with the samples. Thus, the flow rate was adjusted to a reagent temperature of 80 to 90°C dropping onto the sample in the syringe filter.

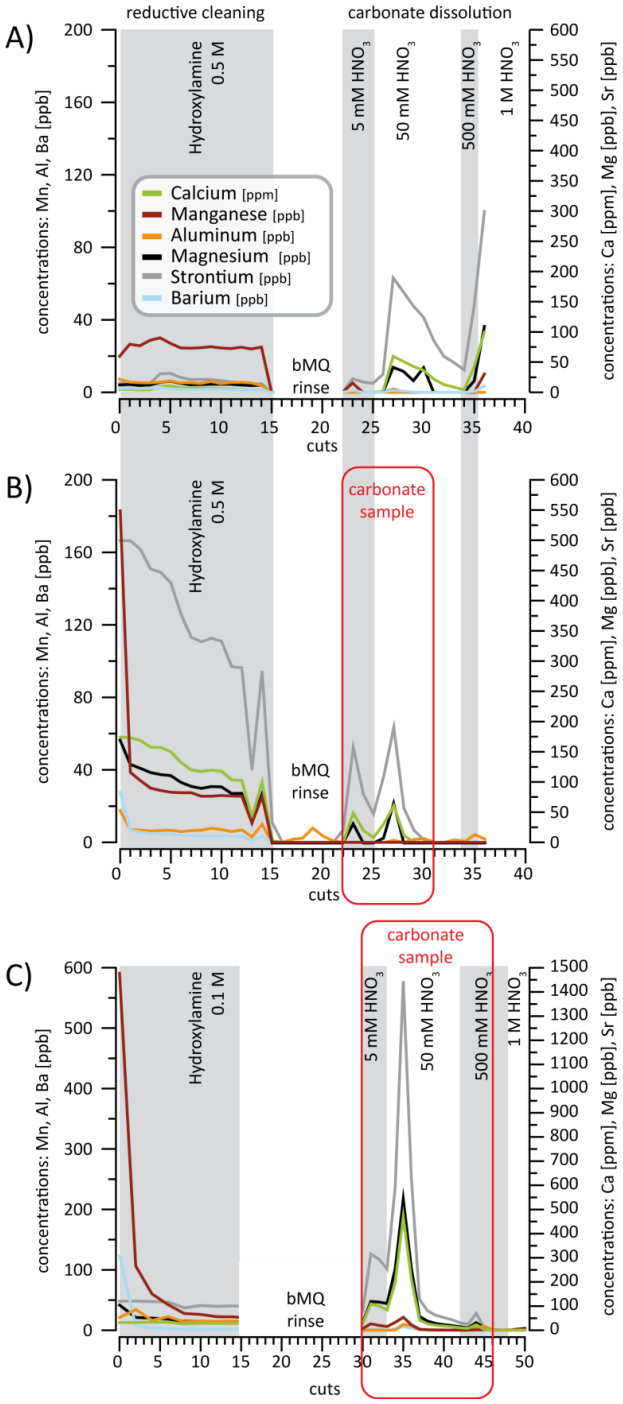

Figure 2.2: *Elemental concentrations in the reductive cleaning solution of the FT cleaning method with* ***A)*** *sample SK-AA-1 large filters (diameter 25 mm) treated as detailed in Table 3.1,* ***B)*** *sample SK-AB 1 with small filters (diameter 13 mm) treated as detailed in Table 3.1 and* ***C)*** *sample SK-AB 10 with small filters (diameter 13 mm) treated as detailed in Table 3.2. Red squares frame the cuts containing the dissolved foraminiferal carbonate which were used for measurements.*

B) Cleaning for Mg/Ca and Ba/Ca analyses

Prior to the analyses of trace element concentrations in foraminiferal shells, the samples were mechanically, reductively and oxidatively cleaned following the standard procedure detailed by Martin and Lea (2002) and adapted from Boyle and Keigwin (1985), Lea and Boyle (1993) and Boyle and Rosenthal (1996) (Table 2.1). The DTPA cleaning described in those studies was not applied because no significant diagenetic influence is expected for the Late-Quaternary time period covered by this study (Chapter 5) as also confirmed by an earlier study (Weldeab et al., 2007a). Following the cleaning procedure the foraminiferal calcite was dissolved in weak nitric acid (0.075 N).

Table 2.1: *Cleaning protocol for trace element analyses*

Step	**Reagents**	**Ultrasonic Bath**	**Procedure**
clay removal + methanol rinse			
mechanical removal of contaminants, such as clays	n-pure water (18.2 MΩ)	45 to 60 seconds	repetition: 3 times, optionally more repetitions were needed, depending on samples and degree of contamination
removal of fat, lipids, especially for core top samples and samples dyed with rose bengal	methanol	45 to 60 seconds	repetition: twice
rinse	n-pure water (18.2 MΩ)	optional	repetition: twice
reductive cleaning: hydrazine/ ammonium citrate solution			
removal of ferromanganese oxides	5 ml ammonium hydroxide, 5 ml ammonium citrate, 375 µl hydrazine	every 2.5 to 3 minutes (optional)	100 µL per sample; heat 30 minutes (in total): rap the rack every 2.5 to 3 minutes
rinse	n-pure water (18.2 MΩ)	optional	repetition: 3 times
oxidative cleaning: hydrogen peroxide			
removal of organic matter	10 ml NaOH, 1 ml H_2O_2 (30%)	every 2 minutes	100 µL per sample; heat 10 minutes (in total): rap every 2 minutes
rinse	n-pure water (18.2 MΩ)	optional	repetition: 3 times
sample transfer	n-pure water (18.2 MΩ)	-	transfer into acid cleaned Eppendorf vials (0.5 ml)

2.2.1.2 Ferromanganese coatings of sediment samples

To extract the Nd isotope composition of past seawater from Fe-Mn coatings of bulk sediments the samples were leached. The leaching procedure (Table 2.2) described by Gutjahr et al. (2007) was applied to leach about 2.5 g of dried and homogenized sediment. For a part of the data set in Chapter 4 100 mg of < 63 µm fraction of bulk sediments were leached (Table A4.2; Weldeab et al., 2011). Prior to the leaching of the sediment samples carbonate was removed using acetic acid. After the reaction with the sediment sample the leach solution (0.05 M hydroxylamine hydrochloride, 15% distilled acetic acid, buffered to pH ~3.5 to 4 with NaOH) was pipetted into a Teflon vial, evaporated to dryness, and treated twice with concentrated HNO_3. Afterward the sample was dissolved in concentrated HNO3 and centrifuged. The supernatant was then further treated for the separation and purification of Nd (column chemistry detailed in Section 2.2.2).

***Table 2.2**: Leaching procedure for removal of the Fe-Mn coating from the sediment*

Step	**Reagents**	**Procedure**	**Description**
1	20 ml n-pure water	shake, centrifuge, decant	
2		repeat step 1	
3	20 ml acetic acid/Na-acetate (40 %)[1] *pH ~4*	shake, centrifuge, decant	de-carbonating
4	10 ml n-pure water + 10 ml acetic acid/Na-acetate (40 %)[1]	shake (overnight), centrifuge, decant	
5	20 ml n-pure water	shake, centrifuge, decant	
6		repeat step 5 twice	
7	20 ml hydroxylamine solution[2] (50%) *pH 3.5 - 4*	shake, centrifuge, pipette supernatant into Teflon vials	Leaching = ***Fe-Mn coating of the sediment samples***
8	20 ml hydroxylamine solution[2] (50%)	shake, keep for 5 days	Preparation of detrital fraction sample
9	20 ml n-pure water	shake, centrifuge, decant	
10		repeat step 9 twice	
11	20 ml n-pure water	store	

[1]258.9 ml n-pure water (ultra pure water 18.2 MΩ/cm), 41.1 g sodium acetate (p.a.), 210 g acetic acid (p.a.)

[2]207 ml n-pure water (ultra pure water 18.2 MΩ/cm), 0.92 g hydroxylamine, 39.3 g acetic acid (s.p.), 5 g sodium hydroxide (30%)

2.2.1.3 Residual sediment fraction

For the determination of the detrital Nd isotope composition the sediment samples were leached following the complete leaching procedure detailed in Table 2.2 including leaching steps 1 to 10. Then the samples were dried. After drying the detrital samples (about 50 mg) were dissolved in several steps using aqua regia and hydrofluoric acid following the procedure detailed in Table 2.3.

***Table 2.3**: Sediment treatment procedure for complete dissolution of the residual sediments*

Step	**Reagents**	**Procedure**	
1	3 ml conc. HCl 1 ml conc. HNO_3 2 ml HF	reflux over night at 140°C	evaporation
2	1 ml conc. HNO_3 5 ml HF	reflux over night at 140°C	evaporation at 120-140°C
3	2.5 ml conc. HNO_3 0.5 ml perchloric acid 2.5 ml HF	reflux over night at 140°C	evaporation at 180°C
4	4 ml 6 M HNO_3	reflux over night at 120°C	evaporation at 180°C
5 & 6	4 ml 6 M HNO_3	evaporate at 180° to 190°C	
7	4 ml 6 M HNO_3	reflux at 120°C	
	100 µl H_2O_2	reaction has to be completed	
	200 µml H_2O_2	reaction has to be completed, min. 1 h	
	200 µml H_2O_2	reaction has to be completed, min. 1 h	
		evaporation to dryness	
8	1 ml 6 M HNO_3	reflux	
9	centrifuge (1.5 ml safe lock tubes), pipette into Teflon and evaporate		
10	preparation for column chemistry		

Chemicals:
HCl ~10.5 M p.a., quartz-distilled,
HNO_3 ~ 14.5 M p.a., quartz-distilled,
HF 40% Merck®, suprapure,
Perchloric acid 70%, H_2O_2 ~30% Merck®, suprapure

2.2.2 Separation and purification of Nd

The separation and purification of neodymium from the different sample material (foraminiferal carbonates, sediment coatings and detrital fraction) for the isotopic analyses was carried out with established ion chromatographic procedures (see Section 2.2.2.2).

2.2.2.1 Foraminiferal samples

Tests have shown that Nd contained in foraminiferal carbonate can be separated and purified using a one-step column procedure with Eichrom Ln-spec resin (Table 2.4, Figure 2.3). Given that the matrix of the foraminiferal samples differs strongly from that of sediment leachates and detrital sediment the established methods for purification of Nd of those samples described in Section 2.2.2.2 had to be modified. Test series and the analysis of cuts of the eluent from the Nd separation procedure (Table 2.4) with an enlarged resin volume of 3.14 ml showed that all disturbing cations (e.g. Ca, Ba, Sr, Mg) were fully removed from the REE cut during the first part of the elution scheme (Figure 2.3) and that the columns were not overloaded with calcium.

Table 2.4: *Nd separation and purification from dissolved foraminifera with 3.14 ml Eichrom Ln-spec resin (50-100 µm)*

Volume	Acid	Stage
8 ml	6 M HCl	pre-clean
0.5 ml	0.1 M HCl	pre-conditioning
1 ml	0.1 M HCl	pre-conditioning
0.5 ml	**0.1 M HCl**	**sample load**
0.5 ml	0.1 M HCl	wash-in
10 ml	0.25 M HCl	elute LREE
2 ml	0.3 M HCl	elute LREE
6 ml	**0.3 M HCl**	**collect Nd sample**
8 ml	6 M HCl	clean
1 + 1 ml	0.3 M HCl	pass and store

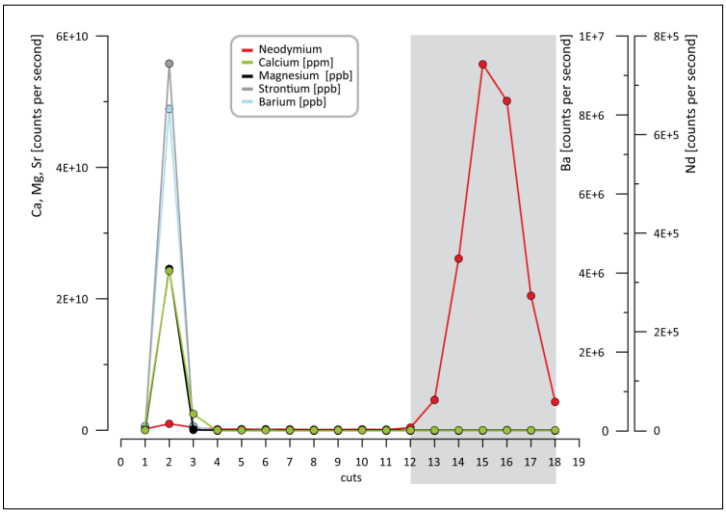

Figure 2.3: *Yield test for adapted neodymium separation (Table 2.4), without Sr-REE separation on cation columns. The plotted elements were measured with Agilent 7500-CX ICP-MS. The sample used for the yield test of the Eichrom Ln-spec columns was a synthetic carbonate solution (~2.8 % Ca, 106 ppb REE, 70 ppm Mg, 65 ppm Sr, 50 ppb Ba). The LREE elution and the Nd collection step (Table 2.4) was divided into 18 cuts of 1 ml each, gray bar frames the cuts which were used for isotopic analyses with Nu instrument ICP-MS.*

2.2.2.2 Sediment samples: Fe-Mn coatings and detrital fraction

The REE separation of the sediment leach and the residual detrital sediment was conducted following the procedures of Horwitz et al. (1992) and Bayon et al. (2002) using AG50W-X12 resin (Table 2.5). The purification of Nd from the REE cut was conducted using Eichrom Ln-spec resin (Cohen et al., 1988; Barrat et al., 1996; Le Fèvre and Pin, 2005) (Table 2.6).

Table 2.5: *Sr-REE separation of sediment leachate samples with 0.8 ml AG50W-X12 cation exchange resin (200-400 µm)*

Volume	Acid	Stage
8 ml	6 M HCl	pre-clean
0.5 ml	1 M HCl	pre-conditioning
1 ml	1 M HCl	pre-conditioning
0.5 ml	**1 M HCl**	**sample load**
3 x 0.5 ml	1 M HCl	wash-in
5 ml	3 M HCl	elute matrix
5 ml	**3 M HCl**	**collection of Sr**
2 x 1 ml	n-pure water	change acid
8 ml	2.5 M HNO_3	elute Ba
6 ml	**6 M HNO_3**	**collection of REE**
6 ml	6 M HNO_3	clean
2 x 1 ml	n-pure water	change acid
1 ml	1 M HCl	store

Table 2.6: *Nd separation of sediment leachate samples with 2 ml Eichrom Ln-spec resin (50 – 100 µm)*

Volume	Acid	Stage
8 ml	6 M HCl	pre-clean
0.5 ml	0.1 M HCl	pre-conditioning
1 ml	0.1 M HCl	pre-conditioning
0.5 ml	**0.1 M HCl**	**sample load**
0.5 ml	0.1 M HCl	wash-in
7.5 ml	0.25 M HCl	elute LREE
5 ml	**0.25 M HCl**	**collection of Nd**
8 ml	6 M HCl	clean
1 + 1 ml	0.3 M HCl	pass and store

2.3 Measurements

2.3.1 Elemental analyses

To evaluate efficiency and calcium loss of the FT and batch cleaning methods, trace and major element concentrations in dissolved foraminiferal samples as well as in some samples of the reductive solutions of the FT method were analyzed. For example, aluminum was used to identify contaminations by clay, manganese for Mn-rich contaminants such as Mn-carbonates and iron for Fe-Mn-oxyhydroxide phases (Chapter 3). To identify those contaminant phases element to calcium ratios of the foraminiferal samples were analyzed by measuring the the concentrations of Al, Ca, Mn, Fe, and Nd with an Agilent 7500-CX inductively coupled plasma mass-spectrometer (ICP-MS) (Chapters 3 and 4).
The uncertainties of repeated measurements (n=3) of two core top and four down core samples (Chapters 3 and 4, respectively) varied between the different element to calcium ratios (maximum 2σ: 9 % for Al/Ca, 27 % for Mn/Ca, 11 % for Nd/Ca and 8 % for Fe/Ca).

2.3.2 Rare earth element analyses

To complement the elemental data sets for examination the contamination of the foraminiferal samples and to determine the origin of the Nd of which the isotopic composition was analyzed, the rare earth element (REE) concentrations were measured in aliquots of the foraminiferal samples (Chapters 3 and 4). The rare earth element (REE) patterns of the foraminiferal samples were determined using online-preconcentration (OP) to remove the calcium matrix before elution of the REEs directly into the spray chamber of the ICP-MS using the ESI SeaFAST system and a method adapted from seawater analysis (Hathorne et al., 2012).
Repeated measurements (n = 3) of one sample gave a maximum uncertainty of 13 % (2σ).

2.3.3 Neodymium isotope analyses

The $^{143}Nd/^{144}Nd$ ratios of the sediment leachates for the section representing the time period between 10 and 20 kyr (Chapter 4) had been measured with a TRITON 1 thermal ionization mass spectrometer (TIMS) at an external reproducibility of ±0.22 (2σ) (Weldeab et al., 2011). For all other samples, the neodymium isotope compositions of the sedimental leachates, the

detrital sediments and the foraminiferal samples were analyzed with a Nu instruments multicollector ICP-MS.

The foraminiferal samples have very low Nd concentrations (Tables A3.1 and A4.1), and most of them thus had to be measured in manual time resolved mode on the Nu multicollector ICP-MS to ensure that all available Nd was used for each measurement. Samples were dissolved in at least 250 µl of 0.3 M HNO_3 to achieve a minimum concentration of 20 ppb, resulting in a total Nd beam intensity of 4 to 5 V. The Nd isotope ratios of these samples were then integrated over a distinct time interval of several minutes depending on sample volume.

Contaminated foraminiferal samples, with elevated Nd concentrations related to ferromanganese oxide coatings, the sediment (Fe-Mn) coatings, and detrital sediment samples had high enough Nd concentrations for measurement in automatic mode using an auto sampler.

The measured $^{143}Nd/^{144}Nd$ ratios were corrected for instrumental mass bias using $^{146}Nd/^{144}Nd = 0.7219$ and an exponential fractionation law. All $^{143}Nd/^{144}Nd$ ratios were normalized to the accepted value of 0.512115 of the JNdi-1 standard (Tanaka et al., 2000) and are expressed in the ε-notation normalized to the value of the Chondritic Uniform Reservoir (CHUR): $\varepsilon Nd=[(^{143}Nd/^{144}Nd)_{sample}/(^{143}Nd/^{144}Nd)_{CHUR}-1]*10{,}000$. The accepted value of CHUR is 0.512638 (Jacobsen and Wasserburg, 1980).

The external reproducibility (2σ) was ±0.6 εNd units for low concentration samples measured in the time resolved mode and ±0.3 εNd units for the bulk sediment leachates and the detrital fraction samples, in both cases assessed by repeated measurements of the JNdi-1 standard at concentrations comparable to those of the corresponding samples (Chapters 3 and 4). The reproducibility of each sample is detailed as external error in Tables A3.1, A3.3, A4.1, A4.3 and A4.4.

The external reproducibility (2σ) of the batch cleaning procedure was estimated to be ±0.4 εNd units by repeated processing of the complete procedure and measurement of 5 aliquots of one large foraminiferal sample (consistency standard).

2.3.4 Trace-Element analyses (Mg/Ca, Ba/Ca)

The trace element ratios (Mg/Ca and Ba/Ca) were analyzed using a Thermo Finnigan Element 2 sector field ICP-MS (Martin and Lea, 2002) at the UCSB.

The analytical reproducibility of 1 % (Mg/Ca) and 2 % (Ba/Ca) was estimated based on measurement of consistency standards (n = 132) during the complete study.

Contamination by silicates and coatings can bias the Mg/Ca ratios. Therefore different element/calcium (Al/Ca, Fe/Ca, Mn/Ca and others) ratios were measured in addition to identify such contamination. The analyzed Element/Ca ratios (Al/Ca, Fe/Ca, Mn/Ca and others) show no correlation with Mg/Ca and Ba/Ca ratios (Figures A5.2 a - d).

2.3.5 Stable isotope ratios ($\delta^{18}O$, $\delta^{13}C$)

The oxygen and carbon isotope compositions of the foraminiferal tests ($\delta^{18}O$ and $\delta^{13}C$) were analyzed using a Stable Isotope Ratio Mass Spectrometer MAT 251 online coupled to Kiel III at the Leibniz-Laboratory for Radiometric Dating and Isotope Research at the University of Kiel. The results of the stable isotopes were expressed as δ-notation, whereas

$$\delta = (R_{sample}/R_{standard}-1)*1000 \quad (2.1)$$

with R being the ratio of heavy to light isotopes ($^{18}O/^{16}O$ and $^{13}C/^{12}C$). The results were calibrated against the NBS19 standard and reported relative to the Pee Dee Belemnite scale (PDB). The analytical uncertainty of the $\delta^{18}O$ and $\delta^{13}C$ measurements is ±0.03 ‰ and ±0.07 ‰, respectively.

Chapter 3

Assessment of seawater Nd isotope signatures extracted from foraminiferal shells and authigenic phases from Gulf of Guinea sediments

Abstract

The radiogenic neodymium (Nd) isotope composition of foraminiferal shells provides a powerful archive to investigate past changes in sources and mixing of water masses. However, seawater Nd isotope ratios extracted from foraminiferal shells can be biased by contaminant phases such as organic matter, silicates, or ferromanganese coatings, the removal of which requires rigorous multiple step cleaning of the samples. Here we investigate the efficiency of flow through and batch cleaning methods to extract seawater Nd isotope compositions from planktonic foraminifera in a shelf setting in the Gulf of Guinea that is strongly influenced by riverine sediment inputs. Nd isotope analyses of reductively and oxidatively cleaned mono-specific planktonic foraminiferal samples and reductively cleaned mixed benthic foraminifera were complemented by analyses of non-reductively cleaned mono-specific planktonic foraminiferal samples, Fe-Mn coatings of de-carbonated bulk sediment leachates, and the residual detrital fraction of the same sediment.

Al/Ca and Mn/Ca ratios of fully cleaned foraminiferal samples reveal indistinguishable levels of cleaning efficiency between the batch and the flow through methods and the Nd isotope compositions obtained from application of both methods are identical within error. Furthermore, non-reductively cleaned foraminiferal samples have the same Nd isotope composition as reductively cleaned foraminifera at our study sites. Close to the Niger River mouth the Nd isotope composition of the foraminifera agree with the seawater Nd isotope composition of nearby stations. Based on the combined extracted Nd isotope signatures and

Published:

***Kraft, S.**, Frank, M., Hathorne, E. C. & Weldeab, S., Assessment of seawater Nd isotope signatures extracted from foraminiferal shells and authigenic phases from Gulf of Guinea sediments, Geochimica et Cosmochimica Acta (2013), Doi: 10.1016/j.gca.2013.07.029*

element to calcium ratios, as well as rare earth element distribution patterns, we infer that the planktonic foraminiferal Nd isotope signatures reflect bottom water/pore water signatures. The isotopic composition of the bulk de-carbonated sediment leachates (Fe-Mn coatings) differs significantly from the foraminiferal data at this site and probably reflects particles that acquired their pre-formed ferromanganese coatings in nearby rivers. Therefore, in such river influenced shelf settings foraminiferal shells should be used to obtain unbiased bottom seawater signatures.

3.1 Introduction

The radiogenic Nd isotope composition of continental rocks varies widely due to elemental fractionation processes in the mantle and as a function of age. Weathering and erosion of continental rocks ultimately control the Nd isotope composition of dissolved Nd in the oceans (cf. Goldstein et al., 1984; Frank, 2002; Jeandel et al., 2007). The main sources of Nd in surface and deep of the oceans have been suggested to be dissolved riverine input and the partial dissolution of aeolian and riverine particulates from the continents (e.g. Frank, 2002 and references therein; Grasse et al., 2012; Singh et al., 2012). Submarine groundwater discharge (Johannesson and Burdige, 2007) and release from reducing sediments (Haley et al., 2004) may also be significant but the sources are essentially continental in origin. Additionally, the Nd isotope composition of seawater can be modified by exchange with sediments on the continental margins and islands without changing the dissolved Nd concentration (e.g. Lacan and Jeandel, 2005). Although the exact mechanism of this process is not yet well understood, recent modelling efforts have demonstrated the importance for the global distribution of seawater Nd isotopes (Arsouze et al., 2009; Rempfer et al., 2011). The Nd oceanic residence time of 200-1000 years (Tachikawa et al., 1999) makes the dissolved Nd isotope composition of seawater a useful tracer of water masses and their mixing. As such Nd isotopes have been applied widely in oceanography and paleo-oceanography and in particular in the tropical Atlantic Ocean (e.g. Piepgras and Wasserburg, 1980, 1982; Goldstein et al., 1984; Goldstein and Jacobsen, 1987; Tachikawa et al., 1999; Rickli et al., 2009; Bayon et al., 2011).

Extracting the seawater Nd isotope composition from marine sediments

The manifestation of the dissolved Nd isotope composition in biogenic and inorganic marine precipitates provides a powerful tool to trace past sources and pathways of water masses and hence past ocean circulation (cf. Frank, 2002). The efficiency of different approaches to clean and separate these precipitates prior to the analysis of past surface and bottom water seawater Nd isotope signatures is the subject of active debate. In this study we investigate various phases and cleaning methods in order to reliably extract seawater Nd isotope composition from sediments of the Gulf of Guinea, in the eastern equatorial Atlantic. Reductively cleaned planktonic foraminifera are tested as archives of surface seawater Nd isotope compositions, non-reductively cleaned planktonic and reductively cleaned benthic foraminifera, as well as Fe-Mn coatings of the bulk sediment are investigated for the extraction of the Nd isotope signature of bottom waters, and the detrital fraction is used to infer the riverine particulate input.

The first studies of trace elements in foraminiferal shells recognized that the foraminiferal tests have to be cleaned thoroughly to remove any contaminant phases, such as ferromanganese oxides (Boyle, 1981; Boyle and Keigwin, 1985). The first measurements of foraminiferal Nd concentrations and Nd isotope composition were carried out by Palmer (1985) and Palmer and Elderfield (1985, 1986), using non-reductively cleaned foraminiferal material. Thus, most of the Nd analyzed originated from the diagenetic Fe-Mn coatings on the foraminifera, which these authors considered to be derived from pore water and bottom waters. More studies have used non-reductively cleaned planktonic foraminifera to reconstruct bottom water signatures (Roberts et al., 2010; Elmore et al., 2011). It has also been shown that the Nd isotope signature of benthic foraminifera reflects bottom waters (Klevenz et al., 2008).

In contrast, reductively cleaned planktonic foraminifera have been proposed to be a reliable archive for surface or subsurface ocean dissolved Nd isotope signatures (Vance and Burton, 1999; Burton and Vance, 2000; Scrivner et al., 2004; Vance et al., 2004; Stoll et al., 2007; Osborne et al., 2008, 2010; Pena et al., 2013). However, a study of plankton tow material suggested accumulation of contaminants within the water column on the tests depending on adsorption/desorption processes and on the redox conditions (Pomiés et al., 2002). Other results indicated that the organic material within foraminiferal shells contains high amounts of rare earth elements and other trace metals such as manganese, considered to be derived

from surface waters (Vance et al., 2004; Haley et al., 2005; Martínez-Botí et al., 2009). More recently, several studies concluded that reductive cleaning does not completely remove the signal acquired during early diagenesis at sediment water interface (Roberts et al., 2010; Tachikawa et al., 2013) and planktonic foraminifera suffering from incomplete removal of ferromanganese coatings were consequently suggested to represent bottom water signatures (e.g. Charbonnier et al., 2012; Piotrowski et al., 2012; Roberts et al., 2012), as demonstrated by the comparison with fish teeth εNd signatures reflecting bottom waters (Martin et al., 2010).

Nd isotope analyses of ferromanganese coatings leached from bulk sediment (Rutberg et al., 2000; Bayon et al., 2002; Piotrowski et al., 2005; Gutjahr et al., 2007, 2008; Pahnke et al., 2008) and from un-cleaned planktonic foraminifera (Roberts et al., 2010; Piotrowski et al., 2012) have provided insights into past bottom water variability. Close to the continental margins, however, the Nd isotope composition extracted from bulk sediment leachates can be altered by the partial dissolution of sedimentary components, such as volcanic ash, other detrital phases (Elmore et al., 2011) and pre-formed oxides (Bayon et al., 2004). This contamination can result in sediment coatings not reflecting pure bottom water signatures. Burial of the sediments and exposure to reducing conditions may also alter the original signatures depending on the region and sedimentary conditions (Elderfield et al., 1981). Piotrowski et al. (2012) showed that in some oceanic settings, the sediment leachates provide reliable bottom water signatures whereas in other settings the leachates can be biased by detrital phases.

The main goal of this study on sediments deposited in the Gulf of Guinea at variable distanced from major river input is to test different cleaning methods of planktonic foraminifera in order to obtain seawater εNd signatures of surface and bottom waters in an attempt to disentangle water mass mixing and riverine input. Our results show that planktonic foraminifera in the Gulf of Guinea cannot be completely cleaned with the applied methods and do not reflect surface water but bottom water signatures. The influence of different river systems can be distinguished by the detrital Nd isotope signatures and those of pre-formed Fe-Mn coatings originating from the rivers in this proximal shelf setting.

3.2 Materials and methods

3.2.1 Study area

Core top and near surface sediments used in this study are from different sampling sites in the Gulf of Guinea in the easternmost equatorial Atlantic (Figure 3.1). The salinity and trace element composition of surface waters as well as the terrigenous sediment in the Gulf of Guinea are strongly influenced by runoff from large river systems draining the West African monsoon area (Zabel et al., 2001; Weldeab et al., 2007a, 2007b). The most important river systems in this region are the Niger, Sanaga, Nyong and Ntem rivers. The catchments of these rivers are characterized by distinct rock types and thus differ markedly in their Nd isotope compositions (Toteu et al., 2001; Weldeab et al., 2011). The Ntem river supplies weathering products from Archean and Early Proterozoic rocks (Toteu et al., 2001) with un-radiogenic Nd isotopic composition (εNd of riverine sediments = -28.1, Weldeab et al., 2011). In contrast, the catchments of the Sanaga and Nyong rivers are dominated by Meso- to Neoproterozoic rocks (Toteu et al., 2001) with more radiogenic signatures (εNd of riverine sediment = -12.4, Weldeab et al., 2011) (Figure 3.1). The catchment area of the Niger river is very complex and highly variable in age, spanning Archean and Proterozoic rocks of the West African Craton in the west (Upper Niger) to young Mesozoic to Quaternary sediments in the east (Lower Niger) (Wright et al., 1985). The Niger thus delivers the most radiogenic Nd isotopic signatures to the study area (εNd of suspended sediments = -10.5, Goldstein et al., 1984) (Figure 3.1). Furthermore, a chain of young volcanic islands located along the Cameroon line within the Gulf of Guinea may provide highly radiogenic signatures (εNd of basaltic material ranges from +2 to +7, Halliday et al., 1988). Given the small areal extent of those islands, we consider their influence very localized.

The Tropical Surface Water (TSW) in the easternmost Gulf of Guinea (Figure 3.1) is affected by contributions of the Guinea Current (GC) from the northwest and by the South Equatorial Current (SEC) from the south. Below the TSW, the Subtropical Underwater (STUW) is advected by the Equatorial Undercurrent (EUC) and the northern South Equatorial Current (nSEC) (Stramma and Schott, 1999; Bayon et al., 2011). Between 100 and 500 m water depth, the South Atlantic Central Water (SACW) is influenced by the EUC and the nSEC (Stramma and Schott, 1999). At intermediate water depth (500-1200 m) the Northern Intermediate Countercurrent (NICC) carries Antarctic Intermediate Water (AAIW). The deep

water (> 1200 m) in the Gulf of Guinea is dominated by North Atlantic Deep Water (NADW).

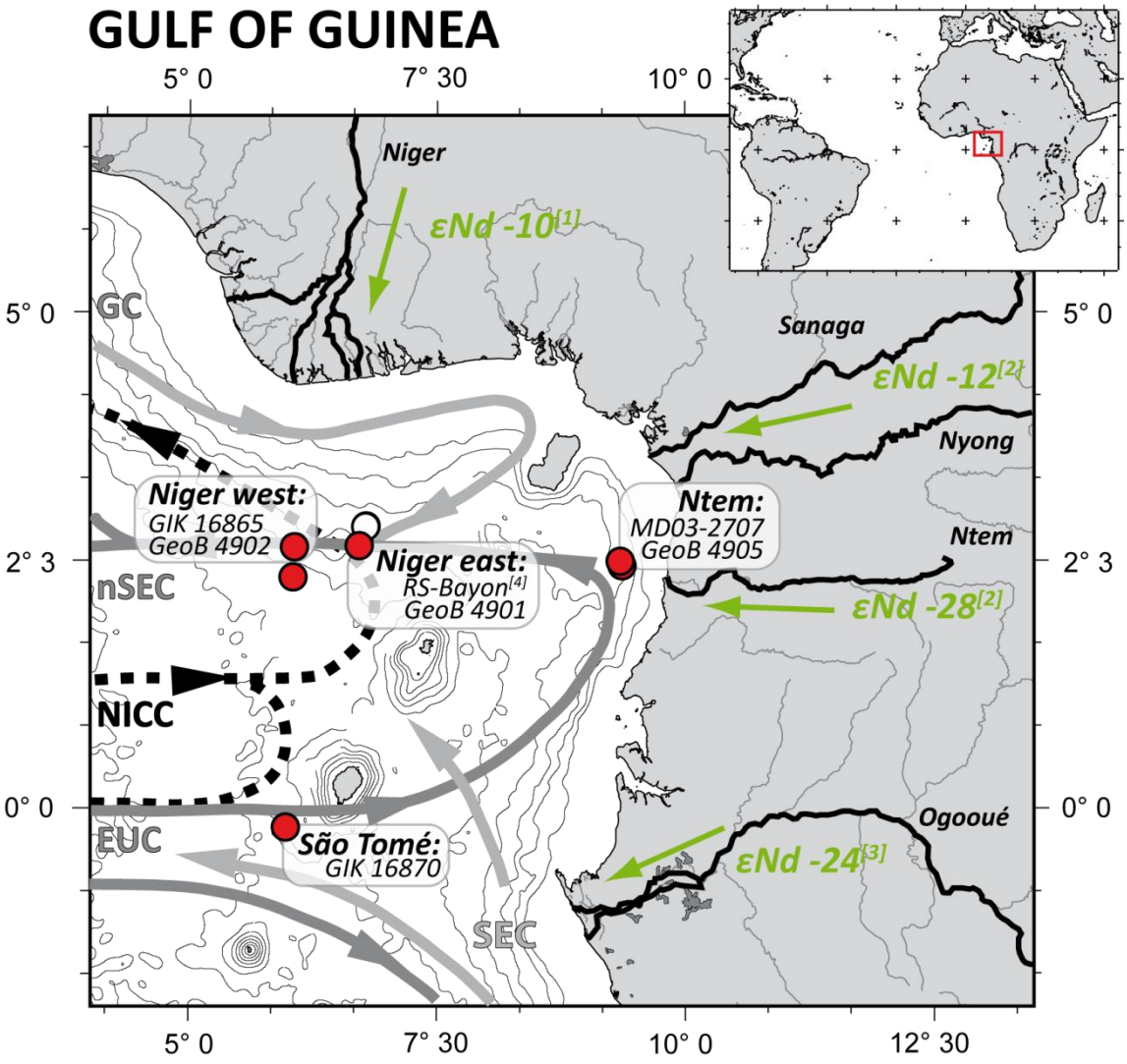

Figure 3.1: *Sampling sites in the Gulf of Guinea ([4]reference site of Bayon et al, 2011) with a simplified schematic current system: surface = light grey line (SEC = South Equatorial Current), subsurface = solid grey line (GC = Guinea Current, NSEC = Northern South Equatorial Current, EUC = Equatorial Undercurrent), deeper currents = dotted black line (NICC = Northern Intermediate Countercurrent) and εNd values of adjacent rivers: [1]Niger sediment (Goldstein et al., 1984), [2]River sediments of Sanaga, Nyong and Ntem (Weldeab et al., 2011), [3]Ogooué river load (suspended or/and dissolved) (Bayon et al., 2011).*

3.2.2 Materials

Core top sample locations (Figure 3.1) and water depths are given in Appendix Table A3.1. Site GIK 16870 (São Tomé) represents the central eastern Gulf of Guinea and sites GIK 16865; GeoB 4902 (Niger west) and GeoB 4901 (Niger east) are located at a distance of about 200 km from the Niger delta. MD03-2707 and GeoB 4905 (Ntem) are located close to the coast between the mouths of the Sanaga/Nyong Rivers and of the Ntem River (Figure 3.1). The GIK samples were taken with a giant box corer during Meteor cruise M6-5 and the uppermost 1 cm was sampled (Lutze et al., 1988). The samples were taken and stained on board (Lutze and Altenbach, 1991), and were sieved and size fractionated as described by Altenbach et al. (2003). The GeoB samples were retrieved during Meteor cruise M41-1 (1986) using a multicorer that was sub-sampled at a sediment depth between 3 and 5 cm. Core top sediment samples of piston core MD03-2707 were not available. Therefore, a sample was obtained from between 25 and 31 cm depth, which is between 550 and 660 years old (Weldeab et al., 2007a). The high accumulation rate of terrigenous material means the abundance of foraminifera in MD03-2707 is low making the use of mixed planktonic foraminifera necessary.

Generally about 20 mg of mono-specific planktonic foraminiferal tests with shell sizes of > 250 µm were separated from the core top sediments. The foraminiferal species, the initial weight and the methods applied to the specific samples are listed in Appendix Table A3.1. All foraminiferal tests were handpicked under a binocular microscope and were gently cracked between two glass plates to open the chambers. During this process, any visible contaminant grains were removed.

A mixture of epibenthic and shallow endobenthic species (e.g. *Oridorsalis umbonata*, *Uvigerina* spp., *Bulimina* spp., *Cibicidoides* spp., *Hoeglundina elegans*) was used because of the low abundance. However, significantly different Nd isotope compositions are not expected between the selected species (Klevenz et al., 2008), which live at or near the sediment surface < 6 cm (Rathburn et al., 1996; Jorissen et al., 1998; Fontanier et al., 2002).

For comparison with the data obtained from the foraminiferal shells, bulk sediment samples were analyzed for the Niger sites and the uppermost part of core MD03-2707 (Ntem).

3.2.3 Methods

3.2.3.1 Cleaning of foraminiferal shells

In this study, we test two cleaning methods for the extraction of seawater Nd isotope composition from foraminifera shells. The first method is a modification of the Flow Through (FT) cleaning method of Haley and Klinkhammer (2002). The main advantage of this method is the prevention of the re-adsorption of rare earth elements originating from contaminant phases onto the foraminifera shells. The second method is a batch cleaning (BC) method originally developed by Boyle (1981) and modified by Vance and Burton (1999) and Vance et al. (2004).

Both methods consist of essentially the same cleaning steps and similar reagents to remove contaminant phases. The first step in both methods is the removal of silicate phases. The cracked foraminifera samples were transferred into 1.5 ml micro-centrifuge tubes (FT method) or 15 ml centrifuge vials (batch method). Then the fine clay particles were brought into suspension using n-pure water (ultra pure water 18.2 MΩ/cm) or methanol (99.9% p.a.). The samples were sonicated (20-60 seconds) and the liquids containing clay fines siphoned off (Tables 3.1 to 3.3).

Organic matter was removed by oxidation, using a hot H_2O_2-NaOH solution (Tables 3.1 to 3.3). For the FT cleaning the oxidation was applied as a pre-cleaning step, not using the FT set up as outlined below. Ferromanganese oxides and early diagenetic oxyhydroxide coatings were removed using a reductive solution of hydroxylamine (FT method) or hydrazine (batch method), (see the following subsections and Tables 3.1 to 3.3). Following the cleaning procedure, the foraminiferal samples were dissolved in dilute nitric acid (< 0.5 M HNO_3, see following sections for further details).

Additionally, six samples were not reductively cleaned. Four of them were directly dissolved after clay removal and two samples were oxidatively cleaned following the clay removal step.

Flow Through cleaning method (FT)

The clay removal and the oxidative cleaning steps were carried out in 1.5 ml micro-centrifuge tubes (Eppendorf). Thereafter the samples were transferred in buffered n-pure water (pH 7 – 8) onto the centre of a 13 mm diameter syringe filter (PTFE-membranes with mesh size of 0.45 µm) and were rinsed with a continuous flow of chemical reagents (Tables 3.1 and 3.2). The setup for the flow-through cleaning method includes a peristaltic pump, with which the

chemicals were pumped through a PTFE tube. Part of the PTFE tube was looped and placed in a water bath at 102°C to heat the cleaning reagents. The tube on which the sample-carrying syringe filter was positioned was insulated to minimize heat loss. The reductive reagent (hydroxylamine solution) was pumped over the samples with a temperature of about 80°C to ensure efficiency of the reductive reaction. The Flow Through cleaning followed the procedures shown in Tables 3.1 and 3.2. Different effects of the two procedures are documented in Figure 2.2 B and C. The purpose of adding buffered n-pure water steps was to improve the rinsing efficiency of the samples and the system in one single step without removing the sample from the system. We slowly dissolved the foraminiferal sample by stepwise addition of weak nitric acid (5, 50 and 500 mM HNO_3, at room temperature) to avoid attacking remaining contaminant particles. To observe the progress of the Flow Through method the cleaning and dissolution solutions were collected in discrete fractions, as described in Tables 3.1 and 3.2. Except for the reductive cleaning reagent, all cuts were collected in 4 ml acid cleaned polystyrene (PS) vials and were acidified with 6 M nitric acid (pH < 2) to ensure that particle reactive elements remained in solution. Two cuts of the reductive cleaning step were immediately combined in 7 ml Teflon vials and dried on a hotplate and were dissolved again in 1 ml of 2% nitric acid for elemental analyses. Between 0.5 and 1 ml of the collected dissolution cuts were taken for elemental analysis with ICP-MS. These elemental analyses were used to evaluate the cleaning efficiency and the calcite loss.

Table 3.1: *Procedure of the Flow Through cleaning method with high concentration reductive solution (0.5 M hydroxylamine)*

Clay removal and oxidative cleaning steps in batch method				
step	**chemical solution**	**amount per sample (ml)**	**repetition**	**ultrasonic**
clay removal	n-pure water (18.2 MΩ/cm)	1 to 1.5	min. 2 to 3 times	min. 30 seconds
	Methanol (99.9% p.a.)	1 to 1.5	min. 2 to 3 times	min. 30 seconds
sample rinse	n-pure water (18.2 MΩ/cm)	1.5	2 times	-
oxidative cleaning	30 ml NaOH (p.a.) + 100 µl H_2O_2 (p.a.)	0.25	only one time for 10 minutes in boiling water, sample rack was rapped several times to remove bubbles	-
sample rinse	n-pure water (18.2 MΩ/cm)	1.5	3 times	-
sample transfer	n-pure water (18.2 MΩ/cm)	Transfer of the samples into 13 mm diameter syringe filters (PTFE-membranes with mesh size of 0.45 µm)		

Reductive cleaning steps and dissolution in flow through method				
main stage	**setting**	**flow rate [ml/min]**	**chemical solution**	**time***
rinse system (without sample)	hot	~3.5	n-pure water (18.2 MΩ/cm)	several minutes
			500 mM HNO_3 (distilled acid)	3 minutes
			n-pure water (18.2 MΩ/cm)	3 minutes
cleaning			0.5 M hydroxylamine (Hydrx)**, pH >9	30 minutes in total (1 minutes cuts)
sample rinse			buffered n-pure water, pH 7-8	6 minutes (1 minutes cuts)
system rinse (without sample)			1 M HNO_3 (distilled acid)	8 minutes
system rinse (without sample)			buffered n-pure water, pH 7-8	5 minutes
sample rinse	room temperature	0.5	buffered n-pure water, pH 7-8	3 minutes
dissolution			5 mM HNO_3 (distilled acid)	30 minutes in total (7.5 minutes cuts)
			50 mM HNO_3 (distilled acid)	60 minutes in total (7.5 minutes cuts)
			500 mM HNO_3 (distilled acid)	10 minutes in total (5 minutes cuts)
			1 M HNO_3 (distilled acid)	3 minutes in total
rinse system (without sample)			n-pure water (18.2 MΩ/cm)	several minutes

**in brackets: the solution was collected for specific time ** 0.5 M Hydroxylamine: 17.38 g NH_4OH*HCl + 400 ml n-pure water + 26 ml 25% NH_3*aq (suprapure)*

Table 3.2: *Advanced procedure of Flow Through cleaning with different reductive solutions*

Clay removal and oxidative cleaning steps in batch method				
step	**chemical solution**	**amount per sample (ml)**	**repetition**	**ultrasonic**
clay removal	n-pure water (18.2 MΩ/cm)	1 to 1.5	min. 2 to 3 times	min. 30 seconds
	Methanol (99.9% p.a.)	1 to 1.5	min. 2 to 3 times	min. 30 seconds
sample rinse	n-pure water (18.2 MΩ/cm)	1.5	2 times	-
oxidative cleaning	30 ml NaOH (p.a.) + 100 µl H_2O_2 (p.a.)	0.25	only one time for 10 minutes in boiling water, sample rack was rapped several times to remove bubbles	-
sample rinse	n-pure water (18.2 MΩ/cm)	1.5	3 times	-
sample transfer	n-pure water (18.2 MΩ/cm)	Transfer of the samples into 13 mm diameter syringe filters (PTFE-membranes with mesh size of 0.45 µm)		

Reductive cleaning steps and dissolution in flow through method				
main stage	**setting**	**flow rate [ml/min]**	**chemical solution**	**time***
rinse system (without sample)	hot	~3.5	n-pure water(18.2 MΩ/cm)	several minutes
			500 mM HNO_3 (distilled acid)	4 minutes
			n-pure water (18.2 MΩ/cm)	3 minutes
cleaning			buffered n-pure water, pH 7-8	5 minutes (1 minute cuts)
			** hydroxylamine (Hydrx), pH >9	30 minutes in total (1 minutes cuts)
sample rinse			buffered n-pure water, pH 7-8	5 minutes (1 minute cuts)
	room temperature (tube removed from water bath)	0.5	buffered n-pure water, pH 7-8	7 minutes (discarded)
			buffered n-pure water, pH 7-8	5 minutes (1 minute cuts)
			buffered n-pure water, pH 7-8	8 minutes (discarded)
			buffered n-pure water, pH 7-8	5 minutes (1 minute cuts)
dissolution			buffered n-pure water, pH 7-8	3 minutes
			5 mM HNO_3 (distilled acid)	30 minutes in total (7.5 minutes cuts)
			50 mM HNO_3 (distilled acid)	75 minutes in total (7.5 minutes cuts)
			500 mM HNO_3 (distilled acid)	37.5 minutes in total (5 minutes cuts)
			1 M HNO_3 (distilled acid)	37.5 minutes in total (5 minutes cuts)
rinse system			n-pure water (18.2 MΩ/cm)	

**in brackets: the solution was collected for specific time, **tests were done with 0.5 M (Hydroxylamine: 17.38 g NH_4OH*HCl + 400 ml n-pure water (18.2 MΩ/cm) + 26 ml 25% NH_3*aq (s.p.)), 0.25 M and 0.1 M hydroxylamine solution*

Batch cleaning method

The batch cleaning method developed by Boyle (1981) was scaled up for larger samples by Vance and Burton (1999) and Vance et al. (2004) so cleaning is conducted with 15 ml polypropylene/polyethylene (PP/PE) centrifuge vials. This method also includes clay removal steps followed by oxidative and reductive cleaning (Table 3.3). In addition, the batch method was tested using a hydroxylamine solution (0.25 and 0.1 M) instead of the usual hydrazine solution for direct comparison with the FT method (Table 3.3). After cleaning and a final rinse with n-pure water the samples were transferred into acid cleaned micro centrifuge tubes (1.5 ml) and dissolved in weak nitric acid by stepwise (50-100 µl) addition of 0.5 M HNO_3 to samples in 0.6 ml n-pure water. The samples were sonicated between the acid addition steps until the dissolution reaction stopped (max. 0.9 ml 0.5 M HNO_3 in 0.6 ml n-pure water). The dissolved samples were centrifuged and the supernatant was immediately siphoned off to prevent the leaching of remaining phases. The supernatant was then dried and re-dissolved in 1 ml 2% nitric acid. An aliquot was used for elemental analyses by ICP-MS, while the remaining sample material was dried again and prepared for Nd isotope analysis (section 3.2.3.3).

Table 3.3: *Steps of the batch cleaning method*

step	**chemical solutions**	**amount per sample (ml)**	**repetition**	**~90°C water bath**	**ultrasonic (seconds)**
clay removal	n-pure water (18.2 MΩ/cm)	5	min. 3 times	no	20 to 60
	methanol	2 to 5	twice	no	20
sample rinse	n-pure water (18.2 MΩ/cm)	5 to 10	min. 3 times	no	-
reductive cleaning*	2.4 g citric acid (p.a.) + 17 ml n-pure water (18.2 MΩ/cm) + 30.5 ml ammonium hydroxide (25%, p.a.) + 2.43 ml hydrazinium hydroxide (about 100%)	10	-	30 minutes	for 20 seconds every 2 minutes
sample rinse	n-pure water (18.2 MΩ/cm)	15 – 10 – 15	3 times	no	no
oxidative cleaning*	50 ml NaOH (0.1 N, p.a.) + 500 µl H_2O_2 (30%, p.a.)	10	-	30 minutes	for 1 minute every 10 minutes
sample rinse	n-pure water (18.2 MΩ/cm)	15 – 10 – 15	3 times	no	no

**order of the steps was changed after Rosenthal et al. (1997)*

3.2.3.2 Fe-Mn coatings of bulk sediment and total dissolution of the residual fraction

The leaching procedure described by Gutjahr et al. (2007) was applied to leach about 2.4 g of dried sediment. Prior to the leaching of the sediment samples carbonate was removed using acetic acid. The leach solution (0.05 M hydroxylamine hydrochloride, 15% distilled acetic acid, buffered to pH ~3.5 to 4 with NaOH) was pipetted into a Teflon vial and further treated for Nd isotope analyses (section 3.2.3.3).

In addition, we analyzed the residual detrital sediment after dissolution, for which the residue of the previously leached samples was treated again with the leach solution (1:1 dilution) and rinsed with n-pure water. After drying, the remaining sediment was dissolved in several steps with aqua regia and hydrofluoric acid. The complete procedure is detailed in Chapter 2, Table 2.3.

3.2.3.3 Separation and purification of Nd

The separation of the REE from the sediment leachates and the dissolved residual detritus was conducted following the procedures of Horwitz et al. (1992) and Bayon et al. (2002) using AG50W-X12 resin. The purification of Nd from the REE cut was conducted using Eichrom Ln-spec resin (Cohen et al., 1988; Barrat et al., 1996; Le Fèvre and Pin, 2005). Given that the matrix of the foraminiferal samples differs strongly from that of sediment leachates and detrital sediment, foraminiferal samples were purified using a one-step column procedure with a larger volume (3.14 ml) of the Ln-spec resin to ensure that the columns were not overloaded with Ca (Chapter 2, Table 2.4, Figure 2.3). Analysis of cuts of the eluent from the neodymium separation procedure showed that all disturbing cations (e.g. Ca, Ba, Sr, Mg) were fully removed from the REE cut during the first part of the elution scheme (Chapter 2, Table 2.4, Figure 2.3).

3.2.4 Measurements

3.2.4.1 Elemental analyses by ICP-MS

The efficiency of both methods, FT and BC, was evaluated by analyzing the trace and major element concentrations in dissolved foraminiferal samples. We used aluminum to identify contaminations by clay, manganese for Mn-rich contaminants such as Mn-carbonates and iron for Fe-Mn-oxyhydroxide phases. In an initial step the calcium concentration was measured and then all samples were diluted to a Ca content of 20 ppm. The isotopes ^{24}Mg,

^{27}Al, ^{43}Ca, ^{55}Mn, ^{56}Fe, ^{88}Sr, ^{137}Ba, and ^{146}Nd were measured with an Agilent 7500-CS inductively coupled plasma mass-spectrometer (ICP-MS). ^{56}Fe was measured with H_2 gas in the collision cell. A standard with element/calcium ratios similar to those found in foraminifera was made from high purity single element solutions and element/Ca ratios were calculated following the method of Rosenthal et al. (1999). The uncertainties of repeated measurements of two samples varied between the different element to calcium ratios (2σ: 9 % for Al/Ca, 5-27 % for Mn/Ca, 8-9 % for Nd/Ca and around 7-8 % for Fe/Ca).

3.2.4.2 REEs by OP-ICP-MS

The rare earth element (REE) patterns of the foraminiferal samples were determined using online-preconcentration (OP) to remove the calcium matrix before elution of the REEs directly into the spray chamber of the ICP-MS using the ESI SeaFAST system and a method adapted from seawater analysis (Hathorne et al., 2012). The samples were diluted to a Ca concentration of 200 ppm and an internal indium spike was added. One ml of sample solution was used to fill a 0.5 ml sample loop, which was then loaded onto the pre-concentration column. The column was washed to remove Ca, Ba and other matrix elements before the pre-concentrated REE were eluted in the ICP-MS. Repeated measurements (n = 3) of one sample gave a maximum uncertainty of 13 % (2σ).

3.2.4.3 Neodymium isotope analyses

Neodymium isotope compositions were analyzed with a Nu instruments multicollector ICP-MS. Since the total amount of Nd available in the foraminiferal samples was very low, most of the samples had to be measured in time resolved mode to ensure that all available Nd was used for each measurement. Samples were dissolved in a minimum of 250 µl of 0.3 M nitric acid to obtain a concentration of at least 20 ppb, resulting in a total Nd beam intensity of 4 to 5 V. The Nd isotope ratios of these samples were integrated over a distinct time interval of several minutes depending on the sample volume. The contaminated foraminifera with elevated Nd concentrations related to ferromanganese oxide coatings, the sediment leachates, and detrital samples had high enough Nd concentrations for measurement in automatic mode using an auto sampler.

The measured $^{143}Nd/^{144}Nd$ ratios were corrected for instrumental mass bias using $^{146}Nd/^{144}Nd = 0.7219$ and an exponential fractionation law. All $^{143}Nd/^{144}Nd$ ratios were normalized to the accepted value of 0.512115 of the JNdi-1 standard (Tanaka et al., 2000) and are expressed in

the ε-notation normalized to the value of the Chondritic Uniform Reservoir (CHUR): $\varepsilon Nd=[(^{143}Nd/^{144}Nd)_{sample}/(^{143}Nd/^{144}Nd)_{CHUR}-1]*10{,}000$. The accepted value of CHUR is 0.512638 (Jacobsen and Wasserburg, 1980). The external reproducibility (2σ) for time resolved measurements, deduced from repeated measurement of the JNdi-1 standard at similar concentrations to the low level samples, ranged between 0.14 and 0.87 εNd units for different analytical sessions (n = 160). The comparable external reproducibility of the ratios measured at higher concentrations in automatic mode was ±0.30 εNd units (2σ). The analytical error of each sample analysis is taken as the external reproducibility (2σ) of the JNdi-1 standard for each analytical session (Table 1). The external reproducibility (2σ) of the BC method was estimated to be 0.39 εNd units by repeating the complete cleaning procedure and measurement (n = 5) of an aliquot of a large foraminiferal sample (consistency standard).

3.3 Results

3.3.1 Element concentrations in the reductive (FT) cleaning solution and in the foraminifera

Calcium, aluminum, and manganese concentrations were measured in hydroxylamine (0.5 M and 0.1 M) fractions collected during the FT cleaning procedure in order to evaluate the cleaning progress and to monitor the sample loss during the cleaning procedure.

3.3.1.1 Calcium concentrations and loss of calcite during the cleaning procedures

The total amount of Ca in the combined cuts (~105 ml, Tables 3.1 and 3.2) of the reductive solution used in the FT method is three times higher (1.48 mg) in the 0.5 M HYDRX solution than in the 0.1 M solution (0.52 mg) (Appendix Figure A3.1 a).

Using the Ca concentration measured in the final dissolved foraminiferal samples, we estimate the loss of calcite during the different cleaning methods assuming that the initial weight (~ 20 mg) of the crushed un-cleaned foraminiferal tests was 100% $CaCO_3$ (Figure 3.2). The weight of residual clay in a sample is likely to be negligible (Yu et al., 2008). The control samples without any reductive cleaning (black triangles in Figure 3.2) have the lowest sample loss (11 to 23%). The FT cleaned samples using 0.5 M HYDRX experienced a calcite loss of 82%, whereas the 0.1 M HYDRX solution resulted in calcite loss ranging between 27 and 44% (Figure 3.2). During the batch cleaning losses between 22% and 79% occurred

(Figure 3.2). The highest calcite losses were found for the *G. ruber pink* samples and for the mixed planktonic foraminifera. The mixed benthic samples suffered a relatively low calcite loss (28%).

3.3.1.2 Manganese concentration in the reductive cleaning solution

Generally, the highest Mn concentrations were found in the first cuts of the reductive hydroxylamine solution. The concentrations decreased exponentially in later cuts (Figure 3.3). The maximum concentration at the site near São Tomé is 40 ppb Mn in the 0.5 M HYDRX solution, as well as for the 0.1 M HYDRX solution. The maximum concentration at the Niger west site is 104 ppb Mn for the 0.1 M HYDRX solution.

3.3.2 Foraminiferal element to calcium ratios

In the dissolved foraminiferal samples the Al/Ca ratios vary between 8 and 136 µmol/mol with only three samples with Al/Ca values > 100 µmol/mol (Figure 3.4, Appendix Table A3.1). There is no correlation with the corresponding Nd/Ca ratios ($r^2 = 0.015$, n = 31) (the Al/Ca and the Nd/Ca ratios are not normally distributed and thus, a Spearman Rank correlation test with a critical value of $p < 0.05$ was carried out to determine if correlations are significant).

All core top samples show Mn/Ca ratios below 51 µmol/mol (Figures 3.5, Appendix Table A3.1). Those samples treated with a complete cleaning procedure have ratios below 25 µmol/mol. There is no significant correlation between Mn/Ca and Nd/Ca ratios and εNd, even when separating the data by location (Figures 3.5; e.g. Niger sites $r^2 = 0.32$, n = 13). The different locations are characterized by different sediment compositions due to riverine influx (Niger and Ntem sites) and distance from a volcanic island (São Tomé site), which may have influenced the elemental composition of the coatings. In addition, different redox conditions have to be taken into account, as indicated by the sample from the Ntem site MD03-2707, which is not a true core top sample and has a higher Mn/Ca ratio of 167 µmol/mol.

The Fe/Ca ratios of the planktonic foraminifera vary between 20 and 83 µmol/mol. At the Niger sites one benthic foraminiferal sample exceeds this with 120 µmol/mol (Figure 3.6 A); the other benthic sample has a Fe/Ca ratio close to the highest value of the planktonic samples (83 µmol/mol). Overall, Fe/Ca ratios correlate significantly with the Nd/Ca ratios with r^2 = of 0.68 (n = 15, $p < 0.05$) (Figure 3.6 A). The correlation is even stronger for the Niger sites ($r^2 = 0.73$, n = 11) possibly caused by different sediment compositions and redox

conditions. The Fe/Ca ratios show no significant correlation with Mn/Ca ratios (Appendix Figure A3.2). The Mn/Fe ratios vary between 0.1 and 1 mol/mol (Appendix Table A3.1) and do not correlate with Nd/Ca (Appendix Figure A3.3).

The Nd/Ca ratios vary overall between 0.2 and 2.5 µmol/mol (Figures 3.5 to 3.7, Table 1). The non-reductively cleaned samples range from 0.8 to 1.7 µmol/mol. The completely cleaned (BC method) benthic foraminiferal samples have a higher average value of 2.0 µmol/mol. The Nd/Ca ratios of the completely cleaned planktonic foraminifera vary between 0.2 and 1.7 µmol/mol, with the exception of one FT (0.5 M HYDRX) cleaned sample exhibiting a value of 2.5 µmol/mol (Appendix Table A3.1, method test detailed in Table 3.1).

3.3.3 REE concentrations in foraminiferal shells

Rare earth element (REE) concentrations were measured for two benthic and six planktonic batch cleaned and two non-reductively cleaned foraminiferal samples at both Niger sites. The results are normalized to Post-Archean Average Australian Sedimentary rock (PAAS values after Nance and Taylor, 1976) and exhibit a similar pattern (Figure 3.7, Appendix Table A3.2) despite covering a large range of absolute concentrations. The REE patterns display pronounced negative Ce-anomalies, yielding PAAS normalized Ce values between 2 and 31 $x10^{-3}$ compared to values between 8 and 97 $x10^{-3}$ for the other REEs.

3.3.4 Neodymium isotope compositions

The εNd signature of the cleaned foraminiferal samples shows a broad spatial variability (Figure 3.8, Appendix Table A3.1). The εNd signatures of the leachates and of the residual detrital fractions obtained from a single location show similar values (Figure 3.8, Appendix Table A3.3). However, a comparison between the different sites in the Gulf of Guinea reveals spatial variability.

At the ***São Tomé site*** (GIK 16870) the reductively cleaned planktonic foraminifera have average εNd values of -11.5 ± 0.8 (SD) (excluding a *G. ruber* pink value of -8.5) with a larger variability than the non-reductively cleaned *G. menardii* samples (-11.1 and -11.8) (Figure 3.8, Appendix Table A3.1). The εNd signatures of flow through and batch cleaned *G. menardii* show the same values within error (-11.7 and -11.9, respectively). The batch cleaned samples treated with hydroxylamine reductive solution (instead of hydrazine solution) also show similar values. The 0.5 M HYDRX leached FT sample reveals a more radiogenic signature (-10.1), as well as the *N. dutertrei* and *G. ruber* pink (-10.4 and -10.9).

The more radiogenic Nd isotope value of one of the *G. ruber* pink samples εNd = -8.5 ± 0.3 is accompanied by an elevated Al/Ca ratio (109 µmol/mol), suggesting that this sample may have been still contaminated by clay.

At the ***Niger west site*** (GIK 16865/GeoB 4902) the FT and the batch cleaned *G. menardii* samples show the same values within error (-12.8 and -13.1, Appendix Table A3.1 and Figures 3.8 and 3.9). The samples of *G. ruber* pink, the benthic foraminifera and the non-reductively cleaned *G. menardii* samples have slightly more radiogenic εNd values (-12.6, -12.5, and -12.6, respectively). The εNd signatures of the foraminifera from the ***Niger east site*** (GeoB 4901) are similar to those of the Niger west site. All analyzed samples (non-reductively and batch cleaned planktonic and benthic foraminifera) show the same εNd value within error (Appendix Table A3.1 and Figures 3.8 and 3.9). In general, the samples of the Niger sites are less radiogenic, than those of the São Tomé site. The sediment leachates and detrital samples, of the Niger west site (GeoB 4902) have more radiogenic εNd values than those of the Niger east site (GeoB 4901).

The mixed planktonic foraminiferal sample from the ***Ntem site*** MD03-2707 (28 cm core depth) shows the least radiogenic εNd value of -15.8 similar to the sediment leachates and detrital compositions at this location (Appendix Tables A3.1 and A3.3, Figure 3.8).

3.4 Discussion

3.4.1 Cleaning efficiency

Carbonate loss

Our results show that the calcite loss applying the BC method is slightly higher (*G. menardii* = 30 - 60%, all samples together = 22-79 %) than that of the FT cleaning method (0.1 M HYDRX = 27 - 44%) (Figure 3.2). The reductive solution obviously attacks the calcite, which is supported by the smaller losses of the non-reductively cleaned control samples (Figure 3.2). Yu et al. (2007) suggested that the most aggressive component of the batch method reductive solution is the citric acid. However, we found similar losses with the FT cleaning method and the use of buffered HYDRX not including citric acid. It is likely that the slightly higher calcite loss of the batch method is at least partly related to mechanical fragmentation caused by frequent ultra-sonication and siphoning. This is consistent with the

observation that the *G. ruber pink* samples with the thinnest shells suffer higher calcite losses than those of *N. dutertrei*, *G. menardii*, and benthic foraminiferal samples (Figure 3.2).

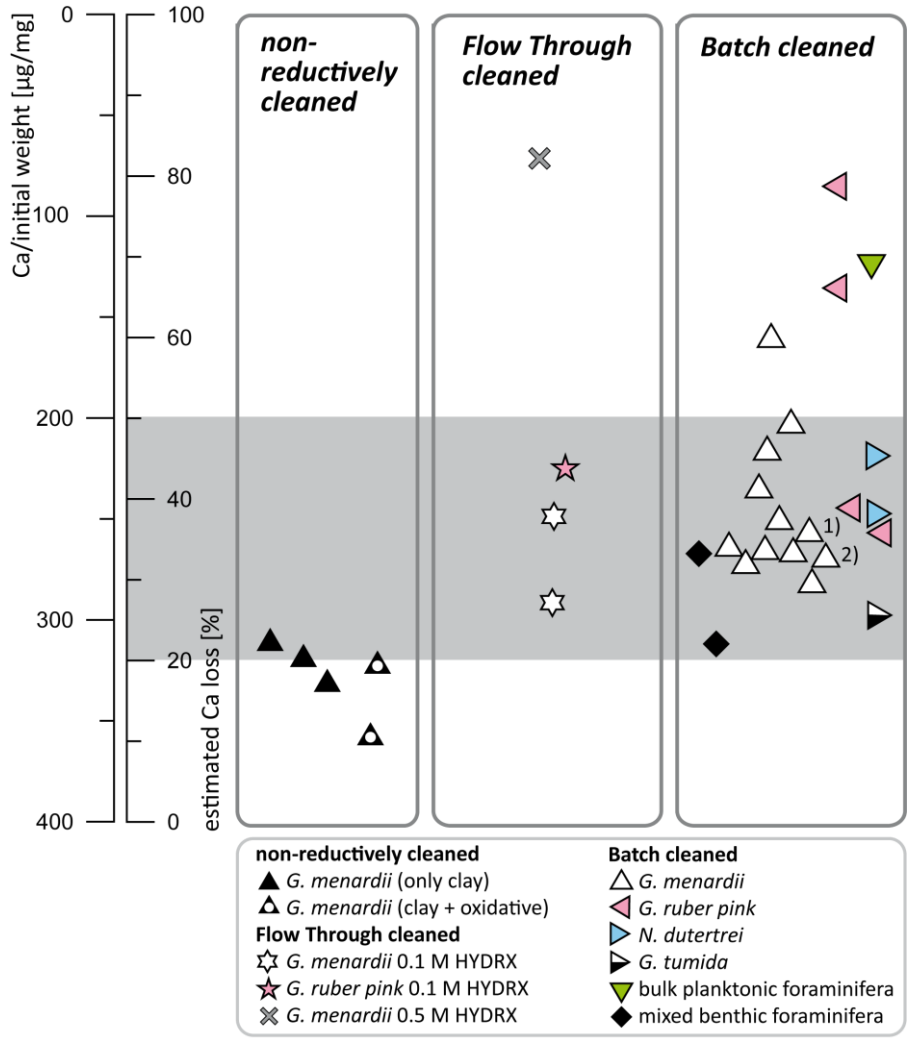

Figure 3.2: *Calcium concentration measured in the differently cleaned foraminiferal samples, related to initial weight of crushed un-cleaned foraminifera and the loss of Ca calculated assuming the sample to be 100% calcite.* [1)] *0.25 M and* [2)] *0.1 M hydroxylamine solution instead of hydrazine*

Element concentrations in the reductive reagent

The sequential release of Mn and Al was monitored during the FT cleaning procedure by continuously collecting the reductive hydroxylamine solution over the course of the cleaning (Figure 3.3, Appendix Figure A3.1b). Our analyses clearly show that Al is low in all samples and there is no clear trend with increasing leach time suggesting that detrital silicate and clay minerals have been successfully separated from the foraminiferal calcite and are not attacked

by the reductive reagent. The Mn concentrations decrease exponentially with reduction time, indicating continuous and efficient removal of Mn-oxide-phases (Figure 3.3). The samples from the São Tomé site show lower initial Mn concentrations than the sample from the Niger west site (Figure 3.3). Mn concentrations decrease to essentially the same values in the last cuts in all samples, demonstrating that the cleaning procedure using the 0.1 HYDRX solution is sufficient to remove Mn-rich contaminant phases from these core top samples.

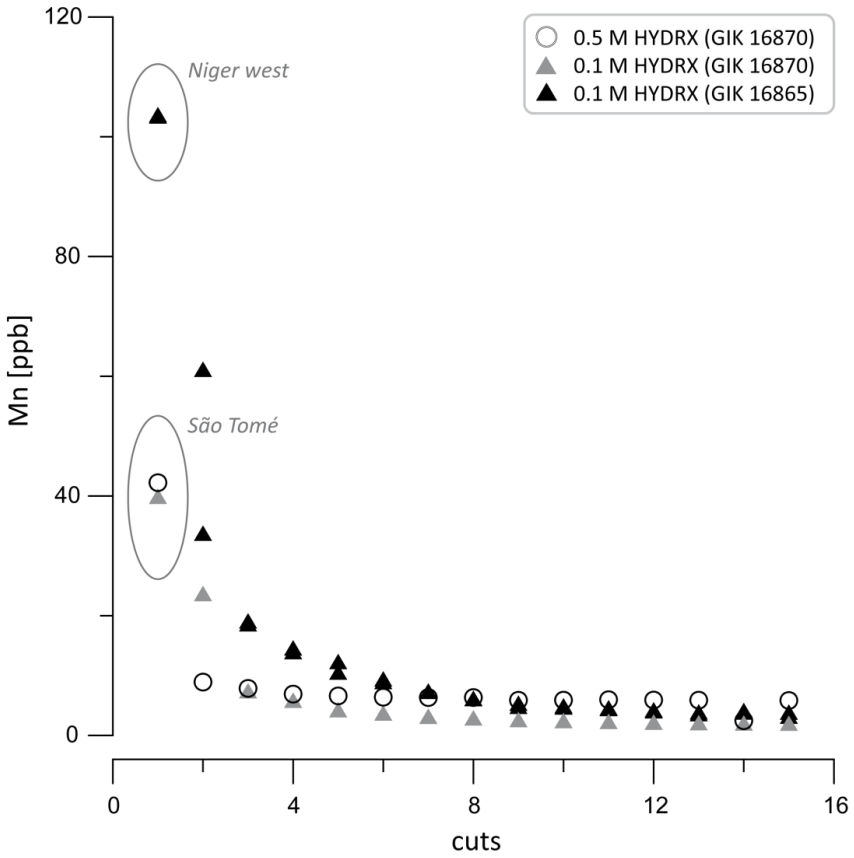

Figure 3.3: *Mn concentration in 1 ml of the reductive solution in the collected cuts (HYDRX = hydroxylamine) of the Flow Through (FT) cleaning, which included clay removal and oxidative cleaning*

Foraminiferal element to calcium ratios

Al/Ca, Mn/Ca and Fe/Ca ratios in dissolved cleaned foraminifera are used to assess the removal of silicate and ferromanganese phases. Following previous work (Ni et al., 2007), we consider that foraminiferal samples with Al/Ca ratios below 100 µmol/mol are not significantly affected by clay contamination. With the exception of three samples the Al/Ca values are all less than 80 µmol/mol, suggesting that Nd contributions from clay phases are

negligible. This is corroborated by the absence of a correlation between Al/Ca and Nd/Ca ratios (Figure 3.4).

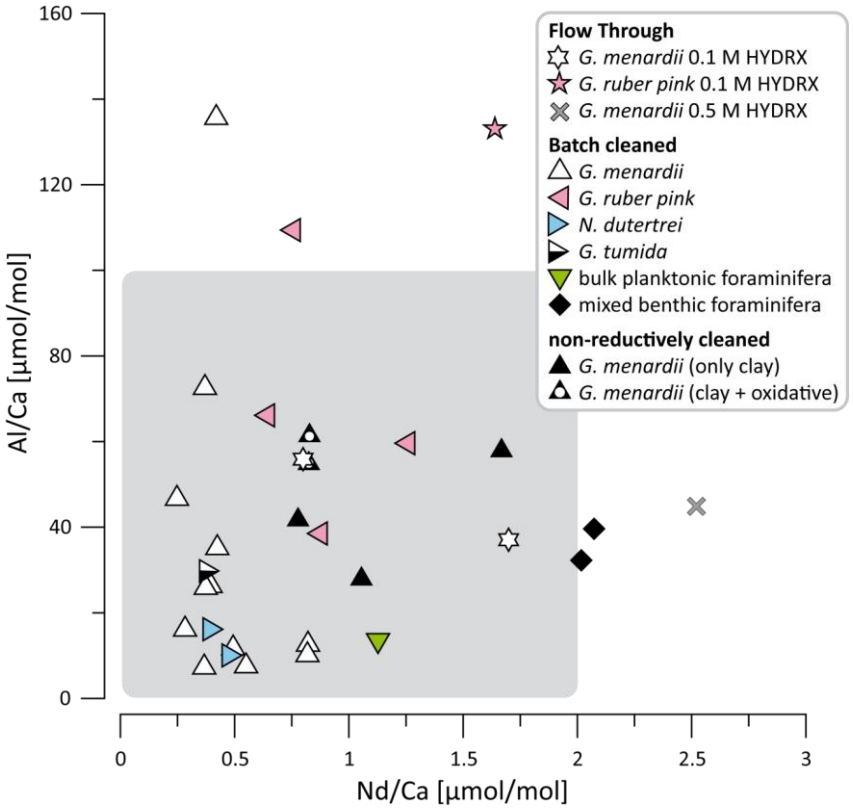

Figure 3.4: *Al/Ca ratios vs. Nd/Ca ratios of the foraminiferal carbonate samples. Samples without clay removal were excluded.*

Mn/Ca ratios were used as an indicator for early diagenetic ferromanganese oxides or Mn-rich carbonates, which can precipitate on the foraminiferal carbonate after deposition in the sediments (Boyle, 1983, Pena et al., 2005, 2008). Mn/Ca ratios below 100 µmol/mol have been interpreted to indicate negligible $MnCO_3$ contamination for Cd/Ca analyses (Boyle, 1983). With the exception of one sample with a Mn/Ca ratio of 167 µmol/mol, all foraminiferal core top samples of our study have Mn/Ca ratios below 51 µmol/mol regardless of the cleaning method applied (Figures 3.5). Reductively cleaned samples show Mn/Ca ratios less than 25 µmol/mol. Low values below 15 µmol/mol are found in planktonic foraminiferal calcite from plankton tows from the Atlantic (0.25 to 15 µmol/mol; Martínez-Botí et al., 2009), nets and sediment traps in the Indian Ocean (1 to 6 µmol/mol, outside the oxygen minimum zone; Pomiès et al., 2002). Similar values were reported by Vance et al. (2004) for cleaned core top foraminifera from the Pacific and the Indian Ocean. Applying those values, only 17 samples were fully cleaned from Mn-bearing contaminant phases

(Appendix Table A3.1). Thus, even if most of the correlations between Mn/Ca, Nd/Ca, and εNd are not significant (Figure 3.5), it cannot be concluded that the reductive cleaning step always removes all contaminating Mn-phases.

The core top samples are characterized by low Fe/Ca values (< 90 µmol/mol). However, given that the Fe/Ca ratios show a correlation with corresponding Nd/Ca ratios (Figure 3.6 A), residual Fe-phases may have contributed to some extent to the analyzed Nd concentrations and Nd isotope compositions. The absence of a correlation between Fe/Ca and εNd may result from the small amount of data available (Figure 3.6 B). Assuming a Nd concentration of 100 µg/g Nd in Fe oxyhydroxide (Bau and Koschinsky, 2006) less than 1% of the Nd could originate from the Fe phase remaining on the foraminifera samples. Thus, either there is much more than 100 µg/g Nd in such coatings or the correlation between Nd and Fe is coincidental. The weak correlation of Mn/Ca with Nd/Ca already implies incomplete cleaning from contaminant phases. However, the Fe/Ca ratios do not correlate with Mn/Ca ratios (Appendix Figure A3.2) and thus, specific contamination with Fe-oxides cannot be excluded.

Another indicator for the presence of early diagenetic ferromanganese oxides is the Mn/Fe ratio, which is very low (< 1 mol/mol) in the cleaned foraminiferal samples. This is inconsistent with the presence of ferromanganese coatings, for which Mn/Fe values considerably above 1 mol/mol are expected because manganese will be mobilized preferentially during diagenesis. Literature data show Mn/Fe values for ferromanganese nodules ranging from 2.0 mol/mol in the Cape basin to 3.7 and 11.6 mol/mol in the Angola Basin (Kasten et al., 1998). In the Brazil Basin the values for nodules vary between 1.05 (bottom) and 1.95 (top) (Dubinin and Rimskaya, 2011). However, incomplete cleaning could also result in low Mn/Fe ratios if the manganese phase will be removed faster than the iron phases. In a pioneering study, Chester and Hughes (1967) found that the hydroxylamine solutions preferentially dissolve manganese, whereas the diluted acid (e.g. acetic acid) will preferentially dissolve iron phases. Furthermore, these authors showed that in their study manganese was completely removed, whereas a small amount of iron remained. The remaining contaminant phases after incomplete cleaning will bias the Nd isotope signal towards bottom water signatures.

Literature data suggest that Nd/Ca ratios in pristine planktonic foraminifera from plankton tows, multinets and sediment traps (Vance and Burton, 1999; Pomiès et al., 2002; Vance et al., 2004; Martínez-Botí et al., 2009) vary between 0.009 and 0.85 µmol/mol. The Nd/Ca

ratio can be up to 1.4 µmol/mol in sedimentary foraminifera suggested to be clean based on Mn/Ca values of < 50 µmol/mol and Al/Ca ratios of < 100 µmol/mol (Vance et al., 2004; Ni et al., 2007). With the exception of two samples, all reductively cleaned planktonic foraminiferal samples show Nd/Ca values below 1.25 µmol/mol supporting efficient cleaning. Benthic foraminifera have higher Nd/Ca values compared to those of planktonic foraminifera, consistent with a previous study (Klevenz et al., 2008).

In summary, these assessments suggest that detrital silicates have been efficiently removed from the foraminiferal carbonates. The removal of the (ferro)manganese phases does not appear to be 100 % complete, as indicated by correlations between Mn/Ca, as well as, Fe/Ca ratios with Nd/Ca ratios and may thus affect the determination of reliable surface seawater Nd isotope signatures.

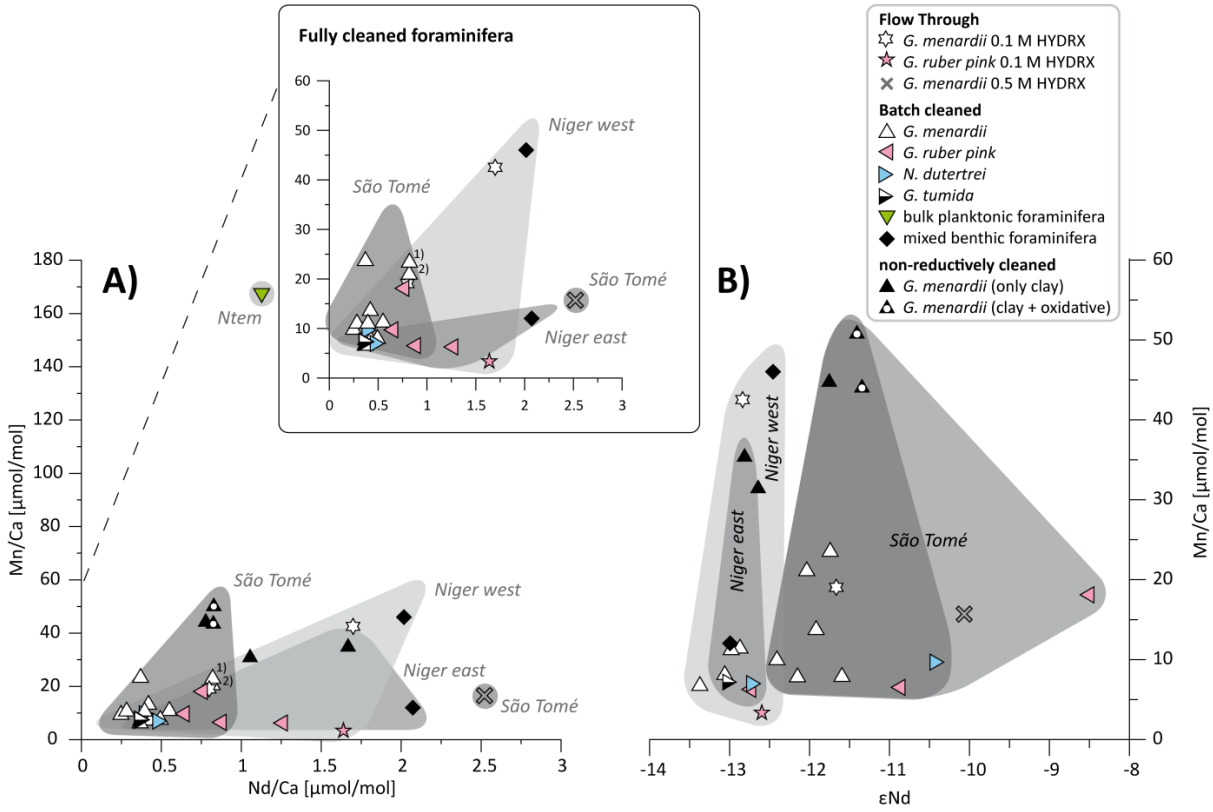

Figure 3.5: *Foraminiferal Mn/Ca ratios versus* ***A)*** *Nd/Ca ratios and* ***B)*** *εNd ratios,*

Most of the completely cleaned core top samples show Mn/Ca < 25 µmol/mol and Nd/Ca < 2 µmol/mol, whereas non-reductively cleaned samples are between 25 and about 50 µmol/mol. The Ntem sample exceeds this value, but this is not a core top sample and assumed to be contaminated by coatings. There are no significant correlations between Mn/Ca and Nd/Ca.

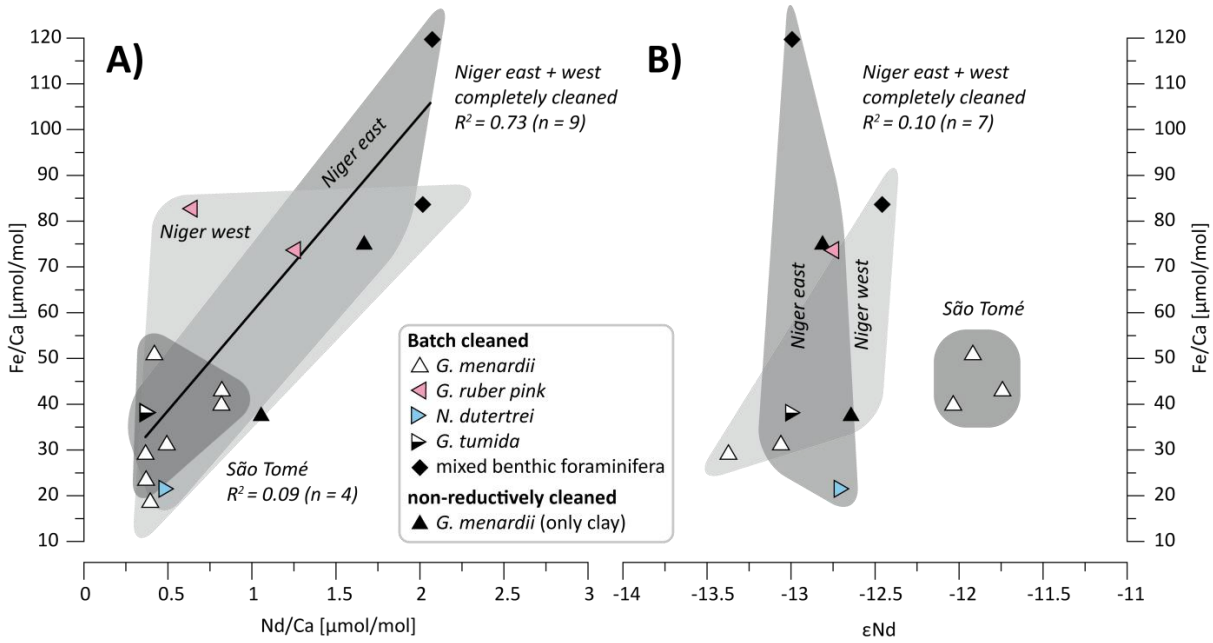

Figure 3.6: *Foraminiferal Fe/Ca versus* ***A)*** *Nd/Ca and* ***B)*** *εNd of batch cleaned samples. The black line is the regression trough values of fully cleaned samples (n = 9) of both Niger sites.*

REE patterns

The REE concentrations of the fully cleaned and non-reductively cleaned foraminifera (normalized to Post-Archean Average Australian Sedimentary rock, PAAS) exhibit similar patterns (Figure 3.7 A, Appendix Table A3.2) despite covering a large range of absolute concentrations. The patterns of all samples have a negative Ce anomaly similar to seawater (e.g. Piepgras and Jacobsen, 1992), but also a middle REE (MREE) enrichment ("MREE-bulge").

The middle bulge could result from three possible processes:

1) Riverine input changed the seawater composition

Modification of the present day seawater pattern by riverine discharge at these sites close to the Niger River mouth (distance approximately 200 km) is possible. MREE bulges similar to our foraminiferal data have been observed for the dissolved phase in various rivers and are thought to be related to phosphate weathering (e.g. Elderfield et al., 1990; Hannigan and Sholkovitz, 2001). Continentally influenced surface water REE patterns at a comparable distance from South Africa have also been observed (Bayon et al., 2004; Stichel et al., 2012). However, given that the present day seawater at the Niger site shows no MREE enrichment (Bayon et al., 2011) it is more likely that the MREE bulge does not result from riverine input to seawater.

2) *Foraminifera incorporated REEs with a MREE bulge*

Another possibility is that planktonic foraminifera fractionate REE during incorporation. MREE enrichment and negative Ce-anomalies were found for reductively cleaned foraminiferal samples cleaned with the flow through method to avoid re-adsorption (Haley and Klinkhammer, 2002). However, the planktonic foraminifera in a later study mostly had seawater like REE patterns, whereas samples from an anoxic setting had a MREE enrichment, but also a positive Ce-anomaly, and were interpreted as diagenetically overprinted (Haley et al., 2005). Our consistency standard (*Globogerina conglomerata*) taken from a large equatorial Pacific core top sample also shows a seawater like pattern without a MREE bulge (Figure 3.7 B) in contrast to the REE patterns of the Gulf of Guinea foraminiferal samples. Furthermore, the non-reductively cleaned and the cleaned foraminifera show exactly the same REE patterns. This suggests the MREE enrichment is unlikely to be a primary signal but probably has a diagenetic origin, indicating that the foraminiferal Nd isotope data of our study reflect bottom or pore waters.

3) Diagenetic origin from pore waters and/or associated phases

Our foraminiferal REE patterns resemble the easily exchangeable REE and carbonate phase of multi-phase leaching studies from ferromanganese oxides given that the Mn and Fe oxide-phases show clear positive Ce-anomalies (Bau and Koschinsky, 2009; Surya Prakash et al., 2012). Also fish teeth that obtain their REE during early diagenesis show REE patterns similar to our foraminiferal samples having a negative Ce-anomaly and a MREE bulge (Martin et al., 2010). Palmer (1985) found a MREE enrichment and a negative Ce-anomaly in the coating phase of the foraminifera, but no MREE bulge in the foraminiferal calcite. Similar patterns were found in non-reductively cleaned foraminifera (Palmer and Elderfield, 1986). The MREE enrichment may originate from pore waters, which under anoxic conditions and the presence of dissolved Fe display a pronounced MREE bulge and a negative Ce-anomaly (Haley et al., 2004).

Considering the information in the literature and the fact that fully cleaned and non-reductively cleaned foraminifera show the same REE pattern (Figure 3.7 A) we argue that the majority of the REE in the cleaned foraminiferal samples in this study are from ferromanganese phases. The fact that fully cleaned and non-reductively cleaned foraminifera are comparable to HH extractions in the MREE/MREE* against HREE/LREE plot (Figure 3.7 C) suggests incomplete cleaning. This is supported by the observation of similar patterns in leachates from a Fe-Mn-standard (Basak et al., 2011). Furthermore, a negative Ce-anomaly has also been observed for some Fe-oxides (Koeppenkastrop and DeCarlo, 1992; Ohta and Kawabe, 2001). Another indicator for remaining Fe-oxides is the correlation between the MREE/MREE* ratios and the Fe/Ca ratios in our foraminiferal samples. In summary, the evidence suggests foraminifera cannot deliver reliable surface seawater signatures, but can be used as reliable archive for bottom water, comparable to fish teeth but more abundant.

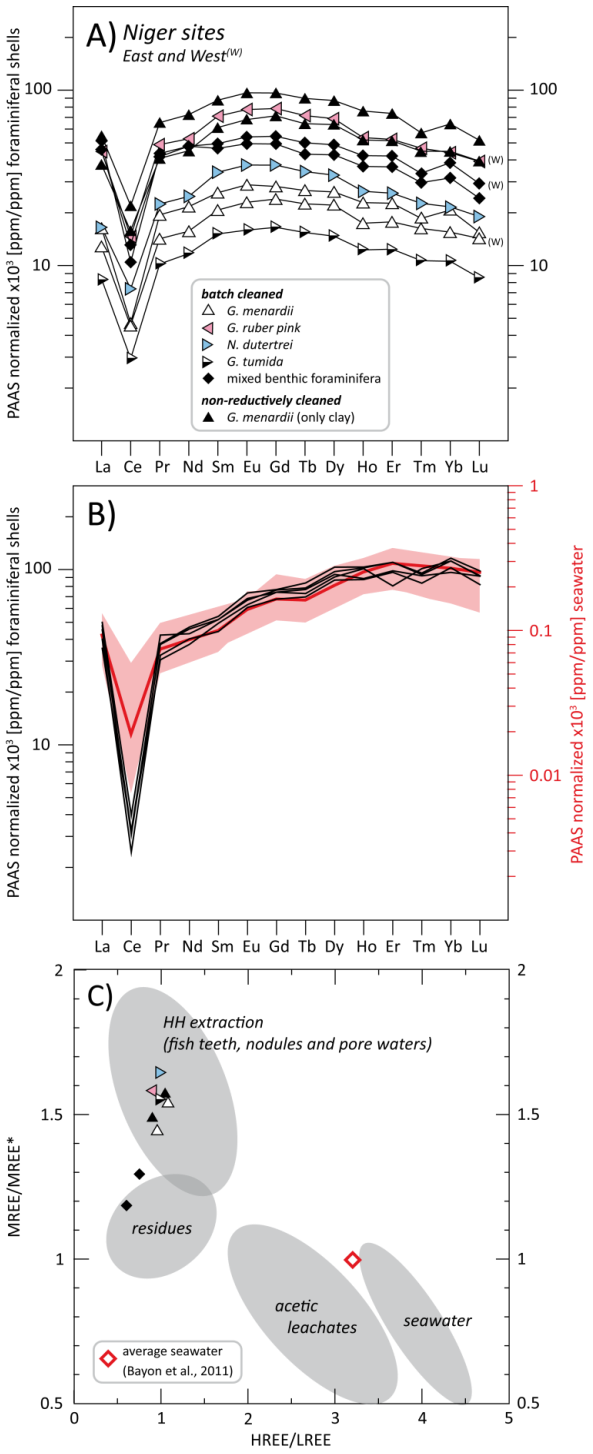

Figure 3.7: A) *REE concentrations normalized to Post-Archean Average Australian Sedimentary rock (PAAS values taken from Nance and Taylor, 1976) from the Niger east and west stations (marked with (W));* ***B)*** *black lines = PAAS normalized REE concentrations of our consistency standard: 5 splits of one large sample consisting of G. conglomerata (equatorial Pacific core top) separately cleaned and processed. Red line = average seawater REE close to Niger site east (Bayon et al., 2011), pink shaded area = range of REE in the water profile (Bayon et al., 2011);* ***C)*** *MREE/MREE*=(Gd+Tb+Dy)/((LREE+HREE)/2) versus HREE/LREE = (Tm+Yb+Lu)/(La+Pr+Nd) plot: shaded gray areas from Martin et al. (2010) and references therein. Symbols are the same as for plot A.*

3.4.2 Neodymium isotope signatures

Nd isotope analyses of splits of the same foraminiferal samples cleaned using the FT and batch methods are identical within error indicating that the efficiency of both cleaning methods in removing contaminant phases is the same (Figure 3.8). This suggests the effects of re-absorption are minimal using the batch method. However, both methods probably do not provide 100% pristine foraminiferal calcite, as indicated by the REE patterns.

Niger sites

Average εNd values (-12.9 ± 0.2 SD, n=13) obtained from all foraminiferal samples (non-reductively cleaned and fully cleaned planktonic and benthic samples) collected at both ***Niger sites*** (GIK 16865, GeoB 4902 and 4901; Figure 3.1) are identical within error to the εNd signature of both Tropical Atlantic Surface Waters (TSW) in the eastern equatorial Atlantic basin (Figure 3.9) (Rickli et al., 2010; Bayon et al., 2011) and North Atlantic Deep Water (NADW) (Figure 3.9, Bayon et al., 2011). However, the water profile published by Bayon et al. (2011) (Figure 3.1) shows similar εNd values (-12.5) for the TSW as well as for the intermediate and deep waters (AAIW and NADW) (Figure 3.9). The recent study of Pena et al. (2013) from an eastern equatorial Pacific site suggests that their cleaned planktonic foraminifera (*N. dutertrei*) reflect subsurface water Nd isotope signatures because of the low Nd concentrations and seawater-like REE patterns. However, the subsurface and deep water Nd isotope signatures measured in the water column at their site also do not differ (Grasse et al., 2012) and thus the cleaned foraminiferal signatures cannot be unambiguous assigned to surface or deep water. The non-reductively cleaned planktonic and the fully cleaned benthic foraminifera reflect the deep water signature (Figure 3.9), as described in previous studies (e.g. Klevenz et al., 2008; Roberts et al., 2010). The εNd values of fully cleaned planktonic foraminiferal species agree well with those obtained in near surface water samples as well as with the deep water samples (Bayon et al., 2011). The body of evidence from this and other recent studies suggests that planktonic foraminifera do not provide a surface water signal (e.g. Roberts et al., 2010, 2012). At our study site the REE patterns in particular strongly suggest that planktonic foraminifera represent bottom water signatures rather than surface seawater. Even after reductive cleaning the Nd isotope signatures of the planktonic foraminifera in our study are suggested to mirror bottom waters, although TSW and NADW have the same εNd signature. In contrast, the Fe-Mn leachates of the bulk sediments clearly

do not represent bottom water signatures and are overprinted by continental εNd signatures in this setting. Nd isotope signatures of marine sediment leachates are generally interpreted to reflect the bottom water composition in the open ocean (e.g. Gutjahr et al., 2007; 2008). The recent study of Charbonnier et al. (2012) based on Cretaceous shallow marine sediment samples (Wissant outcrop in France and Hot Springs outcrop in the USA), suggested that the εNd signatures of Fe-Mn leachates from de-carbonated sediments may have been altered by pre-formed continental oxides and challenges the suitability of sediment leachates for seawater reconstruction in shelf areas. The εNd values of the sediment leachates from the ***Niger west site*** (GIK 16865 and GeoB 4902) differ by more than 2 epsilon units from the benthic foraminiferal values, but are very similar to the εNd values of suspended material from the Niger River (-10.53, Goldstein et al., 1984). Thus, the sediment leachates may reflect the riverine input of particles, which were coated within the river water or in the estuaries and were subsequently transported to the core site. At the ***Niger east site*** (GeoB 4901) the εNd values of sediment leachates and the detrital sediment differ from that of foraminifera by more than one εNd unit. This suggests less riverine influence as a consequence of reduced supply of detrital material compared to the Niger west site (Figures 3.8 and 3.9).

São Tomé site

The averages of the non-reductively (-11.4, n = 4) and fully cleaned (-11.7, n = 8) *G. menardii* samples from the ***São Tomé site*** are about 1 εNd unit more radiogenic than the εNd signature of NADW at neighboring locations (Rickli et al., 2010; Bayon et al., 2011; Figure 3.8). The site is located in the vicinity of the volcanic São Tomé island, the rocks of which (phonolithes, basanites, trachytes, basalts) have highly radiogenic εNd signatures between +3.9 and +6.3 (Halliday et al., 1988). This small offset of the foraminiferal signatures towards more radiogenic values either resulted from the interaction of the waters with Sao Tome via boundary exchange or a small contamination by detrital material from São Tomé. Contamination by clays of the cleaned foraminiferal samples is unlikely because the average Al/Ca ratios are similar to those of the other investigated sites (Appendix Table A3.1). Lacan and Jeandel (2005) and Rickli et al. (2010) demonstrated that boundary exchange and weathering inputs from volcanic islands can strongly influence the Nd isotopic composition of the surrounding seawater. A small contribution of Nd from boundary exchange with the volcanic material (εNd of +3.9) would shift the foraminiferal εNd signatures of both the

seawater and the Fe-Mn coatings formed in bottom or pore waters to slightly more radiogenic Nd isotope compositions.

At the São Tomé site the fully cleaned *N. dutertrei* and *G. ruber* pink samples show considerably more radiogenic values (Figure 3.8). Although the Al/Ca ratios suggest there is no contamination by clays, incomplete cleaning related to the higher porosity of their shell structures compared to *G. menardii* could have caused this small offset. Despite these slight differences the planktonic foraminiferal signatures suggest a bottom water origin.

Ntem site

The ***Ntem sites*** (MD03-2707 and GeoB 4905) are located proximal to the Sanaga/Nyong and Ntem river mouths. The sediments of Sanaga/Nyong and Ntem rivers have εNd values of -12.4 ± 0.4 and -28.1 ± 2.6, respectively (Weldeab et al., 2011). The εNd value obtained from a mixed planktonic foraminiferal sample is significantly less radiogenic (-15.8) than those of the TSW (-12.5) (Figure 3.8). It is possible that this foraminiferal εNd signal from a core depth of 28 cm either reflects the influence of Ntem riverine input or was biased by REE remobilization as a consequence of different redox conditions within the pore waters (Haley et al., 2004). This is supported by an elevated Mn/Ca ratio compared to the core top samples of the other investigated sample sites. The pore water profile of site GeoB 4905 shows a strong increase in iron (Fe^{2+}) concentrations between 9 cm and 18 cm (Sabine Kasten, unpublished data). As many studies of pore water profiles have shown, the dissolved Mn^{2+} concentration will increase at a shallower depth than Fe^{2+} concentration due to the succession of reductive processes (Froelich et al., 1979). This suggests that manganese carbonates may form in these shallow sediment depths < 9 cm, potentially fixing the εNd signatures onto the foraminifera (Roberts et al., 2012). Therefore, down core smearing of the foraminiferal εNd signal is expected to occur over a length scale of < 9 cm at this location. This result is similar to the findings of Roberts et al. (2012) who suggest the signal smoothing, with a length scale of 4 to 16 cm, is of the same order as bioturbation.

The detrital sediment fraction of the Ntem site clearly represents a mixture of sedimentary supply from the Sanaga/Nyong and Ntem rivers (shown by detrital sediment εNd values of Weldeab et al., 2011). The effect on the contaminated foraminiferal sample and the sediment leachate is similar, if both are coated within the pore or bottom waters. The sediment leachate in contrast is more river dominated with coatings pre-formed in the rivers. Bayon et al. (2004) demonstrated the strong influence of pre-formed coatings associated with riverine

material from the Congo River in the Angola basin. The Fe-Mn leachates of the Ntem site (-15.2) and the detrital fraction (-15.8) are much less radiogenic than the expected bottom water (between -12.5 and -13.3; Bayon et al., 2011). Thus, either the bottom water itself has been altered through boundary exchange processes (and thus represents a mixture of NADW and the riverine signature stored in the sediment) or the leachates are contaminated within the pore waters where pre-formed coatings originating from the rivers have been dissolved.

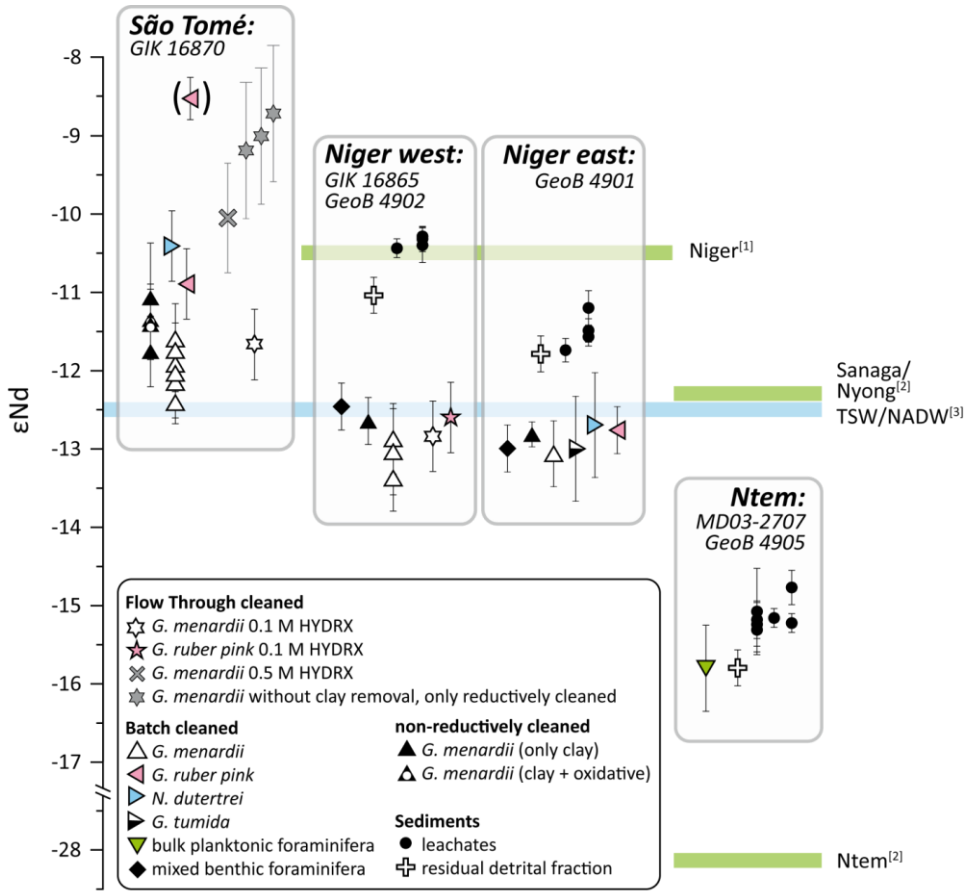

Figure 3.8: *εNd signatures of foraminifera and sediment samples*

Only few samples show elevated Al/Ca (> 100 µmol/mol) and/or Mn/Ca (> 15 µmol/mol). Those sample generally do not differ in εNd values from average clean samples (detailed in Appendix Table A3.1), except of the samples which were not cleaned for clays (gray stars) and the most radiogenic G. ruber pink sample at the São Tomé site (in parenthesis, Al/Ca ratio > 100 µmol/mol).The different used reductive cleaning solution are detailed in Appendix Table A3.1, which is also not influencing the εNd signature, except of the samples which was treated with 0.5 M hydroxylamine (gray cross) following the procedure in Table 3.2.

[1]Niger sediment (Goldstein et al., 1984), [2]Sanaga/Nyong sediment (Weldeab et al., 2011), [3]TSW = Tropical Surface Water (Rickli et al., 2010; Bayon et al., 2011), [3]NADW = North Atlantic Deep Water (Bayon et al., 2011)

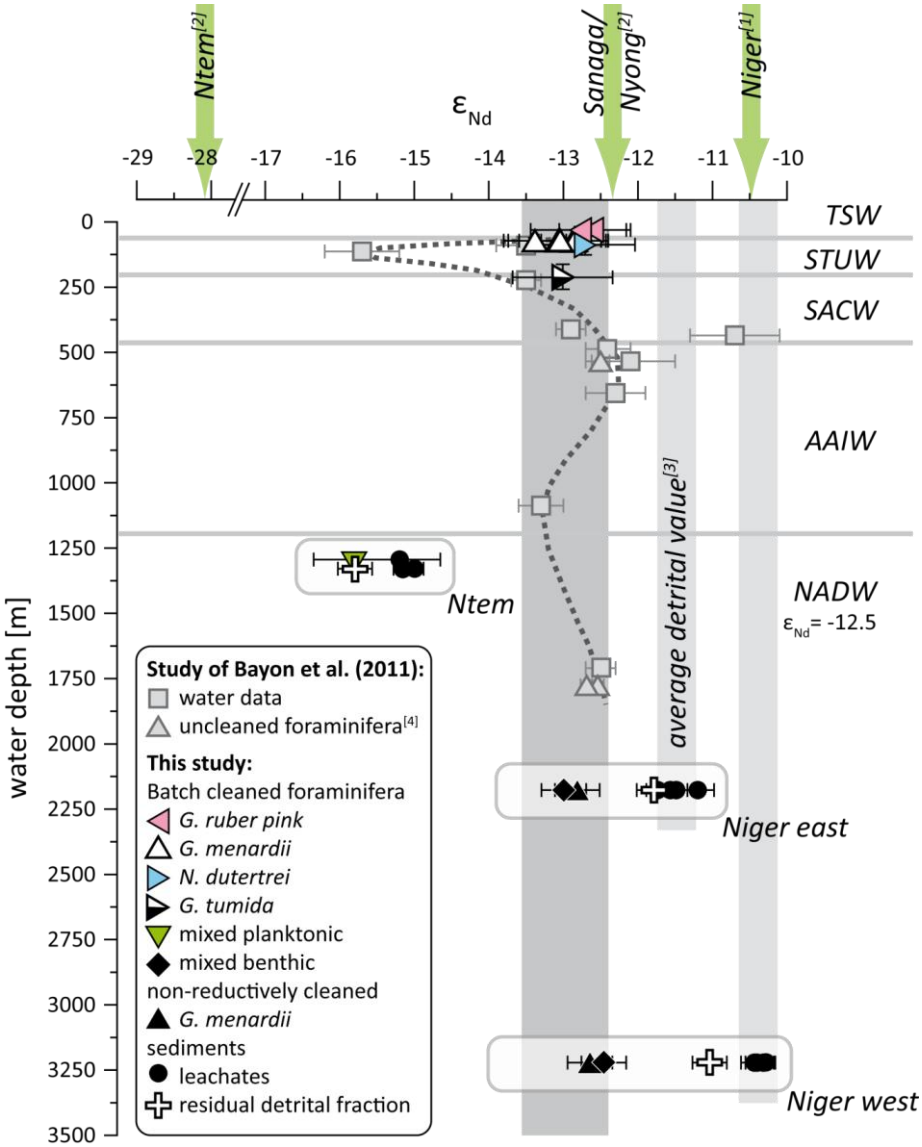

Figure 3.9: *Comparison of water column εNd profiles in the Gulf of Guinea close to Niger sites (Bayon et al., 2011) and uncleaned foraminifera (gray symbols) plotted at the respective core top water depth[4] with foraminiferal and sediment data of this study (black symbols). Fully cleaned foraminifera (with Al/Ca < 100 µmol/mol and Mn/Ca < 15 µmol/mol) are plotted at their estimated calcification depth range, which is mostly smaller than the symbol size (based on Steph et al., 2009). The dark grey bar marks the foraminiferal εNd values, and the light grey bars mark the sediment leachates of both Niger sites consistent with the average values of Bayon et al. (2011)[3].*

The green arrows at the top represent the riverine signatures taken from [1]suspended particles from Goldstein et al. (1984), [2]riverine sediments from Weldeab et al. (2011).

TSW = Tropical Surface Water (eNd = -12,5, 57 m), STUW = Subtropical Underwater (eNd = -15.7, 60 - 180 m) advected by EUC (Equatorial Undercurrent) and NSEC (Northern South Equatorial Current), AAIW = Antarctic Intermediate Water (eNd -12.5 to -13.3, 460 - 500 m, 990 - 1190 m, respectively) transported by NICC (Northern Intermediate Countercurrent), SACW = South Atlantic Central Water, NADW = North Atlantic Deep Water (eNd = -12.)

3.5 Conclusions

Comparison of the elemental (Al/Ca, Mn/Ca, Fe/Ca) and Nd isotope ratios analyzed in foraminiferal core top samples from the Gulf of Guinea that were cleaned applying the Flow Through (FT) and batch (BC) methods show identical levels of cleaning efficiency. Comparison of Nd isotope compositions obtained by both methods suggests the effect of re-adsorption to be minimal during the batch cleaning procedure. Therefore, the well established batch method is preferred to the FT cleaning. Nevertheless, we recommend further tests with various reductive solutions, as well as tests at other sites with variable sedimentary environments, where the water masses and the continental rocks differ more significantly in their Nd isotopic signatures.

The foraminiferal Nd isotope composition provides a useful tool to reconstruct bottom seawater or pore water since the samples could not be completely cleaned of (ferro)manganese contaminant phases. Element to calcium ratios and REE patterns suggest that the planktonic foraminifera acquired REEs during early diagenetic processes. The foraminiferal εNd signatures accordingly represent bottom water masses at the Niger sites.

In contrast, the applicability of Nd isotope signatures in bulk sediment leachates to reconstruct bottom water compositions in the study area is complicated by contributions from pre-formed coatings, most likely originating from the rivers. Our study demonstrates that the bulk leaching method cannot be reliably used for reconstructions of water mass Nd isotope compositions in a setting which is strong influenced by rivers such as the Gulf of Guinea but may, in combination with the signature of the detrital fraction, rather serve to reconstruct changes in the inputs from the nearby rivers.

Acknowledgements

We would like to thank Wolfgang Kuhnt from the Institute of Geoscience of the University of Kiel for providing GIK core top samples. The GeoB samples were kindly provided by the University of Bremen, Geosciences Department and MARUM. Thanks also to A. Eisenhauer for access to the ICP-MS and A. Kolevica for assistance with the measurements. We also thank Germain Bayon, Andrew Bowie (AE) and three anonymous reviewers for their constructive comments that significantly improved the manuscript. This project was funded by the Deutsche Forschungsgemeinschaft (Project No WE2686/5-1).

Chapter 4

Migration of the West African Monsoon over the past 135,000 years: Evidence from sedimentary Nd isotope composition in the Gulf of Guinea

Abstract

The West African Monsoon system has been closely linked to the location and the movement of the ITCZ and the related rain belt. The latitudinal migration of the rain belt across the catchment areas of the major rivers has caused changes of their discharge into the Gulf of Guinea in the easternmost equatorial Atlantic. To investigate the evolution of riverine inputs of two large river systems, Sanaga/Nyong and Ntem during the past 135,000 years, different sedimentary phases of core MD03-2707 were analyzed for their neodymium isotope composition (εNd), as well as for element to calcium (E/Ca) ratios and Rare Earth Element (REE) concentrations. The elemental data indicate that the signatures extracted from cleaned foraminiferal carbonates have been biased by riverine influence and/or changes in bottom water/pore water redox conditions. The εNd record of the detrital fraction indicating changes in riverine influx ranges between values of -23 and -15. The εNd signatures of the sediment coatings, as well as of planktonic and benthic foraminiferal shells reflect past bottom water signatures and show similar trends but a narrower range between -18 and -15. For all phases the glacial εNd signatures were markedly less radiogenic than the interglacial ones, which is interpreted as a consequence of the glacial southward migration of the ITCZ resulting in enhanced runoff of the more southerly located rivers draining Precambrian basement with characteristic unradiogenic εNd signatures during sea level low stands. The detrital εNd record directly reflects the local riverine inputs while the sediment leachates and foraminiferal εNd signal recorded regionally integrated changes of continental inputs, as well as exchange processes between the bottom water and the shelf and/or continental material.

A version of this chapter is going to be submitted as:

***Kraft, S.**, Frank, M., Weldeab S., Hathorne, E., Migration of the West African Monsoon over the past 135,000 years: Evidence from sedimentary Nd isotope composition in the Gulf of Guinea*

4.1 Introduction

The West African Monsoon (WAM) system has been an important component of the global climate system through its impact on the moisture and heat budget, which in turn strongly impacts regional agriculture and economy. Modeling studies (e.g. Broccoli et al., 2006) suggest a linkage between climate oscillations in the high latitudes and changes in atmospheric heat exchange, as well as displacements of the ITCZ on decadal to glacial-interglacial time scales. Close relationships between changes of the global thermohaline circulation and of the West African monsoon system have also been identified (e.g. Chang et al., 2008). The ITCZ has moved across the equator seasonally, as well as on longer time scales (reconstructed positions depicted in Figure 4.1 A: Leroux et al., 1993; Gasse et al., 2000; Talbot et al., 2007; Nicholson et al., 2009; Kim et al., 2010). The position of the African rain belt as well as the associated convergence of trade wind at the ITCZ oscillates seasonally between 17°N and 21°S and controls the distribution of rainfall over tropical Africa (Nicholson, 2000; Nicholson and Grist, 2003). Recent studies have shown variations in rainfall linked to large-scale processes such as atmospheric and ocean circulation in the tropical eastern Atlantic on seasonal and intra-seasonal time scales (Gu and Adler, 2004; Maloney and Shaman, 2008). Consequently, the riverine inputs have varied with the migration of the rain belt and with the intensity of the WAM on longer time scales resulting in changes in salinity and trace element composition of the surface waters, as well as in composition of the terrigenous sediments in the eastern equatorial Atlantic and the Gulf of Guinea (e.g. Schneider et al., 1997; Zabel et al., 2001; Adegbie et al., 2003; Lezine et al., 2005; Weldeab et al., 2005, 2007a, 2007b; Weldeab, 2012a, 2012b).

Radiogenic Nd isotope compositions have been widely used to trace water masses and their mixing in the present and past ocean (e.g. Piepgras and Wasserburg, 1980, 1982; Goldstein et al., 1984; Goldstein and Jacobsen 1987; Tachikawa et al., 1999; Rickli et al., 2009; Bayon et al., 2011). The Nd isotope composition of seawater is influenced by partial dissolution of aeolian and riverine inputs from the continents (e.g. Frank, 2002) and exchange of the continental margins and islands with the ambient deep waters (e.g. Lacan and Jeandel, 2005). The Nd isotope composition of the sediments deposited on continental margins generally reflects those of the continental rocks in the hinterland (e.g. Goldstein et al., 1984; Jeandel et al., 2007) and is determined by the types and ages of the rocks.

For reconstructions of past Nd isotope compositions bulk sediment leachates generally represent bottom water signatures (e.g. Gutjahr et al., 2007, 2008; Pahnke et al., 2008; Stumpf et al., 2010; Piotrowski et al., 2005, 2012) but problems arises from partial dissolution of labile phases such as basaltic glasses have been observed for particular areas, such as in the North Atlantic (e.g. Roberts et al., 2010; Elmore et al., 2011). Furthermore, in shelf areas pre-formed continental oxides may complicate the seawater reconstruction using Nd isotopic compositions of Fe-Mn leachates from de-carbonates sediments as suggested by the recent study of Charbonnier et al. (2012) based on Cretaceous shallow marine sediment samples (Wissant outcrop in France and Hot Springs outcrop in the USA). Close to the Niger River mouth previous studies have also suggested a contribution of the Niger River to the leached bulk sediment signals originating from Nd in pre-formed riverine ferromanganese coatings (Bayon et al., 2011; Kraft et al., 2013). In contrast, several studies have shown that Nd isotope compositions of planktonic and benthic foraminifera with or without (ferro)manganese coatings closely match bottom water Nd isotope signatures (e.g. Klevenz et al., 2008; Roberts et al., 2010; Elmore et al., 2011; Roberts et al., 2012; Piotrowski et al., 2012; Charbonnier et al., 2012).

The evolution and variation of the WAM system and their linkage to northern hemispheric climate oscillations in the past have been studied previously based on sediments from the Gulf of Guinea (core MD03-2707, Figure 4.1) (Weldeab et al., 2007a, 2007b; 2011; Weldeab, 2012a). This core is located close to the West African coast between the Sanaga River mouth (~118 km) and the Ntem River mouth (~50 km; Figure 4.1). The catchment areas of these river systems are dominated by different lithologies (Toteu et al., 2001), resulting in markedly different neodymium isotope compositions (εNd Sanaga/Nyong = -12; Ntem = -28; Weldeab et al., 2011). Weldeab et al. (2011) analyzed the εNd signatures of the detrital sediment fractions of core MD03-2707 for the last deglaciation to determine changes in the riverine influence related to the migration of the ITCZ and the associated rain belt.

In this study we present new Nd isotope data of seawater-derived authigenic phases including foraminiferal carbonates from core MD03-2707 for the last 135,000 years. The detrital εNd record of Weldeab et al. (2011) is extended to cover the same period of time. Element to calcium ratios and rare earth element (REE) concentration patterns obtained from the foraminiferal samples provide additional information on the completeness of the cleaning procedures applied to the foraminiferal shells to remove (ferro)manganese oxide or secondary carbonate coatings and thus on the reliability of the extraction of past seawater signatures.

The new data allow a detailed reconstruction of the consequences of the migration of the WAM reflected by local detrital riverine inputs.

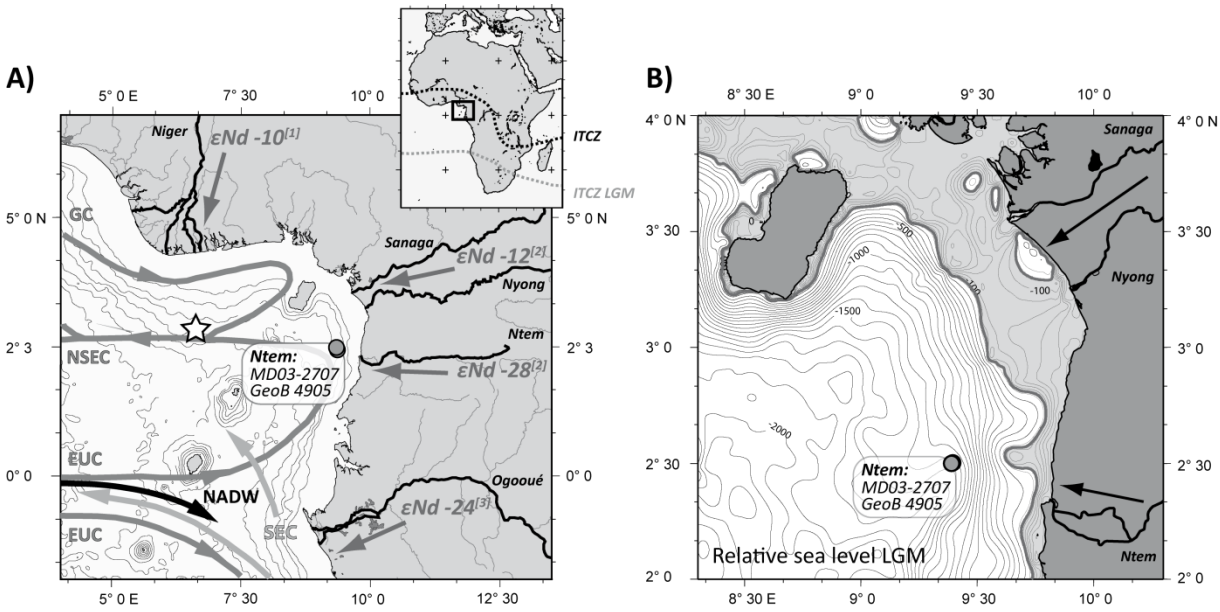

Figure 4.1: A) *Core location MD03-2707 and close by core top sample site GeoB 4905 (circle); Star = core top study site of Kraft et al. (2013) and location of water column data of Bayon et al. (2011); εNd signatures of the different river systems: [1]Goldstein et al., 1984, [2]Weldeab et al., 2011, [3]Bayon et al., 2011; ITCZ location in the upper small figure after Nicholson et al. (2009), Gasse et al. (2000), Leroux et al. (1993), Talbot et al. (2007) and Kim et al. (2010); GC = Guinea Current, NSEC = Northern South Equatorial Current, EUC = Equatorial Undercurrent, SEC = South Equatorial Current, NADW = North Atlantic Deep Water;* ***B)*** *Enlargement of Figure A including the coast line during the Last Glacial Maximum assuming -130 m lower sea level with the exposed shelf area in light grey shading (Giresse et al., 1995; Waelbroeck et al., 2002). Bathymetric contours are given every 20 m between 0 and -140 m water depth and every 100 m below.*

4.2 Material and Methods

Analyses were performed on sediment of core MD03-2707 (1294 m water depth, 2°30'07 N, 9°23'41 E). Additionally, we analyzed core top sediments (3.5 and 4.5 cm core depth) of nearby site GeoB 4905-2, given that core top samples were not available for core MD03-2707.

On average 2.5 g of dried bulk sediment were leached (after carbonate removal) for the extraction of the bottom water Nd isotope signature from oxyhydroxide fraction following the procedure of Gutjahr et al. (2007) detailed in Chapter 2. For the determination of the detrital Nd isotope composition 100 mg of < 63 µm fraction of bulk sediments were first leached

with the same leaching solution as above (Weldeab et al., 2011). Samples of the residual detrital fraction were leached again with the leach solution (1:1 dilution) and were then total dissolved in several steps using aqua regia and hydrofluoric acid (Chapter 2).

In addition to the bulk sediment leaching method to extract bottom water Nd isotope compositions, between 9 and 35 mg of foraminiferal shells > 150 µm (25 mono-specific and 12 mixed planktonic and 32 mixed benthic samples; Appendix Table A4.1) were handpicked under a binocular microscope and gently cracked between glass plates. The foraminiferal samples were cleaned in several steps including oxidative and reductive cleaning following the batch cleaning method developed by Boyle (1981) and scaled up for larger samples by Vance and Burton (1999) and Vance et al. (2004), as described in detail in Kraft et al. (2013). After cleaning, the samples were dissolved in weak HNO_3 by stepwise addition (50 to 100 µl) of 0.5 M HNO_3 to samples in 0.6 ml n-pure water and were then centrifuged. Aliquots were separated for elemental and isotopic analyses (Chapter 2).

The element (e.g. Al, Mn, Fe, and Nd) to calcium ratios of the foraminiferal samples were measured with an Agilent 7500-CX inductively coupled plasma mass-spectrometer (ICP-MS) to identify contaminant phases. The 2σ uncertainties of repeated measurements (n = 3) of four samples were 1-4 % for Al/Ca, 1-3 % for Mn/Ca, 2-11 % for Nd/Ca and 1-2 % for Fe/Ca. To complement the elemental data sets the concentrations of all rare earth elements (REE) were analyzed by ICP-MS with an ESI SeaFAST system and an online-preconcentration method (Hathorne et al., 2012). Repeated measurements (n = 3) of one sample gave an average estimated uncertainty of 3 % (2σ), which is similar to the precision provided in Hathorne et al. (2012).

The $^{143}Nd/^{144}Nd$ ratios of the sediment leachates for the section representing the period between 10 and 20 kyrs had been measured with a TRITON 1 thermal ionization mass spectrometer (TIMS) at an external reproducibility of ±0.22 (2σ) (Weldeab et al., 2011). All other samples, sediment leachates, detrital sediments and the foraminiferal samples were determined using a Nu instruments Multi-collector ICP-MS. The measured $^{143}Nd/^{144}Nd$ ratios were corrected for instrumental mass bias using $^{146}Nd/^{144}Nd = 0.7219$ applying an exponential mass fractionation law. The $^{143}Nd/^{144}Nd$ ratios were normalized to the accepted value of 0.512115 of the JNdi-1 standard (Tanaka et al., 2000) and are expressed in the εNd-notation normalized to the value of the Chondritic Uniform Reservoir (CHUR) = 0.512638 (Jacobsen and Wasserburg, 1980): $\varepsilon Nd=[(^{143}Nd/^{144}Nd)_{sample}/(^{143}Nd/^{144}Nd)_{CHUR}-1]*10{,}000$.

The external reproducibility (2σ) was ±0.6 εNd units for low concentration samples and ±0.3 εNd units for the bulk sediment leachates, in both cases assessed by repeated measurements of the JNdi-1 standard at concentrations comparable to those of the corresponding samples. The external reproducibility (2σ) of the foraminiferal analyses was estimated to be ±0.4 εNd units by repeated processing and measurement (n = 5) of one large foraminiferal sample.

4.3 Results

4.3.1 Foraminiferal element/calcium ratios and REE concentrations

The fully cleaned foraminiferal samples (n = 66) exhibit Al/Ca ratios between 2 and 95 µmol/mol (with the exception of 3 samples with higher ratios), an average Mn/Ca ratio of 166 ± 66 µmol/mol (SD), Fe/Ca ratios between 47 and 447 µmol/mol (with one exception being higher) and an average Nd/Ca ratio of 1.21 ± 0.69 µmol/mol (SD, n = 34) (Appendix Table A4.1). The average Nd/Ca value of the benthic foraminiferal samples is slightly higher (1.67 ± 0.82 µmol/mol, SD) but consistent with a previous study (Klevenz et al., 2008). The average value of Mn/Fe ratios of all analyzed foraminiferal samples is 1.05 ± 0.63 mol/mol (SD, n = 61). Even the three non-oxidatively-reductively cleaned planktonic foraminiferal samples do not exceed a value of 1.31 mol/mol, while they show much higher element to calcium ratios (Mn/Ca 448 to 550 µmol/mol, Fe/Ca 390 to 1055 µmol/mol, Nd/Ca 7 µmol/mol), which documents that the reductive and the oxidative cleaning steps need to be included for successful cleaning (Kraft et al., 2013).

The rare earth element (REE) concentrations of 57 fully cleaned foraminiferal samples (32 benthic and 25 planktonic) were determined. The results were normalized to Post-Archean Sedimentary rocks (PAAS values after Nance and Taylor, 1976). All planktonic and 25 benthic foraminiferal samples show positive Ce anomalies (average 1.35 ± 0.22 SD), whereas only 7 benthic samples have a negative Ce-anomaly (Figure 4.2). All results are detailed in Appendix Table A4.2.

4.3.2 Neodymium isotope signatures

The detrital εNd data of this study complement the MD03-2707 record of Weldeab et al. (2011) (Appendix Table A4.3). The complete data set now covers the last two glacial cycles back to 135 kyr and the εNd signatures range from -23.3 to -15.4, with the least radiogenic value found for the Last Glacial Maximum (LGM) at 20,000 years BP. The εNd values of the

sediment leachates range from -18.2 to -14.8 with the least radiogenic values also occurring at 20 kyr (Appendix Table A4.4). The Holocene samples (GeoB 4905) have an average εNd value of -15.1 ± 0.3 (SD, n = 3). The range of the planktonic foraminiferal εNd values between -17.9 and -15.4 over the studied time interval is significantly narrower (Appendix Table A4.1). The Nd isotope signatures of the foraminiferal samples that were not oxidatively-reductively cleaned are indistinguishable from the corresponding fully cleaned samples. The benthic foraminiferal data cover a εNd range similar to the planktonic samples and vary from -17.3 to -14.7.

4.4 Discussion

4.4.1 Foraminiferal carbonates and changing redox conditions

To obtain reliable seawater data from the foraminiferal carbonates, it has to be demonstrated that any contaminant phases of the carbonates have been removed. There is no significant correlation between Al/Ca ratios and the corresponding Nd/Ca ratios (R^2 = 0.02). This and the low Al/Ca ratios (< 100 µmol/mol; Ni et al., 2007) are supporting that all foraminiferal samples were efficiently cleaned from clays.

The Mn/Ca ratio serves as an indicator for residual ferromanganese coatings or Mn-rich carbonates, which can precipitate on the foraminiferal carbonate after deposition (Boyle, 1983; Pena et al., 2005, 2008). The critical threshold of the Mn/Ca generally assumed to indicate the presence of ferromanganese contamination (100 µmol/mol; Boyle, 1983) is exceeded for most of the analyzed samples (60 out of 69, Figure 4.2) and the down core ratios are much higher than those obtained from cleaned core top foraminifera from the Gulf of Guinea (Kraft et al., 2013). Neither Mn/Ca nor Fe/Ca correlate with Nd/Ca (R^2 = 0.03, R^2 = 0.06, respectively), which suggests that Nd is not associated with contamination originating from the Fe-Mn coatings. In addition, the Mn/Fe ratios are relatively low (0.99 ± 0.62, SD, n = 69) compared to previously published data. In the Cape Basin a range from 2.0 to 3.7 (bottom) and 11.6 (top) was found (Kasten et al., 1998), whereas nodules in the Brazil Basin only varied between 1.05 (bottom) and 1.95 (top) and nearby ferromanganese crusts show values near 1 mol/mol (Dubinin and Rimskaya, 2011). This suggests that contamination by diagenetic ferromanganese coatings cannot be excluded. In addition to diagenetic sources, incomplete cleaning can also result in low Mn/Fe, if Mn is removed faster from the foraminiferal shells. A pioneer study of Chester and Hughes (1967) indicated complete Mn

removal whereas Fe remained to be present in different sediment leaching experiments of foraminiferal shells. On the other hand, the non-reductively cleaned foraminiferal samples show a range of Mn/Fe ratios similar to the fully cleaned foraminiferal shells suggesting that preferential dissolution during the cleaning was not a relevant factor for contamination by ferromanganese coatings.

Furthermore, most of the planktonic foraminiferal samples show no clear indication for additional Nd originating from contaminant phases. In the literature, sedimentary planktonic foraminiferal Nd/Ca values of up to 1.4 µmol/mol have been considered fully cleaned (Vance et al., 2004; Ni et al., 2007). The benthic foraminifera have slightly higher Nd/Ca ratios with an average value of 1.7 ± 0.8 µmol/mol (SD, n = 32), as expected from results of a previous study, which argued for Nd/Ca ratios up to 2 µmol/mol to be still consistent with a pure deep water origin (Klevenz et al., 2008).

The REE patterns show that the signature of the foraminiferal shells does not exclusively originate from surface waters but suggest significant diagenetic contamination. Most of the fully cleaned foraminiferal samples show a pronounced positive Ce-anomaly (Figure 4.2) and are enriched in middle rare earth elements (MREE) (Appendix Figure A4.1). REE patterns of seawater are generally characterized by negative Ce-anomalies and no MREE enrichment. A positive Ce-anomaly can either be caused by contributions of dissolved iron from anoxic pore waters (Haley et al., 2005) or by ferromanganese coatings (Bau and Koschinsky, 2009; Dubinin and Rimskaya, 2011; Surya Prakash et al., 2012). In earlier studies MREE enrichments have, however, also been found in seawater itself and were shown to be caused by riverine inputs and/or contributions from weathering processes on land (e.g. Elderfield et al., 1990; Bayon et al., 2004; Hannigan and Sholkovitz, 2001; Stichel et al., 2012). In anoxic pore waters the MREE enrichment can probably be ascribed to the dissolution of Fe-oxides (Haley et al., 2004).

Analyses of fish teeth show a similar MREE bulge (e.g. Martin et al., 2010) reflecting diagenetic influence, but certainly not the "bell-shaped" pattern of extensive or late diagenesis with MREE/MREE* ratios > 10 (Reynard et al., 1999). Fish teeth from deep sea sediments have MREE/MREE* ratios of about 1.5 (Martin et al., 2010) similar to the foraminifera shells of this study with MREE/MREE* ratios < 1.8 (Figure 4.2; Appendix Table A4.2 and Figure A4.1). The MREE/MREE* ratios of the planktonic foraminiferal samples remained constant over the complete record (Figure 4.2), whereas the benthic samples show a higher variability. The benthic foraminiferal MREE/MREE* record diverges from that of the

planktonic samples especially at the beginning of termination I and II. The benthic foraminifera may have changed their habitat in those intervals, which may have led to a change of the ambient waters, pore or bottom water, whereas the REE patterns of the planktonic foraminifera are expected to generally reflect the waters at the sediment-water interface. The fact that both fully cleaned and non-reductively cleaned planktonic foraminifera obtained near termination II in the core studied here show identical patterns and the agreement of at least the planktonic samples in the MREE/MREE* against HREE/LREE plot including those obtained by HH extractions and fish teeth (Martin et al., 2010; Appendix Figure A4.1) suggests that the REEs reflect early diagenetic phases.

However, the foraminiferal element to calcium ratios cannot be considered as pure coating signals, given that these samples were oxidatively and reductively cleaned and the major part of the metals including Nd will originate from the ferromanganese coating. There is a possibility that the Mn and Fe together with other redox sensitive metals have been mobilized after initial formation of the coatings as a consequence of changes in redox conditions and that therefore also the Nd isotope signatures may have been affected. Results of a recent study suggest that secondary Mn-carbonates can prevent re-dissolution of previously formed coatings such that the original coating signature is 'locked in' the secondary Mn-carbonates (Roberts et al., 2012). Tachikawa et al. (2013) recently found that the Mn-carbonate overgrowth itself has only little impact on the Nd content but that the main carriers of Nd are ferromanganese oxides and Fe sulfides, which has been attached post-mortem to the inner walls and the pores of the foraminiferal tests.

During termination I and II (Figure 4.2) the Mn/Ca ratios and the Ce-anomalies (Ce/Ce*) increased in both benthic and planktonic foraminifera and the Mn/Ca ratios then markedly decreased in the early Holocene and MIS 5e. The highest Fe/Ca ratios are found at the beginning of the last deglaciation and at the end of termination II. This indicates changes in sediment redox conditions during terminations I and II. The oxygen concentration of bottom waters controls the mobility of Mn, Fe and Ce in the pore waters (e.g. Froelich et al., 1979; Sholkovitz et al., 1992). The increase in Ce/Ce* during the de-glaciations may point to a change towards more oxic conditions of the bottom and pore waters in the interglacials and/or increased particle export. The observed glacial-interglacial changes in E/Ca and Ce/Ce* ratios most likely reflect a combination of bottom water oxidation and export productivity, similar to other redox-sensitive trace metals like U, Cd, Mo and V. A recent study of Scholz et al. (2011) depicted a relationship between bottom water oxygen concentration and

accumulation/dissolution of redox-sensitive trace metals (U, V and Mo) together with carrier phases such as Mn and Fe oxy-hydroxides. Another important and closely linked factor influencing the accumulation of redox-sensitive trace metals (U and Cd) in the sediments is the organic carbon flux, which is related to nutrient concentration and productivity in the surface waters (e.g. Rosenthal et al., 1997; Scholz et al., 2011; Boiteau et al., 2012). For example, Boiteau et al. (2012) determined high U/Ca ratios of glacial sediments and foraminifera from the subtropical South Atlantic over the last 600 kyr suggesting lower bottom water oxygen concentrations or higher export productivity, which is difficult to separate because both conditions often occurs together.

We suggest that E/Ca and Ce/Ce* ratios indicate that the foraminiferal shells most probably host a mixture of different contaminant phases, which were 'locked in' and could not completely be removed by the cleaning procedures, thus, containing contributions from pore waters. However, we argue that those contaminant phases are small given that massive overgrowth is not visible and that most contaminations were removed during the cracking procedure before the chemical cleaning procedures were applied.

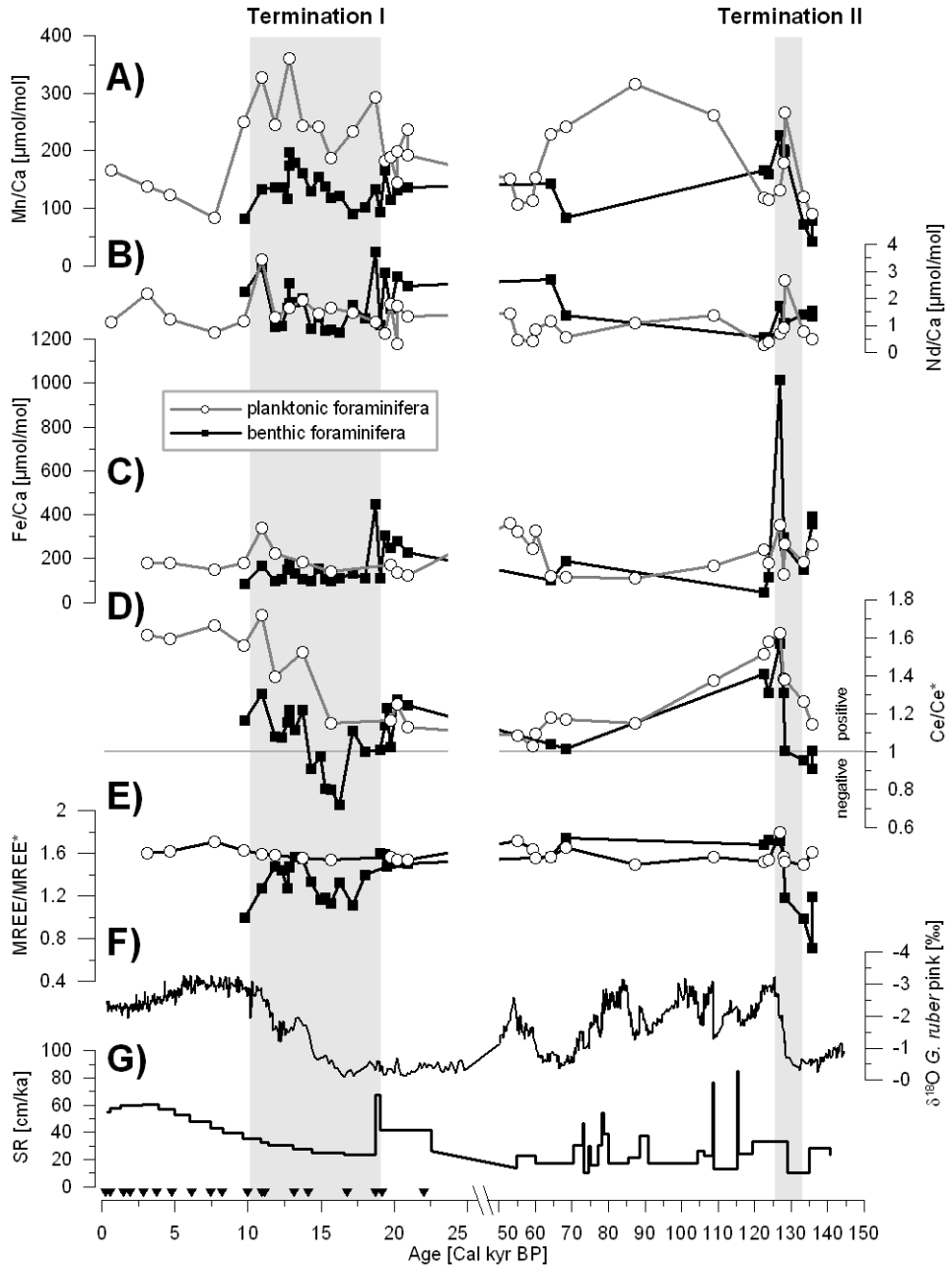

Figure 4.2: ***A)*** *Mn/Ca ratios,* ***B)*** *Nd/Ca ratios,* ***C)*** *Fe/Ca ratios,* ***D)*** *Ce-anomaly calculated with Ce/Ce* = 3(Ce/Ce^{PAAS})/(2La/La^{PAAS}+Nd/Nd^{PAAS}) (after German & Elderfield, 1990),* ***E)*** *MREE/MREE*= (Gd+Tb+Dy)/((LREE+HREE)/2),* ***F)*** *δ^{18}O record of G. ruber pink (Weldeab et al., 2007a),* ***G)*** *Sedimentation rates (Weldeab et al., 2007a); Black triangles along the x-axis indicate age control points of individual calibrated 14C-AMS ages that were used for a polynomial fit to obtain the age model (Weldeab et al., 2007a). Grey bars mark terminations I and II.*

4.4.2 Neodymium isotope compositions

Detrital sediment fraction and sediment leachates of ferromanganese coatings

The least radiogenic εNd values in the detrital sediment record were observed between 19,800 and 20,300 years BP (Figures 4.3). These values were interpreted to represent increased contributions of sediment from the Ntem River (εNd = -28.14, Weldeab et al., 2011), which has discharged into the Gulf of Guinea close to the coring site of MD03-2707 (about 50 km in the Holocene). During this period of time the fraction of terrigenous material originating from the Ntem catchment area amounted to 87 % and resulted from a more southerly location of the ITCZ and the associated rain belt and drier conditions over the Sanaga/Nyong catchment area in the north (Weldeab et al., 2011). However, the sea level was 130 ± 5 m lower during the LGM (Giresse et al., 1995), which substantially reduced the distance between the core site and the river mouth (Weldeab et al., 2011) by more than 10 km and exposed large parts of the shelf (Figure 4.1 B) suggesting that shelf erosion has played an important role for the supply of detrital sediments to the core location during the low stand. Similar conditions with sea level low stand of about -128 m (Waelbroeck et al., 2002) prevailed during MIS 6 (Figure 4.3), although sedimentation rates (Figure 4.2) and thus total riverine input were somewhat lower.

During the last deglaciation the ITCZ and the rain belt migrated northward, resulting in an increased influence of the northern river systems Nyong and Sanaga as reflected by the shift of the detrital εNd signatures at the core site to more radiogenic values (Weldeab et al., 2011). During the transition between MIS 6 and MIS 5e a similar shift in εNd signatures occurred documenting a comparable shift of the rain belt.

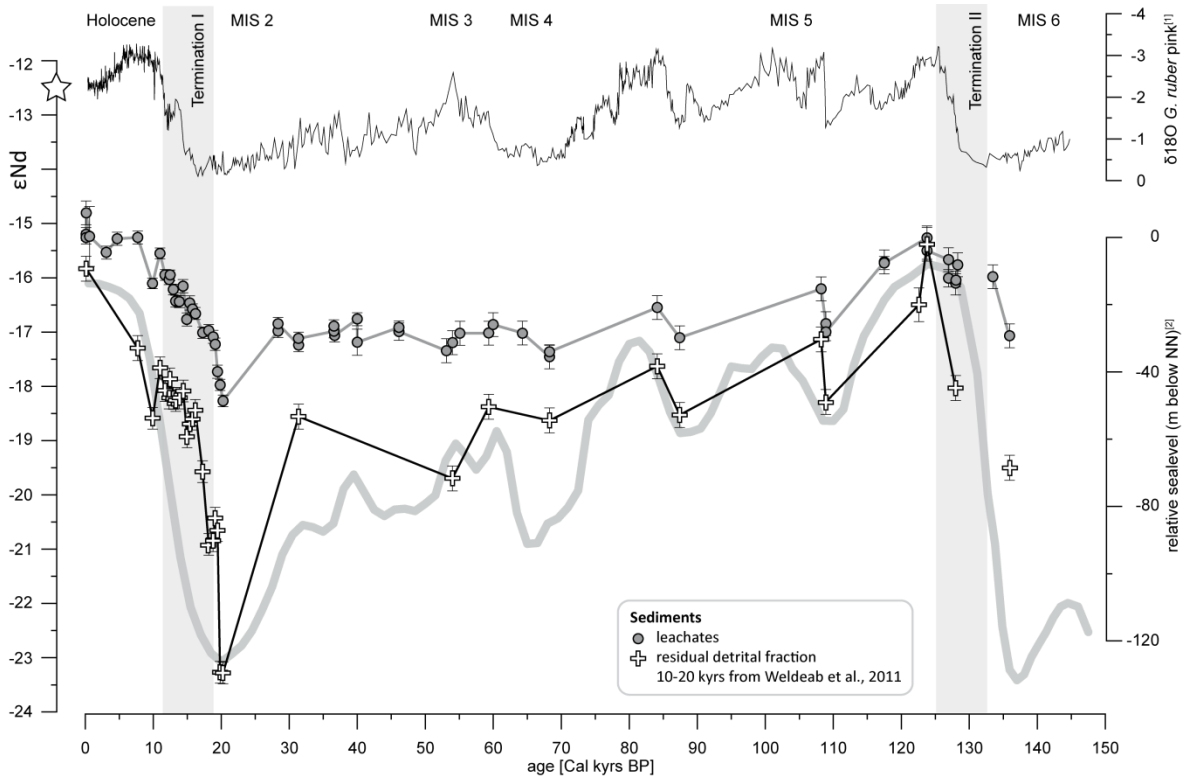

***Figure 4.3**: Down core record of sediment leachates (open circles) and of the detrital fraction (crosses). The age model was adopted from Weldeab et al. (2007a), as well as the $\delta^{18}O$ record[1] of the planktonic foraminifera G. ruber pink, which is shown for reference. [2]The relative sea level (RSL) record is from Waelbroeck et al. (2002). The white star represents the present day εNd signature of the NADW (North Atlantic Deep Water) and TSW (Tropical Surface Water) measured in studies of Rickli et al. (2010) and Bayon et al. (2011) close to our study site.*

The Nd isotope composition of the sediment leachates shows the same trend as that of the detrital fraction but the data are systematically offset towards more radiogenic values by between 0.1 to 5.4 εNd units. The core site (1294 m water depth) is bathed in upper NADW today. The εNd values of the sediment leachates are more radiogenic then modern deep water Nd isotope compositions at the site. The modern NADW εNd value is -12.5 (Rickli et al., 2010; Bayon et al., 2011), as measured in the equatorial Atlantic and close to the Niger River mouth in the Gulf of Guinea, which reflects alteration by significant mixing of the original NADW signature derived from the North Atlantic ocean (North Atlantic εNd = -13.5; Piepgras and Wasserburg, 1987) with other water masses. Thus, it is also possible that the bottom waters at the location of our study site, for which unfortunately no water column data are available to date, have been much less radiogenic than that of the Niger site (εNd of the Niger particles is close to -10) due to partial dissolution of unradiogenic riverine particles. Furthermore, pre-formed coatings originating from the rivers may have been partially

dissolved during leaching of riverine sediments (Bayon et al., 2004). The detrital and dissolved signature of the river closest to the core site is highly un-radiogenic (-28.1; Weldeab et al., 2011) and supports such a mechanism. A recent study of Singh et al. (2012) near the Ganges-Brahmaputra mouth supports release of Nd from particulate matter delivered by the river system and also from margin sediments. Similar influence of particulate processes has also been demonstrated in the eastern equatorial Pacific (Grasse et al., 2012). These authors argued that the supply of particulate matter from rivers and/or sediment water exchange can modify the εNd of surface and bottom water. As stated above there are no water data available close to the coast and we can thus not compare our data directly to bottom or pore water compositions. An influence of riverine inputs on the extracted sediment leachates has, however, been suggested in previous studies (Bayon et al., 2011; Kraft et al., 2013), which suggested, that the εNd signatures of the surface sediment coatings were more similar to those of the Niger River than to local seawater, most likely due to the influence of pre-formed coatings originating in the river.

The largest amounts of the sediments were supplied by the Ntem during the LGM and MIS 6, which is reflected by the largest offset between the Nd isotope signature of the detrital sediments and the sediment coatings. In the higher resolution part of the record between 8 and 15 kyr BP the leachates show less pronounced peaks than the detrital record (Figure 4.3). Particularly during the LGM, the records of the sediment leachates and the detrital sediments diverged strongly. The main amount of terrigenous sediments must have originated from the Ntem River (Weldeab et al., 2011), most likely supplied from the shelf during extensive shelf exposure (Figure 4.1 B). This is supported by several studies suggesting reduced intensities of the wet season during the LGM compared to the late Holocene in equatorial Africa based on sea surface salinity reconstructions (Weldeab et al., 2011) and on δD analyses of leaf waxes (Collins et al., 2013). Although, the $\delta^{13}C$ analyses of leaf waxes (C_3 versus C_4 vegetation) of Collins et al., 2011 depicted a contraction of the wet season length towards the equator, their duration was extended compared to the late Holocene.

The smaller amplitude of the sediment leach record and that of the detrital sediments may have been caused by dilution of the riverine signal by seawater signatures and/or by less variation of the rainfall intensity over the catchment area of the Sanaga and Ntem rivers. That would imply that the detrital sediment record may have been controlled by sea level changes and erosion of the shelf rather than by rainfall induced sediment transport. However, the Nd isotope compositions of the sediment coating reflects the migration of the rain belt over the

catchment areas, as described for the time period from 10 to 20 kyrs by Weldeab et al. (2011) but were most likely to a larger extent controlled by the change of the sea level. Thus, the sediment leachates most likely represent a mixture of bottom water and/or pore water signatures and riverine inputs via pre-formed coatings previously deposited on the shelf. Consequently, the sediment coatings carry a mixture of a regional signature that represents the migration of the rain belt over the river catchment areas and the prevailing bottom water Nd isotope composition.

The εNd signal of the foraminiferal shells

The foraminiferal Nd isotope compositions are very similar to those of the leached sediments and over large sections of the core they are identical within error (Figures 4.4 and 4.5) although the foraminiferal had been reductively cleaned.

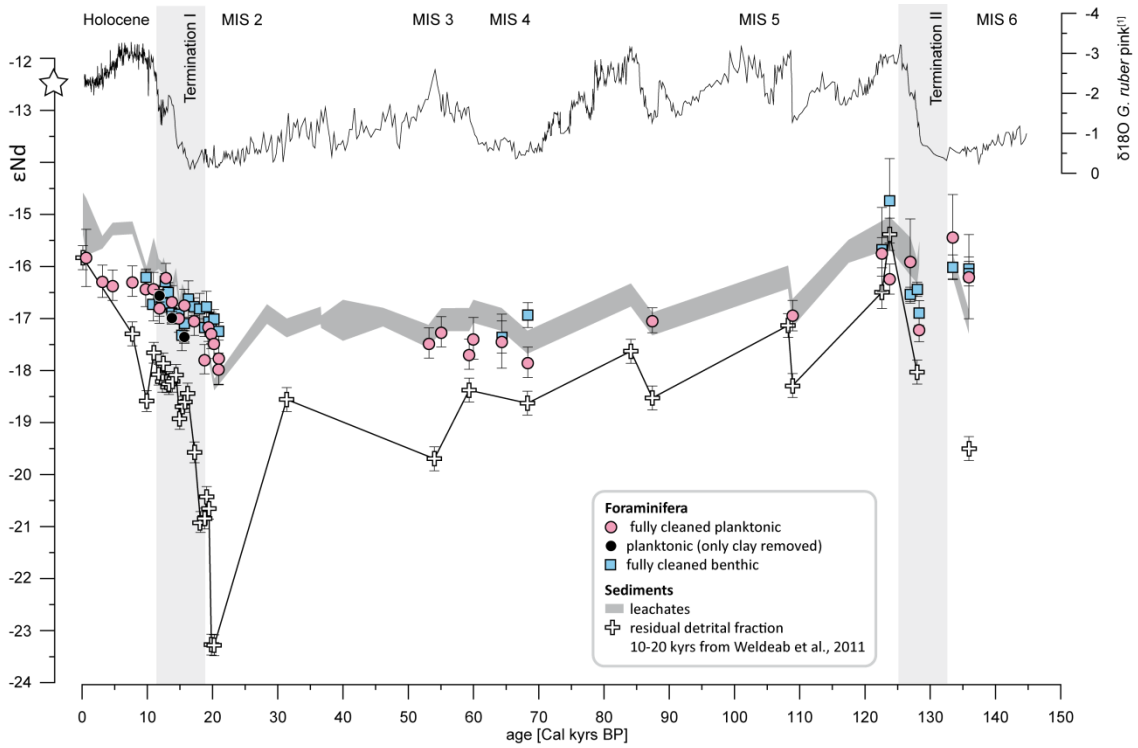

Figure 4.4: *Record of the Nd isotope signatures of planktonic foraminifera, benthic foraminifera, range of the sediment leachates, detrital sediments, and $\delta^{18}O$ record ([1]Weldeab et al., 2007a) as in Figure 4.3. The white star represents the present day εNd signature of the NADW (North Atlantic Deep Water) and TSW (Tropical Surface Water) measured in studies of Rickli et al. (2010) and Bayon et al. (2011) close to our study site.*

The benthic foraminiferal samples are expected to agree with the sediment leachates, given that both are supposed to reflect bottom water compositions (e.g. Gutjahr et al., 2007, 2008; Klevenz et al., 2008; Piotrowski et al., 2012). The influence of riverine signatures is indicated, given that the foraminiferal record is very similar to that of the sediment leachates. This either shows that the riverine contributions also modified the bottom water composition or that the riverine particles and their pre-formed coatings have been deposited at the core site. Despite the general similarity of the foraminiferal and the sediment leachate εNd records, there were periods of divergence of up to 1.4 εNd units. The largest offsets were found for termination II and the Holocene, when the Ce/Ce* was high. High Ce/Ce* ratios point to more oxic conditions of the bottom and pore waters, which would result in less dissolution of pre-formed oxide coatings and thus less contribution of riverine signatures to the foraminiferal signals.

In general, the benthic and planktonic foraminifera show similar values with an average offset of 0.4 εNd units, which is within the analytical uncertainty of the measurements. Overall, the foraminiferal εNd values are less radiogenic then the sediment leachates (Figures 4.4 and 4.5). The benthic foraminifera seem to be slightly more radiogenic than the planktonic samples. The shift of the foraminiferal records to less radiogenic values compared to the sediment leachates may be explained by remobilization processes in the sediments, which cause partial dissolution of the pre-formed riverine coatings (Bayon et al., 2004). The re-dissolved elements may then have been attached to the carbonates via formation of secondary contaminant phases, such as Mn-carbonates (Boyle, 1983). The Nd isotope compositions of the sediment coatings do not contain any contributions from secondary carbonates, because all carbonates were removed from the sediment samples prior to the leaching. However, the observed Nd/Ca ratios of the foraminiferal samples do not show large changes suggesting that there was no major remobilization of Nd.

The foraminiferal shells were reductively cleaned and probably the original oxide coating was ‘locked in’ since they were coated with secondary carbonates (Roberts et al., 2012), which could not be removed during the cleaning procedure. If this is true, the εNd signature of the fully cleaned foraminiferal shells may indeed reflect the actual bottom or pore water signature and was not affected later on by redox changes, given that coatings formed at a later stage on the shells should have been removed during the reductive cleaning procedure. Thus, foraminifera are suggested to reflect bottom or pore water signatures similar to fish teeth (e.g. Martin et al., 2010) with the advantage that foraminifera are in general more abundant.

Our records clearly depict the potential of Nd isotope compositions of foraminifera and bulk sediment leachates to record changes in bottom water composition, caused by changes in origin of the water masses, riverine influence, redox-conditions, oxygen concentration and export productivity during glacial-interglacial cycles. Further studies should include parameters such as bottom and pore water analyses at the same location and additional proxies such as $\delta^{13}C$, Cd/Ca and U/Ca in order to better disentangle the above processes.

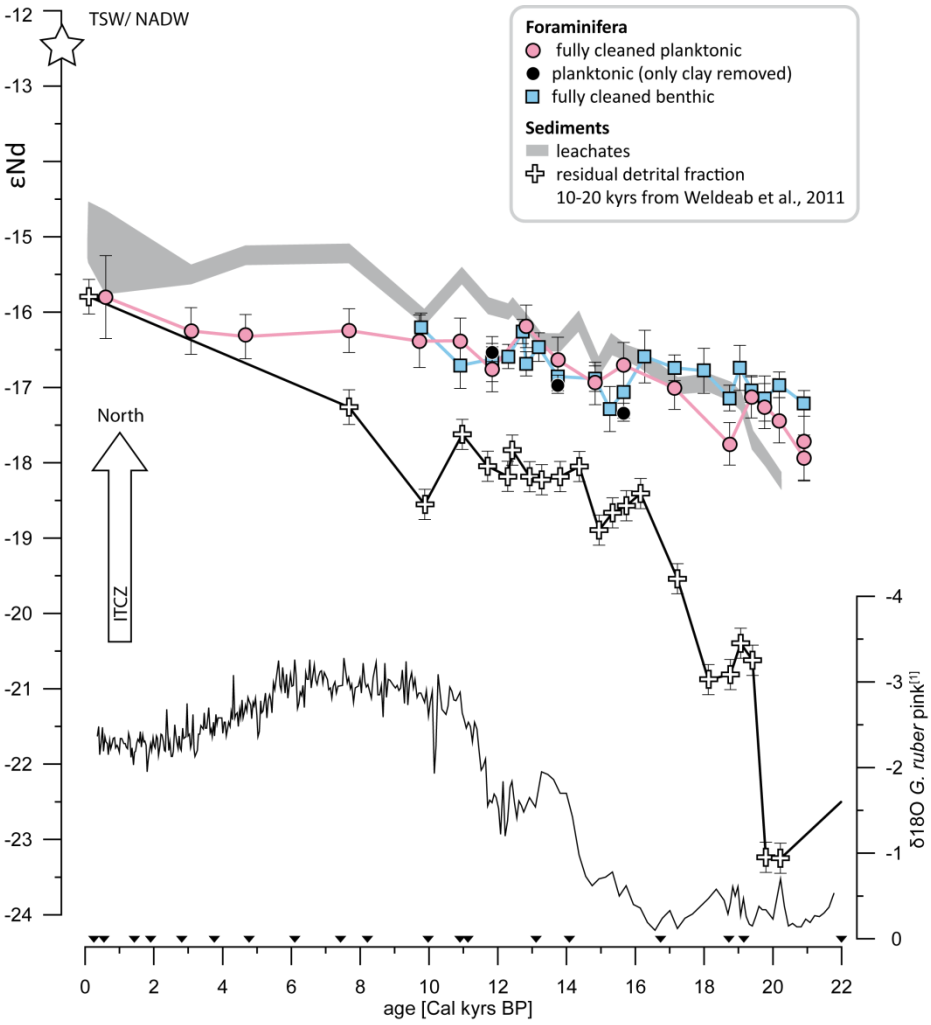

Figure 4.5: *Enlargement of the records since the last deglaciation with symbols identical to Figure 4.4. Black triangles again represent individual calibrated 14C-AMS ages based on which the age model was developed ([1]Weldeab et al., 2007a).*

4.5 Conclusions

In this study we analyzed different geochemical phases obtained from core MD03-2707 to reconstruct changes in riverine influence in the Gulf of Guinea during the past 135,000 years (BP). All analyzed archives have in different ways been related to riverine influence and have followed the same trends with more radiogenic εNd values during the interglacials and un-radiogenic values during glacial periods caused by latitudinal migration of the rain belt over the different catchment areas and changes in supply by these rivers.

The εNd signatures of the detrital sediment fraction of our study reflect changes in riverine input caused by latitudinal shifts of the ITCZ and the rain belt over the catchment areas of the different river systems. In addition, the detrital records were influenced by changes in sea level and thus in nearby shelf exposure.

The sediment leachate record mirrors the riverine inputs as reflected by similar trends as the detrital records. The εNd signals of the sediment coatings show the influence of the river inputs either by pre-formed coatings and/or through modifications of bottom and/or pore waters through partial dissolution of the riverine particles. These effects can only be unambiguously distinguished by comparison to present day water column data, which are unfortunately not available. The leachates thus most likely represent a mixed regionally influenced signal integrating different signatures from the bottom and pore water, rivers and the shelf. The differences in amplitude of the detrital and sediment coating records may be caused by either dilution of the authigenic riverine signature by seawater signatures during early diagenesis and/or less variation of the precipitation over the catchment areas of the rivers than expected from the detrital radiogenic isotope record.

The εNd values of the foraminiferal shells have been similar to the sediment leachate εNd values. However, the carbonates are contaminated with ferromanganese material, as indicated by the E/Ca ratios and the REE concentrations. The observed changes during the glacial-interglacial cycles may thus reflect a combination of bottom water oxygenation and export productivity. In contrast, the Nd isotope composition of the foraminiferal shells reflect bottom or pore waters with contributions of riverine signatures, similar to the sediment leachates, though without the influence of further redox reactions deeper in the sediment.

Acknowledgements

We would like to thank A. Eisenhauer for access to the ICP-MS and A. Kolevica for assistance with the measurements. Thanks also to the University of Bremen, Geosciences Department and MARUM for providing GeoB samples. This project was funded by the Deutsche Forschungsgemeinschaft (Project No WE2686/5-1).

Chapter 5

Changes of temperature and sources of tropical Atlantic subsurface waters in response to the last glacial bipolar oscillation (5-60 kyr BP)

Abstract

To improve our understanding of the response of subsurface water in the tropical Atlantic to the bipolar oscillation and its potential role in modulating the inter-hemispheric heat exchange we represent a detailed record of the evolution of the thermocline and subsurface water masses in the Gulf of Guinea in the easternmost equatorial Atlantic retrieved from core MD03-2707 and provide insights into their coupling to high latitude climate changes during the last glacial period (5-60 kyr BP). In this study, we established a core top-based multi-species temperature calibration of foraminiferal Mg/Ca for the Gulf of Guinea using core top samples from 83 locations. We analyzed trace element compositions (Mg/Ca, Ba/Ca) as well as stable oxygen and carbon isotopes ($\delta^{18}O$ and $\delta^{13}C$) in two planktonic foraminiferal species prevailing at different water depths (*N. dutertrei* and *G. crassaformis*) to reconstruct changes in temperature, salinity, and source of the Subtropical Underwater (STUW) and the South Atlantic Central Water (SACW).

Our study shows that *N. dutertrei* represents conditions within the lower thermocline at the study site and has been influenced by northern hemisphere climate and also by changes in the southern hemisphere due to admixture of water masses of southern origin. *G. crassaformis* represents changes in deeper water masses (SACW) and mainly reflects climatic changes in the southern hemisphere. The SACW pronouncedly influenced the thermocline waters during the time period between 55 and 35 kyr. Enhanced vertical mixing most likely driven by stronger trade winds resulted in a decrease of thermocline depth. Since 32 kyr the trends in the records of *N. dutertrei* and *G. crassaformis* have diverged, suggesting a decrease of the influence of southern water masses and an attenuation of the mixing of the water masses.

A version of this chapter is going to be submitted.

5.1 Introduction

Highly resolved ice core records from Greenland and Antarctica covering the last 70 kyr revealed a centennial-scale rise and drop of air temperature and atmospheric greenhouse gases (Blunier and Brook, 2001; Flückiger et al., 2004; NGRIP, 2004; EPICA, 2006; Ahn and Brook, 2008). High and mid-latitude marine records indicate that the atmospheric fluctuations, as recorded in the ice cores, were accompanied by ice sheet instabilities (Kanfoush et al., 2000; Bond et al., 2001; Anderson et al., 2009; Barker et al., 2009) and perturbations of the thermohaline ocean circulation (McManus et al., 2004; Negre et al., 2010). While the trigger mechanism of these millennial-scale oscillations remains debated (e.g. Petersen et al., 2013), the anti-correlation between air temperature changes in southern and northern high latitudes is consistent with the concept of bipolar oscillation (Stocker, 1998; Knutti et al., 2004; Timmermann et al., 2005).

The response of the tropical Atlantic sea surface temperature to the last glacial bipolar oscillation is characterized by spatially heterogeneous patterns showing asymmetric SST changes across zonal gradients (Jaeschke et al., 2007; Weldeab, 2012a), as well as patchy SST patterns within the western tropical Atlantic (Hüls and Zahn, 2000; Jaeschke et al., 2007). These heterogeneous SST records of the tropical Atlantic may reflect regional imprint of changes in wind strength and direction and surface currents (Weldeab, 2012a) superimposed on basin-wide surface warmth, as predicted by modeling studies (Lohmann, 2003; Chang et al., 2008). Model studies also indicate the importance of shallow subsurface water in the inter-hemispheric heat exchange (Chang et al., 2008). Available records of the subsurface water are, however, limited to the last de-glacial (Rühlemann et al., 2004; Schmidt et al., 2012). A lack of highly resolved and long temperature records of the tropical Atlantic so far hampered our understanding pertaining to the response of subsurface water to the bipolar oscillation and its potential role in modulating the inter-hemispheric heat exchange.

In this study we present detailed temperature records of the thermocline (75 - 150 m) and subsurface water masses (300 - 400 m) of the tropical Atlantic and provide detailed insights into changes of the thermal structure linked to high latitude climate perturbations.

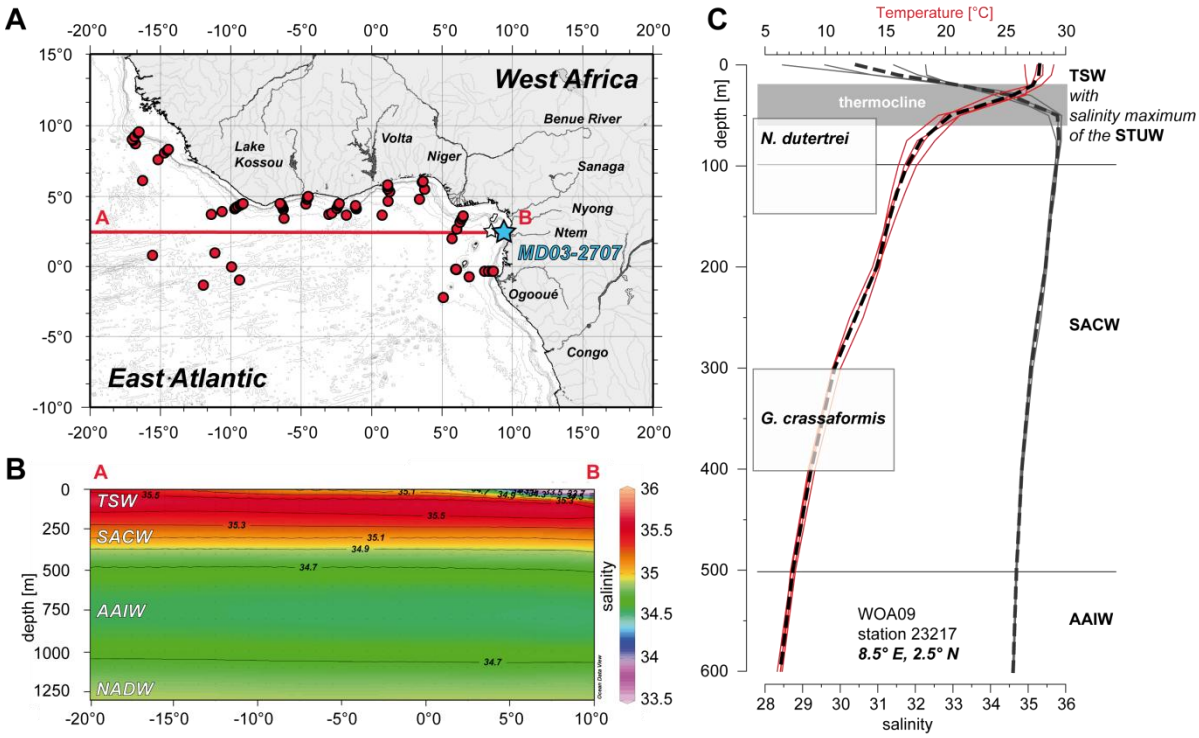

Figure 5.1: A) *Core top locations (circles), location of piston core MD03-2707 (blue star), WOA09 station 23217 (World Ocean Atlas 2009, white star),* ***B)*** *East-West salinity profile along 2.5°N (section A-B, red line in A) and* ***C)*** *temperature (black) and salinity (red): seasonal (solid lines: January-March, April-June, July-September, October-December) and annual (dashed lines) of WOA09 site 23217 (8.5°E, 2.5°N, white star in A), Antonov et al., 2010; Locarnini et al., 2010). The grey box represents the location of the thermocline and the white boxes represent the expected habitat depth of the analyzed planktonic foraminifera in the study area. TSW = Tropical Surface Water, STUW = Subtropical Underwater, SACW = South Atlantic Central Water, AAIW = Antarctic Intermediate Water, NADW = North Atlantic Deep Water (Stramma and Schott, 1999 & references therein; Bayon et al., 2011).*

Oceanographic setting

This study focuses on the paleoceanography of the easternmost equatorial Atlantic, with particular emphasis in the temperature history of the upper 500 m of the water column. On the basis of vertical salinity distribution patterns, the modern water column of the Gulf of Guinea can be subdivided into four main water masses (Figures 5.1 B and 5.1 C): the Tropical Surface Water (TSW), the South Atlantic Central Water (SACW), the Antarctic Intermediate Water (AAIW) and the North Atlantic Deep Water (NADW). The mixed layer is represented by the TSW and the Subtropical Underwater (STUW). The TSW is characterized by low salinity and elevated temperatures between 20 and 28°C (Figure 5.1 C). The STUW is formed by subduction of high salinity surface waters south of 12°S (Sprintall and Tomczak, 1992) and spreads toward the equator below the surface. At WOA09 site

23217 which is close to our core site (Figure 5.1 C) the salinity maximum (35.8 psu) is located in between 50 and 75 m water depth (Antonov et al., 2010). The lower boundary is the marked by the thermocline.

The SACW occupies water depths between 100 and 500 m water depth and is found south of 15°N its northern boundary and is formed in the southern hemisphere subtropical convergence (Stramma and Peterson, 1990; Stramma and England, 1999; Stramma and Schott, 1999) within the confluence of the Brazil and the Falkland Currents. From there it flows eastward as part of the South Atlantic Current. Here the SACW mixes with warm and saline water originating from the South Indian Ocean that enters the Atlantic as the Agulhas Current eddies (Sprintall and Tomczak, 1993; Tomczak and Godfrey, 1994; Stramma and Schott, 1999; Biastoch et al., 2008). After flowing westward with the Benguela Current the North Brazil Undercurrent carries the SACW northward, at the equator the SACW is reflected towards the Gulf of Guinea (Stramma and England, 1999; Stramma and Schott, 1999).

The Antarctic Intermediate Water (AAIW) occupies water depths between 500 and 1200 m. With the exception of the NADW that occupies water depth between 1200 and 4000 m, all water masses in the eastern tropical Atlantic flow northward (Stramma and Schott, 1999; Stramma and England, 1999).

With the exception of the upper meters of the water column, there is little seasonal variation in salinity of only about ±1.7 (psu) at WOA site 23217 close to MD03-2707 (Figure 5.1 C). The very low sea surface salinity at site 23217 is due to fresh water input of large river systems that drain equatorial West Africa. The temperature and salinity profiles from the entire Gulf of Guinea are similar to that of WOA site 23217 (Appendix Figure A5.1).

Within the upper 100 m, a steep temperature gradient of about 11°C exists, which is strongest between 50 and 75 m. The thermocline is located at a water depth between 75 and 100 m.

5.2 Materials and methods

5.2.1 Material and analytical approaches

83 core top samples and a marine sediment sequence of core MD03-2707 (2°30'07 N, 9°23'41 E, 1294 m water depth) were recovered from the Gulf of Guinea (Figure 5.1 A). Core top samples were collected from water depths between 390 m and 4970 m (Figure 5.1 A and Appendix Tables A5.1 and A5.2) during Meteor cruise M 6-5 (Lutze et al., 1988).

Trace-Element analyses (Mg/Ca, Ba/Ca)

We selected tests of *Neogloboquadrina dutertrei* and *Globorotalia crassaformis* to establish a core top-based calibration of foraminiferal Mg/Ca versus temperature and reconstruct changes in thermocline and subsurface water masses in the Gulf of Guinea focusing on the 300 - 400 µm fraction. In sediment samples with low abundances of *N. dutertrei* and *G. crassaformis* we include size fraction larger than 400 µm. A well-defined test range serves to minimize test size dependent fractionation effects on $\delta^{18}O$ and Mg/Ca ratios (Ravelo and Fairbanks, 1995; Elderfield et al., 2002). All foraminiferal shells were handpicked under a binocular microscope. For trace element analyses foraminiferal shells were gently cracked between two glass plates to open the chambers and facilitated effective cleaning. Any visible contaminant grains were manually removed. Ten to 15 cracked specimens, in exceptional cases less but at least 2 to 3, were transferred into 0.5 ml vials. Sample preparation and trace element analysis was carried out in the Department of Earth Science, University of California in Santa Barbara (UCSB). The cleaning procedure of samples for trace element analysis includes reductive and oxidative steps (Chapter 2) following the standard cleaning procedure as described in detail by Martin and Lea (2002). Following the cleaning, foraminiferal shells were dissolved in weak nitric acid (0.075 N) and analyzed using a Thermo Finnigan Element 2 sector field ICP-MS at the UCSB (Martin and Lea, 2002). The analytical reproducibility of 1.02% for Mg/Ca and 2.03% for Ba/Ca was estimated based on repeated measurements of consistency standards (n = 132) during the entire study. Along with Mg/Ca and Ba/Ca several other element/Ca ratios were analyzed to identify possible contaminations by silicates and ferromanganese coatings which may bias the Mg/Ca ratio. The average Al/Ca ratios in *N. dutertrei* core top and down core samples are 15 and 103 µmol/mol, respectively. The *N. dutertrei* Mn/Ca ratios are 11 and 67 µmol/mol and the Fe/Ca ratios are 71 and 274 µmol/mol in core top and down core samples, respectively. The element/Ca ratios of *G. crassaformis* show similar values for Al/Ca (15 and 103 µmol/mol in core top and down core samples, respectively). *G. crassaformis* samples show slightly higher Mn/Ca (22 and 128 µmol/mol, core top and down core samples, respectively) and Fe/Ca values (145 and 232 µmol/mol, core top and down core samples, respectively) than *N. dutertrei*. None of the analyzed Al/Ca. Mn/Ca and Fe/Ca ratios show a significant correlation with Mg/Ca and Ba/Ca ratios (Appendix Figures A5.2 a - d).

Stable isotope analyses (δ18O, δ13C)

The oxygen and carbon isotope compositions of the tests of *N.* dutertrei and *G. crassaformis* ($\delta^{18}O$ and $\delta^{13}C$) were analyzed using a MAT 251 Stable Isotope Ratio Mass Spectrometer coupled to a Kiel III device at the Leibniz-Laboratory for Radiometric Dating and Isotope Research of the University of Kiel. Five to six shells were used for analyses of the stable isotopes.

The stable isotope ratios are expressed in δ-notation, where

$$\delta = (R_{sample}/R_{standard}-1)*1000 \quad (5.1)$$

with R being the ratio of heavy to light isotopes ($^{18}O/^{16}O$ and $^{13}C/^{12}C$). Results were corrected using the NIST NBS19 standard and are reported relative to the (Vienna) Peedee Belemnite (VPDB). The analytical uncertainty of the $\delta^{18}O$ and $\delta^{13}C$ measurements is ± 0.03 ‰ and ± 0.07 ‰, respectively.

Variations of foraminiferal $\delta^{18}O$ time series reflect changes in temperature, salinity and continental ice volume. For extraction of $\delta^{18}O$ variability related to salinity changes, we removed the temperature component from the analyzed $\delta^{18}O_{calcite}$ values using the equation developed by Bemis et al. (1998):

$$\delta^{18}O_{sw} = (T -16.5)/4.8+ (\delta^{18}O_{calcite}+0.27), \quad (5.2)$$

where T is the Mg/Ca-based estimate of calcification temperature (see below) and $\delta^{18}O_{sw}$ (SMOW) is the reconstructed oxygen isotope ratios reported relative to the Standard Mean Ocean Water (SMOW). In a further step, the ice volume component was removed from $\delta^{18}O_{sw}$ following the approach applied by Waelbroeck et al. (2002):

$$\delta^{18}O_{ivf-sw} = \delta^{18}O_{sw}-RSL\ (‰). \quad (5.3)$$

5.2.2 Age model

The age model was taken from Weldeab et al. (2007a, b) and Weldeab (2012a, b). For our record, the age model based on combined ^{14}C age dating points (Weldeab et al., 2007a) and the $\delta^{18}O_{G.\ ruber}$ record (MD03-2707) tuned to the $\delta^{18}O$ record of the Byrd ice core (Blunier and Brook, 2001) was adopted. These records were overlapped at about 1200.5 cm core depth to combine the age models of the different time periods. All analyses presented in this study were carried out on samples used in Weldeab et al. (2007a, b) and Weldeab (2012a, b).

5.3 Results

5.3.1 Core top samples

5.3.1.1 Mg/Ca-temperature ($\delta^{18}O$-based) relationship

Core top sample analyses and culture experiments have revealed that an exponential relationship exists between planktonic foraminiferal Mg/Ca ratios and the temperature of the water from which the foraminifera calcify (Nürnberg, 1995; Nürnberg et al., 1996; Lea et al., 1999; Elderfield and Ganssen, 2000; Dekens et al., 2002). Therefore, Mg/Ca ratios of planktonic foraminiferal tests are commonly used as a powerful tool for reconstructions of past ocean temperatures (e. g. Nürnberg et al., 1996, 2000; Elderfield and Ganssen, 2000; Barker et al., 2003; Lea et al., 2003; Weldeab et al. 2007a; 2007b; Dürkop et al., 2008; Weldeab, 2012a, 2012b). Depending on the oceanographic setting, the application of Mg/Ca as a paleo-thermometer can, however, be complicated by preferential Mg dissolution, post-depositional high Mg-calcite precipitation and the effect of anomalously high salinity. Therefore, we established a regional planktonic foraminiferal Mg/Ca-temperature calibration for the Gulf of Guinea. For the calibration we related analyzed Mg/Ca ratios against $\delta^{18}O$ calcification temperatures. The $\delta^{18}O$ calcification temperature was estimated using analyzed $\delta^{18}O_{cc}$, salinity at the water depth of the estimated habitat depth of the foraminifera (WOA09 data set from Antonov et al., 2010) using the following equations:

$$\delta^{18}O_{sw} = 0.15*\text{salinity}-4.61 \text{ (LeGrande and Schmidt, 2006)} \quad (5.4)$$

and

$$T = 4.8*(\delta^{18}O_{sw} - \delta^{18}O_{cc} + 0.27) + 16.5 \text{ (Bemis et al., 1998)} . \quad (5.5)$$

Our decision to calculate calcification temperatures using salinity instead of temperature from WOA09 data set has the advantage that, in contrast to temperature, salinity varies very little across the subsurface water column. Thus, uncertainty in the estimate of habitat depth has only a small effect on the salinity estimate. The habitat depth of *N. dutertrei* and *G. crassaformis* has been estimated to range between 75 and 150 m and between 300 and 400 m, respectively (see below).

Figure 5.2 shows Mg/Ca ratios analyzed in *N. dutertrei* and *G. crassaformis* plotted versus their respective $\delta^{18}O$ calcification temperature and Mg/Ca in *G. ruber* pink plotted versus summer SST (WOA09) (Weldeab, 2012a). The relationship between the multi-species Mg/Ca

data and $\delta^{18}O$ calcification temperature shows an exponential relationship with a pre-exponential value of 0.50 and an exponential value of 0.077. The latter indicates that a change in temperature of 1°C corresponds to a Mg/Ca change of 7.7% consistent with several culture and core-top results (Nürnberg, 1995; Nürnberg et al., 1996; Lea et al., 1999; Elderfield and Ganssen, 2000, Dekens et al., 2002). The calibration line of our multi-species study plots between the calibration lines obtained from multi-species data of Anand et al. (2003) and the *N. dutertrei* data of Regenberg et al. (2009) (Figure 5.2).

Considering the single species only, the exponential relationships vary significantly from the multi-species calibration line (Figure 5.2). The calibration line of *N. dutertrei* shows a shallower slope resulting in higher temperatures compared to the multi-species calibration for the same Mg/Ca ratios. The data of *N. dutertrei* are very close to the single species calibration (*N. dutertrei*) of Anand et al. (2003) and to the calibration of thermocline/shallow species of Regenberg et al. (2009) but they differ in the slope of the exponential fit. The *N. dutertrei* calibration line of Regenberg et al. (2009) shows a similar slope but also an offset towards lower temperatures (Figure 5.2). The *G. crassaformis* data match the literature calibrations of *N. dutertrei* from Dekens et al. (2002) and Regenberg et al. (2009), as well as the multi-species (8 species) calibration from Elderfield and Ganssen (2000) (Figure 5.2), however with different slopes.

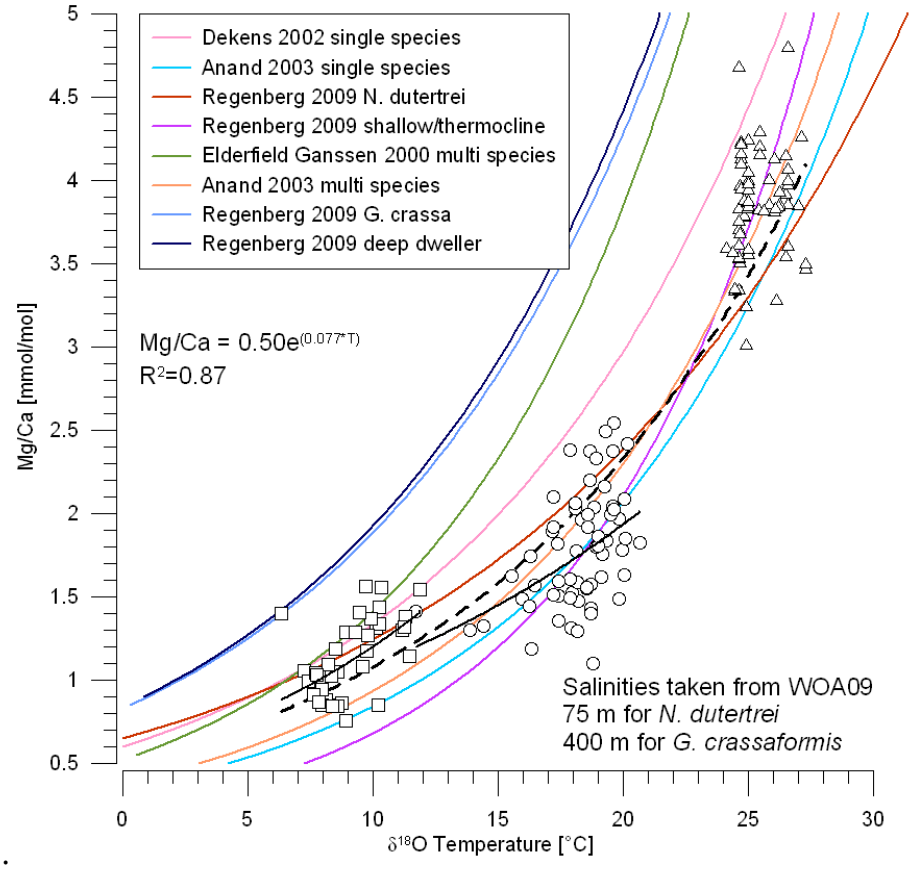

Figure 5.2: *Measured Mg/Ca ratios versus calculated $\delta^{18}O$ temperatures (after Bemis et al., 1998 with salinities from WOA09 data set from Antonov et al., 2010 and $\delta^{18}O_{sw}$ calculated after LeGrande and Schmidt, 2006) of N. dutertrei (circles, 75 m water depth), G. crassaformis (squares, 400 m water depth) and G. ruber pink (triangles, Mg/Ca and summer SST from Weldeab et al., 2007a). The black lines represent the exponential fits through the data of each foraminiferal species (solid line) and through our entire data set (dashed line).*

5.3.1.2 Carbonate ion concentration

The Mg/Ca ratios, in particular those of *N. dutertrei* show a high variability (Figures 5.2, 5.3 and 5.4), which can be caused by various processes including preferential Mg dissolution, spatially or seasonally variable habitat depth within the Gulf of Guinea, and the effect of large salinity variation. We carried out a multivariate analysis to test the relationship of the multi-species Mg/Ca data set to carbonate ion concentration, expressed as

$$\Delta CO_3^{2-} = CO_3^{2-}{}_{insitu} - \Delta CO_3^{2-}{}_{saturation} \qquad (5.6)$$

and to salinity. The results confirm that with an exponential of 0.071±0.002 (7.1±0.2% Mg/Ca change per °C) temperature exerts the most dominant control on planktonic foraminiferal Mg/Ca. The few samples (n = 3) collected below 4500 m (the Calcite

Saturation Horizon = the top of the lysocline) show low Mg/Ca most likely due to corrosive Antarctic Deep Water (Figures 5.3 and 5.4). Those three samples are not included in the calibration data set. The correlation between ΔCO_3^{2-} and Mg/Ca of 0.2% Mg/Ca changes per ΔCO_3^{2-} unit is statistically insignificant indicating that preferential Mg dissolution does not explain the observed scatter. This conclusion is consistent with a poor correlation between the average weight of individual foraminiferal shells and Mg/Ca (Appendix Figure A5.4; Tables A5.1 and A5.2). In addition, the highest variability occurs in samples from oversaturated water masses (Figure 5.3, white symbols). Within the Gulf of Guinea, salinity has also no effect on the Mg/Ca (Figure 5.5 E). Figure 5.5 A shows spatial distribution of Mg/Ca analyzed in *N. dutertrei* and depicts a distinct depth range of low Mg/Ca ratios between 700 and 1800 m. While the range of the water depth overlaps with that of AAIW (500 - 1200 m) which is characterized by low carbonate ion concentration (Figure 5.3 A), the low Mg/Ca ratios, however, do not reflect the spatial distribution of AAIW. This indicates that these low Mg/Ca signatures may be related to processes other than to the relatively low ΔCO_3^{2-}. Spatially and seasonally varying upwelling or shoaling of the thermocline are possible explanations.

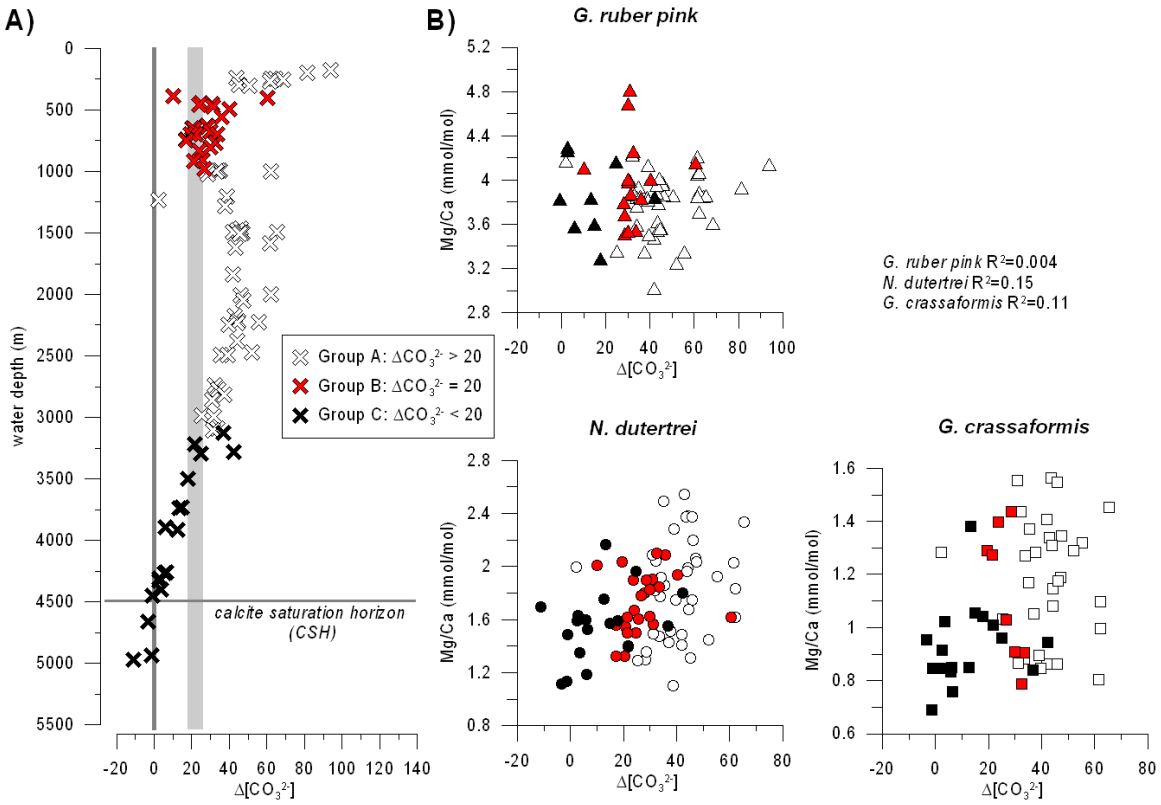

Figure 5.3: *ΔCO_3^{2-} versus water depth and Mg/Ca;* ***A****) ΔCO_3^{2-} water depth profile (calculated ΔCO_3^{2-}* of the core top samples). The grey vertical bar marks the critical range of $\Delta[CO_3^{2-}]$ (>20 µmol/kg), below which preferential Mg^{2+} dissolution may occur (Dekens et al., 2002; Regenberg et al., 2006), the black line mark the calcite saturation horizon representing to top of the lysocline at $\Delta[CO_3^{2-}]$=0.* ***B****) Measured Mg/Ca of core top samples (G. ruber pink values of Weldeab, 2012b) versus calculated ΔCO_3^{2-}* taken from the closest WOCE profiles and from Weldeab et al. (2012b) show no correlation;*

**$\Delta[CO_3^{2-}]$ is the difference between the $[CO_3^{2-}]_{insitu}$ (CO2SYS (Pierrot et al., 2006) using CO_2 constants from Dickson (1990) and Mehrbach et al. (1973) refit by Dickson and Millero (1987)) and $[CO_3^{2-}]_{sat}$ (Jansen et al., 2002). CTD data (salinity, temperature, pressure, total phosphate and total silicate), Alkalinity and TCO_2 taken from WOCE data (Oudot, 1993a and 1993b, Wallace et al., 1995) to calculate $[CO_3^{2-}]_{insitu}$.*

5.3.1.3 Dissolution correction

The Mg/Ca ratios of both species slightly decrease below 3500 m water depth (Figure 5.4). The critical depth, below which dissolution is assumed to occur as calculated following Regenberg et al. (2006) is 4069 m and 3858 m for *N. dutertrei* and *G. crassaformis* (red lines, Figure 5.4). The critical depth ($d_{critical}$) equals the intercept between the average foraminiferal Mg/Ca value (Mg/Ca_{mean}) of the samples < 2000 m (Mg/Ca = 1.8 and 1.2 mmol/mol) and the regression line of the samples > 3500 m and was calculated as follows:

$$d_{critical} = a - b*Mg/Ca_{mean} \quad (5.7)$$

where a is y axis intercept, and b is the slope of the regression line. The Mg/Ca ratios of the samples below the critical depth were corrected using the following equation (Regenberg et al., 2006):

$$Mg/Ca_{initial} = Mg/Ca_{measured}+(d-d_{critical})/b. \quad (5.8)$$

After correction the Mg/Ca values plot inside the range of the standard deviation (Figure 5.4). The correction of Mg/Ca ratios of samples from a water depth >4500 m would lead to overestimated Mg/Ca. Furthermore, those samples from below the calcite saturation horizon (CSH; bottom water depth >4500 m) are not included in the calibration data set.

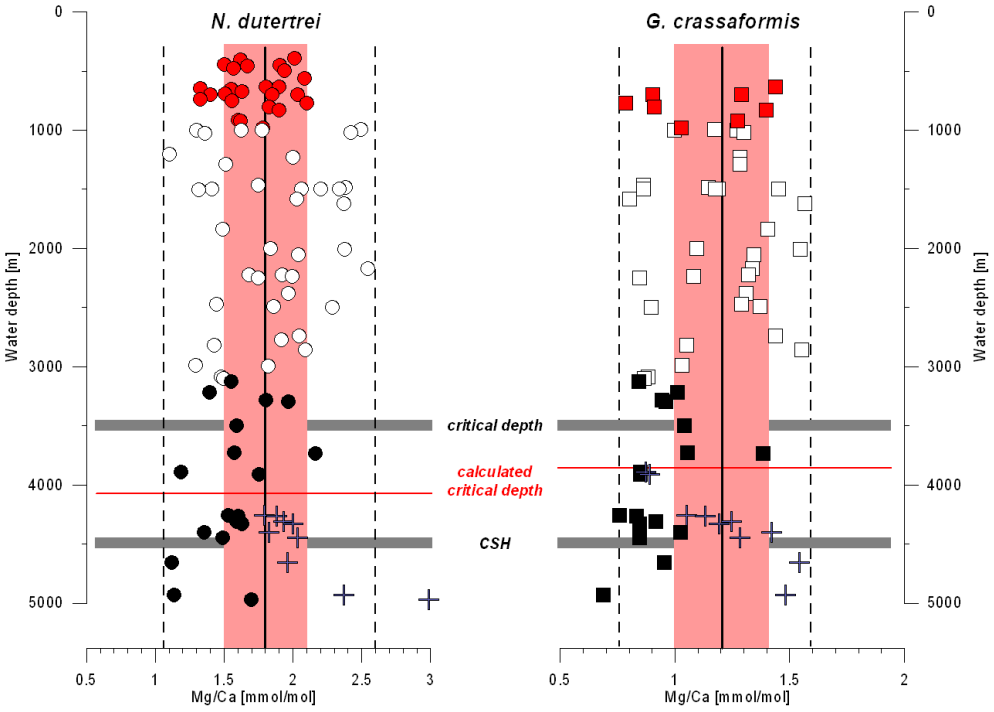

Figure 5.4: *Mg/Ca of N. dutertrei and G. crassaformis versus water depth, scattering around average values of 1.8 ± 0.3 mmol/mol (SD) and 1.2 ± 0.2 mmol/mol (SD) (red bar = standard deviation), respectively. The color code of the data points is taken from Figure 5.3. The dashed lines mark the envelop of the sample scatter < 2000 m water depth. Critical depth (grey) and CSH mark the water depths, below which preferential Mg dissolutions starts and where the calcite saturation is below 0, respectively. The red lines mark the calculated critical depth and blue crosses mark corrected Mg/Ca ratios following Regenberg et al. (2006). The samples from water depths >4500 m are not included in the calibration data set.*

5.3.1.4 Habitat correction

N. dutertrei

In the literature different calcification depths for *N. dutertrei* between surface waters and 150 m depth have been suggested. The shallowest depths of 0 to 20 m were obtained from plankton tows by Schmuker and Schiebel (2002) in the Caribbean. This was supported by analyzing stable isotopes and trace elements by Deuser et al. (1981) and Dekens et al. (2002), respectively. On the basis of sediment trap analyses, Anand et al. (2003) inferred a calcification depth of 75 to 100 m in the Sargasso Sea. This was supported by a study of Steph et al. (2009) in the Eastern Tropical Atlantic. The study of Regenberg et al., 2006 suggested 80 to 190 m for the Caribbean supported by an early study of Hemleben et al. (1989). A number of studies indicate that *N. dutertrei* is a thermocline dweller and its habitat depth ranges between 50 and 100 m water depth. The thermocline depth varies between 50 and 75 m in the Gulf of Guinea (Figures 5.1 C and 5.5 C). To consider possible spatial variations of depth habitat, we calculated δ^{18}O-based calcification temperatures of *N. dutertrei* for 50, 75 and 150 m (Table 5.1). *N. dutertrei* is suggested to calcify during summer between June and September. This is most likely controlled by nitrate concentrations, which varies along the section along 2.5°N during this season (Figure 5.5 D) thus limiting the growth of phytoplankton which is the main food source for *Neogloboquadrina* species (Hemleben et al., 1989 and references therein). Between 7 and 12°W and between 0 and 10°E nutrient rich deeper subsurface waters reach shallower depth. The nutrient concentration can indirectly influence the habitat depth of the non-spinose species *N. dutertrei*, thus we assume shallower habitat depth where nutrient concentrations are higher in shallower depth. Between 20 and 12°W and 7 and 0°W the nutrient concentrations are higher in deeper colder waters, possibly suggesting a deeper habitat depth of *N. dutertrei* of between 100 and 150 m water depth.

G. crassaformis

Few studies have been so far carried out on the calcification depth of deep dweller *G. crassaformis*. The values range from 125 to 800 m water depth. A study of Steph et al., 2009 suggests calcification depths of 400 to 450 m in the Eastern Tropical Atlantic, whereas Elderfield et al. (2002) assume shallower calcification depths of 300 to 450 m in the North Atlantic. The deepest calcification depths (500 to 800 m) were determined in a sediment trap study in the Sargasso Sea (Anand et al., 2003). Depths between 200 and 300 m were found by

Schmuker and Schiebel (2002) by analyzing plankton tows in the Caribbean and are supported by calculations of Regenberg et al. (2006). In general *G. crassaformis* is assumed to calcify below the photic zone in 125 to 200 m water depth (Ravelo and Fairbanks, 1992) and behave similar to *Globorotalia truncatulinoides* (Hemleben et al., 1989) with an average calcification depth of 250 m (Ganssen and Kroon, 2000). According to the analyzed $\delta^{18}O$-based temperatures of our core top calibration we assume a habitat depth of between 300 and 400m.

In summary, we assume habitat depth ranges of *N. dutertrei* and *G. crassaformis* between 75 and 150 m and 300 and 400 m water depth, respectively. On this basis, we calculated the $\delta^{18}O$-based calcification temperature using the analyzed $\delta^{18}O$ and salinity at the respective water depth (Figure 5.2). The relationship between analyzed multi-species Mg/Ca and $\delta^{18}O$ calcification temperatures of our study is described by the following exponential equation (Figure 5.2):

$$Mg/Ca = 0.50e^{0.077*T} \ (R^2=0.87). \qquad (5.9)$$

The relatively large variation of Mg/Ca, particularly those of *N. dutertrei*, for a given $\delta^{18}O$ calcification temperature may arise from seasonally and spatially variable habitat depth of *N. dutertrei*. Thus, we calculated the Mg/Ca-$\delta^{18}O$ temperature calibrations for different assumptions of habitat depth of *N. dutertrei*, whereas *G. crassaformis* is suggested to calcify between 300 and 400 m water depth (Table 5.1). The Mg/Ca ratios of *G. crassaformis* show a much smaller range than *N. dutertrei*. Furthermore, present-day temperature, nutrient concentrations, and salinity do not change significantly across the Gulf of Guinea in water depths below 200 m. We thus do not expect significant changes in the habitat depth of *G. crassaformis* across the study area.

Because the variation of the salinity in these depths is small, the difference of calculated $\delta^{18}O$ calcification temperature is also small (Figure 5.6), indicating that the outcome is less sensitive to the choice of habitat depth between 50 and 150 m. Therefore local calibration provides a robust tool to convert Mg/Ca time series into temperature record.

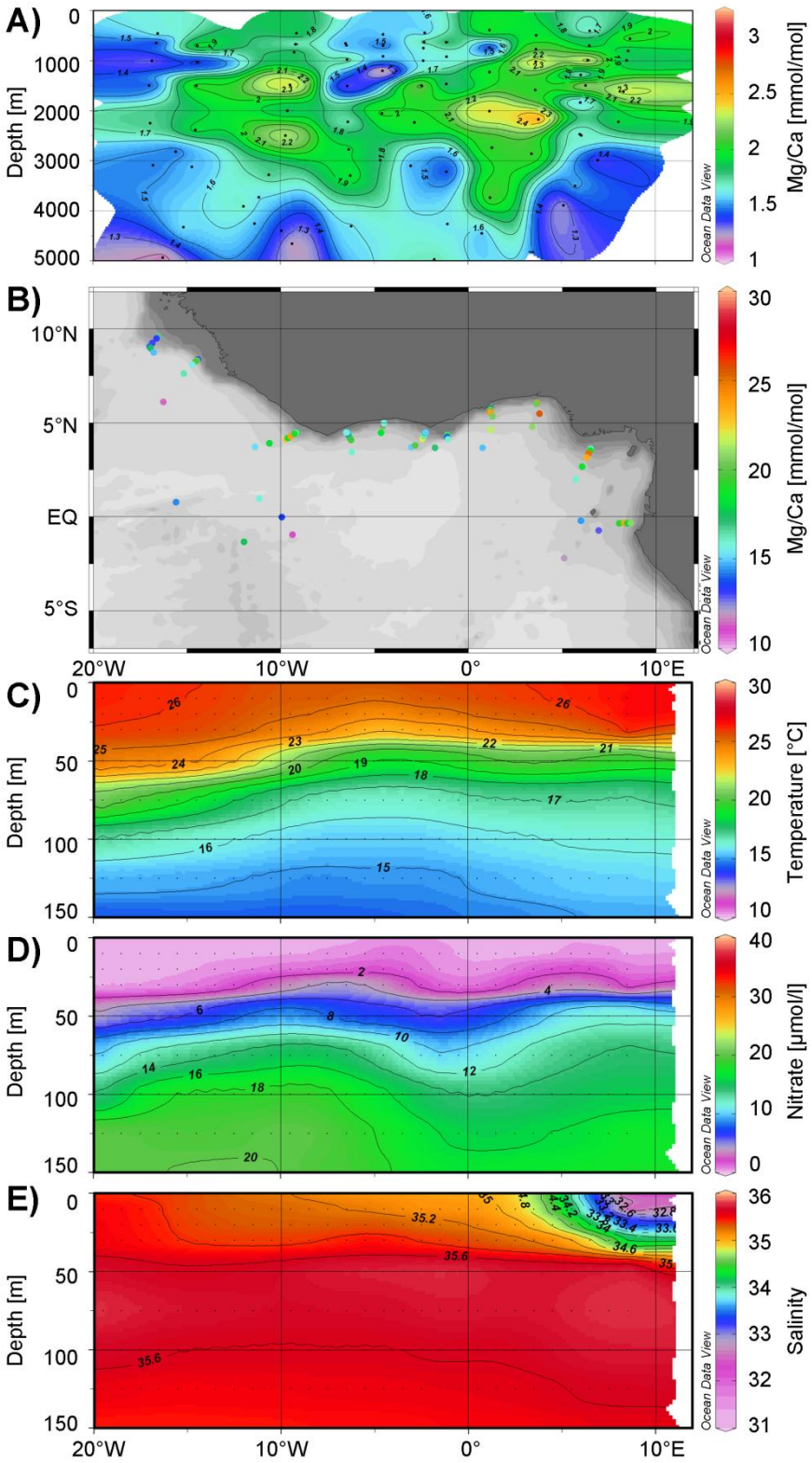

Figure 5.5: *Mg/Ca ratios of N. dutertrei (color code on the right site)* ***A)*** *with corresponding water depth (black dots = core top locations);* ***B)*** *for each location;* ***C)****,* ***D)*** *and* ***E)*** *temperature, nitrate and salinity data taken from WOA09 (Locarnini et al., 2010; Antonov et al., 2010; Garcia et al., 2010) along a transect at 2.5° N from 20° W to 12° E.*

Table 5.1: *Result of different calibrations with different assumptions of habitat depths.*

#	calibration **Mg/Ca =**	**R^2**	**habitat depth** ***N. dutertrei***	**habitat depth** ***G. crassaformis***
1A	$0.4888e^{0.07794*T}$	0.87327	75 m	300 m
1B	$0.4974e^{0.0771*T}$	0.87118	75 m	400 m
1C	$0.5030e^{0.07668*T}$	0.8699	75 m	500 m
1D	$0.5064e^{0.07638*T}$	0.86908	75 m	600 m
Dissolution correction (Regenberg et al., 2006)				
1E	$0.5349e^{0.07431*T}$	0.87094	75 m	400 m
Dissolution correction (Regenberg et al., 2006) and habitat depth correction				
2	$0.5349e^{0.07433*T}$	0.872001	75 + 100 m combination	400 m
3	$0.5350e^{0.07435*T}$	0.872839	75 + 150 m combination	400 m
4	$0.5351e^{0.07433*T}$	0.871935	50 + 100 m combination	400 m
5	$0.5352e^{0.07435*T}$	0.872775	50 + 150 m combination	400 m

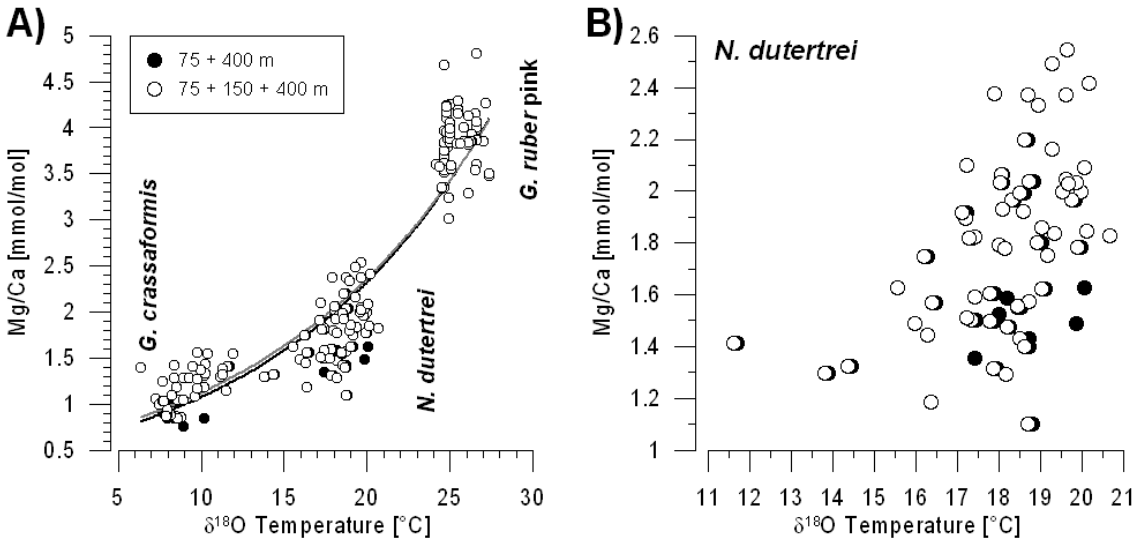

Figure 5.6: A) *comparison core top calibration with Mg/Ca ratios corrected for dissolution effects and habitat depth-corrected $\delta^{18}O$ temperatures;* ***B)*** *zoom of the N. dutertrei data to better visualize the small shift of habitat-corrected $\delta^{18}O$ temperatures towards the calibration line.*

5.3.1.5 Multi-species calibration

Our multi-species calibration, which we applied for our paleo-temperature reconstructions (Table 5.1, # 3)

$$Mg/Ca = 0.54e^{0.074*T} \ (R^2=0.87) \qquad (5.10)$$

plots between that of *N. dutertrei* of Regenberg et al. (2009) and the multi-species calibration of Anand et al. (2003) (Figure 5.7).

The average Mg/Ca-based temperature estimate of thermocline (*N. dutertrei*) using Equation 5.10 developed in this study is 16.0 ± 2.5°C, which closely matches the seasonal average temperature range of the WOA09 sites between 16.8°C and 14.7°C in 75 and 150 water depth (Locarnini et al., 2010). The average annual water column temperatures of 14.9 to 17.3°C between 150 and 75 m water depth observed at WOA09 are slightly warmer.

The average Mg/Ca-based temperature (Equation 5.10) of all analyzed *G. crassaformis* core top samples is 10.1 ± 2.6°C and agrees well with the annual range between 11.0 and 8.9°C of water column temperatures (WOA09) between 300 and 400 m depth (Locarnini et al., 2010).

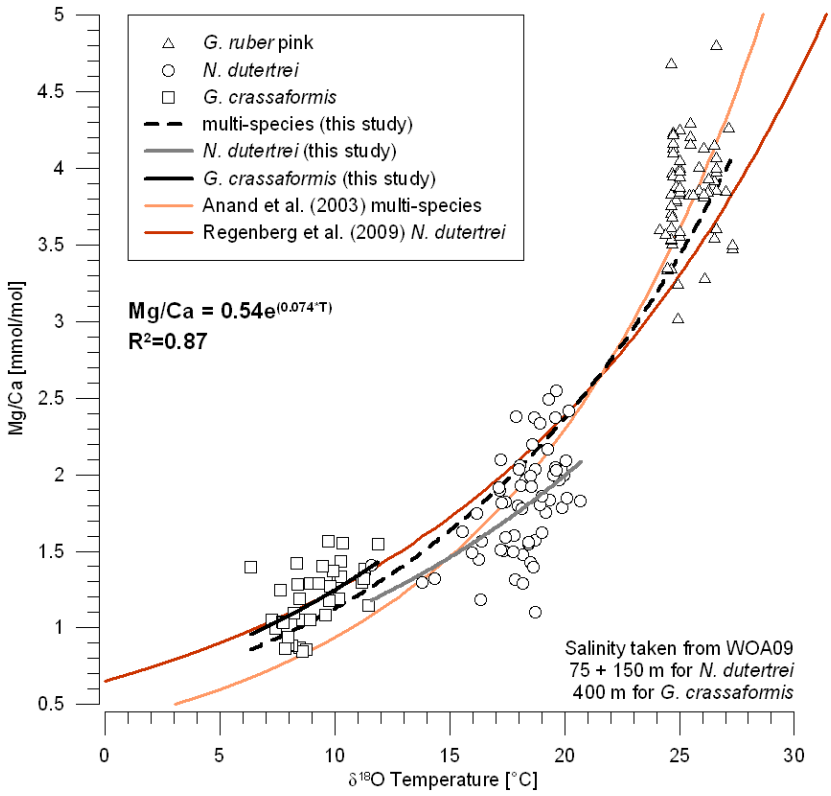

Figure 5.7: *Dissolution corrected (Regenberg et al., 2006) Mg/Ca ratios and habitat depth-corrected $\delta^{18}O$ temperature from the combination of 75 and 150 m habitat depth of N. dutertrei, depending on nutrient distribution, and 400 m habitat depth of G. crassaformis.*

5.3.2 MD03-2707 paleo-record

The core MD03-2707 located in the easternmost Gulf of Guinea has been studied in detail for changes in proxies obtained from surface dwelling foraminifera species G. ruber pink (Weldeab et al., 2007a, 2007b, 2012a, 2012b). In this study we focus on the subsurface water masses and analyze the thermocline and deep dwelling foraminifera species *N. dutertrei* and *G. crassaformis* for paleo-reconstructions of the time period from 60 to 5 kyr BP including Marine Isotope Stage 3 (MIS 3) and the Last Glacial Maximum (LGM).

5.3.2.1 Oxygen ($\delta^{18}O$) and carbon isotopes ($\delta^{13}C$) records

The $\delta^{18}O_{cc}$ values (VPDB) of *N. dutertrei* over the entire record vary between -0.9 and 1.8‰ (Figure 5.8; Appendix Table A5.3). Between 60 and 25 kyr the $\delta^{18}O_{cc}$ values varied between -0.2 and 1.6 ‰. The older (65 - 42 kyr) and last glacial sections of the $\delta^{18}O_{cc}$ record of *N. dutertrei* showed patterns similar to the $\delta^{18}O_{ice}$ record GISP2 (Blunier and Brook, 2001), pertaining the timing and direction of the changes during the Dansgaard-Oeschger (D/O) cycles following the Heinrich Events (H) (Figure 5.8). Most pronounced were the peaks of depleted $\delta^{18}O_{cc}$ values during D/O 12, 14, and 16/17. These peaks showed a rapid $\delta^{18}O_{cc}$ decrease (0.9 to 1.6‰ in 0.6 kyr at the beginning of D/O 12 and 14) and a gradual increase with a duration of 3 to 6 kyr. A trend towards low $\delta^{18}O$ values was evident during D/O 8 and 3/4. Between 27 and 17 kyr the $\delta^{18}O_{cc}$ values were highest and showed little variation. Since Heinrich Event 1 (H 1) the $\delta^{18}O_{cc}$ values decreased continuously, a trend that was interrupted by a drop in $\delta^{18}O_{cc}$ values during the Younger Dryas (Figure 5.8). The $\delta^{18}O_{cc}$ values (PDB) of *G. crassaformis* varied between 1.2 and 3.7‰ (Figure 5.8, Appendix Table A5.4). The lowest values between 60 and 25 kyr corresponded to Heinrich Events 4, 5, 5a and 6 and to the Antarctic Warm Events A 1 to 4. The pattern of the $\delta^{18}O$ record is similar to that of the Byrd ice core $\delta^{18}O_{ice}$ record (Figure 5.8), with gradual decrease and gradual increase of the $\delta^{18}O_{cc}$ values. Furthermore, the Antarctic Cold Reversal (ACR) was also clearly reflected in the $\delta^{18}O_{cc}$ record of *G. crassaformis*. The decrease of $\delta^{18}O_{cc}$ values after 17 kyr resembled the patterns recorded by the Antarctic ice cores but the onset of the decrease lag behind the Byrd record by about 4 kyr (Figure 5.8).

The $\delta^{13}C$ values of *N. dutertrei* vary between 0.9 and 2.1‰ (difference 1.2‰) and the $\delta^{13}C$ record of *G. crassaformis* varies between lower values but with the same amplitude between 0.1 and 1.2‰ (Appendix Tables A5.3 and A5.4). The $\delta^{13}C$ records of *N. dutertrei* and *G.*

crassaformis revealed excursions towards lower values during the Heinrich stadials YD, H1, H3, H4, H5, H5a and H6 (Figures 5.9 C, 5.10 C, 5.11 E and 5.12 E).

5.3.2.2 Mg/Ca and Ba/Ca records

The Mg/Ca-ratios of *N. dutertrei* vary between 1.1 and 2.6 mmol/mol and of *G. crassaformis* between 0.8 and 2.0 mmol/mol (Figures 5.9 B and 5.10 B) over the complete record (Appendix Tables A5.3 and A5.4). Based on these Mg/Ca ratios the temperature estimates range from 9.7 to 21.0°C with an average of 15.6±1.7°C (5.2 and 17.6°C; average 11.7±2.0°C), (Figures 5.11 D and 5.12 D). The temperature reconstruction based on the Mg/Ca data analyzed in *N. dutertrei* tests is interpreted to reflect the temperature history of the lower thermocline. The results of the temperature reconstruction suggested a cooling of the thermocline during D/O events 14, 12 and 8 and a warming during D/O 16/17 and the ACR by up to 3°C on average (Figure 5.11 D). The record showed a general warming of the thermocline during the last 15 kyr with colder phases during H1 and YD. The temperature record of the water column between 300 and 400 m water depth is reconstructed using Mg/Ca ratios of *G. crassaformis*. The record showed pronouncedly elevated temperatures during H2, H4, H5 and H5a (Figure 5.12 D).

The average Ba/Ca ratios of the down core samples of *N. dutertrei* are higher (6.4 µmol/mol) than those of *G. crassaformis* (3.5 µmol/mol) (Appendix Tables A5.3 and A5.4). The average value of the down core *G. crassaformis* samples is similar to the core top Ba/Ca ratio of 3.2 µmol/mol, whereas the Ba/Ca ratios of *N. dutertrei* are much lower in the core top samples (average 2.1 µmol/mol) than in the down core record. The core top Ba/Ca ratios show no correlation with water depth < 4500 m (Appendix Figure A5.5). The down core Ba/Ca record of *N. dutertrei* is characterized by high frequency variation and does not show any co-variability with other parameters analyzed for the same species (Figures 5.9 and 5.11). In contrast, high Ba/Ca in the down core record of *G. crassaformis* correlates with negative $\delta^{13}C$ values, high Mg/Ca ratios and enriched $\delta^{18}O_{cc}$ values during H5a, H5, H4 and H2 (Figures 5.10 and 5.12). Conversely, during the D/O 8, 12 and 13 the subsurface water was characterized by relatively depleted $\delta^{18}O_{cc}$ values, low Mg/Ca ratios, relatively heavy $\delta^{13}C$ values and low Ba/Ca.

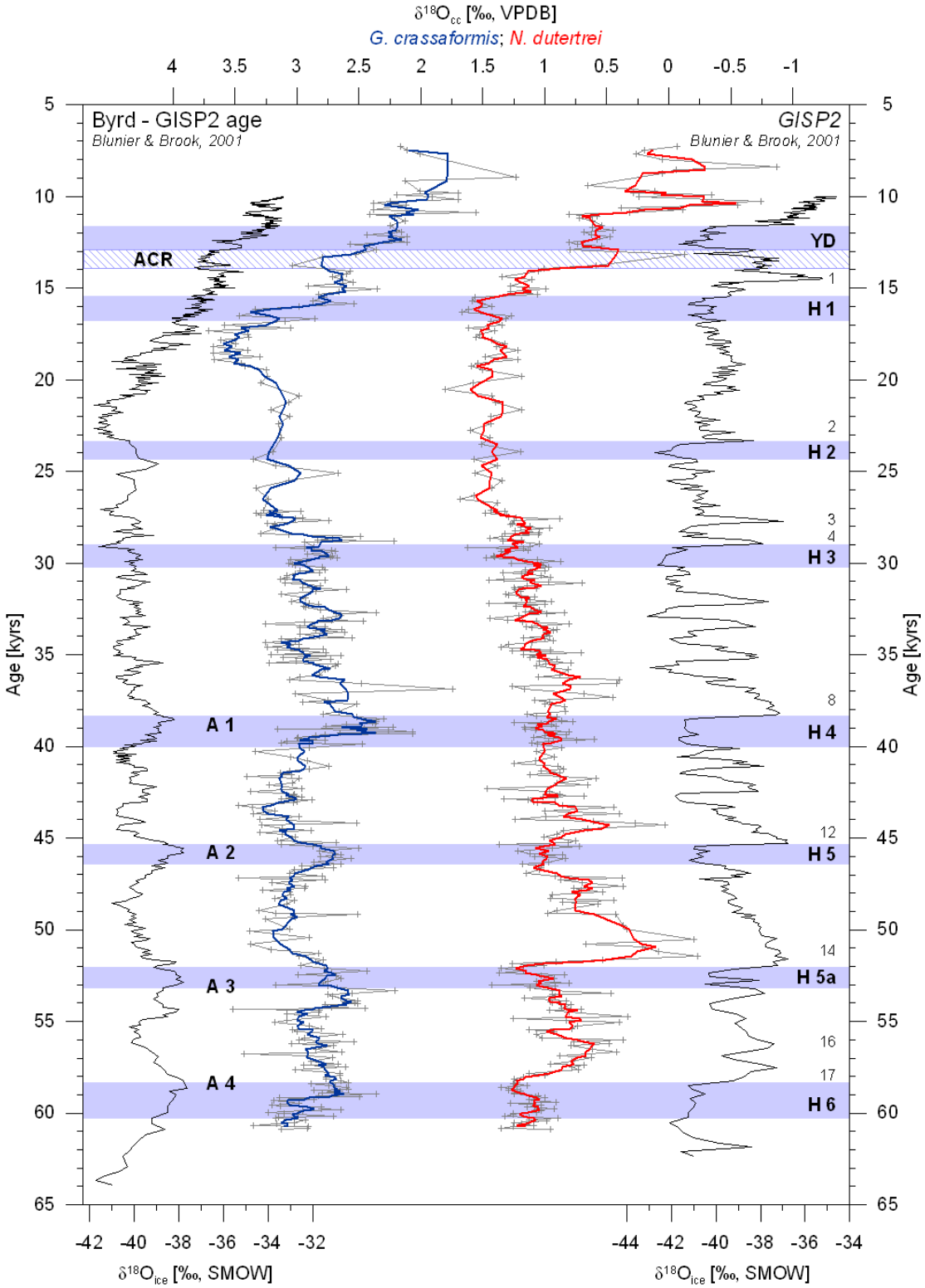

Figure 5.8: *$\delta^{18}O_{cc}$ (VPDB) of N. dutertrei and G. crassaformis (grey lines = all results, 3-point average <27 kyr and 5-point averages >27 kyr in red and blue, respectively) compared to $\delta^{18}O_{ice}$ records from Greenland (GISP 2) and Antarctica (Byrd). Blue bars indicate stadial time intervals of Heinrich Events (H, numbers on the right site of the figure mark longer lasting interstadials (Dansgaard-Oeschger Events) and on the left site Antarctic warm phases are marked (A). YD = Younger Dryas; ACR =Antarctic cold reversal (blue hatched bar).*

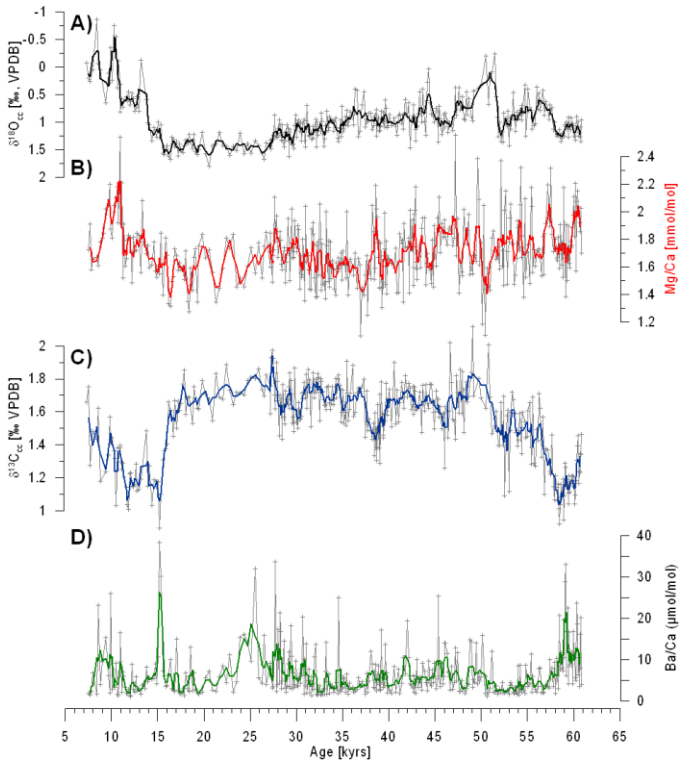

Figure 5.9: A) *$\delta^{18}O_{cc}$ (VPDB),* ***B)*** *Mg/Ca ratios,* ***C)*** *$\delta^{13}C_{cc}$ (VPDB) and* ***D)*** *Ba/Ca analyzed in N. dutertrei from MD03-2707 plotted versus age (Age model from Weldeab et al., 2007a, 2007 b; Weldeab 2012a, 2012b).*

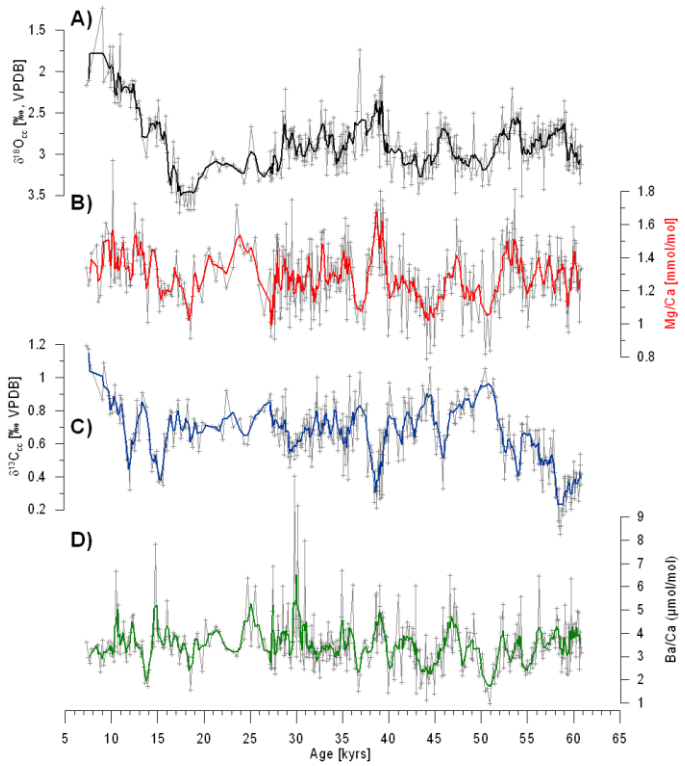

Figure 5.10: A) *$\delta^{18}O_{cc}$ (VPDB),* ***B)*** *Mg/Ca ratios,* ***C)*** *$\delta^{13}C_{cc}$ (VPDB) and* ***D)*** *Ba/Ca analyzed in G. crassaformis from MD03-2707 plotted versus age (Age model from Weldeab et al., 2007a, 2007 b; Weldeab 2012a, 2012b).*

5.4 Discussion

5.4.1 Paleo-salinity reconstructions - oxygen isotopes ($\delta^{18}O_{ivf\text{-}sw}$; SMOW)

The $\delta^{18}O_c$ values (VPDB) of the foraminiferal calcite reflect both past temperature and the $\delta^{18}O$ value of the water, which itself is controlled by salinity and the global ice volume. To reconstruct changes of salinity the $\delta^{18}O_{cc}$ values (VPDB) were corrected for temperature and ice volume effect (Section 5.2.1). Consequently, high $\delta^{18}O_{ivf\text{-}sw}$ (SMOW) values depict high salinity. The relationship between the $\delta^{18}O_{sw}$ of seawater and salinity varies regionally, as well as on different timescales, with the shallowest $\delta^{18}O$-based salinity slope found in low latitudes (Fairbanks et al., 1992; Schmidt, 1999; LeGrande and Schmidt, 2006). This may provide information about water mass mixing and evaporation/precipitation conditions at the source region of a water mass.

Thermocline waters (STUW)

Salinity reconstructions based on $\delta^{18}O_{cc}$ of *N. dutertrei* show decreased salinity (lowest $\delta^{18}O_{ivf\text{-}sw}$ values) during interstadials D/O 16/17, 14, 12, 8, H2 and the ACR (Figure 5.11) and the highest $\delta^{18}O_{ivf\text{-}sw}$ values during Heinrich Events 3, 4, 5, 5a and 6. During the ACR the $\delta^{18}O_{ivf\text{-}sw}$ values were lower than during the YD (Figure 5.11 C).

SACW

Reconstructions based on $\delta^{18}O_{cc}$ of *G. crassaformis* show fresher SACW waters during the YD and the Heinrich Events (H 1 to H 6) and Antarctic Warm Events (A 1 to 4) (Figure 5.12 C). A pronounced freshening occurred around 37 kyr during D/O 8. Overall, the freshest waters were present during the D/O 8, 12 and 14. During the Antarctic Warm events A 1 to 3 the salinity was highest. The salinity was also high during D/O 16/17 and 3/4 H2, H1 and the ACR.

The $\delta^{18}O_{ivf\text{-}sw}$ pattern of *N. dutertrei* is consistent with $\delta^{18}O_{ivf\text{-}sw}$ of *G. ruber* pink (Weldeab, 2012a). The heaviest $\delta^{18}O_{ivf\text{-}sw}$ values were found during Heinrich Events H3, H4, H5, and H5a and the lightest ones during the interstadials, except D/O 3/4. The oscillations of $\delta^{18}O_{ivf\text{-}sw}$ in the surface waters were interpreted as changes in river runoff and/or in the $\delta^{18}O$ of the precipitation in the river catchment area (Weldeab, 2012a). The source region of the thermocline water mass is located in the tropics at about 12°S were subsurface waters with maximum salinities are formed (Figure 1.3; Stramma and England, 1999). Thus, either the salinity of this water mass changed with shifts of the rain belt related to the movement of the

ITCZ or the STUW freshened by upwelling and mixing with fresher deeper water masses, like the SACW. The records of *N. dutertrei* and *G. crassaformis* show comparable patterns with highest $\delta^{18}O_{ivf\text{-}sw}$ values observed at the beginning of Heinrich Events H6, H5a, H5 and H4, however the record of *G. crassaformis* is leading. This suggests mixing of both water masses. The highest salinities were found during the warmest phases in Antarctica, possibly caused by an increased Agulhas leakage and influx of saline waters from the Indian Ocean. At the present day, warming over the Southern Ocean leads the westerlies, as well as the related subtropical front (STF) to shift southward resulting in a widening of the distance between the tip of South African and the STF and thus to an increase of Agulhas leakage and an enhanced influx from the Indian Ocean (Biastoch et al., 2009). Maximum leakage in the past occurred during terminations (Peeters et al., 2004). Variations in the strength of the Agulhas leakage and thus changes in inter-basin flux from the Indian Ocean into the Atlantic has been suggested to strongly influence the AMOC as a consequence of the heat and fresh water additions (Biastoch et al., 2008, 2009; Beal et al., 2011 and references therein).

5.4.2 Temperature and source changes

Modern temperatures at WOA09 site 23217 (white star in Figure 5.1 A) range from 16.8 to 15.1°C (July - September) in water depths between 75 and 150 m and from 10.8 to 8.8°C in 300 and 400 m water depth (Locarnini et al., 2010) with differences of 6°C (8°C) between 75 and 300 (400 m) water depth. The core top samples (*N. dutertrei* - *G. crassaformis*) show a Mg/Ca-based temperature difference of 6.4±3.2°C (SD) using our multi-species calibration (Equation 5.10). Comparable results are achieved applying the *N. dutertrei* and multi-species calibrations of Regenberg et al. (2009) and Anand et al. (2003) of 7.3±3.6°C (SD) and 5.3±2.6°C (SD), respectively. A significantly larger difference of 9.9±3.5°C (SD) results from applying the single species Mg/Ca-T(δ^{18}O-based) relationships (Figure 5.7). Down core the temperature difference between *N. dutertrei* and *G. crassaformis* varies between -2.7 and 11.3°C, suggesting realistic estimates of the past water temperatures by applying the multi-species calibration of this study.

STUW - thermocline

The trace elemental and isotopic composition of *N. dutertrei* reflects changes in the thermocline, which in the Gulf of Guinea occupies water depth between 50 and 100 m (Figures 5.1 C and 5.5 C). The patterns observed in the *N. dutertrei* data resemble other records in the northern hemisphere (e.g. the Greenland ice cores). High $\delta^{18}O_{cc}$ values

correspond to Heinrich Events and low $\delta^{18}O_{cc}$ values to the D/O warm events (Figure 5.8). These climate changes are linked with the tropics by shifts of the ITCZ and the complete wind systems including the trade winds influencing the source region of the STUW in the tropics.

The Mg/Ca-based temperatures in the thermocline indicate a cooling of the thermocline during the transition from Heinrich Events to D/O events 14, 12, 8 and 4 when the northern hemisphere was warm. Contemporaneously, salinity decreased. Conversely, an increase in salinity and relative warm thermocline waters are inferred during H5a, H5, H4, and H2. The thermocline also warmed during D/O 16/17, D/O 2 and the ACR (Figure 5.11) thus showing a temperature pattern opposite to the other D/O events, for which warmer temperatures during the interstadials than during the stadials are indicated.

At least since the temperature minimum during H1 the thermocline has overall warmed with a disruption during the YD which occurred synchronously with a cooling in northern high latitudes. The temperature of the thermocline seems to have been influenced by the northern hemisphere prior to 55 kyr and after 15 kyr. Between 55 and 15 kyr the thermocline temperature variability follow that of SACW and Antarctica (Figures 5.11 D and 5.13 B). This may have been caused by upwelling and mixing with deeper water masses.

Concomitant with the cooling of the thermocline during the interstadial D/O events, surface waters warmed (Weldeab, 2012b) and subsurface waters cooled as indicated by Mg/Ca in *G. crassaformis* (see below). In contrast, the warming of the subsurface waters during the Heinrich events encompassed the entire water column between the surface and 400 m depth.

SACW

The trace element and isotopic compositions of *G. crassaformis* reflect South Atlantic Central Waters (SACW), which in the Gulf of Guinea occupies the water depth between 100 and 500 m (Figure 5.1 C). The patterns of the changes resemble those of the Southern Hemisphere (Antarctic ice cores). Low $\delta^{18}O_{cc}$ values correspond to Antarctic Warm Events (Figure 5.8). The decrease of $\delta^{18}O_{cc}$ values after 17 kyr resembles the changes recorded by the Antarctic ice cores but the onset of the decrease lags the Byrd record by about 4 kyr (Figure 5.8). A lag in onset of changes in $\delta^{18}O_{cc}$ values can be caused by the long distance between Antarctica and the tropics which has to be passed and by the way of transport. The transport of a signal via the ocean currents might be slower than via atmospheric circulation.

The Mg/Ca-based temperature record of *G. crassaformis* shows a gradual increase during periods of Antarctic warming (A1 to A4, Figure 5.12) given by the $\delta^{18}O_{ice}$ (SMOW) record of

the Byrd ice core. Lowest temperatures occurred during D/O 14, 12, 8 and ACR (Figure 5.12 D). The temperature record of *G. crassaformis* thus resembles that of Antarctic ice cores and consequently reflects changes in the source region of the water mass at higher southern latitudes at about 40° S (Figure 1.3; Stramma and England, 1999).

The thermocline (*N. dutertrei*) temperatures show patters very similar to SACW between 55 and 35 kyr (Figure 5.13 B). Upwelling of deeper waters and mixing most likely decreased the temperature of the thermocline. Heinrich Event H3 and D/O 3/4 are not apparent in both temperature records. Between 26 and 18 kyr the temperature records of *N. dutertrei* and *G. crassaformis* are almost anti-correlated (Figure 5.13 B). Thermocline temperatures decreased during H 2, whereas the SACW temperatures increased significantly. The thermocline reflects the cooling of the northern high latitudes while the SACW was controlled by the warming over Antarctica. Since 18 kyr the temperatures have increased in both water masses, with slightly decreased temperatures during H 1 at both water depths and lower temperatures of *G. crassaformis* during the Antarctic cold reversal (ACR) and of *N. dutertrei* during the Younger Dryas (YD). The modeling study of Chang et al. (2008) investigating the link between abrupt changes in the North Atlantic Ocean and the African monsoon suggested that during cold periods in the northern hemisphere (especially Heinrich Events) the thermohaline circulation was weak and the deep water formation decreased, which leads to enhanced stratification of the water column and cold water can be trapped near the surface. This may have caused a warming beneath the surface (Chang et al., 2008) leading to a discrepancy between *G. crassaformis* showing warmer temperatures and *N. dutertrei* showing colder temperatures, in particular between H2 and YD (Figure 5.13 B).

5.4.3 Thermocline movement estimated by Mg/Ca-based temperature differences

To estimate the vertical movement of the thermocline, we compared the Mg/Ca-based temperatures of the surface dwelling species *G. ruber* pink (Weldeab et al. 2007a; Weldeab 2012b) with those obtained from the thermocline dweller *N. dutertrei* and the deep dweller *G. crassaformis*. Large temperature differences suggest a shallow thermocline, whereas small differences imply a deeper thermocline (Figure 5.13 B).

The difference between recent sea surface temperatures (SST, July-September) and thermocline temperatures (TT, annual) in 75 m water depth is about 8.6°C (WOA09 site 23217, Locarnini et al., 2010). The average Mg/Ca-based temperature difference over the complete down core record between *G. ruber* pink (Weldeab et al., 2007; Weldeab 2012b)

and *N. dutertrei* is 8.5±1.8°C (SD), suggesting a reliable paleo-temperature record. The difference between SST (July-September) and water temperatures in 300 m (400 m) water depth (annual) is about 16°C (18°C) (WOA09 site 23217, Locarnini et al., 2010). The down core record suggests lower average temperature differences of about 12.4±2.1°C (SD). This discrepancy may be caused by temperature oscillation in the deeper water masses, with more frequent periods of warmer than colder SACW compared to today. This leads to higher average temperatures covering the last 60,000 years compared to a today temperature average covering only variations of few years in water depths of 300 to 400 m.

The shoaling of the thermocline during D/O 14, 12 and 8 was associated with cooler temperatures and reduced salinity of both water masses. During those periods, the temperatures over Antarctica decreased and temperatures at the source region of the SACW cooled as well. Thus we argue that during these periods the water mass mixing was associated with the thermocline shoaling, which was most likely caused by intensification of equatorial winds and the trade winds. Hessler et al. (2011) suggested an intensification of coastal upwelling due to enhanced trade winds and the increased northward intrusion of cold Benguela Current waters during the period of time between 50 and 25 kyr in the Angola Benguela Front/ Benguela Current system. On the other hand Wolff et al. (1999) suggested that the thermocline fluctuations in the eastern equatorial Atlantic were primarily driven by the intensity of the W-African monsoon and changes in insolation in the low latitudes. However, the shallowest thermocline observed by the highest temperature differences, lowest salinities and coolest temperatures during D/O 14, 12 and 8 (Figure 5.13 B) occurred contemporaneously with low $\delta^{18}O_{sw}$ values and peaks in Ba/Ca ratios (enhanced precipitation) of *G. ruber* pink (Weldeab, 2012a) suggesting a contribution of surface stratification.

5.4.4 Ba/Ca

All species of foraminifera studied to date incorporate Ba into their shells depending on the Ba concentration of the ambient seawater (e.g. Lea and Boyle. 1991; Lea and Spero, 1994). The Ba uptake by foraminifera is not influenced by temperature, salinity, pH or symbiontic photosynthesis (Lea and Boyle, 1991; Lea and Spero, 1992, 1994; Hönisch et al., 2011). Thus, past Ba concentrations of seawater can be estimated from Ba/Ca ratios of foraminifera, but potential contamination by authigenic barite can complicate paleo-reconstructions.

The Ba concentration in seawater increases with depth and varies between the different ocean basins (Turekian and Johnson, 1966; Wolgemuth and Broecker, 1970; Bacon and Edmond, 1972; Chan et al., 1977). Furthermore, the location of the study site close to river mouths can be responsible for high Ba concentrations. Some studies in various estuaries analyzed the Ba release from particles and showed Ba concentrations of 176 nmol/kg (Zaire; Edmond, 1978), 270 nmol/kg (Amazon; Dion, 1983), 385 nmol/kg (Ganges; Carroll et al., 1993), and 600 nmol/kg (Chesapeake; Coffey et al., 1997). The Ba concentrations vary with salinity and distanced from the river mouth. For example in the Bay of Bengal the Ba concentrations vary between 54 (offshore) and 430 (river channels) nmol/kg (Carroll et al., 1993; Singh et al., 2013). The maximum values of those studies are similar to the average values of the core top samples in this study of 494 nmol/kg (*N. dutertrei*) and 753 nmol/kg (*G. crassaformis*), which were calculated with a distribution coefficient D_{Ba} = 0.15 (Hönisch et al., 2011). The core top foraminiferal Ba/Ca ratios of this study are higher than reported in some other studies (between 0.6 to 1.0 µmol/mol, including *N. dutertrei* by Lea and Boyle, 1991; 0.7 to 4.1 µmol/mol by Lea and Spero, 1992). Higher Ba/Ca ratios observed for *Globorotalia* species (between 2 and 13 µmol/mol) in the study of Lea and Boyle (1991) were assumed to be caused by a different mode of shell precipitation mechanisms and/or different temperatures and depth of calcification. The range in Ba/Ca ratios of *G. crassaformis* in our study agrees well with the ratios of Lea and Boyle (1991), even without DTPA cleaning, and thus are asserted to be reliable. The study of Weldeab et al. (2007a) did not find evidence for diagenetic influence on samples younger than 120,000 years BP. Thus we did not clean the foraminiferal samples with DTPA which was used in the common cleaning procedure (Boyle and Keigwin, 1985; Lea and Boyle, 1993; Boyle and Rosenthal, 1996; Martin and Lea, 2002).

The high supply of riverine particles and high Ba release occurring in the river mouths may have contributed to the slightly higher Ba/Ca ratios than published in other studies (Lea and Boyle, 1991; Lea and Spero, 1992). Unfortunately, Ba data are available neither for the close-by rivers nor for the seawater at the core site. However, we suggest the Ba/Ca ratios of the core top samples to be reliable, because we expect elevated Ba concentrations close to the river mouth, in particular because the sedimentation rates are high (average of 23.1 cm/kyrs over the entire record) which will result in high levels of Ba release from the riverine particles. Additionally, there is a strong salinity gradient within the upper 50 m of the water column at the study site (Figure 5.1 C). Consequently, we suggest the range of the Ba/Ca

ratios of the core top samples (with maximum values of 6.0 and 6.5 µmol/mol for *N. dutertrei* and *G. crassaformis*) is reliable and can applied for down core interpretation.

The fact that the core top Ba/Ca ratios of *N. dutertrei* are much lower than in the down core samples can be caused by diagenetic overprint and/or by changes in the Ba concentration in the thermocline due to changes in productivity or salinity despite that the other two both species *G. crassaformis* and *G. ruber* pink (Weldeab et al., 2007a; Weldeab 2012a) analyzed from the same samples do not show unusual values. Barite contamination may have increased the Ba/Ca ratios of *N. dutertrei*, which is consistent with the much higher ratios than in the study of Lea and Boyle (1991). The shell structure of *N. dutertrei* is more porous than *G. crassaformis* and may be more susceptible to contamination, but also *G. ruber* has porous shells. Thus, changes in the thermocline may also have played a role for unusually high Ba/Ca ratios of *N. dutertrei*. However, the Ba/Ca record of *N. dutertrei* shows no significant correlations with any of the other analyzed proxies. The Ba/Ca record is thus probably overprinted by contamination and thus, we decided not to interpret the Ba/Ca record of *N. dutertrei* due to ambiguity of the reliability of the values.

The Ba/Ca ratios in combination with $\delta^{18}O$ records of surface dwelling *G. ruber* pink (Weldeab et al., 2007a; Weldeab 2012a) reflect changes in riverine runoff and monsoon precipitation, with high Ba/Ca values corresponding to low $\delta^{18}O_{ivf\text{-}sw}$ values. In the record of *G. crassaformis* high Ba/Ca ratios correlate with high $\delta^{18}O_{ivf\text{-}sw}$ between 55 and 25 kyr, just opposite to the surface water records (Weldeab et al., 2007a; Weldeab 2012a). Furthermore, between 55 and 25 kyr low Ba/Ca ratios of *G. crassaformis* coincided with cold temperatures and reduced salinity. Barium correlates with alkalinity in seawater (Lea and Boyle, 1989; Lea, 1993). Hall and Chan (2004) measured Ba/Ca of benthic foraminifera in the thermocline and intermediate waters in the Caribbean Sea and the Bahama Bank and suggested that the data reflect increased southern sourced water mass contribution during glacial periods. Thus, we argue that the Ba/Ca record of *G. crassaformis* has most likely been controlled by source changes or changes of the conditions in the source region. The high Ba/Ca ratios of *G. crassaformis* correlate with high $\delta^{18}O_{ivf\text{-}sw}$ values associated with high salinity, warm temperatures, and low $\delta^{13}C$ values, during Antarctic warm phases A3 to A1, suggesting increased influence of southern sourced waters and enhanced upwelling processes in the Southern Ocean and mixture with SACW, which is formed in the southern hemisphere subtropical convergence.

5.4.5 Stable isotope $\delta^{13}C$

The $\delta^{13}C$ (VPDB) of foraminiferal calcite in surface and subsurface waters is influenced by a number of factors and it is not easy to isolate information on particular processes, such as $\delta^{13}C$ changes in the ambient water mass due to changes in productivity, stratification and changes in water mass origin.

The $\delta^{13}C$ records of *N. dutertrei* and *G. crassaformis* mostly follow each other closely ($\Delta\delta^{13}C$ = 0.9 ± 0.2 ‰) implying weak $\delta^{13}C$ vertical gradients between the corresponding waters (Figure 5.13 D). The correlation of the $\delta^{13}C$ records of both species suggest that changes in habitat depth did not dominate the records of the other analyzed proxies but that changes in hydrological properties have been recorded, at least during the time period between 55 and 15 kyr. Since the temperature record partly mirrors the trends in $\delta^{13}C$ it is also possible that the foraminifera migrated though the water column and reflect the temperatures and $\delta^{13}C$ values of the ambient water masses. For example high temperatures correspond to low $\delta^{13}C$ values during Heinrich Events H5a, H5, H4 and slightly lower values during H3, whereas lower temperatures correspond to increased $\delta^{13}C$ values during the subsequent interstadials D/O 14, 12, 8 and 4. Both species show similar trends in temperature, salinity and $\delta^{13}C$ during the period between 55 and 15 kyr suggesting increased water mass mixing and thus similar changes of the conditions in both inhabited water depths.

The decrease in $\delta^{13}C$ differences between the thermocline and the deep dweller since 15 kyr can be caused by changes in the nutrient gradient. At the same time a shoaling of the thermocline depth was observed. A core top study from the western equatorial Atlantic suggests a nutrient depletion in the thermocline and a nutrient enrichment in deep waters during glacials and cold substages (Mulitza et al., 1998).

Prominently low $\delta^{13}C$ values were found in both records during H6 around 59 kyr marking the beginning of Marine Isotope Stage 3 and at about 15 kyr (Figure 5.13 D). Both minima were also observed and discussed in other studies (e.g. Spero and Lea, 2002; Pahnke and Zahn, 2005; Piotrowski et al., 2005; Anderson et al., 2009; Niedermeyer 2009; Zuraida et al., 2009; Krueger et al., 2012) suggesting a common global feature. In the Agulhas Basin Krueger et al. (2012) suggested increased NADW export during interglacials and increased AABW influence at the beginning of glacial stages. The de-glacial $\delta^{13}C$ minimum has been suggested to be caused by enhanced upwelling of nutrient rich deep water in the Southern Ocean which transported the chemical signature (e.g. $\delta^{13}C$ of DIC) into the AAIW and the Mode Waters (Spero and Lea, 2002; Anderson et al., 2009). The latter will feed the SACW

and influence the thermocline in the tropical regions. Thus, excursions toward low $\delta^{13}C$ in the *G. crassaformis* record during H5a, H5 and H4 may also have been caused by enhanced upwelling in the Southern Ocean. This is supported by a study by Niedermeyer et al. (2009) off the coast of Senegal where lighter $\delta^{13}C$ during H1 and H4 in benthic foraminifera indicated enhanced influence of southern sourced deep water suggesting a reduced AMOC and northward heat transport within the North Atlantic Gyre. During H1 the AMOC was most likely significantly weaker (McManus et al., 2004) and thus the production of deep water in the North Atlantic reduced. Thus, the southward export of well ventilated water masses (high $\delta^{13}C$ values) to the south decreased and the influence of poorly ventilated water masses (low $\delta^{13}C$) in the deep Atlantic basin increased. At the end of H1 the AMOC strengthened abruptly (McManus et al., 2004) matching the abrupt decrease in $\delta^{13}C$ of both species. Signatures of enhanced upwelling processes of nutrient rich deep waters in the Southern Ocean (de-glacial $\delta^{13}C$ minimum: Spero and Lea, 2002; Anderson et al., 2009) in the Southern Ocean have been transported to the tropical Atlantic subsurface waters via the AAIW and the SACW (mode waters). Furthermore, low $\delta^{13}C$ values are correlated with higher temperatures in the SACW which occurred simultaneously with a warming over Antarctica (A3 and A1). It is suggested that the deep dwelling species *G. crassaformis* resembles changing conditions in the southern hemisphere. The isotopic and temperature records of *N. dutertrei* are also indirectly influenced by changes in the southern hemisphere due to water mass mixing and changes in the thermocline depth, documented by higher temperatures and low $\delta^{13}C$ values during H5a, H5 and H4. The correlation between high $\delta^{13}C$ values and low temperatures in the *G.* crassaformis record are prominent shortly after D/O 14, 12, 8 and 3.

The changes in climate over the Arctic and Antarctica are mirrored in the subsurface tropical ocean due to a teleconnection between high and low latitudes via ocean circulation processes. Climate signals are transported towards the tropics via oceanic currents influencing the subsurface water masses. The signal from the Northern hemisphere is represented in the thermocline, which is also influenced by signals from the south (SACW) transferred by mixing processes induced by upwelling and trade winds.

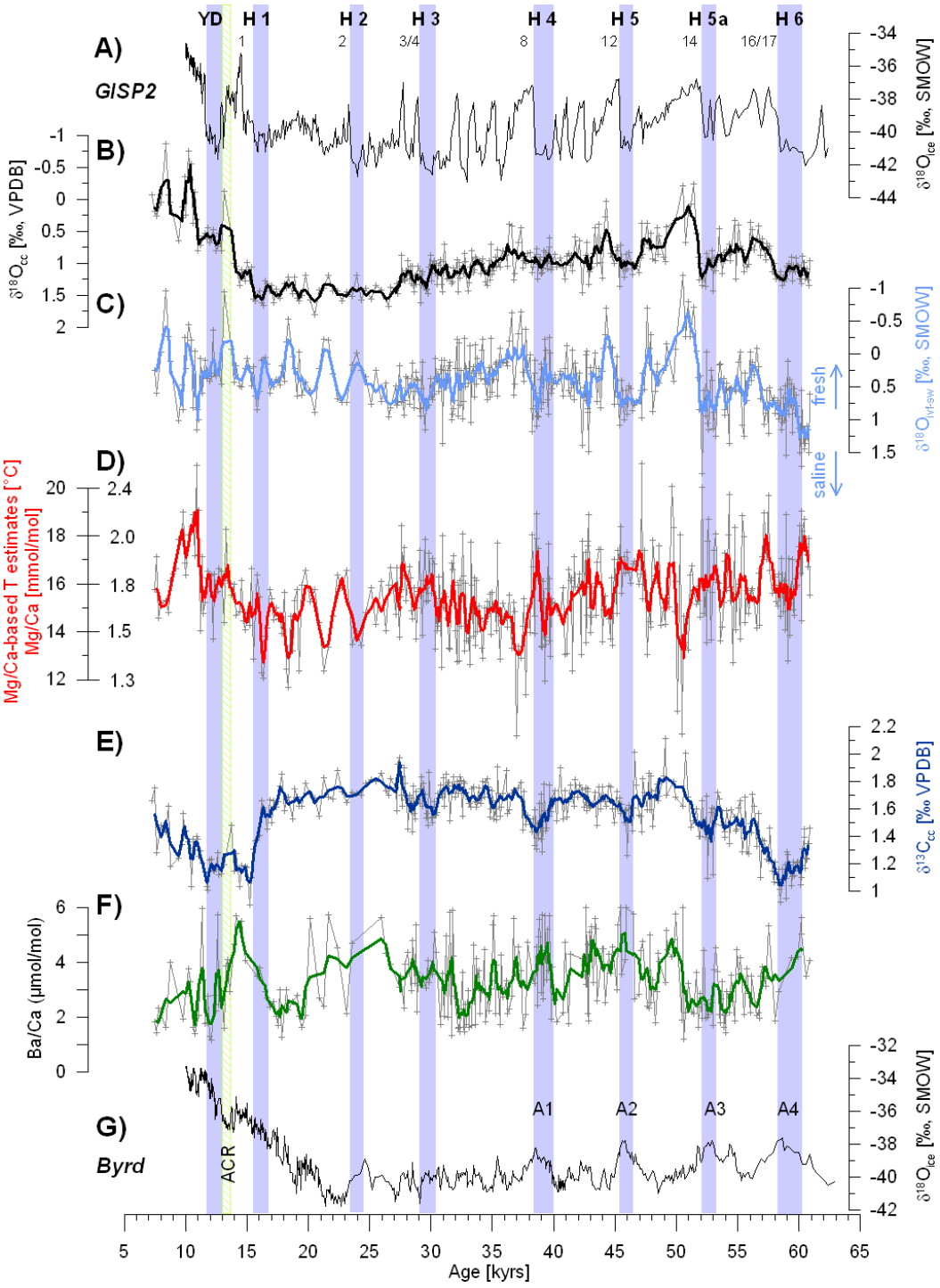

Figure 5.11: N. dutertrei representing thermocline water: B) *$\delta^{18}O_{cc}$ (VPDB),* ***C)*** *$\delta^{18}O_{icf\text{-}sw}$ (SMOW),* ***D)*** *Mg/Ca ratios and Mg/Ca-based temperature estimates,* ***E)*** *$\delta^{13}C_{cc}$ (VPDB) and* ***F)*** *Ba/Ca ratios (< 6 µmol/mol) compared to $\delta^{18}O_{ice}$ (SMOW) ice core records from* ***A)*** *Greenland* ***(****GISP2) an* ***G)*** *Antarctica* ***(****Byrd) (Blunier and Brook, 2001). Blue bars mark stadial time intervals (H = Heinrich Events, YD = Younger Dryas) and the green hatched bar marks the Antarctic Cold Reversal (ACR). The numbers at the top indicate longer lasting interstadials (Dansgaard-Oeschger Events) and on bottom figure G) the Antarctic warm phases are marked (A). Thick colored lines are smoothed: <27 kyr BP = 3-point average, >27 kyr BP = 5-point average.*

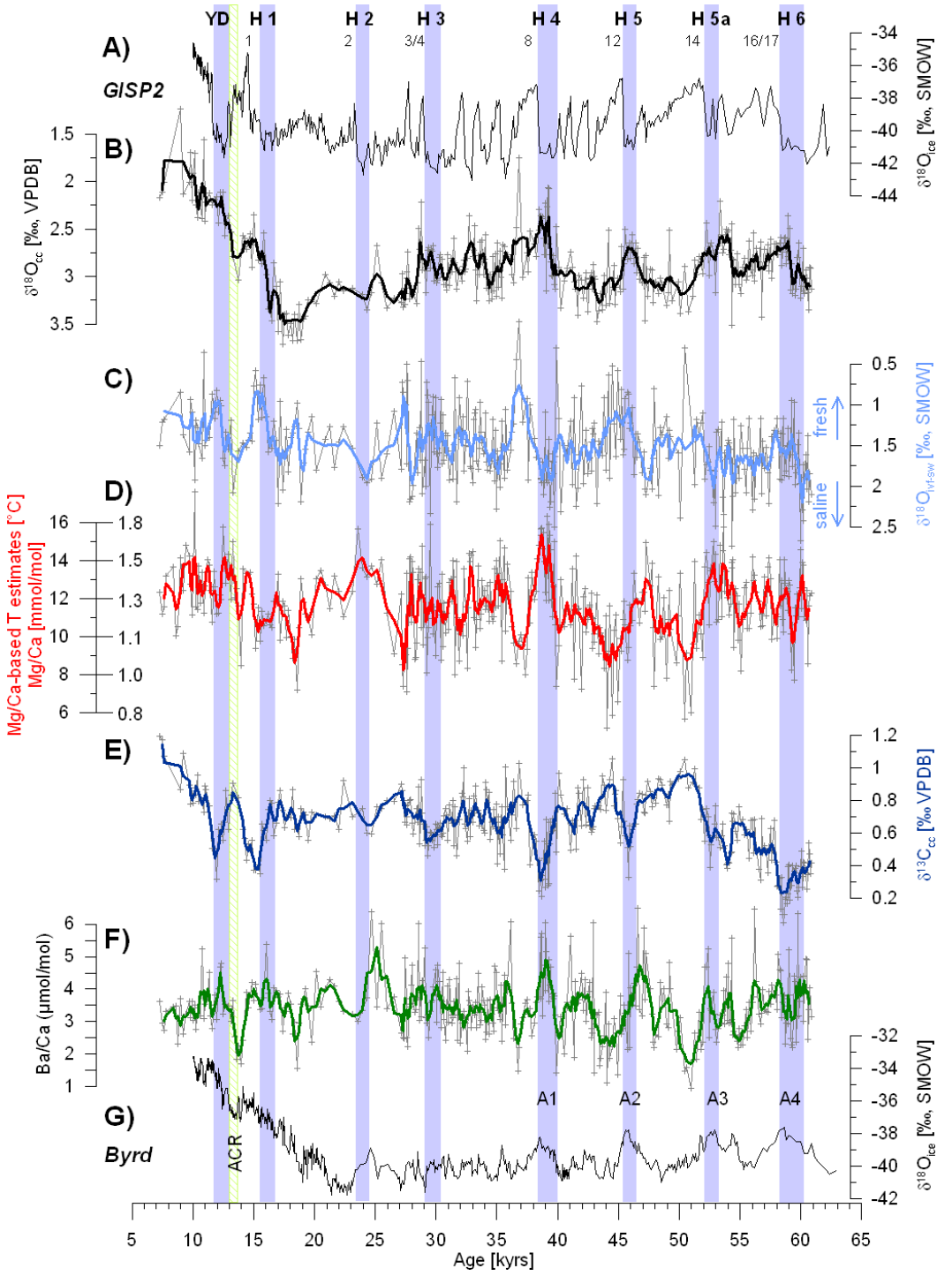

Figure 5.12: G. crassaformis representing sub-thermocline/ intermediate water masses: B) *$\delta^{18}O_{cc}$ (VPDB),* ***C)*** *$\delta^{18}O_{icf\text{-}sw}$ (SMOW),* ***D)*** *Mg/Ca ratios and Mg/Ca-based temperature estimates,* ***E)*** *$\delta^{13}C_{cc}$ (VPDB) and* ***F)*** *Ba/Ca ratios (< 6.5 µmol/mol) compared to $\delta^{18}O_{ice}$ (SMOW) ice core records from* ***A)*** *Greenland* ***(****GISP2) an* ***G)*** *Antarctica* ***(****Byrd) (Blunier and Brook, 2001). Blue bars mark stadial time intervals (H = Heinrich Events, YD = Younger Dryas) and the green hatched bar marks the Antarctic Cold Reversal (ACR). The numbers at the top indicate longer lasting interstadials (Dansgaard-Oeschger Events) and on bottom figure G) the Antarctic warm phases are marked (A). Thick colored lines are smoothed: <27 kyr BP = 3-point average, >27 kyr BP = 5-point average.*

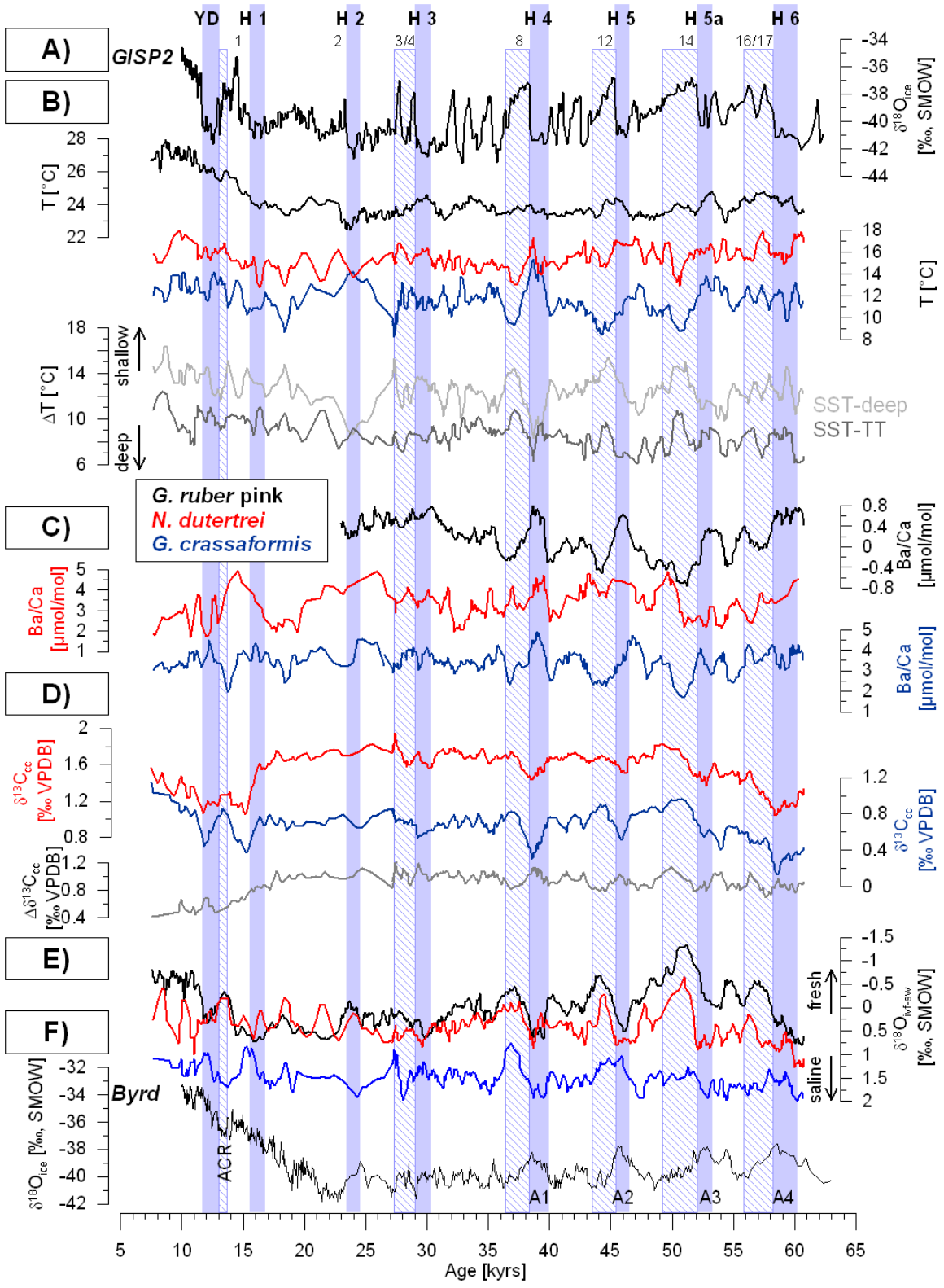

Figure 5.13: ***B)*** *Mg/Ca-based temperatures and ΔT (gray),* ***C)*** *Ba/Ca ratios,* ***D)*** $\delta^{13}C_{cc}$ *(VPDB) and* $\Delta\delta^{13}C_{cc}$ *(VPDB) of N. dutertrei and G. crassaformis (gray) and* ***E)*** $\delta^{18}O_{ivf\text{-}sw}$ *(SMOW) of N. dutertrei (red), G. crassaformis (blue) and G. ruber pink (black) (Weldeab, 2012a, b) compared to* $\delta^{18}O_{ice}$ *(SMOW) ice core records from* ***A)*** *Greenland (GISP2) and* ***F)*** *Antarctica (Byrd) (Blunier and Brook, 2001).*

5.5 Summary and conclusions

This study provide a multi-species Mg/Ca-temperature calibration for the Gulf of Guinea and furthermore, a high resolution temperature and salinity record (average 100 to 200 year interval) from subsurface water masses (< 500 m water depth) covering the last glacial period, as well as the de-glaciation and the early Holocene (60 to 5 kyr).

During D/O stages 14, 12 and 8 cooling of the thermocline as well as the deeper water mass (SACW) were associated with a shallow thermocline, reduced salinity, higher $\delta^{13}C$ values and low Ba/Ca ratios. During these periods the southern hemisphere cooled and the northern hemisphere was warm, implying a southern source of the SACW. Mixing with thermocline waters resulting from upwelling was likely caused by enhanced SE trade winds.

During Heinrich Events and Antarctic warm events both the thermocline and the SACW waters appear to have been warmer and more saline corresponding to a deeper thermocline, low $\delta^{13}C$ values and high Ba/Ca (*G. crassaformis*). The northern hemisphere cooled, the thermohaline circulation was reduced and the thermocline warmed during these periods. Minima in $\delta^{13}C$ values are suggested to indicate enhanced the influence of southern sources waters to the subsurface tropical Atlantic, as they represent upwelling of deeper nutrient rich water masses in the Southern Ocean (Spero and Lea, 2002; Anderson et al., 2009) mixing with the mode waters and transport with the SACW. Furthermore, the minima in $\delta^{13}C$ values match the maxima in Ba/Ca ratios (*G. crassaformis*).

During a large part of the investigated period of time temperature and salinity recorded by the two species followed the same trends reflecting similar conditions in both water masses. This suggests the strong influence of southern waters, strong mixing effects and possibly strong trade winds which resulted in a decrease of the thermocline depth.

At 32 kyr the trends in the different records of *N. dutertrei* and *G. crassaformis* started to diverge. In particular, during H2, H1 and the YD the thermocline cooled and the SACW warmed. Furthermore, the $\delta^{18}O_{ivf\text{-}sw}$ records of both water masses are anti-correlated. This divergence in the records suggests that during those times the influence of southern water masses decreased and attenuated the mixing of the water masses.

Acknowledgements

The core top samples were provided by Wolfgang Kuhnt, University of Kiel. We like to thank Georges L. Paradis and Jen Massey from the Marine Science Institute at University of California Santa Barbara and Nils Andersen from the Leibniz-Laboratory for Radiometric Dating and Isotope Research at the University of Kiel for analyzing the samples. This project was funded by the Deutsche Forschungsgemeinschaft (Project No WE2686/5-1).

Chapter 6

Summary and Conclusions

The first main objective of this study is the reconstruction of the evolution of riverine input into the Gulf of Guinea as a function of glacial-interglacial variations in monsoonal precipitation, as well as water mass mixing during the past 135,000 years. The second main objective is the high resolution reconstruction (100 to 200 years sampling interval) of changes in physical parameters such as temperature and salinity, as well as changes of the sources of subsurface water masses (< 500 m) in the eastern tropical Atlantic. The overall goal was the determination of the linkages between high latitude climate changes and the response of tropical water masses during the past 60,000 years.

To achieve our objectives various proxies (εNd, REE, element/calcium ratios, Mg/Ca, Ba/Ca, $\delta^{18}O$, $\delta^{13}C$) of different authigenic phases (planktonic and benthic foraminifera, sediment coatings, detrital sediments) of core top sediments and one sediment core (MD03-2707) were determined. Furthermore, two different cleaning methods were analyzed to obtain seawater neodymium isotope compositions from foraminiferal shells. In addition, a multi-species Mg/Ca-temperature calibration for the Gulf of Guinea was developed to obtain reliable paleo-temperature reconstructions.

The main conclusions and outcomes of this thesis are summarized below by answering the questions raised in the introduction (Chapter 1).

The following questions and answers summarize the first part of the thesis, consisting of Chapters 3 and 4.

→ How efficient is the cleaning of planktonic foraminiferal carbonates from contaminant phases with regard to extraction of the water mass Nd isotope signature inhabited by the foraminifera and can reliable surface and subsurface water mass neodymium isotope compositions be extracted?

During the extensive method tests the core top foraminiferal carbonates of this study could not be completely cleaned from (ferro)manganese contaminant phases, as documented by element/calcium ratios and REE concentration patterns. Thus, we were not able to obtain

reliable surface seawater neodymium isotope compositions from planktonic foraminiferal shells. Nevertheless, the foraminiferal carbonates provide reliable bottom or pore water signatures.

→ How do the cleaning methods differ?

During the batch cleaning method the foraminiferal samples were cleaned reductively and oxidatively, as well as mechanically in vials, in which the samples remained during the procedure. In contrast, for the Flow Through (FT) cleaning method the samples were rinsed with a continuous flow of the reductive cleaning solution. The proposed advantage of the FT cleaning is the preventing of re-adsorption processes of particle reactive elements back onto the foraminiferal calcite.

Both tested cleaning methods show identical levels of cleaning efficiency. The elemental (Al/Ca, Mn/Ca, Fe/Ca) and Nd isotope ratios analyzed in foraminiferal core top samples of both methods reveal within error identical results in the same samples suggesting that re-adsorption of Nd onto the foraminifera was minimal. Accordingly, we applied the well established batch cleaning method for all further analyses in this thesis.

→ How does the input of the different rivers influence the neodymium isotope compositions of bottom waters and of the authigenic phases of sediments?

All analyzed archives (planktonic and benthic foraminifera, sediment leachates, detrital sediment fractions) of the down core study on core MD03-2707 have in different ways been affected by riverine influence. This is supported by similar trends of all archives with more radiogenic εNd values during the interglacials and less radiogenic values during glacial periods caused by latitudinal migration of the rain belt over the different catchment areas and changes in supply of the dissolved and particulate load of these rivers.

The similarity in the trends of the records of the authigenic phases has probably been caused by pre-formed coatings originating from the surrounding river systems. Those coatings can bias the sediment leachate signature, as a part of the detrital sediments and their coatings originated from the rivers. Pre-formed coatings and riverine particles partially dissolve in seawater and modify the bottom and/or pore water Nd isotope signatures. Thus, also the authigenic signatures extracted from the foraminiferal carbonates can be biased by riverine signatures.

→ How reliable are sediment leachates as recorders of bottom water signatures in river influenced shelf settings? What does the sediment leachate record tell us?

The applicability of Nd isotope compositions of bulk sediment leachates to reconstruct bottom water compositions can be complicated by contribution from pre-formed coatings originating from the rivers and/or through modification of bottom and/or pore waters by partial dissolution of the riverine particles.

This study shows a shift in sediment leachate Nd signatures toward riverine signatures, depending on their location. Thus, in such a strongly riverine influenced setting like our study site sediment leachates cannot be reliably used for reconstructions of water mass Nd isotope compositions. However, in combination with the records of the detrital sediment fraction changes in inputs from the nearby rivers can be reliably reconstructed, given that the leachates most likely represent a mixed signal from bottom and pore water, rivers and the shelf.

→ What are the factors influencing the detrital sediment record?

The record of the neodymium isotope composition of the detrital sediment fraction reflects changes in riverine input caused by movement of the rain belt and the intensity of the precipitation over the catchment areas of the various river systems. The sedimental input from the different rivers is to some extent mixed with sediments transported by currents and is also influenced by changes in sea level and thus in nearby shelf exposure and erosion.

→ What is the information potential of foraminiferal records?

The foraminiferal neodymium isotope composition provides a useful tool to reconstruct bottom or pore water signatures, caused by changes in origin of the water masses, riverine influence, redox-conditions, oxygen concentration and export productivity during glacial-interglacial cycles. Element/calcium ratios and REE pattern imply that planktonic foraminifera acquire REEs during early diagenetic processes. The results of samples close to the Niger show an agreement between Nd isotope signatures of planktonic foraminifera and bottom water data (Bayon et al., 2011). In the paleo-records of MD03-2707 the patterns of the Nd isotope signatures of foraminiferal shells and sediment leachates are similar. Thus, the foraminiferal shells are supposed to reflect bottom or pore waters with contribution of riverine signatures, similar to sediment leachates, though without being influenced by further

redox reactions deeper in the sediment, as the original coating signature is 'locked in' the secondary Mn-carbonates (Roberts et al., 2012).

→ Outlook

To improve studies dealing with different cleaning methods to obtain neodymium isotope compositions from foraminiferal calcites, we recommend further tests with various reductive solutions.

Furthermore, we recommend further studies at other sites with variable sedimentary environments, where the water masses and the continental rocks differ more significantly in their Nd isotope compositions than at the Niger site. In particular, sites with significantly different dissolved surface and deep water Nd isotope signatures should be investigated in detail.

Further studies should include parameter analyses of water column profiles and surface seawater signatures at the same sites in the Gulf of Guinea and from different water depths. Additional proxies, such as $\delta^{13}C$, Cd/Ca and U/Ca should be applied on the foraminiferal carbonates in order to prove our findings and help to disentangle the different possible origins of the neodymium isotope signatures. Furthermore, the gap in the paleo-data set around termination II should be closed to reconstruct the conditions of this de-glacial phase and to compare the results with termination I.

The following questions and answers summarize the second part of the thesis (Chapter 5).

→ How did temperature and salinity in subsurface waters in the tropics vary between 60,000 and 5,000 years BP? How were those changes in water mass parameters linked to high latitude climate oscillations?

Based on the records of the oxygen isotope compositions of *N. dutertrei* and *G. crassaformis* the changes in the thermocline waters resemble the patterns of Greenland ice cores, whereas the SACW variability is comparable to the Antarctic ice core records.

Between 60,000 and 32,000 years ago the records of the thermocline and the SACW follow the same trends. During D/O events both water masses cooled, show reduced salinity, and the thermocline was shoaling coinciding with cool climate trends in the southern hemisphere and a warm northern hemisphere. During Heinrich Events and Antarctic warm phases both water masses warmed, became more saline and the thermocline deepened contemporaneously with

a cool northern hemisphere. During such phases the thermohaline circulation is supposed to be reduced causing a thermocline warming. The similarity of the records of both water masses suggests enhanced influence of southern sourced waters and enhanced mixing processes as a result of upwelling probably caused by enhanced trade winds. This increase in influence of southern sourced waters in the tropical Atlantic is also supported by the match of minima of carbon isotope ratios with Ba/Ca maxima of *G. crassaformis*.

Since 32,000 years BP ago the records of the foraminiferal species *N. dutertrei* and *G. crassaformis* have diverged. This was particularly pronounced during Heinrich Events; the thermocline cooled and the SACW warmed. The salinity reconstructions are anti-correlated. This implies a reduction of the influence of southern water masses and attenuated mixing between the thermocline waters and SACW.

→ What caused the changes in depth and temperature of the thermocline during the past 60,000 years?

Changes in the depth of the thermocline in the tropics can be caused by changes in upwelling which is mainly driven by equatorial and trade winds. Another possible factor causing thermocline fluctuations is the intensity of the West African monsoon and changes in insolation in low latitudes (Wolff et al., 1999). The temperature fluctuations of the thermocline were most likely influenced by the underlying SACW and mixing processes and associated influence of southern sourced waters during the time period between 60,000 and 32,000 years. Furthermore, the reduced thermohaline circulation during Heinrich Events may have been cause for a warming of the thermocline. Changes in near surface water stratification also played a role for changes in temperature and thermocline depth. At 32,000 years the records of the thermocline and the SACW started to diverge, suggesting decreasing influence of the southern sourced waters to the thermocline waters due to reduced mixing processes.

→ What was the consequence of increasing influence of southern sourced waters in the tropical Atlantic during the last glacial?

Caused by enhanced mixing processes and increasing strength of the trade winds a strong influence of southern sourced waters was the reason for similar conditions in both subsurface water masses as suggested by temperature and salinity records of the thermocline and the SACW.

→ Outlook

Similar analyses of a second core at an open ocean site could prove our findings and provide more detailed insights into the spatial evolution of the different water masses in the Gulf of Guinea. Additional proxy analysis of planktonic foraminifera inhibiting water depth deeper than *G. crassaformis* and of benthic foraminifera would complement the records of this study and the surface analyses (Weldeab et al., 2007 a, b; Weldeab, 2012a, b) by completing the insights into changes in the entire water column.

References

Adegbie, A. T., Schneider, R. R., Rohl, U., and Wefer, G., 2003. Glacial Millennial-Scale Fluctuations in Central African Precipitation Recorded in Terrigenous Sediment Supply and Freshwater Signals Offshore Cameroon. *Palaeogeography Palaeoclimatology Palaeoecology* **197**, 323-333. DOI: 10.1016/s0031-0182(03)00474-7.

Ahn, J. and Brook, E. J., 2008. Atmospheric CO2 and Climate on Millennial Time Scales During the Last Glacial Period. *Science* **322**, 83-85. Doi: 10.1126/science.1160832.

Altenbach, A. V., Lutze, G. F., Schiebel, R., and Schönfeld, J., 2003. Impact of Interrelated and Interdependent Ecological Controls on Benthic Foraminifera: An Example from the Gulf of Guinea. *Palaeogeography, Palaeoclimatology, Palaeoecology* **197**, 213-238. DOI: 10.1016/S0031-0182(03)00463-2.

Anand, P., Elderfield, H., and Conte, M. H., 2003. Calibration of Mg/Ca Thermometry in Planktonic Foraminifera from a Sediment Trap Time Series. *Paleoceanography* **18**, -. 1050, DOI: 10.1029/2002kpa000846.

Anderson, R. F., Ali, S., Bradtmiller, L. I., Nielsen, S. H. H., Fleisher, M. Q., Anderson, B. E., and Burckle, L. H., 2009. Wind-Driven Upwelling in the Southern Ocean and the Deglacial Rise in Atmospheric CO2. *Science* **323**, 1443-1448. DOI: 10.1126/science.1167441.

Antonov, J. I., Seidov, D., Boyer, T. P., Locarnini, R. A., Mishonov, A. V., Garcia, H. E., Baranova, O. K., Zweng, M. M., and Johnson, D. R., 2010. *World Ocean Atlas 2009, Volume 2: Salinity*. S. Levitus Ed. NOAA Atlas NESDIS 69, U.S. Gov. Printing Office, Washington, D.C.

Arsouze, T., Dutay, J. C., Lacan, F., and Jeandel, C., 2009. Reconstructing the Nd Oceanic Cycle Using a Coupled Dynamical - Biogeochemical Model. *Biogeosciences* **6**, 2829-2846. DOI:10.5194/bg-6-2829-2009.

Bacon, M. P. and Edmond, J. M., 1972. Barium at Geosecs III in the Southwest Pacific. *Earth and Planetary Science Letters* **16**, 66-74. DOI: 10.1016/0012-821X(72)90237-3.

Barker, S., Greaves, M., and Elderfield, H., 2003. A Study of Cleaning Procedures Used for Foraminiferal Mg/Ca Paleothermometry. *Geochemistry Geophysics Geosystems* **4**, 20. 8407, DOI: 10.1029/2003gc000559.

Barker, S., Diz, P., Vautravers, M. J., Pike, J., Knorr, G., Hall, I. R., and Broecker, W. S., 2009. Interhemispheric Atlantic Seesaw Response During the Last Deglaciation. *Nature* **457**, 1097-U50. DOI: 10.1038/Nature07770.

Barrat, J. A., Keller, F., Amossé, J., Taylor, R. N., Nesbitt, R. W., and Hirata, T., 1996. Determination of Rare Earth Elements in Sixteen Silicate Reference Samples by Icp-Ms after Tm Addition and Ion Exchange Separation. *Geostandards Newsletter* **20**, 133-139. DOI: 10.1111/j.1751-908X.1996.tb00177.x.

Basak, C., Martin, E. E., and Kamenov, G. D., 2011. Seawater Pb Isotopes Extracted from Cenozoic Marine Sediments. *Chemical Geology* **286**, 94-108. DOI: 10.1016/j.chemgeo.2011.04.007.

Bau, M. and Koschinsky, A., 2006. Hafnium and Neodymium Isotopes in Seawater and in Ferromanganese Crusts: The "Element Perspective". *Earth and Planetary Science Letters* **241**, 952-961. DOI: 10.1016/j.epsl.2005.09.067.

Bau, M. and Koschinsky, A., 2009. Oxidative Scavenging of Cerium on Hydrous Fe Oxide: Evidence from the Distribution of Rare Earth Elements and Yttrium between Fe Oxides and Mn Oxides in Hydrogenetic Ferromanganese Crusts. *Geochemical Journal* **43**, 37-47. DOI: 10.2343/geochemj.1.0005.

Bayon, G., German, C. R., Boella, R. M., Milton, J. A., Taylor, R. N., and Nesbitt, R. W., 2002. An Improved Method for Extracting Marine Sediment Fractions and Its Application to Sr and Nd Isotopic Analysis. *Chemical Geology* **187**, 179-199. DOI: 10.1016/s0009-2541(01)00416-8.

Bayon, G., German, C. R., Burton, K. W., Nesbitt, R. W., and Rogers, N., 2004. Sedimentary Fe-Mn Oxyhydroxides as Paleoceanographic Archives and the Role of Aeolian Flux in Regulating Oceanic Dissolved Ree. *Earth and Planetary Science Letters* **224**, 477-492. DOI: 10.1016/j.epsl.2004.05.033.

Bayon, G., Birot, D., Ruffine, L., Caprais, J. C., Ponzevera, E., Bollinger, C., Donval, J. P., Charlou, J. L., Voisset, M., and Grimaud, S., 2011. Evidence for Intense Ree Scavenging at Cold Seeps from the Niger Delta Margin. *Earth and Planetary Science Letters* **312**, 443-452. DOI: 10.1016/j.epsl.2011.10.008.

Beal, L. M., De Ruijter, W. P. M., Biastoch, A., Zahn, R., and Grp, S. W. I. W., 2011. On the Role of the Agulhas System in Ocean Circulation and Climate. *Nature* **472**, 429-436. DOI: 10.1038/nature09983.

Bemis, B. E., Spero, H. J., Bijma, J., and Lea, D. W., 1998. Reevaluation of the Oxygen Isotopic Composition of Planktonic Foraminifera: Experimental Results and Revised Paleotemperature Equations. *Paleoceanography* **13**, 150-160. DOI: 10.1029/98pa00070.

Biastoch, A., Boning, C. W., and Lutjeharms, J. R. E., 2008. Agulhas Leakage Dynamics Affects Decadal Variability in Atlantic Overturning Circulation. *Nature* **456**, 489-492. DOI: 10.1038/nature07426.

Biastoch, A., Boning, C. W., Schwarzkopf, F. U., and Lutjeharms, J. R. E., 2009. Increase in Agulhas Leakage Due to Poleward Shift of Southern Hemisphere Westerlies. *Nature* **462**, 495-U188. DOI: 10.1038/nature08519.

Blunier, T. and Brook, E. J., 2001. Timing of Millennial-Scale Climate Change in Antarctica and Greenland During the Last Glacial Period. *Science* **291**, 109-112. DOI: 10.1126/science.291.5501.109.

Boiteau, R., Greaves, M., and Elderfield, H., 2012. Authigenic Uranium in Foraminiferal Coatings: A Proxy for Ocean Redox Chemistry. *Paleoceanography* **27**, 8. DOI: 10.1029/2012pa002335.

Bond, G., Kromer, B., Beer, J., Muscheler, R., Evans, M. N., Showers, W., Hoffmann, S., Lotti-Bond, R., Hajdas, I., and Bonani, G., 2001. Persistent Solar Influence on North Atlantic Climate During the Holocene. *Science* **294**, 2130-2136. DOI: 10.1126/science.1065680.

Boyle, E. A., 1981. Cadmium, Zinc, Copper, and Barium in Foraminifera Tests. *Earth and Planetary Science Letters* **53**, 11-35. DOI: 10.1016/0012-821x(81)90022-4.

Boyle, E. A., 1983. Manganese Carbonate Overgrowths on Foraminifera Tests. *Geochimica Et Cosmochimica Acta* **47**, 1815-1819. DOI: 10.1016/0016-7037(83)90029-7.

Boyle, E. A. and Keigwin, L. D., 1985. Comparison of Atlantic and Pacific Paleochemical Records for the Last 215,000 Years - Changes in Deep Ocean Circulation and Chemical Inventories. *Earth and Planetary Science Letters* **76**, 135-150. DOI: 10.1016/0012-821x(85)90154-2.

Boyle, E. A. and Rosenthal, Y., 1996. Chemical Hydrography of the South Atlantic During the Last Glacial Maximum: Cd Vs. Δ13C. In: Wefer, G., Berger, W. H., Sielder, G., and Webb, D. (Eds.), *The South Atlantic: Present and Past Circulation*. Springer-Verlag, New York., 644 p., ISBN 3540620796, 9783540620792.

Broccoli, A. J., Dahl, K. A., and Stouffer, R. J., 2006. Response of the Itcz to Northern Hemisphere Cooling. *Geophysical Research Letters* **33**, 4. DOI: 10.1029/2005gl024546.

Burton, K. W. and Vance, D., 2000. Glacial-Interglacial Variations in the Neodymium Isotope Composition of Seawater in the Bay of Bengal Recorded by Planktonic Foraminifera. *Earth and Planetary Science Letters* **176**, 425-441. DOI: 10.1016/s0012-821x(00)00011-x.

Carroll, J., Falkner, k. K., Brown, E. T., and Moore, W. S., 1993. The Role of the Ganges-Brahmaputra Mixing Zone in Supplying Barium And226ra to the Bay of Bengal. *Geochimica Et Cosmochimica Acta* **57**, 2981-2990. DOI: 10.1016/0016-7037(93)90287-7.

Chan, L. H., Drummond, D., Edmond, J. M., and Grant, B., 1977. On the Barium Data from the Atlantic Geosecs Expedition. *Deep Sea Research* **24**, 613-649. DOI: 10.1016/0146-6291(77)90505-7.

Chang, P., Zhang, R., Hazeleger, W., Wen, C., Wan, X. Q., Ji, L., Haarsma, R. J., Breugem, W. P., and Seidel, H., 2008. Oceanic Link between Abrupt Changes in the North Atlantic Ocean and the African Monsoon. *Nature Geoscience* **1**, 444-448. DOI: 10.1038/Ngeo218.

Charbonnier, G., Puceat, E., Bayon, G., Desmares, D., Dera, G., Durlet, C., Deconinck, J. F., Amedro, F., Gourlan, A. T., Pellenard, P., and Bomou, B., 2012. Reconstruction of the Nd Isotope Composition of Seawater on Epicontinental Seas: Testing the Potential of Fe-Mn Oxyhydroxide Coatings on Foraminifera Tests for Deep-Time Investigations. *Geochimica Et Cosmochimica Acta* **99**, 39-56. DOI: 10.1016/j.gca.2012.09.012.

Chester, R. and Hughes, M. J., 1967. A Chemical Technique for the Separation of Ferro-Manganese Minerals, Carbonate Minerals and Adsorbed Trace Elements from Pelagic Sediments. *Chemical Geology* **2**, 249-262. DOI: 10.1016/0009-2541(67)90025-3

Coffey, M., Dehairs, F., Collette, O., Luther, G., Church, T., and Jickells, T., 1997. The Behaviour of Dissolved Barium in Estuaries. *Estuarine, Coastal and Shelf Science* **45**, 113-121. DOI: 10.1006/ecss.1996.0157.

Cohen, A. S., O'Nions, R. K., Siegenthaler, R., and Griffin, W. L., 1988. Chronology of the Pressure-Temperature History Recorded by a Granulite Terrain. *Contributions to Mineralogy and Petrology* **98**, 303-311. DOI: 10.1007/bf00375181.

Collins, J. A., Schefusz, E., Heslop, D., Mulitza, S., Prange, M., Zabel, M., Tjallingii, R., Dokken, T. M., Huang, E., Mackensen, A., Schulz, M., Tian, J., Zarriess, M., and Wefer,

G., 2011. Interhemispheric Symmetry of the Tropical African Rainbelt over the Past 23,000 Years. *Nature Geosci* **4**, 42-45. DOI: 10.1038/ngeo1039.

Collins, J. A., Schefuss, E., Mulitza, S., Prange, M., Werner, M., Tharammal, T., Paul, A., and Wefer, G., 2013. Estimating the Hydrogen Isotopic Composition of Past Precipitation Using Leaf-Waxes from Western Africa. *Quat. Sci. Rev.* **65**, 88-101. DOI: 10.1016/j.quascirev.2013.01.007.

Dekens, P. S., Lea, D. W., Pak, D. K., and Spero, H. J., 2002. Core Top Calibration of Mg/Ca in Tropical Foraminifera: Refining Paleotemperature Estimation. *Geochemistry Geophysics Geosystems* **3**, 29. DOI: 10.1029/2001gc000200.

Deuser, W. G., Ross, E. H., Hemleben, C., and Spindler, M., 1981. Seasonal-Changes in Species Composition, Numbers, Mass, Size, and Isotopic Composition of Planktonic-Foraminifera Settling into the Deep Sargasso Sea. *Palaeogeography Palaeoclimatology Palaeoecology* **33**, 103-127. DOI: 10.1016/0031-0182(81)90034-1.

Dickson, A. G. and Millero, F. J., 1987. A Comparison of the Equilibrium Constants for the Dissociation of Carbonic Acid in Seawater Media. *Deep Sea Research Part A. Oceanographic Research Papers* **34**, 1733-1743. DOI: 10.1016/0198-0149(87)90021-5.

Dickson, A. G., 1990. Thermodynamics of the Dissociation of Boric Acid in Synthetic Seawater from 273.15 to 318.15 K. *Deep Sea Research Part A. Oceanographic Research Papers* **37**, 755-766. DOI: 10.1016/0198-0149(90)90004-F.

Dion, P. 1983 *Trace Elements and Radionuclides in the Connecticut River and Amazon River Estuary*. Ph.D. Thesis, Yale University, 233 pp.

Dubinin, A. V. and Rimskaya, M. N., 2011. Geochemistry of Rare Earth Elements in Bottom Sediments of the Brazil Basin, Atlantic Ocean. *Lithol. Miner. Resour.* **46**, 1-16. DOI: 10.1134/s0024490211010032.

Dürkop, A., Holbourn, A., Kuhnt, W., Zuraida, R., Andersen, N., and Grootes, P. M., 2008. Centennial-Scale Climate Variability in the Timor Sea During Marine Isotope Stage 3. *Marine Micropaleontology* **66**, 208-221. DOI: 10.1016/j.marmicro.2007.10.002.

Edmond, J. M., Boyle, E. D., Drummond, D., Grant, B., and Mislick, T., 1978. Desorption of Barium in the Plume of the Zaire (Congo) River. *Netherlands Journal of Sea Research* **12**, 324-328. DOI: 10.1016/0077-7579(78)90034-0.

Elderfield, H., Hawkesworth, C. J., Greaves, M. J., and Calvert, S. E., 1981. Rare Earth Element Geochemistry of Oceanic Ferromanganese Nodules and Associated Sediments. *Geochimica Et Cosmochimica Acta* **45**, 513-528.

Elderfield, H., Upstillgoddard, R., and Sholkovitz, E. R., 1990. The Rare-Earth Elements in Rivers, Estuaries, and Coastal Seas and Their Significance to the Composition of Ocean Waters. *Geochimica Et Cosmochimica Acta* **54**, 971-991. DOI: 10.1016/0016-7037(90)90432-k.

Elderfield, H. and Ganssen, G., 2000. Past Temperature and $\delta^{18}O$ of Surface Ocean Waters Inferred from Foraminiferal Mg/Ca Ratios. *Nature* **405**, 442-445. DOI: 10.1038/35013033.

Elderfield, H., Vautravers, M., and Cooper, M., 2002. The Relationship between Shell Size and Mg/Ca, Sr/Ca, Delta O-18, and Delta C-13 of Species of Planktonic Foraminifera. *Geochemistry Geophysics Geosystems* **3**. DOI: 10.1029/2001gc000194.

Elmore, A. C., Piotrowski, A. M., Wright, J. D., and Scrivner, A. E., 2011. Testing the Extraction of Past Seawater Nd Isotopic Composition from North Atlantic Deep Sea Sediments and Foraminifera. *Geochem. Geophys. Geosyst.* **12**, Q09008. DOI: 10.1029/2011gc003741.

EPICA Community Members, 2006. One-to-One Coupling of Glacial Climate Variability in Greenland and Antarctica. *Nature* **444**, 195-198. DOI: 10.1038/nature05301.

Fairbanks, R. G., Charles, C. D., and Wright, J. D., 1992. Origin of Global Meltwater Pulse. In: Taylor, R. E., Long, A., and Kra, R. S. (Eds.), *Radiocarbon after Four Decades*. Springer New York. ISBN: 978-1-4757-4251-0, DOI: Doi: 10.1007/978-1-4757-4249-7_30.

Flückiger, J., Blunier, T., Stauffer, B., Chappellaz, J., Spahni, R., Kawamura, K., Schwander, J., Stocker, T. F., and Dahl-Jensen, D., 2004. N_2O and CH_4 Variations During the Last Glacial Epoch: Insight into Global Processes. *Glob. Biogeochem. Cycle* **18**, GB1020. DOI: 10.1029/2003gb002122.

Fontanier, C., Jorissen, F. J., Licari, L., Alexandre, A., Anschutz, P., and Carbonel, P., 2002. Live Benthic Foraminiferal Faunas from the Bay of Biscay: Faunal Density, Composition, and Microhabitats. *Deep-Sea Research Part I-Oceanographic Research Papers* **49**, 751-785. DOI: 10.1016/s0967-0637(01)00078-4.

Frank, M., 2002. Radiogenic Isotopes: Tracers of Past Ocean Circulation and Erosional Input. *Rev. Geophys.* **40**, 1001. DOI: 10.1029/2000rg000094.

Froelich, P. N., Klinkhammer, G. P., Bender, M. L., Luedtke, N. A., Heath, G. R., Cullen, D., Dauphin, P., Hammond, D., Hartman, B., and Maynard, V., 1979. Early Oxidation of Organic Matter in Pelagic Sediments of the Eastern Equatorial Atlantic: Suboxic Diagenesis. *Geochimica Et Cosmochimica Acta* **43**, 1075-1090. DOI: 10.1016/0016-7037(79)90095-4.

Ganachaud, A. and Wunsch, C., 2000. Improved Estimates of Global Ocean Circulation, Heat Transport and Mixing from Hydrographic Data. *Nature* **408**, 453-457. DOI: 10.1038/35044048.

Ganssen, G. M. and Kroon, D., 2000. The Isotopic Signature of Planktonic Foraminifera from Ne Atlantic Surface Sediments: Implications for the Reconstruction of Past Oceanic Conditions. *J. Geol. Soc.* **157**, 693-699. DOI: 10.1144/jgs.157.3.693.

Garcia, A. C., Locarnini, R. A., Boyer, T. P., Antonov, J. I., Zweng, M. M., Baranova, O. K., and Johnson, D. R., 2010. *World Ocean Atlas 2009, Volume 4: Nutrients (Phosphate, Nitrate, Silicate).* S. Levitus Ed. NOAA Atlas NESDIS 71, U.S. Gov. Printing Office, Washington, D.C.

Gasse, F., 2000. Hydrological Changes in the African Tropics since the Last Glacial Maximum. *Quat. Sci. Rev.* **19**, 189-211. DOI: 10.1016/S0277-3791(99)00061-X.

German, C. R. and Elderfield, H., 1990. Application of the Ce Anomaly as a Paleoredox Indicator: The Ground Rules. *Paleoceanography* **5**, 823-833. DOI: 10.1029/PA005i005p00823.

Giresse, P., Aloisi, J.-C., Kuete, M., Monteillet, J., and Ngueutchoua, G., 1995. Quaternary Sedimentary Deposits on the Cameroon Shelf: Characterization of Facies and Late Quaternary Shorelines. *Quaternary International* **29-30**, 75-82. DOI: 10.1016/1040-6182(95)00009-8

Goldstein, S. L., O'Nions, R. K., and Hamilton, P. J., 1984. A Sm-Nd Isotopic Study of Atmospheric Dusts and Particulates from Major River Systems. *Earth and Planetary Science Letters* **70**, 221-236. DOI: 10.1016/0012-821X(84)90007-4.

Goldstein, S. J. and Jacobsen, S. B., 1987. The Nd and Sr Isotopic Systematics of River-Water Dissolved Material: Implications for the Sources of Nd and Sr in Seawater. *Chemical Geology: Isotope Geoscience section* **66**, 245-272. DOI: 10.1016/0168-9622(87)90045-5

Grasse, P., Stichel, T., Stumpf, R., Stramma, L., and Frank, M., 2012. The Distribution of Neodymium Isotopes and Concentrations in the Eastern Equatorial Pacific: Water Mass Advection Versus Particle Exchange. *Earth and Planetary Science Letters* **353**, 198-207. DOI 10.1016/j.epsl.2012.07.044.

Griffiths, J. F. (ed.), 1972. *Climates of Africa*, World survey of climatology. Vol. 10, 604 p., Amsterdam [etc.]: Elsevier, ISBN: 0444408932.

Gu, G. and Adler, R. F., 2004. Seasonal Evolution and Variability Associated with the West African Monsoon System. *Journal of Climate* **17**, 3364-3377. DOI: 10.1175/1520-0442(2004)017<3364:seavaw>2.0.co;2.

Gutjahr, M., Frank, M., Stirling, C. H., Klemm, V., van de Flierdt, T., and Halliday, A. N., 2007. Reliable Extraction of a Deepwater Trace Metal Isotope Signal from Fe-Mn Oxyhydroxide Coatings of Marine Sediments. *Chemical Geology* **242**, 351-370. DOI: 10.1016/j.chemgeo.2007.03.021.

Gutjahr, M., Frank, M., Stirling, C. H., Keigwin, L. D., and Halliday, A. N., 2008. Tracing the Nd Isotope Evolution of North Atlantic Deep and Intermediate Waters in the Western North Atlantic since the Last Glacial Maximum from Blake Ridge Sediments. *Earth and Planetary Science Letters* **266**, 61-77. DOI: 10.1016/j.epsl.2007.10.037.

Haley, B. A. and Klinkhammer, G. P., 2002. Development of a Flow-through System for Cleaning and Dissolving Foraminiferal Tests. *Chemical Geology* **185**, 51-69. DOI: 10.1016/s0009-2541(01)00399-0.

Haley, B. A., Klinkhammer, G. P., and McManus, J., 2004. Rare Earth Elements in Pore Waters of Marine Sediments. *Geochimica Et Cosmochimica Acta* **68**, 1265-1279. DOI: 10.1016/j.gca.2003.09.012.

Haley, B. A., Klinkhammer, G. P., and Mix, A. C., 2005. Revisiting the Rare Earth Elements in Foraminiferal Tests. *Earth and Planetary Science Letters* **239**, 79-97. DOI: 10.1016/j.epsl.2005.08.014.

Hall, J. M. and Chan, L. H., 2004. Ba/Ca in Benthic Foraminifera: Thermocline and Middepth Circulation in the North Atlantic During the Last Glaciation. *Paleoceanography* **19**. DOI: 10.1029/2004pa001028.

Halliday, A. N., Dickin, A. P., Fallick, A. E., and Fitton, J. G., 1988. Mantle Dynamics: A Nd, Sr, Pb and O Isotopic Study of the Cameroon Line Volcanic Chain. *Journal of Petrology* **29**, 181-211. DOI: 10.1093/petrology/29.1.181.

Hannigan, R. E. and Sholkovitz, E. R., 2001. The Development of Middle Rare Earth Element Enrichments in Freshwaters: Weathering of Phosphate Minerals. *Chemical Geology* **175**, 495-508. DOI: 10.1016/s0009-2541(00)00355-7.

Hathorne, E. C., Haley, B., Stichel, T., Grasse, P., Zieringer, M., and Frank, M., 2012. Online Preconcentration Icp-Ms Analysis of Rare Earth Elements in Seawater. *Geochemistry Geophysics Geosystems* **13**, 12. DOI: 10.1029/2011gc003907.

Hemleben, C., Spindler, M., and Anderson, O. R., 1989. *Modern Planktonic Foraminifera*. Springer-Verlag, New York. ISBN: 3540968156, 9783540968153.

Hessler, I., Steinke, S., Groeneveld, J., Dupont, L., and Wefer, G., 2011. Impact of Abrupt Climate Change in the Tropical Southeast Atlantic During Marine Isotope Stage (Mis) 3. *Paleoceanography* **26**, 11. DOI: 10.1029/2011pa002118.

Hönisch, B., Allen, K. A., Russell, A. D., Eggins, S. M., Bijma, J., Spero, H. J., Lea, D. W., and Yu, J., 2011. Planktic Foraminifers as Recorders of Seawater Ba/Ca. *Marine Micropaleontology* **79**, 52-57. DOI: 10.1016/j.marmicro.2011.01.003.

Horwitz, E. P., Chiarizia, R., and Dietz, M. L., 1992. A Novel Strontium-Selective Extraction Chromatographic Resin. *Solvent Extr. Ion Exch.* **10**, 313-336. DOI: 10.1080/07366299208918107.

Hüls, M. and Zahn, R., 2000. Millennial-Scale Sea Surface Temperature Variability in the Western Tropical North Atlantic from Planktonic Foraminiferal Census Counts. *Paleoceanography* **15**, 659-678. DOI: 10.1029/1999pa000462.

Jacobsen, S. B. and Wasserburg, G. J., 1980. Sm-Nd Isotopic Evolution of Chondrites. *Earth and Planetary Science Letters* **50**, 139-155. DOI: 10.1016/0012-821X(80)90125-9.

Jaeschke, A., Ruhlemann, C., Arz, H., Heil, G., and Lohmann, G., 2007. Coupling of Millennial-Scale Changes in Sea Surface Temperature and Precipitation Off Northeastern Brazil with High-Latitude Climate Shifts During the Last Glacial Period. *Paleoceanography* **22**. Pa4206, DOI: 10.1029/2006pa001391.

Jansen, H., Zeebe, R. E., and Wolf-Gladrow, D. A., 2002. Modeling the Dissolution of Settling $CaCo_3$ in the Ocean. *Glob. Biogeochem. Cycle* **16**, 16. DOIi: 10.1029/2000gb001279.

Jeandel, C., Arsouze, T., Lacan, F., Téchiné, P., and Dutay, J. C., 2007. Isotopic Nd Compositions and Concentrations of the Lithogenic Inputs into the Ocean: A Compilation, with an Emphasis on the Margins. *Chemical Geology* **239**, 156-164. DOI: 10.1016/j.chemgeo.2006.11.013.

Johannesson, K. H. and Burdige, D. J., 2007. Balancing the Global Oceanic Neodymium Budget: Evaluating the Role of Groundwater. *Earth and Planetary Science Letters* **253**, 129-142. DOI: 10.1016/j.epsl.2006.10.021.

Jorissen, F. J., Wittling, I., Peypouquet, J. P., Rabouille, C., and Relexans, J. C., 1998. Live Benthic Foraminiferal Faunas Off Cape Blanc, Nw-Africa: Community Structure and Microhabitats. *Deep-Sea Research Part I-Oceanographic Research Papers* **45**, 2157-2188. DOI: 10.1016/s0967-0637(98)00056-9.

Kanfoush, S. L., Hodell, D. A., Charles, C. D., Guilderson, T. P., Mortyn, P. G., and Ninnemann, U. S., 2000. Millennial-Scale Instability of the Antarctic Ice Sheet During the Last Glaciation. *Science* **288**, 1815-1818. DOI: 10.1126/science.288.5472.1815.

Kasten, S., Glasby, G. P., Schulz, H. D., Friedrich, G., and Andreev, S. I., 1998. Rare Earth Elements in Manganese Nodules from the South Atlantic Ocean as Indicators of Oceanic Bottom Water Flow. *Mar. Geol.* **146**, 33-52. DOI: 10.1016/s0025-3227(97)00128-x.

Kim, S.-Y., Scourse, J., Marret, F., and Lim, D.-I., 2010. A 26,000-Year Integrated Record of Marine and Terrestrial Environmental Change Off Gabon, West Equatorial Africa. *Palaeogeography, Palaeoclimatology, Palaeoecology* **297**, 428-438. DOI: 10.1016/j.palaeo.2010.08.026.

Klevenz, V., Vance, D., Schmidt, D. N., and Mezger, K., 2008. Neodymium Isotopes in Benthic Foraminifera: Core-Top Systematics and a Down-Core Record from the Neogene South Atlantic. *Earth and Planetary Science Letters* **265**, 571-587. DOI: 10.1016/j.epsl.2007.10.053.

Knorr, G. and Lohmann, G., 2007. Rapid Transitions in the Atlantic Thermohaline Circulation Triggered by Global Warming and Meltwater During the Last Deglaciation. *Geochemistry, Geophysics, Geosystems* **8**, Q12006. DOI: 10.1029/2007gc001604.

Knutti, R., Fluckiger, J., Stocker, T. F., and Timmermann, A., 2004. Strong Hemispheric Coupling of Glacial Climate through Freshwater Discharge and Ocean Circulation. *Nature* **430**, 851-856. DOI: 10.1038/Nature02786.

Koeppenkastrop, D. and De Carlo, E. H., 1992. Sorption of Rare-Earth Elements from Seawater onto Synthetic Mineral Particles: An Experimental Approach. *Chemical Geology* **95**, 251-263. DOI: 10.1016/0009-2541(92)90015-W.

Kraft, S., Frank, M., Hathorne, E. C., and Weldeab, S., 2013. Assessment of Seawater Nd Isotope Signatures Extracted from Foraminiferal Shells and Authigenic Phases of Gulf of Guinea Sediments. *Geochimica Et Cosmochimica Acta* **121**, 414-435. DOI: 10.1016/j.gca.2013.07.029.

Krueger, S., Leuschner, D. C., Ehrmann, W., Schmiedl, G., and Mackensen, A., 2012. North Atlantic Deep Water and Antarctic Bottom Water Variability During the Last 200 ka Recorded in an Abyssal Sediment Core Off South Africa. *Global and Planetary Change* **80-81**, 180-189. DOI: 10.1016/j.gloplacha.2011.10.001.

Lacan, F. and Jeandel, C., 2005. Neodymium Isotopes as a New Tool for Quantifying Exchange Fluxes at the Continent-Ocean Interface. *Earth and Planetary Science Letters* **232**, 245-257. DOI: 10.1016/j.epsl.2005.01.004.

Le Fèvre, B. and Pin, C., 2005. A Straightforward Separation Scheme for Concomitant Lu-Hf and Sm-Nd Isotope Ratio and Isotope Dilution Analysis. *Analytica Chimica Acta* **543**, 209-221. DOI: 10.1016/j.aca.2005.04.044.

Lea, D. and Boyle, E., 1989. Barium Content of Benthic Foraminifera Controlled by Bottom-Water Composition. *Nature* **338**, 751-753. DOI: 10.1038/338751a0.

Lea, D. W. and Boyle, E. A., 1991. Barium in Planktonic Foraminifera. *Geochimica Et Cosmochimica Acta* **55**, 3321-3331. DOI: 10.1016/0016-7037(91)90491-M.

Lea, D. W. and Spero, H. J., 1992. Experimental-Determination of Barium Uptake in Shells of the Planktonic-Foraminifera Orbulina-Universa at 22-Degrees-C. *Geochimica Et Cosmochimica Acta* **56**, 2673-2680. DOI: 10.1016/0016-7037(92)90352-J.

Lea, D. W., 1993. Constraints on the Alkalinity and Circulation of Glacial Circumpolar Deep-Water from Benthic Foraminiferal Barium. *Glob. Biogeochem. Cycle* **7**, 695-710. DOI: 10.1029/93gb01536.

Lea, D. W. and Boyle, E. A., 1993. Determination of Carbonate-Bound Barium in Foraminifera and Corals by Isotope Dilution Plasma-Mass Spectrometry. *Chemical Geology* **103**, 73-84. DOI: 10.1016/0009-2541(93)90292-Q.

Lea, D. W. and Spero, H. J., 1994. Assessing the Reliability of Paleochemical Tracers: Barium Uptake in the Shells of Planktonic Foraminifera. *Paleoceanography* **9**, 445-452. DOI: 10.1029/94pa00151.

Lea, D. W., Mashiotta, T. A., and Spero, H. J., 1999. Controls on Magnesium and Strontium Uptake in Planktonic Foraminifera Determined by Live Culturing. *Geochimica Et Cosmochimica Acta* **63**, 2369-2379. DOI: 10.1016/S0016-7037(99)00197-0.

Lea, D. W., Pak, D. K., Peterson, L. C., and Hughen, K. A., 2003. Synchroneity of Tropical and High-Latitude Atlantic Temperatures over the Last Glacial Termination. *Science* **301**, 1361-1364. DOI: 10.1126/science.1088470.

LeGrande, A. N. and Schmidt, G. A., 2006. Global Gridded Data Set of the Oxygen Isotopic Composition in Seawater. *Geophysical Research Letters* **33**, L12604. DOI: 10.1029/2006gl026011.

Leroux, M., 1993. The Mobile Polar High: A New Concept Explaining Present Mechanisms of Meridional Air-Mass and Energy Exchanges and Global Propagation of Palaeoclimatic Changes. *Global and Planetary Change* **7**, 69-93. DOI: 10.1016/0921-8181(93)90041-L.

Lezine, A. M., Duplessy, J. C., and Cazet, J. P., 2005. West African Monsoon Variability During the Last Deglaciation and the Holocene: Evidence from Fresh Water Algae, Pollen and Isotope Data from Core Kw31, Gulf of Guinea. *Palaeogeography Palaeoclimatology Palaeoecology* **219**, 225-237. DOI: 10.1016/j.palaeo.2004.12.027.

Locarnini, R. A., Mishonov, A. V., Antonov, J. I., Boyer, T. P., Garcia, H. E., Baranova, O. K., Zweng, M. M., and Johnson, D. R., 2010. *World Ocean Atlas 2009, Volume 1: Temperature.* S. Levitus Ed. NOAA Atlas NESDIS 68, U.S. Gov. Printing Office, Washington, D.C.

Lohmann, G., 2003. Atmospheric and Oceanic Freshwater Transport During Weak Atlantic Overturning Circulation. *Tellus A* **55**, 438-449. DOI: 10.1034/j.1600-0870.2003.00028.x.

Lutze, G. F., Agwu, C. O. C., Altenbach, A. V., Henken-Mellies, U., Kothe, C., Mühlhan, N., Pflaumann, U., Samtleben, C., Sarnthein, M., Segl, M., Soltwedel, T., Stute, U., Tiedemann, R., and Weinholz, P., 1988. Berichte Über Die `Meteor´-Fahrt 6-5, Dakar-Libreville 15.1.-16.2.1988. *Berichte-Reports, Geologisch-Paläontologisches Institut Universität Kiel* **22**.

Lutze, G. F. and Altenbach, A. V., 1991. Technik Und Signifikanz Der Lebendfärbung Benthischer Foraminiferen Mit Bengal-Rosa. *Geologisches Jahrbuch* **A 128**, 251-265.

Maloney, E. D. and Shaman, J., 2008. Intraseasonal Variability of the West African Monsoon and Atlantic Itcz. *Journal of Climate* **21**, 2898-2918. DOI: 10.1175/2007jcli1999.1.

Marchitto, T. M., Oppo, D. W., and Curry, W. B., 2002. Paired Benthic Foraminiferal Cd/Ca and Zn/Ca Evidence for a Greatly Increased Presence of Southern Ocean Water in the Glacial North Atlantic. *Paleoceanography* **17**, 16. DOI: 10.1029/2000pa000598.

Martin, P. A. and Lea, D. W., 2002. A Simple Evaluation of Cleaning Procedures on Fossil Benthic Foraminiferal Mg/Ca. *Geochemistry Geophysics Geosystems* **3**, 8. 8401, DOI: 10.1029/2001gc000280.

Martin, E. E., Blair, S. W., Kamenov, G. D., Scher, H. D., Bourbon, E., Basak, C., and Newkirk, D. N., 2010. Extraction of Nd Isotopes from Bulk Deep Sea Sediments for Paleoceanographic Studies on Cenozoic Time Scales. *Chemical Geology* **269**, 414-431. DOI: 10.1016/j.chemgeo.2009.10.016.

Martínez-Botí, M. A., Vance, D., and Mortyn, P. G., 2009. Nd/Ca Ratios in Plankton-Towed and Core Top Foraminifera: Confirmation of the Water Column Acquisition of Nd. *Geochemistry Geophysics Geosystems* **10**, 16. Q08018, DOI: 10.1029/2009gc002701.

McManus, J. F., Francois, R., Gherardi, J. M., Keigwin, L. D., and Brown-Leger, S., 2004. Collapse and Rapid Resumption of Atlantic Meridional Circulation Linked to Deglacial Climate Changes. *Nature* **428**, 834-837. DOI: 10.1038/Nature02494.

Mehrbach, C., Culberson, C. H., Hawley, J. E., and Pytkowicz, R. M., 1973. Measurement of Apparent Dissociation-Constants of Carbonic-Acid in Seawater at Atmospheric-Pressure. *Limnology and Oceanography* **18**, 897-907.

Mulitza, S., Rühlemann, C., Bickert, T., Hale, W., Patzold, J., and Wefer, G., 1998. Late Quaternary δ13C Gradients and Carbonate Accumulation in the Western Equatorial Atlantic. *Earth and Planetary Science Letters* **155**, 237-249. DOI: 10.1016/S0012-821x(98)00012-0.

Nance, W. B. and Taylor, S. R., 1976. Rare-Earth Element Patterns and Crustal Evolution .1. Australian Post-Archean Sedimentary-Rocks. *Geochimica Et Cosmochimica Acta* **40**, 1539-1551. doi: 10.1016/0016-7037(76)90093-4.

Negre, C., Zahn, R., Thomas, A. L., Masque, P., Henderson, G. M., Martinez-Mendez, G., Hall, I. R., and Mas, J. L., 2010. Reversed Flow of Atlantic Deep Water During the Last Glacial Maximum. *Nature* **468**, 84-88. DOI: 10.1038/nature09508.

NGRIP, North Greenland Ice Core Project Members, 2004. High-Resolution Record of Northern Hemisphere Climate Extending into the Last Interglacial Period. *Nature* **431**, 147-151. DOI: 10.1038/Nature02805.

Ni, Y. Y., Foster, G. L., Bailey, T., Elliott, T., Schmidt, D. N., Pearson, P., Haley, B., and Coath, C., 2007. A Core Top Assessment of Proxies for the Ocean Carbonate System in Surface-Dwelling Foraminifers. *Paleoceanography* **22**. DOI: 10.1029/2006pa001337.

Nicholson, S. E., 1996. A Review of Climate Dynamics and Climate Variability in Eastern Africa. In: Johnson, T. C. and Odada, E. O. (Eds.), *The Limnology, Climatology and Paleoclimatology of the East African Lakes*. Gordon and Breach, Amsterdam. ISBN: 2884492348, 9782884492348.

Nicholson, S. E., 2000. The Nature of Rainfall Variability over Africa on Time Scales of Decades to Millenia. *Global and Planetary Change* **26**, 137-158. DOI: 10.1016/S0921-8181(00)00040-0.

Nicholson, S. E. and Grist, J. P., 2003. The Seasonal Evolution of the Atmospheric Circulation over West Africa and Equatorial Africa. *Journal of Climate* **16**, 1013-1030. DOI: 10.1175/1520-0442(2003)016<1013:tseota>2.0.co;2.

Nicholson, S. E., 2009. A Revised Picture of the Structure of The "Monsoon" And Land ITCZ over West Africa. *Climate Dynamics* **32**, 1155-1171. DOI: 10.1007/s00382-008-0514-3.

Niedermeyer, E. M., Prange, M., Mulitza, S., Mollenhauer, G., Schefuss, E., and Schulz, M., 2009. Extratropical Forcing of Sahel Aridity During Heinrich Stadials. *Geophysical Research Letters* **36**. DOI: 10.1029/2009gl039687.

Nürnberg, D., 1995. Magnesium in Tests of *Neogloboquadrina pachyderma* sinistral from High Northern and Southern Latitudes. *Journal of Foraminiferal Research* **25**, 350-368. DOI:10.2113/gsjfr.25.4.350.

Nürnberg, D., Bijma, J., and Hemleben, C., 1996. Assessing the Reliability of Magnesium in Foraminiferal Calcite as a Proxy for Water Mass Temperatures. *Geochimica Et Cosmochimica Acta* **60**, 803-814. DOI: 10.1016/0016-7037(95)00446-7.

Nürnberg, D., Müller, A., and Schneider, R. R., 2000. Paleo-Sea Surface Temperature Calculations in the Equatorial East Atlantic from Mg/Ca Ratios in Planktic Foraminifera: A Comparison to Sea Surface Temperature Estimates from U-37(K '), Oxygen Isotopes, and Foraminiferal Transfer Function. *Paleoceanography* **15**, 124-134. DOI: 10.1029/1999PA000370.

Ohta, A. and Kawabe, I., 2001. Ree(III) Adsorption onto Mn Dioxide (δ-MnO_2) and Fe Oxyhydroxide: Ce(III) Oxidation by δ-MnO_2. *Geochimica Et Cosmochimica Acta* **65**, 695-703. DOI: 10.1016/S0016-7037(00)00578-0.

Osborne, A. H., Vance, D., Rohling, E. J., Barton, N., Rogerson, M., and Fello, N., 2008. A Humid Corridor across the Sahara for the Migration of Early Modern Humans out of Africa 120,000 Years Ago. *Proceedings of the National Academy of Sciences of the United States of America* **105**, 16444-16447. DOI: 10.1073/pnas.0804472105.

Osborne, A. H., Marino, G., Vance, D., and Rohling, E. J., 2010. Eastern Mediterranean Surface Water Nd During Eemian Sapropel S5: Monitoring Northerly (Mid-Latitude) Versus Southerly (Sub-Tropical) Freshwater Contributions. *Quat. Sci. Rev.* **29**, 2473-2483. doi: DOI: 10.1016/j.quascirev.2010.05.015.

Oudot, C., 1993a. Total Co2 and Total Alkalinity Data Obtained During the R/V L'atalante Cruise in the Atlantic Ocean (WOCE Section A06, 02 Jan. - 10 Feb., 1993). Carbon Dioxide Information Analysis Center, Oak Ridge National Laboratory, US Department of Energy, Oak Ridge, Tennessee.

Oudot, C., 1993b. Carbon Data Obtained During the R/V L'atalante Cruise in the Atlantic Ocean (WOCE Section A07, 13 Feb. - 19 Mar., 1993). Carbon Dioxide Information Analysis Center, Oak Ridge National Laboratory, US Department of Energy, Oak Ridge, Tennessee.

Pahnke, K. and Zahn, R., 2005. Southern Hemisphere Water Mass Conversion Linked with North Atlantic Climate Variability. *Science* **307**, 1741-1746. DOI: 10.1126/science.1102163.

Pahnke, K., Goldstein, S. L., and Hemming, S. R., 2008. Abrupt Changes in Antarctic Intermediate Water Circulation over the Past 25,000 Years. *Nature Geoscience* **1**, 870-874. DOI: 10.1038/ngeo360.

Palmer, M. R., 1985. Rare-Earth Elements in Foraminfera Tests. *Earth and Planetary Science Letters* **73**, 285-298. DOI: 10.1016/0012-821x(85)90077-9.

Palmer, M. R. and Elderfield, H., 1985. Variations in the Nd Isotopic Composition of Foraminifera from Atlantic-Ocean Sediments. *Earth and Planetary Science Letters* **73**, 299-305. DOI: 10.1016/0012-821x(85)90078-0.

Palmer, M. R. and Elderfield, H., 1986. Rare-Earth Elements and Neodymium Isotopes in Ferromanganese Oxide Coatings of Cenozoic Foraminifera from the Atlantic-Ocean. *Geochimica Et Cosmochimica Acta* **50**, 409-417. DOI: 10.1016/0016-7037(86)90194-8.

Peeters, F. J. C., Acheson, R., Brummer, G. J. A., de Ruijter, W. P. M., Schneider, R. R., Ganssen, G. M., Ufkes, E., and Kroon, D., 2004. Vigorous Exchange between the Indian and Atlantic Oceans at the End of the Past Five Glacial Periods. *Nature* **430**, 661-665. DOI: 10.1038/nature02785.

Pena, L. D., Calvo, E., Cacho, I., Eggins, S., and Pelejero, C., 2005. Identification and Removal of Mn-Mg-Rich Contaminant Phases on Foraminiferal Tests: Implications for Mg/Ca Past Temperature Reconstructions. *Geochemistry Geophysics Geosystems* **6**, 25. Q09p02, DOI: 10.1029/2005gc000930.

Pena, L. D., Cacho, I., Calvo, E., Pelejero, C., Eggins, S., and Sadekov, A., 2008. Characterization of Contaminant Phases in Foraminifera Carbonates by Electron Microprobe Mapping. *Geochemistry Geophysics Geosystems* **9**, 12. Q07012, DOI: 10.1029/2008gc002018.

Pena, L. D., Goldstein, S. L., Hemming, S. R., Jones, K. M., Calvo, E., Pelejero, C., and Cacho, I., 2013. Rapid Changes in Meridional Advection of Southern Ocean Intermediate Waters to the Tropical Pacific During the Last 30 Kyr. *Earth and Planetary Science Letters* **368**, 20-32. DOI: 10.1016/j.epsl.2013.02.028.

Petersen, S. V., Schrag, D. P., and Clark, P. U., 2013. A New Mechanism for Dansgaard-Oeschger Cycles. *Paleoceanography* **28**, 24-30. DOI: 10.1029/2012pa002364.

Piepgras, D. J. and Wasserburg, G. J., 1980. Neodymium Isotopic Variations in Seawater. *Earth and Planetary Science Letters* **50**, 128-138. DOI: 10.1016/0012-821x(80)90124-7.

Piepgras, D. J. and Wasserburg, G. J., 1982. Isotopic Composition of Neodymium in Waters from the Drake Passage. *Science* **217**, 207-214. DOI: 10.1126/science.217.4556.207.

Piepgras, D. J. and Wasserburg, G. J., 1987. Rare Earth Element Transport in the Western North Atlantic Inferred from Nd Isotopic Observations. *Geochimica Et Cosmochimica Acta* **51**, 1257-1271. DOI: 10.1016/0016-7037(87)90217-1.

Piepgras, D. J. and Jacobsen, S. B., 1992. The Behavior of Rare Earth Elements in Seawater: Precise Determination of Variations in the North Pacific Water Column. *Geochimica Et Cosmochimica Acta* **56**, 1851-1862. DOI: 10.1016/0016-7037(92)90315-a.

Pierrot, D., Lewis, E., and Wallace, D. W. R., 2006. MS Excel Program Developed for CO2 System Calculations. ORNL/CDIAC-105a. Carbon Dioxide Information Analysis Center, Oak Ridge National Laboratory, U.S. Department of Energy, Oak Ridge, Tennessee. DOI: 10.3334/CDIAC/otg.CO2SYS_XLS_CDIAC105a.

Piotrowski, A. M., Goldstein, S. L., Hemming, S. R., and Fairbanks, R. G., 2005. Temporal Relationships of Carbon Cycling and Ocean Circulation at Glacial Boundaries. *Science* **307**, 1933-1938. DOI: 10.1126/science.1104883.

Piotrowski, A. M., Galy, A., Nicholl, J. A. L., Roberts, N., Wilson, D. J., Clegg, J. A., and Yu, J., 2012. Reconstructing Deglacial North and South Atlantic Deep Water Sourcing Using Foraminiferal Nd Isotopes. *Earth and Planetary Science Letters* **357-358**, 289-297. DOI: 10.1016/j.epsl.2012.09.036.

Pomies, C., Davies, G. R., and Conan, S. M. H., 2002. Neodymium in Modern Foraminifera from the Indian Ocean: Implications for the Use of Foraminiferal Nd Isotope Compositions in Paleo-Oceanography. *Earth and Planetary Science Letters* **203**, 1031-1045. DOI: 10.1016/s0012-821x(02)00924-x.

Rathburn, A. E., Corliss, B. H., Tappa, K. D., and Lohmann, K. C., 1996. Comparisons of the Ecology and Stable Isotopic Compositions of Living (Stained) Benthic Foraminifera from the Sulu and South China Seas. *Deep Sea Research Part I: Oceanographic Research Papers* **43**, 1617-1646. DOI: 10.1016/S0967-0637(96)00071-4.

Ravelo, A. C. and Fairbanks, R. G., 1992. Oxygen Isotopic Composition of Multiple Species of Planktonic Foraminifera: Recorders of the Modern Photic Zone Temperature Gradient. *Paleoceanography* **7**, 815-831. DOI: 10.1029/92pa02092.

Ravelo, A. C. and Fairbanks, R. G., 1995. Carbon Isotopic Fractionation in Multiple Species of Planktonic-Foraminifera from Core-Tops in the Tropical Atlantic. *Journal of Foraminiferal Research* **25**, 53-74. DOI: 10.2113/gsjfr.25.1.53.

Regenberg, M., Nürnberg, D., Steph, S., Groeneveld, J., Garbe-Schonberg, D., Tiedemann, R., and Dullo, W. C., 2006. Assessing the Effect of Dissolution on Planktonic Foraminiferal Mg/Ca Ratios: Evidence from Caribbean Core Tops. *Geochemistry Geophysics Geosystems* **7**, 23. DOI: 10.1029/2005gc001019.

Regenberg, M., Steph, S., Nürnberg, D., Tiedemann, R., and Garbe-Schonberg, D., 2009. Calibrating Mg/Ca Ratios of Multiple Planktonic Foraminiferal Species with Delta O-18-Calcification Temperatures: Paleothermometry for the Upper Water Column. *Earth and Planetary Science Letters* **278**, 324-336. DOI: 10.1016/j.epsl.2008.12.019.

Rempfer, J., Stocker, T. F., Joos, F., Dutay, J.-C., and Siddall, M., 2011. Modelling Nd-Isotopes with a Coarse Resolution Ocean Circulation Model: Sensitivities to Model Parameters and Source/Sink Distributions. *Geochimica Et Cosmochimica Acta* **75**, 5927-5950. DOI: 10.1016/j.gca.2011.07.044.

Reynard, B., Lécuyer, C., and Grandjean, P., 1999. Crystal-Chemical Controls on Rare-Earth Element Concentrations in Fossil Biogenic Apatites and Implications for Paleoenvironmental Reconstructions. *Chemical Geology* **155**, 233-241. DOI: 10.1016/S0009-2541(98)00169-7.

Rickli, J., Frank, M., and Halliday, A. N., 2009. The Hafnium-Neodymium Isotopic Composition of Atlantic Seawater. *Earth and Planetary Science Letters* **280**, 118-127. DOI: 10.1016/j.epsl.2009.01.026.

Rickli, J., Frank, M., Baker, A. R., Aciego, S., de Souza, G., Georg, R. B., and Halliday, A. N., 2010. Hafnium and Neodymium Isotopes in Surface Waters of the Eastern Atlantic Ocean: Implications for Sources and Inputs of Trace Metals to the Ocean. *Geochimica Et Cosmochimica Acta* **74**, 540-557. DOI: 10.1016/j.gca.2009.10.006.

Roberts, N. L., Piotrowski, A. M., McManus, J. F., and Keigwin, L. D., 2010. Synchronous Deglacial Overturning and Water Mass Source Changes. *Science* **327**, 75-78. DOI: 10.1126/science.1178068.

Roberts, N. L., Piotrowski, A. M., Elderfield, H., Eglinton, T. I., and Lomas, M. W., 2012. Rare Earth Element Association with Foraminifera. *Geochimica Et Cosmochimica Acta* **94**, 57-71. DOI: 10.1016/j.gca.2012.07.009.

Rosenthal, Y., Boyle, E. A., and Labeyrie, L., 1997. Last Glacial Maximum Paleochemistry and Deepwater Circulation in the Southern Ocean: Evidence from Foraminiferal Cadmium. *Paleoceanography* **12**, 787-796. DOI: 10.1029/97pa02508.

Rosenthal, Y., Field, M. P., and Sherrell, R. M., 1999. Precise Determination of Element/Calcium Ratios in Calcareous Samples Using Sector Field Inductively Coupled Plasma Mass Spectrometry. *Anal. Chem.* **71**, 3248-3253. DOI: 10.1021/ac981410x.

Ruddiman, W. F., 2008. *Earth's Climate, Past and Future*. W. H. Freeman, ISBN 978-0-7167-8490-6.

Rühlemann, C., Mulitza, S., Lohmann, G., Paul, A., Prange, M., and Wefer, G., 2004. Intermediate Depth Warming in the Tropical Atlantic Related to Weakened Thermohaline Circulation: Combining Paleoclimate Data and Modeling Results for the Last Deglaciation. *Paleoceanography* **19**, PA1025. DOI: 10.1029/2003pa000948.

Rutberg, R. L., Hemming, S. R., and Goldstein, S. L., 2000. Reduced North Atlantic Deep Water Flux to the Glacial Southern Ocean Inferred from Neodymium Isotope Ratios. *Nature* **405**, 935-938. DOI: 10.1038/35016049.

Schlitzer, R., 2000. Electronic Atlas of Woce Hydrographic and Tracer Data Now Available. *Eos, Transactions American Geophysical Union* **81**, 45-45. DOI: 10.1029/00eo00028.

Schmidt, G. A., Bigg, G. R., and Rohling, E. J., 1999. "Global Seawater Oxygen-18 Database - V1.21" http://data.giss.nasa.gov/o18data/

Schmidt, M. W., Chang, P., Hertzberg, J. E., Them, T. R., Link, J., and Otto-Bliesner, B. L., 2012. Impact of Abrupt Deglacial Climate Change on Tropical Atlantic Subsurface Temperatures. *Proceedings of the National Academy of Sciences of the United States of America* **109**, 14348-14352. DOI: 10.1073/pnas.1207806109.

Schmuker, B. and Schiebel, R., 2002. Planktic Foraminifers and Hydrography of the Eastern and Northern Caribbean Sea. *Marine Micropaleontology* **46**, 387-403. DOI: 10.1016/s0377-8398(02)00082-8.

Schneider, R. R., Price, B., Muller, P. J., Kroon, D., and Alexander, I., 1997. Monsoon Related Variations in Zaire (Congo) Sediment Load and Influence of Fluvial Silicate Supply on Marine Productivity in the East Equatorial Atlantic During the Last 200,000 Years. *Paleoceanography* **12**, 463-481. DOI: 10.1029/96pa03640.

Scholz, F., Hensen, C., Noffke, A., Rohde, A., Liebetrau, V., and Wallmann, K., 2011. Early Diagenesis of Redox-Sensitive Trace Metals in the Peru Upwelling Area - Response to Enso-Related Oxygen Fluctuations in the Water Column. *Geochimica Et Cosmochimica Acta* **75**, 7257-7276. DOIi: 10.1016/j.gca.2011.08.007.

Scrivner, A. E., Vance, D., and Rohling, E. J., 2004. New Neodymium Isotope Data Quantify Nile Involvement in Mediterranean Anoxic Episodes. *Geology* **32**, 565-568. doi: 10.1130/g20419.1.

Sholkovitz, E. R., Shaw, T. J., and Schneider, D. L., 1992. The Geochemistry of Rare-Earth Elements in the Seasonally Anoxic Water Column and Porewaters of Chesapeake Bay. *Geochimica Et Cosmochimica Acta* **56**, 3389-3402.

Singh, S. P., Singh, S. K., Goswami, V., Bhushan, R., and Rai, V. K., 2012. Spatial Distribution of Dissolved Neodymium and Epsilon(Nd) in the Bay of Bengal: Role of Particulate Matter and Mixing of Water Masses. *Geochimica Et Cosmochimica Acta* **94**, 38-56. DOI: 10.1016/j.gca.2012.07.017.

Singh, S. P., Singh, S. K., and Bhushan, R., 2013. Internal Cycling of Dissolved Barium in Water Column of the Bay of Bengal. *Marine Chemistry* **154**, 12-23. DOI: 10.1016/j.marchem.2013.04.013.

Spero, H. J. and Lea, D. W., 2002. The Cause of Carbon Isotope Minimum Events on Glacial Terminations. *Science* **296**, 522-525. DOI: 10.1126/science.1069401.

Sprintall, J. and Tomczak, M., 1992. Evidence of the Barrier Layer in the Surface-Layer of the Tropics. *Journal of Geophysical Research-Oceans* **97**, 7305-7316. DOI: 10.1029/92jc00407.

Sprintall, J. and Tomczak, M., 1993. On the Formation of Central Water and Thermocline Ventilation in the Southern Hemisphere. *Deep Sea Research Part I: Oceanographic Research Papers* **40**, 827-848. DOI: 10.1016/0967-0637(93)90074-D.

Steph, S., Regenberg, M., Tiedemann, R., Mulitza, S., and Nurnberg, D., 2009. Stable Isotopes of Planktonic Foraminifera from Tropical Atlantic/Caribbean Core-Tops: Implications for Reconstructing Upper Ocean Stratification. *Marine Micropaleontology* **71**, 1-19. DOI: 10.1016/j.marmicro.2008.12.004.

Stichel, T., Frank, M., Rickli, J., Hathorne, E. C., Haley, B. A., Jeandel, C., and Pradoux, C., 2012. Sources and Input Mechanisms of Hafnium and Neodymium in Surface Waters of the Atlantic Sector of the Southern Ocean. *Geochimica Et Cosmochimica Acta* **94**, 22-37. DOI: 10.1016/j.gca.2012.07.005

Stocker, T. F., 1998. Climate Change - the Seesaw Effect. *Science* **282**, 61-62. DOI: 10.1126/science.282.5386.61.

Stoll, H. M., Vance, D., and Arevalos, A., 2007. Records of the Nd Isotope Composition of Seawater from the Bay of Bengal: Implications for the Impact of Northern Hemisphere Cooling on Itcz Movement. *Earth and Planetary Science Letters* **255**, 213-228. DOI: 10.1016/j.epsl.2006.12.016.

Stramma, L. and Peterson, R. G., 1990. The South-Atlantic Current. *J. Phys. Oceanogr.* **20**, 846-859. DOI: 10.1175/1520-0485(1990)020<0846:Tsac>2.0.Co;2.

Stramma, L. and England, M. H., 1999. On the Water Masses and Mean Circulation of the South Atlantic Ocean. *Journal of Geophysical Research-Oceans* **104**, 20863-20883. DOI: 10.1029/1999jc900139.

Stramma, L. and Schott, F., 1999. The Mean Flow Field of the Tropical Atlantic Ocean. *Deep-Sea Research Part Ii-Topical Studies in Oceanography* **46**, 279-303. DOI: 10.1016/s0967-0645(98)00109-x.

Stumpf, R., Frank, M., Schonfeld, J., and Haley, B. A., 2010. Late Quaternary Variability of Mediterranean Outflow Water from Radiogenic Nd and Pb Isotopes. *Quat. Sci. Rev.* **29**, 2462-2472. DOI 10.1016/j.quascirev.2010.06.021.

Surya Prakash, L., Ray, D., Paropkari, A. L., Mudholkar, A. V., Satyanarayanan, M., Sreenivas, B., Chandrasekharam, D., Kota, D., Kamesh Raju, K. A., Kaisary, S., Balaram, V., and Gurav, T., 2012. Distribution of Rees and Yttrium among Major Geochemical Phases of Marine Fe-Mn-Oxides: Comparative Study between Hydrogenous and Hydrothermal Deposits. *Chemical Geology* **312-313**, 127-137. DOI: 10.1016/j.chemgeo.2012.03.024.

Tachikawa, K., Jeandel, C., and Roy-Barman, M., 1999. A New Approach to the Nd Residence Time in the Ocean: The Role of Atmospheric Inputs. *Earth and Planetary Science Letters* **170**, 433-446. DOI: 10.1016/S0012-821X(99)00127-2.

Tachikawa, K., Toyofuku, T., Basile-Doelsch, I., and Delhaye, T., 2013. Microscale Neodymium Distribution in Sedimentary Planktonic Foraminiferal Tests and Associated Mineral Phases. *Geochimica Et Cosmochimica Acta* **100**, 11-23. DOI: 10.1016/j.gca.2012.10.010.

Talbot, M. R., Filippi, M. L., Jensen, N. B., and Tiercelin, J. J., 2007. An Abrupt Change in the African Monsoon at the End of the Younger Dryas. *Geochemistry Geophysics Geosystems* **8**, DOI: 10.1029/2006gc001465.

Tanaka, T., Togashi, S., Kamioka, H., Amakawa, H., Kagami, H., Hamamoto, T., Yuhara, M., Orihashi, Y., Yoneda, S., Shimizu, H., Kunimaru, T., Takahashi, K., Yanagi, T., Nakano, T., Fujimaki, H., Shinjo, R., Asahara, Y., Tanimizu, M., and Dragusanu, C., 2000. Jndi-1: A Neodymium Isotopic Reference in Consistency with Lajolla Neodymium. *Chemical Geology* **168**, 279-281. DOI:10.1016/s0009-2541(00)00198-4.

Timmermann, A., Krebs, U., Justino, F., Goosse, H., and Ivanochko, T., 2005. Mechanisms for Millennial-Scale Global Synchronization During the Last Glacial Period. *Paleoceanography* **20**. Pa4008, DOI: 10.1029/2004pa001090.

Tomczak, M. and Godfrey, J. S., 1994. *Regional Oceanography: An Introduction*. Pergamon. New York. ISBN 0080410219.

Toteu, S. F., Van Schmus, W. R., Penaye, J., and Michard, A., 2001. New U-Pb and Sm-Nd Data from North-Central Cameroon and Its Bearing on the Pre-Pan African History of Central Africa. *Precambrian Research* **108**, 45-73. DOI: 10.1016/S0301-9268(00)00149-2.

Turekian, K. K. and Johnson, D. G., 1966. The Barium Distribution in Sea Water. *Geochimica Et Cosmochimica Acta* **30**, 1153-1174. DOI: 10.1016/0016-7037(66)90035-4.

Vance, D. and Burton, K., 1999. Neodymium Isotopes in Planktonic Foraminifera: A Record of the Response of Continental Weathering and Ocean Circulation Rates to Climate Change. *Earth and Planetary Science Letters* **173**, 365-379. DOI: 10.1016/s0012-821x(99)00244-7.

Vance, D., Scrivner, A. E., Beney, P., Staubwasser, M., Henderson, G. M., and Slowey, N. C., 2004. The Use of Foraminifera as a Record of the Past Neodymium Isotope Composition of Seawater. *Paleoceanography* **19**, 17. DOI: 10.1029/2003pa000957.

Waelbroeck, C., Labeyrie, L., Michel, E., Duplessy, J. C., McManus, J. F., Lambeck, K., Balbon, E., and Labracherie, M., 2002. Sea-Level and Deep Water Temperature Changes Derived from Benthic Foraminifera Isotopic Records. *Quat. Sci. Rev.* **21**, 295-305. DOI: 10.1016/S0277-3791(01)00101-9

Wallace, D., Johnson, K., Rios, A., and Gonzalez-Davila, M., 1995. Total CO_2 and Total Alkalinity Data Obtained During the R/V L'atalante Cruise in the Atlantic Ocean (Woce Sections A13 and A14, 12 Jan. - 02 Mar., 1995). Carbon Dioxide Information Analysis Center, Oak Ridge National Laboratory, US Department of Energy, Oak Ridge, Tennessee.

Weldeab, S., Schneider, R. R., Kolling, M., and Wefer, G., 2005. Holocene African Droughts Relate to Eastern Equatorial Atlantic Cooling. *Geology* **33**, 981-984. DOI: 10.1130/g21874.1.

Weldeab, S., Lea, D. W., Schneider, R. R., and Andersen, N., 2007a. 155,000 Years of West African Monsoon and Ocean Thermal Evolution. *Science* **316**, 1303-1307. DOI: 10.1126/science.1140461.

Weldeab, S., Lea, D. W., Schneider, R. R., and Andersen, N., 2007b. Centennial Scale Climate Instabilities in a Wet Early Holocene West African Monsoon. *Geophysical Research Letters* **34**, 6. L24702, DOI: 10.1029/2007gl031898.

Weldeab, S., Frank, M., Stichel, T., Haley, B., and Sangen, M., 2011. Spatio-Temporal Evolution of the West African Monsoon During the Last Deglaciation. *Geophysical Research Letters* **38**, 5. DOI: 10.1029/2011gl047805.

Weldeab, S., 2012a. Bipolar Modulation of Millennial-Scale West African Monsoon Variability During the Last Glacial (75,000 - 25,000 Years Ago). *Quat. Sci. Rev.* **40**, 21-29. DOI: 10.1016/j.quascirev.2012.02.014.

Weldeab, S., 2012b. Timing and Magnitude of Equatorial Atlantic Surface Warming During the Last Glacial Bipolar Oscillation. *Climate of the Past* **8**, 1705-1716. DOI: 10.5194/cp-8-1705-2012.

Wolff, T., Mulitza, S., Rühlemann, C., and Wefer, G., 1999. Response of the Tropical Atlantic Thermocline to Late Quaternary Trade Wind Changes. *Paleoceanography* **14**, 374-383. DOI: 10.1029/1999pa900011.

Wolgemuth, K. and Broecker, W. S., 1970. Barium in Sea Water. *Earth and Planetary Science Letters* **8**, 372-378. DOI: 10.1016/0012-821X(70)90110-X.

Wright, J. B., Hastings, D. A., Jones, W. B., and Williams, H. R., 1985. *Geology and Mineral Resources of West Africa*. Allan and Unwin, London, ISBN 0045560013.

Yu, J. M., Elderfield, H., Greaves, M., and Day, J., 2007. Preferential Dissolution of Benthic Foraminiferal Calcite During Laboratory Reductive Cleaning. *Geochemistry Geophysics Geosystems* **8**, 17. DOI: 10.1029/2006gc001571.

Yu, J., Elderfield, H., Jin, Z., and Booth, L., 2008. A Strong Temperature Effect on U/Ca in Planktonic Foraminiferal Carbonates. *Geochimica Et Cosmochimica Acta* **72**, 4988-5000. doi: 10.1016/j.gca.2008.07.011.

Zabel, M., Schneider, R. R., Wagner, T., Adegbie, A. T., de Vries, U., and Kolonic, S., 2001. Late Quaternary Climate Changes in Central Africa as Inferred from Terrigenous Input to the Niger Fan. *Quat. Res.* **56**, 207-217. DOI: 10.1006/qres.2001.2261.

Zuraida, R., Holbourn, A., Nurnberg, D., Kuhnt, W., Durkop, A., and Erichsen, A., 2009. Evidence for Indonesian Throughflow Slowdown During Heinrich Events 3-5. *Paleoceanography* **24**. DOI: 10.1029/2008pa001653.

Appendix

TABLES

Table A3.1: *Measurement results of element and isotopic composition of foraminiferal tests*

Site	Sample	Species	Initial weight [mg]	Cleaning procedure*	Ca [µg]	Al/Ca [µmol/mol]	Mn/Ca [µmol/mol]	Fe/Ca [µmol/mol]	Nd/Ca [µmol/mol]	Mn/Fe [mol/mol]	Nd [ng]	εNd (2σ)**	Ext. error
GIK 16870-1A	SK-T1	*G. menardii*	20.8	C	6441.5	42.5	45.0	-	0.77	-	18.0	-11.8	0.5
2469 m water depth	SK-T2	*G. menardii*	20.2	C	-	-	-	-	-	-	-	-11.1	0.7
0-1 cm core depth	SK-AB 8	G. menardii	22.8	CO	8111.0	55.6	44.3	-	0.83	-	22.9	-11.3	0.5
0°12'90 S, 5°58'1E	SK-AB 9	*G. menardii*	23.2	CO	7431.8	62.3	50.9	-	0.83	-	20.9	-11.4	0.5
	SK-AB 4	*G. menardii*	20.2	R-FT (0.5 M HYDRX)	2109.2	1252.6	39.6	-	4.48	-	34.1	-8.7	0.9
	SK-AB 5	*G. menardii*	20.9	R-FT (0.25 M HYDRX)	5739.3	570.0	53.3	-	2.04	-	42.2	-9.2	0.9
	SK-AB 6	*G. menardii*	20.3	R-FT (0.1 M HYDRX)	6182.8	423.1	84.5	-	1.63	-	36.4	-9.0	0.9
	SK-AB 1	*G. menardii*	19	COR-FT (0.5 M HYDRX)[1]	1356.9	44.9	15.7	-	2.52	-	12.3	-10.1	0.7
	SK-AB 7	*G. menardii*	22.4	COR-FT (0.1 M HYDRX)	6528.5	55.9	19.1	-	0.80	-	18.8	-11.7	0.5
	SK-AC 3	*G. menardii*	20.4	COR-B	5355.4	26.6	8.1	-	0.37	-	7.2	-11.6	0.5
	SK-AC 4	*G. menardii*	21	COR-B	5693.1	35.9	8.1	-	0.42	-	8.7	-12.2	0.5
	SK-AC 9	*G. menardii*	20.8	COR-B	5507.2	47.4	10.2	-	0.25	-	4.9	-12.4	0.3
	SK-AC 9 (re-measured)	*G. menardii*	20.8	COR-B	4184.7	73.3	24.1	23.9	0.37	1.011	5.6	-	-
	SK-AC 11	*G. menardii*	20	COR-B	4672.9	136.4	14.0	51.3	0.42	0.273	7.1	-11.9	0.4
	SK-AC 12	*G. menardii*	20.4	COR-B (0.25 M HYDRX)	5086.0	10.9	21.4	40.3	0.82	0.530	15.0	-12.0	0.4
	SK-AC 13	*G. menardii*	21.4	COR-B (0.1 M HYDRX)	5733.4	13.4	23.8	43.4	0.82	0.548	16.9	-11.7	0.4
	SK-AC 7	*G. ruber pink*	20.5	COR-B	2779.4	38.5	6.5	-	0.86	-	8.6	-10.9	0.5
	SK-AC 8	*G. ruber pink*	19.8	COR-B	1689.2	109.4	18.1	-	0.74	-	4.5	-8.5	0.3
	SK-AC 6	*N. dutertrei*	20.1	COR-B	4397.2	16.2	9.7	-	0.41	-	6.4	-10.4	0.5
GIK 16865-1A	SK-AB 10	*G. menardii*	21.2	COR-FT (0.1 M HYDRX)	5272.9	37.1	42.5	-	1.70	-	32.2	-12.8	0.5
2492 m water depth	SK-AC 5	*G. menardii*	20.1	COR-B	5309.0	8.3	11.7	-	0.55	-	10.5	-12.9	0.5
0-1 cm core depth	SK-AC 10	*G. menardii*	21.6	COR-B	4636.3	16.9	11.5	-	0.28	-	4.7	-13.0	0.6
2°40'3 N, 6°03'3 E	SK-AC 10 (re-measured)	*G. menardii*	21.6	COR-B	3432.8	27.1	11.5	19.0	0.40	0.602	4.9	-	-
	SK-AB 13	*G. ruber pink*	21.1	COR-FT (0.1 M HYDRX)	4750.7	133.0	3.3	-	1.64	-	28.0	-12.6	0.5

Table A3.1: *Measurement results of element and isotopic composition of foraminiferal tests (continued)*

Site	Sample	Species	Initial weight [mg]	Cleaning procedure*	Ca	Al/Ca	Mn/Ca	Fe/Ca	Nd/Ca	Mn/Fe	Nd	εNd	Ext. error
					[µg]	[µmol/ mol]	[µmol/ mol]	[µmol/ mol]	[µmol/ mol]	[mol/ mol]	[ng]		(2σ)**
GeoB 4902-4	SK-AD 44	*G. menardii*	21.9	C	6955.9	28.7	31.7	37.9	1.06	0.836	26.4	-12.6	0.3
3221 m water depth	SK-AD 45	*G. menardii*	23.6	COR-B	6023.9	8.0	7.0	29.5	0.37	0.237	8.0	-13.4	0.4
3-5 cm core depth	SK-AD 48	*G. ruber pink*	7.7	COR-B	1880.3	66.1	9.7	82.7	0.63	0.118	4.3	-	-
2°21'12 N, 6°01'48 E	SK-AD 49	*Benthos mix*	13	COR-B	4054.8	32.3	46.0	83.7	2.02	0.550	29.4	-12.5	0.3
GeoB 4901-5	SK-AD 42	*G. menardii*	24	C	7918.0	58.6	35.6	75.4	1.67	0.473	47.5	-12.8	0.2
2177 m water depth	SK-AD 43	*G. menardii*	26.7	COR-B	7491.4	12.5	8.4	31.6	0.49	0.265	13.3	-13.1	0.4
3-5 cm core depth	SK-AD 46	*G. ruber pink*	23.5	COR-B	6037.0	59.6	6.3	73.7	1.25	0.085	27.0	-12.8	0.3
2°40'54 N, 6°43'12 E	SK-AD 51	*N. dutertrei*	23.5	COR-B	5813.1	9.9	7.0	21.5	0.49	0.325	10.2	-12.7	0.1
	SK-AD 52	*G. tumida*	30.4	COR-B	9065.8	29.7	7.1	38.0	0.38	0.187	12.3	-13.0	0.1
	SK-AD 47	*Benthos mix*	10.4	COR-B	2778.6	39.6	12.0	119.7	2.07	0.101	20.7	-13.0	0.3
MD03-2707	SK-AD 8	bulk planktonic foraminifera	16.6	COR-B	2075.3	12.8	166.7	-	1.13	-	8.4	-15.8	0.6
1294 m water depth													
27-29 cm core depth													
2°30'07 N, 9°23'41 E													

*C = Clay removal, O = Oxidative cleaning, R-FT = Reductive Flow Through cleaning, R-B = Reductive batch cleaning; **External long-term error ±0.67 (2σ) (n = 160);
[1]FT cleaning method applied after Table 3.1, all other FT samples were cleaned following the procedure in Table 3.2

Table A3.2: *Rare Earth element (REE) concentrations Normalized to PAAS (ppm) (Nance and Taylor, 1976) results x10e^{3}*

sample	La	Ce	Pr	Nd	Sm	Eu	Gd	Tb	Dy	Ho	Er	Tm	Yb	Lu
Niger site east														
SK-AD 46, ***G. ruber pink***	45	15	49	53	71	78	79	72	69	54	52	47	44	39
SK-AD 43, ***G. menardii***	16	5	19	22	26	29	28	27	26	23	23	19	21	15
SK-AD 51, ***N. dutertrei***	16	7	22	25	34	37	37	34	33	26	26	23	22	19
SK-AD 52, ***G. tumida***	6	2	7	9	11	11	12	11	10	9	9	7	8	6
SK-AD 52, ***G. tumida***	6	2	8	9	11	11	11	11	11	10	10	7	9	6
SK-AD 52, ***G. tumida***	13	5	16	17	24	25	26	24	23	18	19	18	15	13
SK-AD 47, **mixed benthic foraminifera**	51	10	44	48	47	50	49	43	43	37	36	30	32	24
SK-AD 42, ***G. menardii***, non-reductively cleaned	55	22	65	73	88	97	96	90	87	76	74	57	64	52
Niger site west														
SK-AD 45, ***G. menardii***	13	5	14	16	21	23	24	22	22	17	18	16	16	14
SK-AD 49, **mixed benthic foraminifera**	46	13	42	48	50	54	55	50	49	42	42	34	39	29
SK-AD 44, ***G. menardii***, non-reductively cleaned	38	16	41	45	61	68	71	64	64	52	51	45	45	39

Table A3.3: *Results of sediment analyses*

Sample	Sediment	Core depth	Initial weight [g]	εNd	External error (2σ)
GeoB 4902-4, 3221 m water depth, 2°21'12 N, 6°01'48 E					
SK-L 4	sediment leach	3-4 cm	2.45	-10.4	0.1
SK-L 5	sediment leach	4-5 cm	2.47	-10.3	0.1
SK-L 42	sediment leach	4-5 cm	2.51	-10.4	0.2
SK-L 42 (re-measured)	sediment leach	4-5 cm	2.51	-10.3	0.2
SK-TD 42	residual total dissolution	4-5 cm	0.054	-11.0	0.2
GeoB 4901-5, 2177 m water depth, 2°40'54 N, 6°43'12 E					
SK-L 2	sediment leach	3-4 cm	2.48	-11.7	0.2
SK-L 3	sediment leach	4-5 cm	2.45	-11.5	0.2
SK-L 3 (re-measured)	sediment leach	4-5 cm	2.45	-11.6	0.1
SK-L 41	sediment leach	4-5 cm	2.50	-11.2	0.2
SK-TD 41	residual total dissolution	4-5 cm	0.053	-11.8	0.2
MD03-2707, 1294 m water depth, 2°30'07 N, 9°23'41 E					
SK-L 1	sediment leach	27-29 cm	2.40	-15.0	0.6
SK-L 1(re-measured)	sediment leach	27-29 cm	2.40	-15.2	0.2
SK-L 1 (re-measured)	sediment leach	27-29 cm	2.40	-15.3	0.3
SK-L 1 (re-measured)	sediment leach	27-29 cm	2.40	-15.2	0.3
GeoB 4905-2, 1329 m water depth, 2°30'0 N, 9°23'24 E					
SK-L 6	sediment leach	3-4 cm	2.47	-15.2	0.1
SK-L 7	sediment leach	4-5 cm	2.55	-15.2	0.1
SK-L 43	sediment leach	4-5 cm	2.51	-14.8	0.2
SK-TD 43	residual total dissolution	4-5 cm	0.053	-15.8	0.2

Table A4.1: *Element to Ca ratios and εNd of foraminiferal samples*

core depth [cm]	age* [Cal. Kyr BP]	species	initial weight [mg]	Ca [µg]	Al/Ca [µmol/mol]	Mn/ Ca [µmol/mol]	Fe/Ca [µmol/mol]	Nd/Ca [µmol/mol]	Mn/Fe [mol/mol]	Nd [ng]	εNd	external error (2σ)
planktonic foraminifera, fully cleaned												
28	0.6	*Bulk plankton*	16.6	2075	12.8	166.8	-	1.13	-	8.4	-15.8	0.6
175.25	3.08	*Bulk plankton*	22.4	5157	9.0	138.7	179.9	2.18	0.771	40.5	-16.3	0.3
268.25	4.67	*Bulk plankton*	19.9	3800	11.0	123.3	180.5	1.23	0.683	16.9	-16.3	0.3
418.75	7.68	*Bulk plankton*	13.2	2310	19.9	82.9	148.4	0.75	0.558	6.2	-16.3	0.3
501	9.73	*G. ruber pink*	20.1	3943	14.1	249.6	178.6	1.15	1.398	16.3	-16.3	0.4
542.5	10.91	*G. ruber pink*	26	5806	74.2	328.2	339.2	3.45	0.968	72.2	-16.4	0.3
572.5	11.84	*G. ruber pink*	26.8	6230	27.0	244.9	224.6	1.29	1.090	28.9	-16.8	0.3
602.5	12.83	*G. ruber pink*	20.42	4796	1.5	360.3	-	1.64	-	28.3	-16.2	0.5
628.5	13.74	*G. ruber pink*	23.7	5378	16.2	243.3	184.5	1.93	1.318	37.3	-16.6	0.3
657.5	14.83	*G. ruber pink*	20.57	5814	2.5	242.5	-	1.43	-	29.8	-17.0	0.5
678.5	15.66	*G. ruber pink*	27.1	7222	7.6	188.0	142.0	1.66	1.324	43.0	-16.7	0.3
713.5	17.14	*G. ruber pink*	20.42	3748	2.7	234.3	-	1.48	-	20.0	-17.0	0.3
753.5	18.74	*G. ruber pink*	19.7	3539	6.2	292.9	-	1.14	-	14.5	-17.8	0.3
793.5	19.37	*G. ruber pink*	19.8	3553	4.7	182.3	-	0.71	-	9.0	-17.1	0.3
813.5	19.76	*G. ruber pink*	24.6	4433	13.3	189.1	173.1	1.78	1.093	28.3	-17.3	0.3
833.5	20.19	*G. ruber pink*	19.96	2227	19.2	144.9	-	0.32	-	2.6	-17.4	0.9
833.5	20.19	*G. ruber pink*	28.6	5982	16.1	198.6	138.2	1.72	1.437	37.0	-17.4	0.3
863.5	20.91	*G. ruber pink*	20.28	5416	3.0	236.8	-	1.33	-	25.8	-17.7	0.5
863.5	20.91	*G. ruber pink*	27.9	6497	11.2	192.5	124.5	1.35	1.546	31.6	-17.9	0.3
1447	53.13	*Bulk plankton*	9.2	1526	23.0	151.8	361.0	1.46	0.420	8.0	-17.4	0.3
1474.25	55.02	*Bulk plankton*	28.1	4081	19.7	106.2	322.1	0.46	0.330	6.8	-17.2	0.3
1570.75	59.28	*Bulk plankton*	22.2	3835	7.7	113.7	246.2	0.42	0.462	5.8	-17.7	0.3
1585.5	59.94	*Bulk plankton*	21.9	3013	7.1	153.6	329.0	0.84	0.467	9.1	-17.4	0.4

Table A4.1: *Element to Ca ratios and εNd of foraminiferal samples (continued)*

core depth [cm]	age* [Cal. Kyr BP]	species	initial weight [mg]	Ca [µg]	Al/Ca [µmol/mol]	Mn/Ca [µmol/mol]	Fe/Ca [µmol/mol]	Nd/Ca [µmol/mol]	Mn/Fe [mol/mol]	Nd [ng]	εNd	external error (2σ)
1662.5	64.3	*G. ruber pink*	21.5	5328	9.3	228.5	121.9	1.15	1.876	22.0	-17.4	0.5
1732.5	68.28	*G. ruber pink*	23.1	4159	6.1	241.5	114.0	0.57	2.119	8.5	-17.8	0.3
2167.5	87.36	*G. ruber pink*	22.9	5857	15.1	316.6	110.3	1.07	2.870	22.6	-17.0	0.2
2640.5	108.9	*Bulk plankton*	25.7	5519	10.5	261.2	165.8	1.36	1.576	27.0	-16.9	0.3
2935.5	122.5	*Bulk plankton*	22.7	5460	7.9	117.7	240.4	0.28	0.490	5.4	-15.7	0.3
2975.5	123.7	*Bulk plankton*	22.9	5080	5.3	115.1	178.9	0.38	0.644	6.9	-16.2	0.3
3080.5	126.9	*Bulk plankton*	20	2753	5.5	131.9	353.3	0.69	0.373	6.8	-15.9	0.8
3115.5	128	*G. ruber pink*	19.3	1212	9.2	178.7	129.4	0.93	1.381	4.0	-	-
3125.5	128.3	*G. ruber pink*	15.3	3784	18.9	267.0	267.7	2.69	0.998	36.6	-17.2	0.2
3194.5	133.4	*G. ruber pink*	22.3	3351	21.7	119.4	183.2	0.78	0.652	9.4	-15.4	0.8
3235.5	135.9	*G. ruber pink*	29.7	1252	22.7	91.0	263.9	0.47	0.345	2.1	-16.2	0.8
planktonic foraminifera, only clay removed												
572.5	11.84	*G. ruber pink*	18.6	6547	52.1	518.6	395.1	5.54	1.312	130.5	-16.5	0.1
628.5	13.74	*G. ruber pink*	13.7	4915	110.3	549.8	1054.7	8.86	0.521	156.7	-17.0	0.1
678.5	15.66	*G. ruber pink*	18.7	7582	30.1	447.5	390.4	6.45	1.146	176.0	-17.3	0.1
benthic foraminifera, fully cleaned												
502.5	9.77	*mixed benthos*	16.9	5039	42.1	81.6	85.8	2.23	0.950	40.5	-16.2	0.2
542.5	10.91	*mixed benthos*	25	8338	44.6	133.2	166.0	3.17	0.803	95.3	-16.3	0.3
572.5	11.84	*mixed benthos*	26.7	6633	117.5	136.0	97.0	0.93	1.403	22.2	-16.6	0.3
587	12.31	*mixed benthos*	28.2	7355	46.8	135.6	104.7	0.98	1.295	25.8	-16.6	0.2
599.5	12.73	*mixed benthos*	16.4	4957	95.1	116.3	150.0	1.64	0.775	29.3	-16.3	0.2
602.5	12.82	*mixed benthos*	25.5	8360	38.2	197.1	177.2	2.56	1.112	76.9	-	-
602.5	12.83	*mixed benthos*	25.5	4077	89.4	174.2	170.5	1.84	1.022	27.1	-16.7	0.2
613	13.19	*mixed benthos*	27.2	7615	772.7	179.6	134.9	1.85	1.332	50.7	-16.5	0.2

Table A4.1: *Element to Ca ratios and εNd of foraminiferal samples (continued)*

core depth [cm]	age* [Cal. Kyr BP]	species	initial weight [mg]	Ca [µg]	Al/Ca [µmol/mol]	Mn/Ca [µmol/mol]	Fe/Ca [µmol/mol]	Nd/Ca [µmol/mol]	Mn/Fe [mol/mol]	Nd [ng]	εNd	external error (2σ)
628.5	13.74	*mixed benthos*	27.6	6573	49.5	161.4	107.8	1.99	1.498	47.1	-16.9	0.2
643.5	14.29	*mixed benthos*	27.2	5777	52.0	129.7	98.7	0.87	1.314	18.1	-	-
657.5	14.83	*mixed benthos*	26.8	7313	55.8	155.1	154.4	1.31	1.005	34.5	*-16.8*	0.2
668.5	15.26	*mixed benthos*	27.8	7533	47.1	137.5	107.3	0.82	1.282	22.3	-17.3	0.3
678.5	15.66	*mixed benthos*	28.6	6400	86.3	118.1	99.7	0.83	1.184	19.2	-17.0	0.4
693.5	16.28	*mixed benthos*	28.5	6122	53.2	122.0	109.9	0.75	1.110	16.6	-16.5	0.4
713.5	17.14	*mixed benthos*	26.1	6355	35.1	89.8	132.6	1.76	0.677	40.2	*-16.7*	0.2
732.5	17.99	*mixed benthos*	25.7	5826	32.1	102.6	111.9	1.28	0.917	26.8	-16.8	0.3
753.5	18.74	*mixed benthos*	35.2	9208	72.1	132.7	446.7	3.73	0.297	123.6	-17.1	0.2
773.5	19.04	*mixed benthos*	26.5	6627	56.0	94.1	110.9	1.02	0.848	24.2	-16.7	0.3
793.5	19.37	*mixed benthos*	20.6	6836	47.3	165.4	305.4	2.95	0.542	72.5	-17.0	0.2
813.5	19.76	*mixed benthos*	19.8	6310	68.7	114.1	249.8	1.63	0.457	37.0	-17.2	0.3
833.5	20.186	*mixed benthos*	20.8	6004	54.4	131.3	279.2	2.82	0.470	61.0	-17.0	0.2
863.5	20.908	*mixed benthos*	22.8	6717	72.3	136.7	227.5	2.47	0.601	59.7	-17.2	0.2
1662.5	64.296	*mixed benthos*	17.1	4469	25.0	143.5	102.7	2.71	1.397	43.6	-17.3	0.3
1732.5	68.276	*mixed benthos*	16	3545	21.3	83.1	187.7	1.38	0.442	17.5	-16.9	0.2
2935.5	122.54	*mixed benthos*	14.5	2553	11.3	165.7	47.0	0.57	3.522	5.2	-15.6	0.8
2975.5	123.74	*mixed benthos*	16.1	2906	16.9	159.1	113.5	0.52	1.401	5.4	-14.7	0.8
3080.5	126.9	*mixed benthos*	23	4227	23.0	227.0	1012.6	1.73	0.224	26.3	-16.5	0.1
3115.5	127.95	*mixed benthos*	28.4	7851	56.9	203.2	296.0	1.08	0.686	30.4	-16.4	0.1
3125.5	128.25	*mixed benthos*	21.4	5008	50.6	198.6	257.9	1.09	0.770	19.7	-16.9	0.2
3194.5	133.4	*mixed benthos*	32.4	7855	30.2	71.8	149.0	1.40	0.482	39.6	-16.0	0.2
3235.5	135.87	*mixed benthos*	25.2	6965	48.5	42.2	359.1	1.55	0.118	38.7	-16.0	0.2
3235.5	135.87	*mixed benthos*	21.2	5024	29.7	78.7	392.9	1.34	0.200	24.3	-16.1	0.2

*Age model from Weldeab et al. (2007a)

Table A4.2: *REE concentrations of foraminiferal samples, normalized to PAAS (ppm) (Nance and Taylor, 1976), results x10e^3*

core depth (cm)	Age* (Cal kyr BP)	species	La	Ce	Pr	Nd	Sm	Eu	Gd	Tb	Dy	Ho	Er	Tm	Yb	Lu	Ce/Ce*[1]	LREE/ HREE[2]	MREE/ MREE*[3]
PAAS (ppm)			38	80	8.9	32	5.6	1.1	4.7	0.8	4.4	1	2.9	1	2.8	0.5			
planktonic foraminifera, fully cleaned																			
175.25	3.08	Bulk plankton	9	15	11	12	13	15	15	14	13	10	10	8	8	4	1.61	1.31	1.61
268.25	4.67	Bulk plankton	6	11	7	8	10	11	11	10	9	8	7	6	6	59	1.59	1.24	1.62
418.75	7.68	Bulk plankton	4	7	5	6	7	8	8	7	7	6	5	4	4	10	1.66	1.19	1.71
501	9.73	*G. ruber pink*	31	52	33	39	45	49	52	44	41	34	31	25	24	5	1.56	1.4	1.63
542.5	10.91	*G. ruber pink*	133	240	140	151	173	196	207	166	153	125	113	87	87	4	1.72	1.61	1.59
572.5	11.84	*G. ruber pink*	47	69	51	55	64	74	78	65	60	50	48	36	38	3	1.4	1.36	1.58
628.5	13.74	*G. ruber pink*	74	118	78	85	94	107	111	89	82	66	62	45	47	17	1.52	1.66	1.55
678.5	15.66	*G. ruber pink*	50	56	43	47	59	65	69	57	54	43	41	35	32	64	1.15	1.33	1.54
813.5	19.76	*G. ruber pink*	47	59	51	59	63	71	72	60	56	46	41	31	31	29	1.16	1.65	1.56
833.5	20.19	*G. ruber pink*	66	86	69	75	80	92	96	80	72	58	55	40	42	35	1.25	1.68	1.54
863.5	20.91	*G. ruber pink*	52	61	54	59	63	74	76	61	57	46	43	31	33	28	1.13	1.68	1.54
1474.25	55.02	Bulk plankton	2	2	2	2	3	3	3	3	3	2	2	1	2	2	1.08	1.47	1.72
1570.75	59.28	Bulk plankton	2	2	2	3	3	4	3	3	3	3	2	2	2	2	1.03	1.29	1.64
1585.5	59.94	Bulk plankton	4	5	5	5	6	6	7	6	6	5	5	4	4	10	1.09	1.24	1.55
1662.5	64.3	*G. ruber pink*	6	8	7	8	9	10	10	9	8	7	7	5	5	4	1.18	1.37	1.56
1732.5	68.28	*G. ruber pink*	3	4	3	4	4	5	5	5	4	3	3	2	2	24	1.17	1.38	1.65
2167.5	87.36	*G. ruber pink*	32	38	34	35	35	52	57	35	35	33	34	31	27	3	1.15	1.28	1.49
2640.5	108.87	Bulk plankton	5	8	6	7	9	9	10	8	8	7	7	5	5	14	1.37	1.18	1.57
2935.5	122.54	Bulk plankton	1	2	1	2	2	3	2	2	2	2	2	1	1	1	1.52	0.99	1.52
2975.5	123.74	Bulk plankton	2	3	2	2	2	3	3	3	3	2	2	2	2	14	1.58	0.99	1.54
3080.5	126.9	Bulk plankton	7	14	10	12	17	20	20	19	17	14	14	12	11	30	1.62	0.82	1.8
3115.5	127.95	*G. ruber pink*	21	34	26	33	36	43	47	40	39	35	33	26	29	24	1.38	0.94	1.57

Table A4.2: *REE concentrations of foraminiferal samples (continued)*

core depth (cm)	Age* (Cal kyr BP)	species	La	Ce	Pr	Nd	Sm	Eu	Gd	Tb	Dy	Ho	Er	Tm	Yb	Lu	Ce/Ce*[1]	LREE/ HREE[2]	MREE/ MREE*[3]
3125.5	128.25	*G. ruber pink*	75	113	88	95	105	131	136	118	102	95	85	73	80	1	1.38	1.16	1.52
3194.5	133.4	*G. ruber pink*	25	33	26	28	33	43	40	28	30	23	25	18	19	1	1.27	1.38	1.5
3235.5	135.87	*G. ruber pink*	11	15	13	17	18	19	23	20	19	18	18	13	13	22	1.14	1.02	1.61
planktonic foraminifera, only clay removed																			
572.5	11.84	*G. ruber pink*	189	307	222	247	289	347	350	296	276	226	211	164	172	132	1.47	1.47	1.64
628.5	13.74	*G. ruber pink*	253	351	285	346	377	423	424	350	328	265	249	187	191	142	1.24	1.65	1.57
678.5	15.66	*G. ruber pink*	250	320	257	285	328	377	383	323	303	252	241	186	200	151	1.22	1.44	1.52
benthic foraminifera, fully cleaned																			
502.5	9.77	*mixed benthos*	91	94	59	60	55	52	57	38	32	24	23	18	16	13	1.17	3.86	1
542.5	10.91	*mixed benthos*	117	143	94	94	99	103	110	81	70	52	49	40	36	29	1.31	2.61	1.27
572.5	11.84	*mixed benthos*	29	31	26	28	33	36	38	31	29	23	21	18	17	15	1.08	1.54	1.48
587	12.31	*mixed benthos*	31	32	26	29	33	36	37	29	26	20	19	16	15	12	1.07	1.83	1.44
599.5	12.73	*mixed benthos*	58	69	54	63	57	58	62	47	41	33	31	21	22	17	1.15	2.53	1.27
602.5	12.83	*mixed benthos*	41	52	44	52	53	58	59	46	42	35	31	24	24	17	1.17	1.88	1.47
602.5	12.83	*mixed benthos*	54	71	57	67	70	77	78	61	55	45	41	30	31	23	1.22	1.89	1.48
613	13.19	*mixed benthos*	61	67	53	57	70	78	80	64	58	44	41	33	30	24	1.11	1.75	1.57
628.5	13.74	*mixed benthos*	74	96	79	88	98	112	114	94	89	74	69	52	53	37	1.22	1.52	1.55
643.5	14.29	*mixed benthos*	31	28	28	31	30	35	35	27	25	22	20	14	15	12	0.91	1.94	1.33
657.5	14.95	*mixed benthos*	66	64	61	64	59	68	66	56	44	40	36	35	28	31	0.98	1.93	1.16
668.5	15.26	*mixed benthos*	41	32	35	38	33	38	39	28	27	23	22	16	17	13	0.81	2.21	1.18
678.5	15.66	*mixed benthos*	42	33	36	38	33	37	37	27	25	21	20	15	15	12	0.8	2.48	1.13
693.5	16.28	*mixed benthos*	32	23	30	33	31	34	38	29	26	23	21	16	17	13	0.72	1.84	1.32
713.5	17.14	*mixed benthos*	96	103	82	85	73	75	82	57	49	40	37	27	28	20	1.11	3.06	1.11
732.5	17.99	*mixed benthos*	39	38	34	37	41	43	45	35	31	23	21	18	16	14	1	2.06	1.4

Table A4.2: *REE concentrations of foraminiferal samples (continued)*

core depth (cm)	Age* (Cal kyr BP)	species	La	Ce	Pr	Nd	Sm	Eu	Gd	Tb	Dy	Ho	Er	Tm	Yb	Lu	Ce/Ce*[1]	LREE/ HREE[2]	MREE/ MREE*[3]
753.5	19.5	*mixed benthos*	144	188	159	170	181	202	199	158	136	106	96	70	71	52	1.01	2.19	1.48
773.5	19.04	*mixed benthos*	28	28	26	29	35	38	39	32	29	21	20	17	14	12	1.14	1.75	1.6
793.5	19.37	*mixed benthos*	33	43	40	48	52	56	58	47	42	35	32	25	23	17	1.23	1.66	1.59
813.5	19.76	*mixed benthos*	52	53	46	50	59	63	65	50	45	33	30	25	22	18	1.03	2.04	1.5
833.5	20.19	*mixed benthos*	113	154	126	137	146	166	165	129	114	91	81	59	60	45	1.27	2.04	1.51
863.5	20.91	*mixed benthos*	95	127	107	115	125	135	138	109	95	76	68	49	51	38	1.25	2.07	1.5
1662.5	64.3	*mixed benthos*	12	15	15	17	19	22	22	18	18	15	14	11	11	8	1.04	1.41	1.57
1732.5	68.28	*mixed benthos*	10	14	17	20	25	29	28	24	24	19	18	14	14	11	1.02	1.11	1.74
2935.5	122.54	*mixed benthos*	5	10	9	10	16	20	19	21	18	16	15	17	12	15	1.41	0.58	1.68
2975.5	123.74	*mixed benthos*	7	11	9	11	16	18	18	17	17	13	13	12	12	9	1.31	0.78	1.73
3080.5	126.9	*mixed benthos*	29	55	40	46	64	72	76	67	64	52	51	46	43	38	1.57	0.87	1.71
3115.5	127.95	*mixed benthos*	25	36	29	33	40	46	48	40	39	32	32	27	27	23	1.31	1.06	1.56
3125.5	128.25	*mixed benthos*	35	38	34	42	46	54	48	31	37	44	37	35	30	20	1	1.2	1.18
3194.5	133.4	*mixed benthos*	49	45	41	43	34	38	38	23	24	28	21	13	20	4	0.95	3.09	0.99
3235.5	135.87	*mixed benthos*	54	49	48	52	38	33	28	19	16	18	17	9	8	5	0.91	5.26	0.72
3235.5	135.87	*mixed benthos*	43	44	43	44	29	45	44	30	27	22	23	10	18	10	1.01	2.85	1.19

*Age model from Weldeab et al. (2007a),
[1] German & Elderfield (1990), [2] Dubinin & Rimskaya (2011), [3] MREE/MREE*=(Gd+Tb+Dy)/((LREE+HREE)/2)

Table A4.3: *εNd of detrital sediment fraction (total dissolution)*

core depth [cm]	age* [Cal. kyr BP]	initial weight [mg]	εNd	external error (2σ)
GeoB 4905-2, ***1329 m water depth, 2°30'0 N, 9°23'24 E***				
4.5	0.25	52.9	-15.80	0.23
MD03-2707, ***1294 m water depth, 2°30'07 N, 9°23'41 E***				
418.8	7.68	51.5	-17.26	0.23
1125.25	31.34	52.3	-18.52	0.23
1458.25	53.95	50.1	-19.66	0.23
1570.75	59.28	52.1	-18.34	0.23
1731.75	68.23	54.2	-18.59	0.23
2102.5	84.07	53.9	-17.59	0.23
2167.5	87.36	52.2	-18.49	0.23
2610.5	108.17	54.7	-17.10	0.23
2640.5	108.87	54.4	-18.25	0.23
2935.5	122.54	53.8	-16.46	0.31
2975.5	123.74	54.2	-15.35	0.31
3115.5	127.95	54.3	-18.00	0.23
3235.5	135.87	52.8	-19.47	0.23

*Age model of GeoB 4905 from Weldeab et al. (2005) and MD03-2707 from Weldeab et al. (2007a)

Table A4.4: *εNd of sediment leachates*

core depth [cm]	age* [Cal. Kyr BP]	initial weight [g]	de-carbonated sediment	εNd	external error (2σ)
GeoB 4905-2, ***1329 m water depth, 2°30'0 N, 9°23'24 E***					
3.50	0.12	2.47	bulk	-15.16	0.12
4.50	0.25	2.55	bulk	-15.22	0.12
4.50	0.25	2.51	bulk	-14.77	0.22
MD03-2707, ***1294 m water depth, 2°30'07 N, 9°23'41 E***					
28.00	0.60	2.14	bulk	-15.20	0.55
175.25	3.08	2.47	bulk	-15.50	0.12
268.25	4.67	2.46	bulk	-15.24	0.12
418.75	7.68	2.50	bulk	-15.22	0.12
506.00	9.87	0.1	< 63 µm	-16.07	0.10
544.00	10.96	0.1	< 63 µm	-15.51	0.10
569.00	11.73	0.1	< 63 µm	-15.91	0.10
587.00	12.31	0.1	< 63 µm	-15.99	0.10
591.00	12.44	0.1	< 63 µm	-15.92	0.10
605.00	12.91	0.1	< 63 µm	-16.18	0.10
615.00	13.26	0.1	< 63 µm	-16.39	0.11
630.00	13.80	0.1	< 63 µm	-16.40	0.11
645.00	14.35	0.1	< 63 µm	-16.12	0.12
660.00	14.93	0.1	< 63 µm	-16.73	0.12
670.00	15.32	0.1	< 63 µm	-16.43	0.13
680.50	15.74	0.1	< 63 µm	-16.54	0.10
690.50	16.15	0.1	< 63 µm	-16.62	0.11
715.50	17.23	0.1	< 63 µm	-16.98	0.10
735.50	18.13	0.1	< 63 µm	-16.94	0.11
755.50	18.77	0.1	< 63 µm	-17.05	0.12
776.50	19.09	0.1	< 63 µm	-17.19	0.11
795.50	19.41	0.1	< 63 µm	-17.70	0.12
815.50	19.80	0.1	< 63 µm	-17.94	0.10
835.50	20.23	0.1	< 63 µm	-18.23	0.11
1065.75	28.31	2.52	bulk	-16.95	0.12
1065.75	28.31	2.51	bulk	-16.81	0.12
1125.25	31.34	2.49	bulk	-17.21	0.12
1125.25	31.34	2.50	bulk	-17.08	0.12
1213.75	36.54	2.46	bulk	-16.95	0.12
1213.75	36.54	2.51	bulk	-16.86	0.12
1215.25	36.63	2.49	bulk	-17.03	0.12
1265.25	39.95	2.47	bulk	-16.73	0.12
1265.25	39.95	2.52	bulk	-17.15	0.24
1350.25	46.09	2.54	bulk	-16.88	0.12
1350.25	46.09	2.51	bulk	-16.96	0.16

Table A4.4: *εNd of sediment leachates (continued)*

core depth [cm]	age* [Cal. Kyr BP]	initial weight [g]	de-carbonated sediment	εNd	external error (2σ)
1446.25	53.08	2.47	bulk	-17.31	0.22
1458.25	53.95	2.49	bulk	-17.16	0.22
1475.25	55.06	2.50	bulk	-16.99	0.22
1570.75	59.28	2.48	bulk	-16.98	0.22
1585.50	59.94	2.49	bulk	-16.83	0.22
1661.75	64.25	2.51	bulk	-16.98	0.22
1731.75	68.23	2.51	bulk	-17.42	0.22
1731.75	68.23	2.51	bulk	-17.33	0.12
2102.50	84.07	2.51	bulk	-16.51	0.22
2167.50	87.36	2.52	bulk	-17.07	0.22
2610.50	108.17	2.51	bulk	-16.17	0.22
2640.50	108.87	2.50	bulk	-16.81	0.22
2640.50	108.87	2.50	bulk	-16.96	0.16
2785.50	117.45	2.50	bulk	-15.67	0.22
2785.50	117.45	2.50	bulk	-15.69	0.12
2975.50	123.74	2.50	bulk	-15.23	0.22
2975.50	123.74	2.50	bulk	-15.46	0.16
3080.50	126.90	2.51	bulk	-15.63	0.22
3080.50	126.90	2.51	bulk	-15.97	0.16
3115.50	127.95	2.51	bulk	-16.06	0.22
3115.50	127.95	2.51	bulk	-16.01	0.12
3125.50	128.25	2.52	bulk	-15.73	0.22
3194.50	133.40	2.52	bulk	-15.95	0.22
3235.50	135.87	2.50	bulk	-17.03	0.22

*Age model of GeoB 4905 from Weldeab et al. (2005) and MD03-2707 from Weldeab et al. (2007a)

Table A5.1: *Trace element and results of stable isotope analyses of N. dutertrei core top samples. Test size = 300-400 µm.*

Core (GIK)	latitude	longitude	bottom water depth m	weight/ specimen µg	Mg/Ca mmol/ mol	Mg/Ca[1] mmol/ mol	Ba/Ca µmol/ mol	$\delta^{18}O$ ‰ VPDB	$\delta^{13}C$ ‰ VPDB	T_{calc}[2] °C
16756-1A	9.07	-17.00	1495	35	1.411	1.411		1.46	1.26	11.59
16757-1A	8.98	-16.94	2250	36	1.746	1.746	4.51	0.51	1.34	16.19
16755-1A	9.25	-16.85	1002	31	1.296	1.296	1.86	1.00	1.23	13.81
16758-2A	8.75	-16.79	3089	28	1.477	1.477	2.45	0.10	1.71	18.19
16754-1A	9.50	-16.62	646	29	1.324	1.324	1.13	0.89	1.36	14.36
16753-1A	9.58	-16.54	457	33	1.669	1.669				
16769-1A	6.12	-16.27	4933	25	1.134		0.94	0.39	1.48	
16770-2A	0.79	-15.58	2818	38	1.430	1.430	3.39	0.03	1.52	18.50
16768-1A	7.62	-15.17	4327	27	1.628	1.997	1.05	-0.28	1.45	19.97
16767-1A	8.10	-14.72	3123	26	1.552	1.552	1.22			
16766-1A	8.28	-14.53	2383	33	1.965	1.965	1.49	0.07	1.15	18.32
16765-1A	8.32	-14.48	1500	24	2.063	2.063	0.83	0.13	1.28	18.04
16763-1A	8.37	-14.43	701	31	2.032	2.032	1.55	0.13	1.59	18.02
16764-1A	8.37	-14.43	1025	26	1.358	1.358	5.86			
16772-1A	-1.33	-11.97	3911	37	1.754	1.754	1.61	-0.08	1.68	19.17
16776-2A	3.73	-11.38	4257	30	1.526	1.794	1.06	0.16	1.75	17.99
16775-2A	0.98	-11.15	3730	36	1.572	1.572	4.90	0.01	1.70	18.74
16777-1A	3.92	-10.62	3282	31	1.801	1.801	1.36	-0.03	1.93	18.92
16774-3A	-0.02	-9.95	4398	34	1.354	1.82	1.77	0.29	1.67	17.42
16778-2A	4.12	-9.73	2496	29	2.283	2.283	1.74			
16779-1A	4.20	-9.63	2002	31	1.835	1.835	3.21	-0.12	1.70	19.34
16780-1A	4.29	-9.49	1483	32	2.378	2.378	2.64	0.18	1.65	17.88
16773-2A	-0.95	-9.38	4658	32	1.117		0.85	0.20	1.71	
16788-1A	4.43	-9.27	831	34	1.895	1.895	1.49	0.33	1.43	17.19
16787-1A	4.47	-9.19	674	25	1.627	1.627	1.33	0.67	1.41	15.55
16786-1A	4.50	-9.14	451	37	1.905	1.905	3.11			
16803-1A	4.50	-6.52	653	24	1.549	1.549	0.64	0.05	1.17	18.44
16802-1A	4.50	-6.47	691	28	1.503	1.503	0.72	0.28	1.28	17.35
16800-1A	4.47	-6.44	982	28	1.782	1.782	0.84	-0.25	1.71	19.88
16799-1A	4.44	-6.43	1505	25	1.315	1.315	0.84	0.18	1.50	17.85
16798-1A	4.34	-6.40	2221	24	1.680	1.680	4.41			
16797-2A	4.24	-6.35	2773	30	1.915	1.915	1.90	0.33	1.34	17.12
16796-1A	4.10	-6.27	3296	33	1.966	1.966	1.72	-0.22	1.63	19.74
16795-1A	3.45	-6.22	4307	26	1.589	1.93	1.30	0.13	1.45	18.09
16804-1A	4.47	-4.67	2992	29	1.819	1.819	1.83	0.30	1.34	17.27
16805-1A	4.80	-4.58	2053	32	2.036	2.036	1.87	-0.01	1.36	18.74
16806-1A	4.95	-4.55	1204	23	1.100	1.100	0.53	0.00	1.40	18.70
16815-2A	4.97	-4.52	913	21	1.604	1.604	1.18	0.19	1.35	17.79

Table A5.1: *Trace element and results of stable isotope analyses of N. dutertrei core top samples. Test size = 300-400 µm (continued).*

Core (GIK)	latitude	longitude	bottom water depth m	weight/ specimen µg	Mg/Ca mmol/ mol	Mg/Ca[1] mmol/ mol	Ba/Ca µmol/ mol	$\delta^{18}O$ ‰ VPDB	$\delta^{13}C$ ‰ VPDB	T_{calc}[2] °C
16816-1A	5.00	-4.52	475	26	1.568	1.568	0.77	0.48	1.09	16.39
16814-1A	4.98	-4.52	698	24	1.399	1.399	0.89	0.02	1.37	18.62
16807-1A	3.72	-3.05	3102	26	1.496	1.496	3.22	0.19	1.65	17.77
16808-2A	3.80	-2.85	2234	38	1.991	1.991	2.46	0.04	1.54	18.50
16809-2A	4.15	-2.47	1500	33	2.199	2.199	2.17	0.02	1.73	18.61
16817-1A	4.32	-2.38	1001	29	1.621	1.621	0.74	-0.07	1.52	19.04
16818-1A	4.38	-2.37	749	24	1.557	1.557	2.27	0.06	1.45	18.44
16819-2A	4.45	-2.33	631	26	1.803	1.803	1.23	-0.05	1.43	18.93
16820-1A	4.50	-2.30	445	30	1.501	1.501	0.87			
16825-1C	3.67	-1.79	4970	31	1.698		1.43	-0.22	1.32	
16833-2A	4.30	-1.15	1466	27	1.747	1.747	3.38	0.53	1.35	
16835-1A	4.24	-1.15	3219	26	1.394	1.394	1.26	0.27	1.59	
16831-1A	4.35	-1.15	632	31	1.899	1.899	1.13	0.27	1.28	
16832-1A	4.33	-1.14	920	29	1.618	1.618	1.23	-0.10	1.60	
16836-1A	4.12	-1.09	4264	28	1.601	1.88	1.15	-0.03	1.40	
16837-1A	3.67	0.74	4449	31	1.490	2.033	1.20	-0.22	1.51	19.87
16845-1A	5.55	1.15	2007	33	2.372	2.372	3.02	0.02	1.39	18.69
16842-1A	5.82	1.15	390	25	2.010	2.010	4.92			
16843-1A	5.77	1.15	740	27	1.326	1.326	1.16			
16844-1A	5.72	1.15	1230	28	1.996	1.996	3.07	-0.15	1.28	19.52
16838-1A	4.65	1.18	3736	33	2.163	2.163	1.91	-0.10	1.49	19.27
16846-1A	5.35	1.28	2739	31	2.045	2.045	1.99	-0.17	1.33	19.62
16856-1A	4.80	3.40	2860	32	2.090	2.090	2.58	-0.26	1.60	20.05
16854-1A	6.02	3.60	1583	30	2.027	2.027	1.94	-0.18	1.35	19.66
16853-2A	6.05	3.63	1018	27	2.418	2.418	2.23	-0.29	1.33	20.17
16852-1A	6.07	3.64	770	30	2.098	2.098	0.95	0.33	1.34	17.23
16851-1A	6.07	3.65	495	25	1.939	1.939	1.55			
16855-1A	5.50	3.77	2173	32	2.545	2.545	3.68	-0.18	1.67	19.65
16867	-2.20	5.10	3891	31	1.186	1.186	1.06	0.52	1.63	16.35
16866-1A	2.00	5.72	3501	29	1.592	1.592	2.74	0.30	1.75	17.42
16870-1A	-0.20	5.97	2469	35	1.446	1.446	2.85	0.54	1.67	16.27
16869-1A	-0.20	6.00	1837	37	1.489	1.489	3.18	0.60	1.76	15.98
16868-2A	-0.22	6.02	1284	37	1.513	1.513	3.99	0.34	1.66	17.22
16865-1A	2.67	6.05	2492	31	1.860	1.860	3.08	-0.03	1.84	19.03
16864-1A	3.15	6.28	1495	33	2.334	2.334		-0.01	1.59	18.94
16863-2A	3.39	6.40	993	30	2.492	2.492	3.84	-0.09	1.72	19.29
16862-1A	3.54	6.48	698	26	1.847	1.847	2.54	-0.26	1.56	20.11
16861-1A	3.62	6.50	403	31	1.616	1.616	1.94			

Table A5.1: *Trace element and results of stable isotope analyses of N. dutertrei core top samples. Test size = 300-400 µm (continued).*

Core (GIK)	latitude	longitude	bottom water depth	weight/ specimen	Mg/Ca	Mg/Ca[1]	Ba/Ca	$\delta^{18}O$	$\delta^{13}C$	T_{calc}[2]
			m	µg	mmol/ mol	mmol/ mol	µmol/ mol	‰ VPDB	‰ VPDB	°C
16871-1A	-0.72	6.93	2987	32	1.290	1.290	3.47	0.15	2.04	18.16
16872-1A	-0.34	8.03	2223	32	1.921	1.921	3.67	0.08	1.48	18.57
16873-1A	-0.33	8.30	1619	32	2.372	2.372	2.73	-0.14	1.31	19.61
16874-2A	-0.34	8.47	997	28	1.777	1.777	2.77	0.17	1.48	18.15
16875-1A	-0.33	8.55	803	26	1.828	1.828	2.19	-0.36	1.49	20.68
16880-1A	-0.33	8.65	560	28	2.085	2.085	1.37			

[1] *Mg/Ca values corrected after Regenberg et al. (2006), samples > 4500 m are excluded*
[2] *T_{calc} temperature calculation based on $\delta^{18}O_{sw}$ and calculated after Bemis et al. (1998), $\delta^{18}O_{sw}$ calculated after LeGrande and Schmidt (2006) with salinity in 75m (12-7° W, & 0-10°E) and 150 m (20-12°W & 7-0°W) from WOA09 (Locarnini et al., 2010)*

Table A5.2: *Trace element and results of stable isotope analyses of G. crassaformis core top samples. Test size = 300-400 µm.*

Core (GIK)	latitude	longitude	bottom water depth	weight/ specimen	Mg/Ca	Mg/Ca[1]	Ba/Ca	$\delta^{18}O$	$\delta^{13}C$	T_{calc}[2]
			m	µg	mmol/ mol	mmol/ mol	µmol/ mol	‰ VPDB	‰ VPDB	°C
16756-1A	9.07	-17.00	1495	38	0.861	0.861	2.41	0.73	1.99	8.77
16757-1A	8.98	-16.94	2250	35	0.845	0.845	1.64	0.99	2.02	8.59
16755-1A	9.25	-16.85	1002					0.85	2.20	7.77
16758-2A	8.75	-16.79	3089	32	0.882	0.882	2.40	0.99	2.12	8.13
16769-1A	6.12	-16.27	4933	26	0.688		0.77	1.06	2.40	
16770-2A	0.79	-15.58	2818	41	1.052	1.052	3.10	0.93	1.98	8.60
16768-1A	7.62	-15.17	4327	27	0.846	1.192	2.54	0.75	1.68	10.19
16767-1A	8.10	-14.72	3123	28	0.841	0.841	2.30			
16766-1A	8.28	-14.53	2383	35	1.309	1.309	4.17	0.86	1.70	10.15
16765-1A	8.32	-14.48	1500	25	1.188	1.188	3.91	0.86	2.04	8.49
16763-1A	8.37	-14.43	701	32	1.290	1.290	3.30	0.86	1.95	8.91
16772-1A	-1.33	-11.97	3911	39	0.850	0.889	2.82	0.97	2.12	7.95
16776-2A	3.73	-11.38	4257	34	0.757	1.051	1.18	1.20	1.92	8.91
16775-2A	0.98	-11.15	3730	39	1.055	1.055	3.79	0.97	2.26	7.26
16777-1A	3.92	-10.62	3282	31	0.943	0.943	2.55	1.14	2.12	7.96
16774-3A	-0.02	-9.95	4398	39	1.023	1.421	2.92	1.01	2.04	8.35
16778-2A	4.12	-9.73	2496	25	0.896	0.896	2.34			
16779-1A	4.20	-9.63	2002	32	1.096	1.096	3.49	1.20	2.07	8.20
16780-1A	4.29	-9.49	1483	29	1.146	1.146	2.45	0.95	1.39	11.47
16773-2A	-0.95	-9.38	4658	40	0.953		1.65	1.02	1.89	
16788-1A	4.43	-9.27	831	34	1.397	1.397	4.23	0.66	2.46	6.36
16800-1A	4.47	-6.44	982	25	1.028	1.028	2.67	0.51	3.73	
16799-1A	4.44	-6.43	1505					0.85	1.87	9.18
16797-2A	4.24	-6.35	2773					0.75	1.63	10.33
16796-1A	4.10	-6.27	3296	28	0.960	0.960	3.50			
16795-1A	3.45	-6.22	4307	26	0.915	1.246	2.44	1.05	2.19	7.64
16805-1A	4.80	-4.58	2053	30	1.344	1.344	3.61			
16806-1A	4.95	-4.55	1204					1.04	1.89	9.06
16807-1A	3.72	-3.05	3102	22	0.866	0.866	2.24	1.15	2.14	7.85
16808-2A	3.80	-2.85	2234	24	1.082	1.082	2.78	1.14	1.78	9.60
16809-2A	4.15	-2.47	1500	31	1.176	1.176	2.74	1.12	1.74	9.78
16817-1A	4.32	-2.38	1001	20	0.995	0.995	2.08	1.29	2.23	7.43
16818-1A	4.38	-2.37	749					0.77	1.97	8.67
16833-2A	4.30	-1.15	1466	24	0.862	0.862	1.97	1.03	2.18	
16835-1A	4.24	-1.15	3219	32	1.011	1.011	3.27			
16831-1A	4.35	-1.15	632	34	1.437	1.437	4.10			
16832-1A	4.33	-1.14	920	32	1.273	1.273	4.23	1.00	1.87	

Table A5.2: *Trace element and results of stable isotope analyses of G. crassaformis core top samples. Test size = 300-400 µm (continued).*

Core (GIK)	latitude	longitude	bottom water depth	weight/ specimen	Mg/Ca	Mg/Ca[1]	Ba/Ca	$\delta^{18}O$	$\delta^{13}C$	T_{calc}[2]
			m	µg	mmol/ mol	mmol/ mol	µmol/ mol	‰ VPDB	‰ VPDB	°C
16836-1A	4.12	-1.09	4264	27	0.832	1.131	2.19	0.90	1.71	
16837-1A	3.67	0.74	4449	26	0.846	1.281	1.61	0.93	2.03	8.40
16845-1A	5.55	1.15	2007	30	1.546	1.546	4.54	0.61	1.30	11.89
16844-1A	5.72	1.15	1230	27	1.283	1.283	3.68			
16838-1A	4.65	1.18	3736	33	1.382	1.382	5.13	0.88	1.43	11.30
16846-1A	5.35	1.28	2739	29	1.437	1.437	4.24	0.78	1.65	10.25
16856-1A	4.80	3.40	2860	33	1.553	1.553	5.67	0.98	1.62	10.36
16854-1A	6.02	3.60	1583	26	0.803	0.803	1.65			
16853-2A	6.05	3.63	1018	24	1.299	1.299	5.32	0.32	1.46	11.16
16852-1A	6.07	3.64	770	22	0.786	0.786	1.57			
16855-1A	5.50	3.77	2173	32	1.337	1.337	3.55	1.00	1.65	10.26
16867	-2.20	5.10	3891	29	0.850	0.874	2.41	1.17	2.02	8.45
16866-1A	2.00	5.72	3501	29	1.042	1.042	3.56	1.24	2.18	7.69
16870-1A	-0.20	5.97	2469	35	1.289	1.289	5.36	0.73	1.84	9.29
16869-1A	-0.20	6.00	1837	40	1.406	1.406	6.31	1.03	1.81	9.46
16868-2A	-0.22	6.02	1284	37	1.284	1.284	4.99			
16865-1A	2.67	6.05	2492	29	1.370	1.370	5.01	1.09	1.71	9.93
16864-1A	3.15	6.28	1495	28	1.452	1.452	4.72	1.03	1.56	
16863-2A	3.39	6.40	993	24	1.171	1.171	3.12			
16862-1A	3.54	6.48	698	20	0.904	0.904	2.17	0.71	1.40	
16871-1A	-0.72	6.93	2987	29	1.031	1.031	2.44	1.12	2.17	7.74
16872-1A	-0.34	8.03	2223	30	1.320	1.320	5.35	0.86	1.43	11.26
16873-1A	-0.33	8.30	1619	27	1.564	1.564	5.21	0.95	1.75	9.72
16874-2A	-0.34	8.47	997	28	1.269	1.269	3.01	1.02	1.74	9.78
16875-1A	-0.33	8.55	803	24	0.909	0.909	2.01			

[1]Mg/Ca values corrected after Regenberg et al. (2006), samples > 4500 m are excluded
[2]T_{calc} temperature calculation based on $\delta^{18}O_{sw}$ and calculated after Bemis et al. (1998), $\delta^{18}O_{sw}$ calculated after LeGrande and Schmidt (2006) with salinity in 400 m from WOA09 (Locarnini et al., 2010)

Table A5.3: *Trace element and results of stable isotope analyses of N. dutertrei down core samples. Test size = 300-400 µm.*

depth	age	$\delta^{18}O$	$\delta^{13}C$	Mg/Ca	Ba/Ca	T[1]	$\delta^{18}O_{sw}$[2]	$\delta^{18}O_{ivf\ sw}$[3]
cm	kyr	‰ VPDB	‰ VPDB	mmol/mol	µmol/mol	°C	‰ SMOW	‰ SMOW
400.5	7.27	-0.07	1.66					
410.5	7.49	0.20	1.75	1.725	1.83	15.7	0.31	0.24
418.5	7.67	0.26	1.28	1.911	1.43	17.1	0.66	0.59
424.5	7.81			1.579	2.32	14.6		
432.5	8.00	0.05	1.48	1.655	(6.81)	15.2	0.05	-0.03
448.5	8.38	-0.87	1.44	1.671	1.62	15.3	-0.85	-0.96
456.5	8.57	-0.06	1.62	1.608	(23.25)	14.8	-0.15	-0.28
464.5	8.77	0.05	1.18	1.779	4.01	16.2	0.25	0.10
472.5	8.97			1.810	(9.49)	16.4		
480.5	9.18			1.842		16.6		
488.5	9.39	0.65	1.24	2.020	(15.40)	17.9	1.21	1.01
500.5	9.71	0.12	1.34	2.043	(6.17)	18.0	0.70	0.47
504.5	9.82	0.29	1.57	2.198	1.93	19.0	1.08	0.84
508.5	9.93	-0.35	1.41	1.874	(26.02)	16.9	0.00	-0.26
512.5	10.04	0.24	1.44	1.808	2.86	16.4	0.49	0.22
520.5	10.27	-0.75	1.36	2.046	3.78	18.0	-0.16	-0.45
524.5	10.38	-0.31	1.32		3.29			
528.5	10.50	-0.56	1.04	2.102	(9.13)	18.4	0.11	-0.21
532.5	10.61	0.38	1.38	2.181	1.62	18.9	1.15	0.81
536.5	10.73	-0.12	1.30	1.920	1.39	17.2	0.30	-0.05
542.5	10.91	0.32	1.40	2.539	(9.51)	20.9	1.51	1.14
544.5	10.97	0.81	1.38	1.921	(16.54)	17.2	1.22	0.84
548.5	11.09	0.58	1.25	2.208	2.08	19.1	1.38	0.99
552.5	11.21	0.72	1.29	1.520	(7.02)	14.0	0.48	0.07
556.5	11.33	0.62	1.21	1.912	5.96	17.1	1.02	0.60
560.5	11.46			1.604	3.35	14.8		
564.5	11.58	0.54	1.14	1.661	1.77	15.2	0.55	0.09
568.5	11.71	0.61	1.04	1.792	1.80	16.3	0.83	0.36
572.5	11.84	0.45	1.01	1.829	2.77	16.5	0.73	0.24
576.5	11.96	0.68	1.23	1.803	1.30	16.3	0.92	0.42
580.5	12.09	0.62	1.23	1.806	1.18	16.4	0.86	0.34
584.5	12.22	0.48	1.15	1.483	(8.90)	13.7	0.17	-0.37
588.5	12.36	0.58	1.15	1.813	2.78	16.4	0.83	0.28
592.5	12.49	0.80	1.16	1.713	2.22	15.7	0.90	0.33
596.5	12.62	0.74	1.28	1.716	5.75	15.7	0.83	0.25
598.5	12.69	0.54	1.12	1.845	2.46	16.6	0.84	0.25
605.5	12.93	0.80	1.13	1.830	2.97	16.5	1.08	0.45
610.5	13.16	-0.13	1.19	1.559	1.61	14.4	-0.30	-0.95
615.5	13.31			2.080	3.87	18.3		

Table A5.3: *Trace element and results of stable isotope analyses of N. dutertrei down core samples. Test size = 300-400 µm (continued).*

depth	age	$\delta^{18}O$	$\delta^{13}C$	Mg/Ca	Ba/Ca	T[1]	$\delta^{18}O_{sw}$[2]	$\delta^{18}O_{ivf\ sw}$[3]
cm	kyr	‰ VPDB	‰ VPDB	mmol/mol	µmol/mol	°C	‰ SMOW	‰ SMOW
620.5	13.47			1.777	4.11	16.1		
625.5	13.62			1.759	2.94	16.0		
630.5	13.77	0.58	1.48	1.695	(8.07)	15.5	0.65	-0.08
635.5	13.93	1.01	1.15	1.756	4.66	16.0	1.17	0.43
640.5	14.09	1.05	1.27	1.595	5.70	14.7	0.94	0.18
650.5	14.40	1.34	1.03	1.613	5.27	14.8	1.27	0.48
655.5	14.56	1.10	1.19	1.778	5.50	16.2	1.30	0.50
660.5	14.71			1.567	(9.00)	14.4		
665.5	14.87	1.28	1.18	1.526	4.08	14.1	1.05	0.22
670.5	15.03	1.00	1.18	1.606	(10.72)	14.8	0.91	0.06
675.5	15.19	1.28	0.90	1.547	(38.38)	14.3	1.08	0.22
680.5	15.36	1.06	1.10	1.846	(30.12)	16.7	1.36	0.48
685.5	15.52	1.56	1.31	1.392	(7.35)	12.9	1.08	0.18
690.5	15.68	1.59	1.37	1.626	(6.22)	15.0	1.53	0.63
695.5	15.84	1.50	1.38	1.810	3.50	16.4	1.75	0.84
700.5	16.01	1.43	1.41	1.686	3.79	15.4	1.48	0.56
705.5	16.17	1.62	1.66	1.334	(6.18)	12.3	1.01	0.09
710.5	16.34	1.67	1.61	1.312	(9.95)	12.1	1.02	0.08
715.5	16.51	1.27	1.57	1.495	2.93	13.8	0.99	0.04
720.5	16.67	1.32	1.45	1.531	2.70	14.1	1.09	0.14
725.5	16.84	1.44	1.67	1.729	2.36	15.8	1.56	0.60
730.5	17.01	1.34	1.50	1.678	(14.94)	15.4	1.38	0.41
735.5	17.18	1.62	1.66	1.573	2.58	14.5	1.47	0.50
740.5	17.35	1.40	1.61	1.630	2.02	15.0	1.36	0.38
745.5	17.52	1.53	1.65	1.578	1.69	14.5	1.39	0.40
750.5	17.69	1.55	1.77	1.599	3.01	14.7	1.46	0.46
755.5	17.86	1.43	1.85	1.509	1.25	13.9	1.17	0.17
760.5	18.04	1.32	1.59	1.712	(6.79)	15.6	1.41	0.41
765.5	18.21	1.39	1.68	1.350	3.00	12.4	0.82	-0.19
770.5	18.38	1.22	1.69	1.274	2.26	11.7	0.48	-0.53
775.5	18.56			1.589	(12.95)	14.6		
780.5	18.73	1.48	1.53	1.427	2.56	13.2	1.06	0.04
785.5	18.91	1.22	1.75	1.670	(6.79)	15.3	1.24	0.22
790.5	19.09	1.54	1.69	1.728	2.79	15.8	1.66	0.63
795.5	19.26	1.59	1.62	1.342	2.03	12.4	1.00	-0.03
800.5	19.44	1.51	1.62	1.750	1.64	15.9	1.66	0.63
810.5	19.80	1.19	1.79	1.834	2.07	16.6	1.47	0.43
820.5	20.16	1.58	1.71	1.664	5.61	15.3	1.59	0.55
830.5	20.53	1.80	1.68	1.726	(7.08)	15.8	1.92	0.88

Table A5.3: *Trace element and results of stable isotope analyses of N. dutertrei down core samples. Test size = 300-400 µm (continued).*

depth	age	$\delta^{18}O$	$\delta^{13}C$	Mg/Ca	Ba/Ca	T[1]	$\delta^{18}O_{sw}$[2]	$\delta^{18}O_{ivf\ sw}$[3]
cm	kyr	‰ VPDB	‰ VPDB	mmol/mol	µmol/mol	°C	‰ SMOW	‰ SMOW
840.5	20.89	1.43	1.55	1.558	2.70	14.4	1.25	0.22
850.5	21.26	1.40	1.83	1.342	2.39	12.4	0.80	-0.22
860.5	21.64	1.19	1.69	1.444	5.74	13.4	0.80	-0.22
870.5	22.01	1.43	1.68	1.591	(8.49)	14.7	1.32	0.31
880.5	22.39	1.44	1.88	1.807	4.52	16.4	1.68	0.67
890.5	22.77	1.60	1.73	1.735	(11.20)	15.8	1.73	0.72
900.5	23.15	1.44	1.65	1.833	2.12	16.6	1.73	0.73
910.5	23.54	1.51	1.72	1.455	4.71	13.5	1.15	0.17
920.5	23.93	1.20	1.72	1.517	(15.29)	14.0	0.95	-0.02
930.5	24.32	1.57	1.70	1.453	(16.19)	13.4	1.21	0.24
940.5	24.72	1.39	1.79	1.606	(14.18)	14.8	1.30	0.35
950.5	25.11	1.57	1.81	1.738	(9.62)	15.8	1.70	0.76
960.5	25.51	1.34	1.80	1.551	(31.99)	14.3	1.16	0.24
970.5	25.92	1.43	1.86	1.772	5.62	16.1	1.61	0.71
980.5	26.32	1.57	1.74	1.521	4.31	14.1	1.33	0.44
985.5	26.52	1.68	1.70	1.749	(15.84)	15.9	1.83	0.96
990.5	26.73	1.38	1.82	1.847	3.93	16.7	1.69	0.82
1000.5	27.14	1.44	1.76	1.600	(9.11)	14.7	1.34	0.49
1002.0	27.20	1.32	1.59	1.846	(6.79)	16.7	1.63	0.78
1004.0	27.28	1.48	1.93	1.707	(7.70)	15.6	1.57	0.72
1007.0	27.41	1.31	1.97	1.490	3.08	13.8	1.01	0.17
1009.0	27.49	1.30	1.92	1.686	3.50	15.4	1.35	0.51
1010.5	27.55	1.23	1.84	1.725		15.7	1.35	0.51
1012.0	27.61	0.88	1.70	2.106	(11.77)	18.4	1.55	0.73
1014.0	27.70	1.25	1.62	1.791	(33.66)	16.3	1.46	0.64
1017.0	27.82	1.27	1.90	1.968	2.31	17.5	1.75	0.93
1019.0	27.90	1.28	1.79	1.802	3.93	16.3	1.52	0.70
1020.5	27.97	1.12	1.67	1.671	(17.25)	15.3	1.15	0.34
1022.0	28.03	1.19	1.70					
1024.0	28.11	0.96	1.45	1.783	4.37	16.2	1.17	0.37
1027.0	28.24	1.24	1.70	1.854	(21.28)	16.7	1.56	0.77
1029.0	28.32	1.05	1.63	1.793	(16.82)	16.3	1.27	0.48
1030.5	28.39	1.33	1.68	1.618	2.96	14.9	1.26	0.48
1032.0	28.45	1.05	1.44	1.577	4.80	14.5	0.91	0.13
1034.0	28.53	1.34	1.77	1.650	(7.41)	15.1	1.33	0.56
1037.0	28.66	1.45	1.57	1.739	(14.51)	15.9	1.58	0.81
1039.0	28.74	1.19	1.53	1.669	3.22	15.3	1.21	0.45
1040.5	28.81	1.34	1.73	1.484	5.37	13.7	1.03	0.27
1042.0	28.87	1.19	1.65	1.632	2.20	15.0	1.14	0.39

Table A5.3: *Trace element and results of stable isotope analyses of N. dutertrei down core samples. Test size = 300-400 µm (continued).*

depth	age	$\delta^{18}O$	$\delta^{13}C$	Mg/Ca	Ba/Ca	T[1]	$\delta^{18}O_{sw}$[2]	$\delta^{18}O_{ivf\ sw}$[3]
cm	kyr	‰ VPDB	‰ VPDB	mmol/mol	µmol/mol	°C	‰ SMOW	‰ SMOW
1044.0	28.95	1.05	1.67	1.717	3.63	15.7	1.14	0.40
1047.0	29.08	1.12	1.64	1.948	(8.93)	17.4	1.57	0.83
1049.0	29.17	1.62	1.75	1.694	(11.87)	15.5	1.68	0.94
1050.5	29.23	1.17	1.84	1.713	3.17	15.7	1.27	0.53
1052.0	29.29	1.14	1.62	1.499	3.45	13.9	0.86	0.12
1054.0	29.38	1.35	1.79	1.775	(18.19)	16.1	1.55	0.81
1057.0	29.51	1.32	1.71	2.021	(10.90)	17.9	1.88	1.15
1059.0	29.59	1.41	1.53	1.665	3.07	15.3	1.43	0.70
1060.5	29.66	1.41	1.57	1.737	(6.73)	15.8	1.54	0.82
1062.0	29.72	1.47	1.48	1.669	4.06	15.3	1.49	0.77
1064.0	29.81	1.06	1.87	1.935	3.26	17.3	1.49	0.78
1067.0	29.94	0.87	1.62	1.783	(9.67)	16.2	1.08	0.37
1069.0	30.02	1.27	1.53	1.707	(6.06)	15.6	1.35	0.64
1070.5	30.09	1.03	1.54	1.748	3.78	15.9	1.18	0.47
1072.0	30.15	1.02	1.50	1.900	3.56	17.0	1.40	0.69
1074.0	30.24	0.97	1.66	1.871	5.10	16.8	1.31	0.60
1077.0	30.37	1.16	1.56	1.438	(6.73)	13.3	0.76	0.06
1079.0	30.45	1.00	1.56	1.679	4.38	15.4	1.04	0.34
1080.5	30.52	1.34	1.57	1.522	(7.65)	14.1	1.10	0.41
1082.0	30.58	1.19	1.72	1.541	(6.12)	14.2	0.98	0.29
1084.0	30.67	1.03	1.68	1.797	(20.30)	16.3	1.26	0.57
1087.0	30.80	0.95	1.78	1.640	1.71	15.1	0.92	0.24
1089.0	30.89	1.33	1.72	1.356	(10.21)	12.5	0.77	0.08
1090.5	30.95	1.45	1.69	2.041	3.59	18.0	2.03	1.35
1092.0	31.02	0.97	1.83	1.633	(13.79)	15.0	0.93	0.25
1094.0	31.10	0.70	1.62	1.705	2.05	15.6	0.78	0.10
1097.0	31.23	1.14	1.86	1.686	4.97	15.4	1.19	0.51
1099.0	31.32	1.25	1.75	1.581	(7.63)	14.6	1.12	0.44
1100.5	31.39	1.07	1.80	1.571	2.01	14.5	0.92	0.25
1102.0	31.45	1.24	1.80	1.440	3.47	13.3	0.85	0.17
1104.0	31.54	1.19	1.51	1.436	5.84	13.3	0.79	0.12
1107.0	31.67	1.31	1.72	1.874	1.32	16.9	1.66	0.99
1109.0	31.76	1.29	1.77	1.837	5.91	16.6	1.58	0.91
1110.5	31.83	1.08	1.83	1.920	4.22	17.2	1.49	0.82
1112.0	31.89	1.19	1.78	1.764	2.77	16.0	1.36	0.70
1114.0	31.98	1.12	1.69	1.519	(10.70)	14.0	0.88	0.21
1117.0	32.11	0.95	1.80	1.379	(13.67)	12.7	0.43	-0.23
1119.0	32.20	1.45	1.72	1.752	1.61	16.0	1.61	0.94
1120.5	32.27	1.00	1.76	1.383	1.64	12.8	0.49	-0.17

Table A5.3: *Trace element and results of stable isotope analyses of N. dutertrei down core samples. Test size = 300-400 µm (continued).*

depth	age	$\delta^{18}O$	$\delta^{13}C$	Mg/Ca	Ba/Ca	T[1]	$\delta^{18}O_{sw}$[2]	$\delta^{18}O_{ivf\ sw}$[3]
cm	kyr	‰ VPDB	‰ VPDB	mmol/mol	µmol/mol	°C	‰ SMOW	‰ SMOW
1122.0	32.34	1.24	1.83	1.779	1.45	16.2	1.43	0.77
1124.0	32.42	1.11	1.81	1.540	2.28	14.2	0.91	0.24
1127.0	32.56	1.05	1.55	2.055	3.63	18.1	1.65	0.98
1129.0	32.65	1.16	1.80	1.800	1.63	16.3	1.39	0.72
1130.5	32.71	0.84	1.79	1.428	1.47	13.2	0.43	-0.24
1132.0	32.78	0.98	1.72	1.764	2.47	16.0	1.16	0.49
1134.0	32.87	1.21	1.72	1.473	1.73	13.6	0.88	0.21
1137.0	33.00	1.44	1.67	1.472	2.97	13.6	1.11	0.44
1139.0	33.09	1.30	1.64	1.486	1.63	13.7	1.00	0.33
1140.5	33.16	1.07	1.64	1.370	(7.20)	12.7	0.54	-0.13
1142.0	33.23	1.18	1.62	2.002	(14.10)	17.7	1.71	1.04
1144.0	33.32	0.80	1.75	1.753	1.70	16.0	0.96	0.29
1147.0	33.45	1.15	1.76	1.494	4.62	13.8	0.86	0.19
1149.0	33.54	1.11	1.69	1.791	(6.54)	16.2	1.32	0.65
1150.5	33.61	0.90	1.66	1.453	1.74	13.4	0.53	-0.14
1152.0	33.68	0.93	1.61	1.778	4.14	16.2	1.13	0.46
1154.0	33.77	0.99	1.65	1.515	3.48	14.0	0.74	0.07
1157.0	33.90	0.99	1.75	1.642	3.69	15.1	0.96	0.29
1159.0	33.99	0.96	1.68	1.578	2.13	14.5	0.83	0.15
1160.5	34.06	1.17	1.64	1.582	2.96	14.6	1.04	0.36
1162.0	34.13	1.00	1.68	1.441	3.00	13.3	0.61	-0.07
1164.0	34.22	0.93	1.80	1.394	2.95	12.9	0.45	-0.23
1167.0	34.36	1.10	1.69	1.630	4.46	15.0	1.06	0.38
1169.0	34.45	1.29	1.80	1.564	1.82	14.4	1.13	0.45
1172.0	34.59	1.36	1.82	1.665	(25.07)	15.3	1.37	0.69
1174.0	34.68	1.11	1.76	1.589	2.73	14.6	1.00	0.32
1175.5	34.75	0.96	1.74	1.616	2.24	14.9	0.89	0.21
1177.0	34.81	1.26	1.54	1.700	(6.19)	15.6	1.34	0.65
1179.0	34.91	0.71	1.60	1.504	3.04	13.9	0.44	-0.24
1180.5	34.97	1.17	1.73	1.712	3.34	15.6	1.27	0.58
1182.0	35.04	1.06	1.66	1.626	5.36	15.0	1.01	0.32
1184.0	35.13	1.12	1.53	1.623	5.69	14.9	1.06	0.38
1187.0	35.27	0.90	1.60	1.611	2.14	14.8	0.82	0.14
1189.0	35.36	1.04	1.52	1.518	3.91	14.0	0.80	0.12
1190.5	35.43	0.79	1.91	1.998	(6.49)	17.7	1.32	0.64
1192.0	35.50	1.00	1.71	1.590	3.00	14.6	0.88	0.20
1194.0	35.60	1.07	1.55	1.394	1.72	12.9	0.58	-0.09
1197.0	35.73	0.92	1.62	1.570	4.25	14.5	0.76	0.09
1199.0	35.83	0.81	1.72	1.656	2.73	15.2	0.81	0.14

Table A5.3: *Trace element and results of stable isotope analyses of N. dutertrei down core samples. Test size = 300-400 µm (continued).*

depth	age	$\delta^{18}O$	$\delta^{13}C$	Mg/Ca	Ba/Ca	T[1]	$\delta^{18}O_{sw}$[2]	$\delta^{18}O_{ivf\ sw}$[3]
cm	kyr	‰ VPDB	‰ VPDB	mmol/mol	µmol/mol	°C	‰ SMOW	‰ SMOW
1200.5	36.13	0.88	1.88	1.602	3.34	14.7	0.78	0.12
1202.0	36.22	1.05	1.57	1.539	2.13	14.2	0.84	0.18
1204.0	36.37	0.40	1.60	1.699	2.31	15.5	0.47	-0.20
1207.0	36.59	0.42	1.72	1.442	2.75	13.3	0.03	-0.62
1209.0	36.74	1.26	1.74	1.661	5.59	15.2	1.27	0.62
1210.5	36.85	1.17	1.72	1.612	3.64	14.8	1.09	0.45
1212.0	36.96			1.097	3.50	9.7		
1214.0	37.11	0.68	1.75	1.449	4.57	13.4	0.31	-0.31
1217.0	37.34	0.45	1.80	1.395	3.69	12.9	-0.03	-0.64
1219.0	37.49	1.08	1.45	1.540	1.58	14.2	0.88	0.28
1220.5	37.60	0.96	1.73	1.678	(6.67)	15.4	1.00	0.41
1222.0	37.71	1.00	1.49	1.248	2.11	11.4	0.21	-0.37
1224.0	37.86	0.84	1.55	1.640	4.74	15.1	0.82	0.24
1227.0	38.08	0.84	1.49	1.511	(11.97)	14.0	0.58	0.02
1229.0	38.23	1.14	1.44	2.045	(9.02)	18.0	1.73	1.17
1230.5	38.35	1.06	1.53	1.856	3.40	16.7	1.38	0.82
1232.0	38.42	0.90	1.34	1.509	(7.12)	13.9	0.64	0.08
1234.0	38.48	0.95	1.59	1.588	3.22	14.6	0.83	0.28
1237.0	38.57	0.86	1.43	2.187	(8.86)	18.9	1.64	1.09
1239.0	38.64	0.78	1.31	2.021	4.55	17.9	1.33	0.78
1240.5	38.68	1.25	1.49	1.804	2.43	16.3	1.49	0.94
1242.0	38.73	1.03	1.39	1.959	4.93	17.5	1.50	0.95
1244.0	38.79	0.95	1.64	1.775	5.57	16.1	1.14	0.60
1247.0	38.89	0.91	1.49	1.668	(8.44)	15.3	0.93	0.38
1249.0	38.95	1.17	1.38	1.785	3.93	16.2	1.38	0.83
1250.5	39.00	1.07	1.71	1.450	2.88	13.4	0.69	0.15
1252.0	39.04	1.16	1.29	1.446	5.73	13.4	0.77	0.23
1254.0	39.11	1.08	1.51	1.771	2.66	16.1	1.26	0.72
1257.0	39.20	0.80	1.78	1.681	(17.11)	15.4	0.84	0.31
1259.0	39.26	0.99	1.53	1.301	4.42	12.0	0.31	-0.22
1260.5	39.31	0.97	1.59	1.490	5.71	13.8	0.68	0.14
1262.0	39.36	0.83	1.44	1.455	(7.02)	13.5	0.47	-0.06
1264.0	39.42	1.00	1.46	1.604	3.37	14.8	0.91	0.38
1267.0	39.51	1.09	1.55	1.730	5.19	15.8	1.21	0.68
1269.0	39.57	0.93	1.59	1.989	3.68	17.7	1.44	0.92
1270.5	39.62	0.60	1.55	1.474	(13.64)	13.6	0.27	-0.26
1272.0	39.67	0.75	1.77	1.784	5.71	16.2	0.95	0.42
1274.0	39.73	0.97	1.61	1.405	(6.75)	13.0	0.51	-0.02
1277.0	39.82	1.10	1.58	1.676	1.92	15.4	1.13	0.60

Table A5.3: *Trace element and results of stable isotope analyses of N. dutertrei down core samples. Test size = 300-400 µm (continued).*

depth	age	$\delta^{18}O$	$\delta^{13}C$	Mg/Ca	Ba/Ca	T[1]	$\delta^{18}O_{sw}$[2]	$\delta^{18}O_{ivf\ sw}$[3]
cm	kyr	‰ VPDB	‰ VPDB	mmol/mol	µmol/mol	°C	‰ SMOW	‰ SMOW
1279.0	39.89	1.06	1.68	1.659	3.83	15.2	1.06	0.52
1282.0	40.08	0.86	1.74	1.653	2.62	15.2	0.86	0.31
1284.0	40.27	1.07	1.51	1.622	1.84	14.9	1.01	0.45
1287.0	40.57	0.93	1.90	1.595	(8.33)	14.7	0.82	0.26
1289.0	40.77	1.07	1.53	1.736	2.15	15.8	1.21	0.64
1290.5	40.91	1.24	1.73	1.410	4.74	13.0	0.79	0.22
1292.0	41.06	0.89	1.54	1.414	(7.65)	13.1	0.45	-0.13
1294.0	41.21	0.85	1.66	1.837	1.78	16.6	1.13	0.55
1297.0	41.36	1.03	1.78	1.776	4.29	16.1	1.23	0.64
1299.0	41.46	0.88	1.72	1.793	(6.22)	16.3	1.10	0.51
1300.5	41.54	1.12	1.69	1.342	(10.56)	12.4	0.53	-0.06
1302.0	41.62	0.88	1.62	1.914	(8.42)	17.1	1.28	0.69
1304.0	41.77	0.59	1.82	1.743	(6.64)	15.9	0.73	0.13
1307.0	41.98	0.91	1.69	1.741	(19.25)	15.9	1.04	0.44
1309.0	42.12	0.65	1.77	1.810	(10.43)	16.4	0.90	0.29
1310.5	42.22			1.411	(6.19)	13.0		
1312.0	42.33	1.47	1.74	2.008	4.12	17.8	2.01	1.39
1314.0	42.47	0.96	1.61	1.761	3.89	16.0	1.13	0.51
1317.0	42.60	0.88	1.65	1.938	3.18	17.3	1.32	0.70
1319.0	42.66	0.99	1.76	1.463	5.99	13.5	0.64	0.01
1320.5	42.70	0.68	1.59	1.594	(6.09)	14.7	0.58	-0.05
1322.0	42.74	1.01	1.75	1.978	2.12	17.6	1.51	0.88
1324.0	42.80	0.91	1.73	2.008	4.68	17.8	1.45	0.83
1327.0	42.88	1.33	1.63	2.181	1.86	18.9	2.10	1.47
1329.0	42.93	1.14	1.61	1.744	5.09	15.9	1.28	0.65
1330.5	42.97			1.633	4.61	15.0		
1332.0	43.02	1.09	1.62	1.510	(9.93)	14.0	0.83	0.20
1334.0	43.07	1.06	1.63	1.585	5.30	14.6	0.94	0.31
1337.0	43.21	0.86	1.64	1.709	3.25	15.6	0.94	0.31
1339.0	43.34	0.45	1.72	1.759	5.61	16.0	0.61	-0.02
1340.5	43.43			1.594	5.23	14.7		
1342.0	43.53	1.00	1.48	1.880	2.61	16.9	1.36	0.72
1344.0	43.66	0.40	1.76	1.954	(9.21)	17.4	0.86	0.22
1347.0	43.85	0.99	1.60	1.954	(7.14)	17.4	1.45	0.82
1349.0	43.98	1.24	1.76	1.469	4.51	13.6	0.90	0.26
1350.5	44.07	0.61	1.69	1.623	4.51	14.9	0.55	-0.09
1352.0	44.17	0.27	1.65	1.694	2.54	15.5	0.34	-0.30
1354.0	44.29	0.03	1.62	1.603	(9.66)	14.8	-0.06	-0.70
1357.0	44.49	0.66	1.77	1.576	4.31	14.5	0.51	-0.12

Table A5.3: *Trace element and results of stable isotope analyses of N. dutertrei down core samples. Test size = 300-400 µm (continued).*

depth	age	$\delta^{18}O$	$\delta^{13}C$	Mg/Ca	Ba/Ca	T[1]	$\delta^{18}O_{sw}$[2]	$\delta^{18}O_{ivf\ sw}$[3]
cm	kyr	‰ VPDB	‰ VPDB	mmol/mol	µmol/mol	°C	‰ SMOW	‰ SMOW
1359.0	44.61	0.85	1.76	1.480	3.59	13.7	0.53	-0.10
1360.5	44.71			1.792	(7.42)	16.3		
1362.0	44.80	0.90	1.60	1.453	4.57	13.4	0.53	-0.10
1364.0	44.93	1.01	1.50	1.897	(9.15)	17.0	1.38	0.75
1367.0	45.12	0.75	1.73	1.605	3.01	14.8	0.66	0.03
1369.0	45.25	0.81	1.60	1.952	5.38	17.4	1.27	0.64
1370.5	45.34	1.37	1.68	1.874	(25.30)	16.9	1.71	1.09
1372.0	45.43	0.72	1.57	2.103	5.98	18.4	1.39	0.76
1374.0	45.55	0.94	1.63	1.705	3.56	15.6	1.02	0.40
1377.0	45.72	1.22	1.50	1.912	(9.10)	17.1	1.62	1.00
1379.0	45.84	1.12	1.59	1.815	4.11	16.4	1.38	0.75
1380.5	45.92	0.86	1.59	1.856	5.99	16.7	1.18	0.55
1382.0	46.01	1.09	1.26	1.940	(13.99)	17.3	1.53	0.91
1384.0	46.12	0.84	1.63	1.821	(14.03)	16.5	1.10	0.48
1387.0	46.30	0.97	1.60	1.759	(11.57)	16.0	1.14	0.52
1389.0	46.41	1.18	1.44	1.841	(6.95)	16.6	1.48	0.86
1390.5	46.51	1.03	1.61	1.872	5.75	16.8	1.37	0.75
1392.0	46.61	1.03	2.02	1.887	2.66	17.0	1.40	0.77
1394.0	46.74	1.05	1.78	1.840	(8.38)	16.6	1.34	0.72
1397.0	46.94	1.15	1.56	1.756	2.82	16.0	1.31	0.69
1399.0	47.08	0.92	1.55	1.810	4.43	16.4	1.17	0.55
1400.5	47.18	0.37	1.43	2.553	(12.87)	21.0	1.59	0.96
1402.0	47.28	0.87	1.82	1.678	4.77	15.4	0.90	0.28
1404.0	47.41	0.70	1.72	1.951	(11.70)	17.4	1.16	0.54
1407.0	47.61	0.37	1.59	1.411	2.41	13.0	-0.08	-0.70
1409.0	47.75	0.77	1.86	1.651	2.32	15.2	0.76	0.14
1410.5	47.85	0.70	1.60	1.564	4.99	14.4	0.54	-0.08
1412.0	47.95	0.54	1.84	1.536	2.53	14.2	0.32	-0.30
1414.0	48.08	0.94	1.48	2.014	3.36	17.8	1.49	0.86
1417.0	48.28	0.96	1.74	1.802	1.79	16.3	1.19	0.57
1419.0	48.42	0.45	1.78	1.865	2.94	16.8	0.78	0.15
1420.5	48.52	0.86	1.66	1.763	4.34	16.0	1.03	0.41
1422.0	48.62	0.57	1.69	1.978	4.01	17.6	1.07	0.44
1424.0	48.75			1.544	(14.90)	14.3		
1427.0	48.95	0.90	1.84	1.631	(14.28)	15.0	0.86	0.24
1429.0	49.08	0.98	2.12	1.551	3.27	14.3	0.79	0.17
1430.5	49.19	0.43	1.70	1.677	5.16	15.4	0.46	-0.15
1432.0	49.29			1.683	4.45	15.4		
1434.0	49.42			1.638	(13.98)	15.1		

Table A5.3: *Trace element and results of stable isotope analyses of N. dutertrei down core samples. Test size = 300-400 µm (continued).*

depth	age	$\delta^{18}O$	$\delta^{13}C$	Mg/Ca	Ba/Ca	T[1]	$\delta^{18}O_{sw}$[2]	$\delta^{18}O_{ivf\ sw}$[3]
cm	kyr	‰ VPDB	‰ VPDB	mmol/mol	µmol/mol	°C	‰ SMOW	‰ SMOW
1437.0	49.62			2.382	4.21	20.1		
1439.0	49.75	0.37	1.80	2.091	(6.59)	18.3	1.02	0.41
1440.5	49.85			1.614	4.82	14.9		
1442.0	49.95	0.34	1.69	1.773	5.77	16.1	0.53	-0.08
1444.0	50.09			1.183	(15.81)	10.7		
1447.0	50.29			2.044		18.0		
1449.0	50.42			1.103	1.88	9.7		
1450.5	50.52	-0.20	1.62	1.433	5.99	13.3	-0.61	-1.21
1452.0	50.62			1.591	1.20	14.7		
1454.0	50.76	0.67	2.01	1.466	2.17	13.6	0.33	-0.27
1457.0	50.96	0.21	1.69	1.431	3.23	13.2	-0.20	-0.79
1460.5	51.19287	0.08	1.47	1.806	(12.01)	16.4	0.32	-0.26
1462.0	51.29			1.861	2.20	16.8		
1464.0	51.43	-0.23	1.51	1.722	2.14	15.7	-0.13	-0.71
1467.0	51.63	0.53	1.60	1.652	3.63	15.2	0.52	-0.05
1469.0	51.76	0.91	1.48	1.670	1.63	15.3	0.93	0.36
1470.5	51.86	1.26	1.40	1.746	2.36	15.9	1.41	0.85
1472.0	51.96	1.01	1.40	1.584	2.86	14.6	0.88	0.33
1474.0	52.09	1.36	1.66	2.372	1.97	20.0	2.36	1.82
1477.0	52.25	1.18	1.46	1.603	4.43	14.8	1.08	0.55
1479.0	52.36	1.37	1.40	1.719	1.95	15.7	1.47	0.94
1480.5	52.45	0.84	1.69	1.463	2.45	13.5	0.49	-0.03
1482.0	52.53	1.03	1.10	2.009	2.00	17.8	1.57	1.05
1484.0	52.64	0.93	1.42	2.149	2.11	18.7	1.65	1.14
1487.0	52.80	1.07	1.58	1.476	2.62	13.7	0.75	0.25
1489.0	52.91	0.80	1.61	1.711	2.52	15.6	0.89	0.40
1490.5	52.99	1.43	1.12	1.779	1.70	16.2	1.63	1.14
1492.0	53.07	0.92	1.60	1.952	3.73	17.4	1.37	0.89
1494.0	53.18	1.12	1.49	2.056	4.54	18.1	1.73	1.24
1497.0	53.35	0.94	1.72	1.766	3.68	16.1	1.12	0.64
1499.0	53.46	0.46	1.67	1.764	2.09	16.0	0.64	0.17
1500.5	53.54	0.94	1.59	1.475	1.80	13.6	0.62	0.15
1502.0	53.62	0.92	1.59		2.65			
1504.0	53.73	1.16	1.48	1.539	3.30	14.2	0.95	0.49
1507.0	53.86	0.83	1.49	1.658	1.62	15.2	0.83	0.37
1509.0	53.93	0.96	1.39	1.932	2.05	17.3	1.39	0.93
1510.5	53.98	0.94	1.43	1.883	(8.53)	16.9	1.30	0.84
1512.0	54.03	0.88	1.47	1.735	1.43	15.8	1.00	0.55
1514.0	54.11	0.79	1.59	1.720	2.93	15.7	0.89	0.44

Table A5.3: *Trace element and results of stable isotope analyses of N. dutertrei down core samples. Test size = 300-400 µm (continued).*

depth	age	$\delta^{18}O$	$\delta^{13}C$	Mg/Ca	Ba/Ca	T[1]	$\delta^{18}O_{sw}$[2]	$\delta^{18}O_{ivf\ sw}$[3]
cm	kyr	‰ VPDB	‰ VPDB	mmol/mol	µmol/mol	°C	‰ SMOW	‰ SMOW
1517.0	54.21			2.048	(8.69)	18.1		
1519.0	54.29	0.86	1.48	2.319	2.69	19.7	1.80	1.36
1520.5	54.34	0.71	1.35	1.824	2.17	16.5	0.97	0.53
1522.0	54.39	0.97	1.50	1.669	2.76	15.3	0.99	0.54
1524.0	54.47	0.80	1.60	1.743	3.54	15.9	0.95	0.50
1527.0	54.61			1.378	2.58	12.7		
1529.0	54.74	0.33	1.54	2.096	1.86	18.4	0.99	0.54
1530.5	54.83	1.25	1.44	1.524	(8.64)	14.1	1.02	0.57
1532.0	54.93	0.83	1.45	1.704	4.48	15.6	0.91	0.46
1534.0	55.06	0.40	1.61	1.758	3.55	16.0	0.57	0.11
1537.0	55.25	0.74	1.66	1.480	4.17	13.7	0.42	-0.03
1539.0	55.38	0.79	1.29	2.172	(11.32)	18.8	1.54	1.08
1540.5	55.47	1.13	1.39	2.038	2.11	18.0	1.71	1.24
1542.0	55.57	0.93	1.69	1.558	(6.02)	14.4	0.75	0.29
1544.0	55.70	1.06	1.29	1.723	3.76	15.7	1.17	0.71
1547.0	55.89	1.03	1.27	1.604	2.86	14.8	0.93	0.46
1549.0	56.02	0.37	1.50	1.705	2.17	15.6	0.45	-0.03
1550.5	56.12	0.77	1.43	1.719	3.49	15.7	0.87	0.39
1552.0	56.21	0.48	1.71	1.729	(7.79)	15.8	0.60	0.12
1554.0	56.34	0.79	1.62	1.663	(7.99)	15.3	0.80	0.32
1557.0	56.53	0.62	1.33	1.532	2.07	14.1	0.40	-0.09
1559.0	56.66	0.42	1.57	1.818	2.17	16.5	0.68	0.19
1560.5	56.76			1.546	1.98	14.3		
1562.0	56.86	0.88	1.10	1.841	3.51	16.6	1.18	0.68
1564.0	56.98	0.63	1.38	1.914	3.82	17.1	1.03	0.53
1567.0	57.18	0.78	1.37	2.192	3.43	19.0	1.57	1.06
1569.0	57.31	0.96	1.30	1.948	3.12	17.4	1.41	0.90
1570.5	57.40	0.69	1.24	1.896	(9.95)	17.0	1.06	0.55
1572.0	57.50	0.78	1.22	2.314	5.33	19.7	1.72	1.20
1574.0	57.63	0.73	1.46	1.832	(8.06)	16.6	1.01	0.50
1577.0	57.82	1.13	1.15	1.708	3.47	15.6	1.21	0.71
1579.0	57.95	1.00	1.07	1.751	(9.34)	15.9	1.16	0.65
1580.5	58.04	1.17	1.21	1.799	1.86	16.3	1.40	0.90
1582.0	58.14	1.25	1.14	1.666	(10.34)	15.3	1.26	0.77
1584.0	58.27	1.23	1.06	1.641	(6.31)	15.1	1.20	0.71
1585.5	58.33	1.22	1.16	1.815	2.94	16.4	1.48	0.99
1587.0	58.40	1.25	1.01	1.744	(8.35)	15.9	1.40	0.91
1589.0	58.48	1.14	0.92	1.589	(20.70)	14.6	1.02	0.54
1590.5	58.55	1.25	1.04	1.904	(7.65)	17.1	1.64	1.15

Table A5.3: *Trace element and results of stable isotope analyses of N. dutertrei down core samples. Test size = 300-400 µm (continued).*

depth	age	$\delta^{18}O$	$\delta^{13}C$	Mg/Ca	Ba/Ca	T[1]	$\delta^{18}O_{sw}$[2]	$\delta^{18}O_{ivf\ sw}$[3]
cm	kyr	‰ VPDB	‰ VPDB	mmol/mol	µmol/mol	°C	‰ SMOW	‰ SMOW
1592.0	58.61	1.35	1.16	1.758	(11.71)	16.0	1.52	1.03
1594.0	58.69	1.22	1.09	1.613	(9.53)	14.8	1.15	0.66
1595.5	58.76	1.29	1.10	1.775	(7.97)	16.1	1.49	1.00
1597.0	58.82	1.19	1.19	1.524	(7.34)	14.1	0.96	0.48
1599.0	58.91	1.25	0.95	2.177	(19.65)	18.9	2.01	1.53
1600.5	58.97	1.25	1.10	1.706	(10.53)	15.6	1.33	0.85
1602.0	59.03	1.05	1.29	1.666	(28.86)	15.3	1.06	0.59
1604.0	59.12	1.08	1.27	1.383	(32.99)	12.8	0.57	0.10
1605.5	59.18	1.00	1.15	1.902	(6.12)	17.1	1.39	0.92
1607.0	59.24	1.13	1.19	1.497	(16.84)	13.8	0.84	0.38
1609.0	59.33	1.09	1.17	1.740	(22.44)	15.9	1.23	0.77
1610.5	59.39	0.91	1.04	1.657	4.17	15.2	0.91	0.45
1612.0	59.46	1.28	1.11	1.895	(8.33)	17.0	1.65	1.20
1614.0	59.54	1.03	1.22	1.625	(16.69)	14.9	0.98	0.52
1615.5	59.60	1.08	1.11	1.596	(8.81)	14.7	0.98	0.53
1617.0	59.67	1.14	1.18	1.785	(9.91)	16.2	1.35	0.90
1619.0	59.75	0.93	1.17	1.740	(10.90)	15.9	1.06	0.62
1620.5	59.81	1.07	1.21	1.754	(11.78)	16.0	1.23	0.79
1622.0	59.88	1.03	1.21	1.884	4.18	16.9	1.39	0.95
1624.0	59.96	1.06	1.15	1.972	(16.83)	17.5	1.55	1.12
1625.5	60.03	1.26	1.21	2.107	(11.55)	18.4	1.93	1.50
1627.0	60.09	1.26	1.05	1.819	(11.32)	16.5	1.52	1.09
1629.0	60.17	1.33	1.10	2.205	5.62	19.0	2.13	1.70
1630.5	60.24	1.13	1.19	1.568	5.02	14.5	0.97	0.55
1632.0	60.30	0.90	1.31	2.072	(23.63)	18.2	1.52	1.11
1634.0	60.39	1.13	1.39	2.150	(18.65)	18.7	1.86	1.45
1635.5	60.45	0.99	1.46	2.036	(6.32)	18.0	1.56	1.15
1637.0	60.51	1.25	1.17	1.990	(10.43)	17.7	1.76	1.35
1639.0	60.60	1.19	1.24	1.967	3.51	17.5	1.67	1.26
1640.5	60.66	1.09	1.24	1.921	(16.16)	17.2	1.51	1.09
1642.0	60.72	1.26	1.35	1.853	(7.96)	16.7	1.57	1.15
1644.0	60.81	1.35	1.35	2.024	(20.09)	17.9	1.91	1.49
1645.5	60.87	0.96	1.46	1.697	4.06	15.5	1.02	0.60

[1]*Mg/Ca-based temperature estimates calculated with Equation 5.10 from Chapter 5*

[2]*calculated after Bemis et al., (1998)*

[3]*corrected for the relative sea level following the approach of Waelbroeck et al. (2002)*

The age model was taken from Weldeab et al. (2007a, b) and Weldeab (2012a, b). For our record the models were overlapped at about 1200.5 cm core depth. We analyzed samples from the same core depth as done in the studies (Weldeab et al., 2007a, b; Weldeab, 2012a, b).

Table A5.4: *Trace element and results of stable isotope analyses of G. crassaformis down core samples. Test size = 300-400 µm.*

depth	age	$\delta^{18}O$	$\delta^{13}C$	Mg/Ca	Ba/Ca	T[1]	$\delta^{18}O_{sw}$[2]	$\delta^{18}O_{ivf\ sw}$[3]
cm	kyr	‰ VPDB	‰ VPDB	mmol/mol	µmol/mol	°C	‰ SMOW	‰ SMOW
400.5	7.27	2.17	1.19	1.338	3.62	12.3	1.57	1.50
410.5	7.49	2.11	1.17	1.231	2.97	11.2	1.28	1.21
418.5	7.67	2.01	1.07	1.266	2.73	11.6	1.25	1.18
424.5	7.81			1.424	3.32	13.2		
448.5	8.38			1.475	3.47	13.6		
456.5	8.57			1.131	3.49	10.1		
464.5	8.77			1.168	2.32	10.5		
472.5	8.97	1.23	0.86	1.531	3.70	14.1	1.01	0.85
480.5	9.18	2.13	1.09	1.349	2.64	12.4	1.55	1.37
488.5	9.39			1.606	3.22	14.8		
500.5	9.71	2.01	0.89	1.543	3.64	14.3	1.81	1.58
504.5	9.82	1.70	0.78	1.380	3.12	12.7	1.19	0.94
508.5	9.93	2.20	0.85	1.225	3.63	11.1	1.35	1.10
512.5	10.04	1.91	0.79	1.443	3.03	13.3	1.53	1.26
516.5	10.16	1.70	0.88	1.986	3.52	17.6	2.21	1.93
520.5	10.27	2.25	0.84	1.265	2.76	11.6	1.49	1.20
524.5	10.38	2.38	0.95	1.251	3.42	11.4	1.59	1.28
528.5	10.50	2.12	0.80	1.481	(6.66)	13.7	1.80	1.48
532.5	10.61			1.280	3.18	11.7		
536.5	10.73	2.39	0.80	1.448	5.22	13.4	2.01	1.66
542.5	10.91	1.56	0.73	1.232	3.10	11.2	0.73	0.36
544.5	10.97	2.42	0.89	1.371	3.54	12.7	1.88	1.51
548.5	11.09	2.21	0.87	1.445	3.81	13.4	1.83	1.44
552.5	11.21			1.519	3.73	14.0		
556.5	11.33	2.13	0.77	1.490	4.50	13.8	1.83	1.41
560.5	11.46			1.348	3.17	12.4		
564.5	11.58	2.25	0.51	1.192	2.79	10.8	1.33	0.87
568.5	11.71			1.449	3.52	13.4		
572.5	11.84	2.19	0.51	1.368	3.83	12.6	1.66	1.17
576.5	11.96	2.16	0.32	1.229	3.07	11.2	1.32	0.82
580.5	12.09	2.44	0.62	1.231	4.03	11.2	1.61	1.09
584.5	12.22	2.11	0.58	1.325	4.68	12.2	1.48	0.95
588.5	12.36	2.24	0.66	1.300	4.80	11.9	1.56	1.01
592.5	12.49	2.12	0.56	1.726	3.22	15.8	2.23	1.66
596.5	12.62	2.57	0.67	1.519	3.55	14.0	2.33	1.75
598.5	12.69	2.43	0.86	1.384	3.54	12.8	1.93	1.34
605.5	12.93	2.36	0.62	1.551	3.49	14.3	2.17	1.55
610.5	13.16	2.53	0.83	1.299	3.01	11.9	1.85	1.20
615.5	13.31	2.79	0.91	1.631	3.66	15.0	2.75	2.08

Table A5.4: *Trace element and results of stable isotope analyses of G. crassaformis down core samples. Test size = 300-400 µm. (continued)*

depth	age	$\delta^{18}O$	$\delta^{13}C$	Mg/Ca	Ba/Ca	T[1]	$\delta^{18}O_{sw}$[2]	$\delta^{18}O_{ivf\ sw}$[3]
cm	kyr	‰ VPDB	‰ VPDB	mmol/mol	µmol/mol	°C	‰ SMOW	‰ SMOW
620.5	13.47			1.309	2.55	12.0		
625.5	13.62			1.358	1.85	12.5		
630.5	13.77	3.04	0.82	1.268	2.26	11.6	2.29	1.57
635.5	13.93			1.005	1.71	8.5		
640.5	14.09	2.57	0.62	1.468	2.43	13.6	2.23	1.47
645.5	14.24	2.60	0.56					
650.5	14.40	2.71	0.43	1.440	3.89	13.3	2.32	1.53
655.5	14.56	2.63	0.53	1.438	3.43	13.3	2.24	1.43
660.5	14.71	2.55	0.49	1.448	7.81	13.4	2.17	1.35
665.5	14.87	2.91	0.56	1.327	4.20	12.2	2.28	1.45
670.5	15.03	2.35	0.37	1.278	3.66	11.7	1.62	0.77
675.5	15.19	2.66	0.37	1.072	4.16	9.4	1.44	0.58
680.5	15.36	2.83	0.41	1.259	3.66	11.5	2.05	1.18
685.5	15.52	2.78	0.35	1.107	3.38	9.8	1.65	0.76
690.5	15.68	2.87	0.66	1.241	3.41	11.3	2.06	1.16
695.5	15.84	2.54	0.62	1.172	3.72	10.5	1.57	0.66
700.5	16.01	2.99	0.56	1.195	5.38	10.8	2.07	1.15
705.5	16.17	3.34	0.75	1.229	3.88	11.2	2.50	1.58
710.5	16.34	3.33	0.80	1.178	3.31	10.6	2.37	1.44
715.5	16.51	3.46	0.79	1.166	3.08	10.5	2.48	1.54
720.5	16.67	2.86	0.58	1.292	4.04	11.9	2.16	1.21
725.5	16.84	3.10	0.66	1.291	3.95	11.8	2.40	1.44
730.5	17.01	3.58	0.79	1.435	3.77	13.3	3.18	2.21
735.5	17.18	3.05	0.86	1.111	3.84	9.8	1.93	0.96
740.5	17.35	3.72	0.74	1.294	2.70	11.9	3.02	2.04
745.5	17.52	3.40	0.63	1.268	3.42	11.6	2.64	1.66
750.5	17.69	3.39	0.70	1.121	3.33	9.9	2.29	1.30
755.5	17.86	3.62	0.70	1.246	3.87	11.4	2.82	1.82
760.5	18.04	3.50	0.70	1.123	3.54	10.0	2.41	1.40
765.5	18.21	3.67	0.87	1.034	2.62	8.9	2.35	1.34
770.5	18.38	3.40	0.62	1.112	2.98	9.8	2.28	1.27
775.5	18.56	3.68	0.63	0.911	1.57	7.2	2.00	0.98
780.5	18.73	3.30	0.58	1.167	2.95	10.5	2.32	1.29
785.5	18.91	3.67	0.75	1.410	3.55	13.0	3.22	2.19
790.5	19.09	3.45	0.73	1.287	3.71	11.8	2.74	1.72
795.5	19.26	3.42	0.71	1.228	4.00	11.2	2.58	1.55
800.5	19.44	3.25	0.56	1.213	3.48	11.0	2.37	1.34
810.5	19.80	3.24	0.73	1.135	2.37	10.1	2.18	1.14

Table A5.4: *Trace element and results of stable isotope analyses of G. crassaformis down core samples. Test size = 300-400 µm. (continued)*

depth	age	$\delta^{18}O$	$\delta^{13}C$	Mg/Ca	Ba/Ca	T[1]	$\delta^{18}O_{sw}$[2]	$\delta^{18}O_{ivf\ sw}$[3]
cm	kyr	‰ VPDB	‰ VPDB	mmol/mol	µmol/mol	°C	‰ SMOW	‰ SMOW
820.5	20.16	3.29	0.71	1.413	4.55	13.1	2.84	1.80
830.5	20.53			1.457	3.46	13.5		
840.5	20.89	2.98	0.70	1.376	4.01	12.7	2.46	1.43
850.5	21.26	3.07	0.69	1.255	4.30	11.5	2.29	1.27
860.5	21.64	3.21	0.71	1.424	4.09	13.2	2.79	1.77
870.5	22.01	3.06	0.62	1.342	3.62	12.4	2.47	1.45
880.5	22.39	3.15	0.92	1.215	3.32	11.0	2.28	1.27
900.5	23.15	3.13	0.70	1.341	3.23	12.4	2.53	1.54
910.5	23.54			1.715	3.02	15.7		
920.5	23.93	3.19	0.75	1.474	3.36	13.6	2.87	1.89
930.5	24.32	3.35	0.60	1.419	3.75	13.1	2.92	1.96
940.5	24.72	3.17	0.59	1.482	6.37	13.7	2.86	1.91
950.5	25.11	2.67	0.76	1.383	3.47	12.8	2.16	1.23
960.5	25.51	3.06	0.75	1.518	6.02	14.0	2.82	1.90
970.5	25.92	3.33	0.80	1.235	3.39	11.2	2.51	1.61
985.5	26.52	3.23	0.79	1.052	3.77	9.1	1.96	1.08
1000.5	27.14	3.27	0.90	1.326	2.65	12.2	2.65	1.80
1002.0	27.20	2.97	0.86	1.009	3.16	8.5	1.58	0.73
1004.0	27.28	3.33	0.80	0.925	2.52	7.4	1.69	0.85
1005.5	27.34			1.033	2.48	8.8		
1007.0	27.41	3.29	0.67	1.023	4.95	8.7	1.94	1.10
1009.0	27.49	3.12	0.77	1.047	(6.88)	9.0	1.84	1.00
1010.5	27.55	2.95	0.70	1.440	3.70	13.3	2.56	1.73
1012.0	27.61	3.02	0.65	0.907	2.51	7.1	1.33	0.50
1014.0	27.70	2.75	0.77	1.072	2.23	9.4	1.53	0.70
1017.0	27.82	3.24	0.80	1.527	3.55	14.1	3.01	2.20
1019.0	27.90	3.18	0.81	1.538	3.45	14.2	2.97	2.16
1020.5	27.97			1.189	4.12	10.7		
1022.0	28.03	3.19	0.66	1.511	4.73	14.0	2.93	2.13
1024.0	28.11	3.17	0.59	1.445	3.56	13.4	2.79	1.99
1027.0	28.24			1.029	3.30	8.8		
1029.0	28.32			1.036	3.38	8.9		
1030.5	28.39	3.29	0.75	1.095	3.67	9.6	2.13	1.35
1032.0	28.45	3.07	0.67	1.408	3.73	13.0	2.61	1.83
1034.0	28.53	2.49	0.88	1.465	6.01	13.5	2.14	1.37
1037.0	28.66	2.71	0.53	1.306	3.04	12.0	2.05	1.28
1039.0	28.74	2.83	0.66	1.445	3.90	13.4	2.45	1.69
1040.5	28.81	2.22	0.93	1.165	3.14	10.5	1.23	0.47
1042.0	28.87	2.94	0.72	1.603	4.26	14.8	2.84	2.09

Table A5.4: *Trace element and results of stable isotope analyses of G. crassaformis down core samples. Test size = 300-400 µm. (continued)*

depth	age	$\delta^{18}O$	$\delta^{13}C$	Mg/Ca	Ba/Ca	T[1]	$\delta^{18}O_{sw}$[2]	$\delta^{18}O_{ivf\ sw}$[3]
cm	kyr	‰ VPDB	‰ VPDB	mmol/mol	µmol/mol	°C	‰ SMOW	‰ SMOW
1044.0	28.95			1.090	4.08	9.6		
1047.0	29.08	2.87	0.52	1.413	5.27	13.1	2.42	1.68
1049.0	29.17	3.17	0.56	1.420	3.13	13.1	2.74	2.00
1050.5	29.23	2.94	0.64	0.976	2.97	8.1	1.46	0.72
1052.0	29.29	2.72	0.46	1.119	3.22	9.9	1.62	0.89
1054.0	29.38	2.69	0.52	1.166	2.52	10.5	1.71	0.97
1057.0	29.51	2.92	0.61	1.748	3.33	15.9	3.07	2.34
1059.0	29.59	2.72	0.60	1.259	3.60	11.5	1.95	1.22
1060.5	29.66	2.73	0.56	1.207	3.65	10.9	1.84	1.12
1062.0	29.72	2.68	0.58	1.137	4.06	10.1	1.62	0.90
1064.0	29.81	3.05	0.51	1.266	(10.76)	11.6	2.30	1.58
1067.0	29.94	2.92	0.66	1.044	4.61	9.0	1.63	0.92
1069.0	30.02	3.06	0.62	1.265	2.99	11.6	2.31	1.60
1070.5	30.09	3.04	0.53	1.247	4.74	11.4	2.24	1.53
1072.0	30.15	3.01	0.65	1.368	(9.48)	12.6	2.48	1.77
1074.0	30.24	2.80	0.63	1.387	4.25	12.8	2.30	1.60
1077.0	30.37	2.77	0.66	1.225	3.68	11.1	1.93	1.23
1079.0	30.45	2.97	0.59	1.025	2.81	8.8	1.63	0.94
1080.5	30.52	2.82	0.58	1.438	3.63	13.3	2.42	1.73
1082.0	30.58	3.01	0.60	1.081	4.51	9.5	1.82	1.12
1084.0	30.67	3.08	0.71	1.283	3.08	11.8	2.37	1.68
1087.0	30.80	3.08	0.75	1.142	2.44	10.2	2.04	1.35
1089.0	30.89	3.14	0.71	1.233	(7.98)	11.2	2.31	1.62
1090.5	30.95	2.77	0.56	1.287	4.10	11.8	2.07	1.38
1092.0	31.02			1.157	2.98	10.4		
1094.0	31.10	3.10	0.77	1.390	4.29	12.8	2.60	1.92
1097.0	31.23	2.81	0.68	1.410	3.21	13.0	2.36	1.68
1099.0	31.32	2.95	0.66	1.290	2.95	11.8	2.25	1.57
1100.5	31.39	2.84	0.80	1.512	3.12	14.0	2.59	1.91
1102.0	31.45	2.60	0.52	1.422	3.63	13.1	2.17	1.49
1104.0	31.54	2.85	0.76	0.968	3.22	8.0	1.35	0.67
1107.0	31.67	3.13	0.46	1.509	4.32	13.9	2.87	2.20
1109.0	31.76			1.211	2.42	11.0		
1112.0	31.89	2.93	0.68	1.022	4.78	8.7	1.58	0.91
1114.0	31.98			1.136	2.34	10.1		
1117.0	32.11	3.05	0.84	1.177	2.95	10.6	2.09	1.42
1119.0	32.20	2.90	0.82	1.127	2.81	10.0	1.82	1.15
1120.5	32.27	2.82	1.00	1.466	3.33	13.6	2.48	1.81
1122.0	32.34	2.95	0.65					

Table A5.4: *Trace element and results of stable isotope analyses of G. crassaformis down core samples. Test size = 300-400 µm. (continued)*

depth	age	$\delta^{18}O$	$\delta^{13}C$	Mg/Ca	Ba/Ca	T[1]	$\delta^{18}O_{sw}$[2]	$\delta^{18}O_{ivf\ sw}$[3]
cm	kyr	‰ VPDB	‰ VPDB	mmol/mol	µmol/mol	°C	‰ SMOW	‰ SMOW
1124.0	32.42	2.93	0.63	1.264	2.96	11.6	2.17	1.50
1127.0	32.56	2.81	0.55	0.995	2.09	8.3	1.38	0.71
1129.0	32.65			1.259	3.92	11.5		
1130.5	32.71	2.36	0.81	1.555	3.64	14.4	2.18	1.51
1132.0	32.78	2.68	0.58	1.512	3.52	14.0	2.42	1.76
1134.0	32.87	2.64	0.74	1.548	2.83	14.3	2.45	1.78
1137.0	33.00	2.79	0.66	1.566	3.45	14.4	2.63	1.96
1139.0	33.09	2.72	0.83	1.212	3.41	11.0	1.85	1.18
1140.5	33.16	2.47	0.72	1.293	3.21	11.9	1.77	1.10
1142.0	33.23	2.94	0.89	1.078	3.58	9.4	1.73	1.06
1144.0	33.32	3.26	0.74	1.203	2.81	10.9	2.36	1.69
1147.0	33.45	2.78	0.74	1.485	4.47	13.7	2.47	1.80
1149.0	33.54	2.98	0.64	1.258	3.29	11.5	2.20	1.53
1150.5	33.61	2.64	0.70	1.162	2.90	10.4	1.64	0.97
1152.0	33.68	2.85	0.71	1.227	3.05	11.2	2.01	1.33
1154.0	33.77	2.62	0.65	1.400	4.06	12.9	2.14	1.47
1157.0	33.90	2.98	0.62	1.292	3.65	11.9	2.28	1.61
1159.0	33.99	2.82	0.60	1.348	3.52	12.4	2.24	1.56
1160.5	34.06	2.56	0.91	1.253	2.46	11.4	1.77	1.10
1162.0	34.13	3.13	0.87	1.267	2.68	11.6	2.38	1.70
1164.0	34.22	3.01	0.79	1.371	3.65	12.7	2.48	1.80
1167.0	34.36	3.26	0.85	1.193	2.62	10.8	2.34	1.66
1169.0	34.45	2.98	0.56	1.392	3.69	12.9	2.50	1.82
1172.0	34.59	3.24	0.67	1.216	3.24	11.0	2.37	1.69
1174.0	34.68	2.79	0.64	1.193	2.95	10.8	1.87	1.19
1175.5	34.75	3.15	0.74	1.216	2.71	11.0	2.29	1.60
1177.0	34.81	2.96	0.67	1.469	4.72	13.6	2.62	1.94
1179.0	34.91	2.76	0.63	1.260	(6.70)	11.5	1.99	1.31
1180.5	34.97	3.21	0.78	1.517	4.52	14.0	2.96	2.28
1182.0	35.04	2.64	0.41	1.440	3.43	13.3	2.25	1.57
1184.0	35.13	3.11	0.70	1.267	3.35	11.6	2.36	1.68
1187.0	35.27	2.73	0.47	1.638	3.07	15.1	2.70	2.02
1189.0	35.36	3.01	0.67	1.334	4.14	12.3	2.40	1.72
1190.5	35.43	3.23	0.76	1.023	2.40	8.7	1.88	1.20
1192.0	35.50	2.67	0.59	1.404	3.58	13.0	2.21	1.53
1194.0	35.60	2.69	0.38	1.593	4.42	14.7	2.58	1.90
1197.0	35.73	2.75	1.01	1.150	2.89	10.3	1.73	1.05
1199.0	35.83	2.77	0.76	1.491	4.16	13.8	2.47	1.80
1200.5	36.13	2.82	0.56	1.341	6.07	12.4	2.23	1.56

Table A5.4: *Trace element and results of stable isotope analyses of G. crassaformis down core samples. Test size = 300-400 µm. (continued)*

depth	age	$\delta^{18}O$	$\delta^{13}C$	Mg/Ca	Ba/Ca	T[1]	$\delta^{18}O_{sw}$[2]	$\delta^{18}O_{ivf\ sw}$[3]
cm	kyr	‰ VPDB	‰ VPDB	mmol/mol	µmol/mol	°C	‰ SMOW	‰ SMOW
1202.0	36.22	2.98	0.71	1.170	3.57	10.5	2.00	1.34
1204.0	36.37	3.06	0.92	1.096	2.49	9.6	1.90	1.24
1207.0	36.59	2.48	0.63	1.013	2.44	8.6	1.10	0.45
1209.0	36.74			1.087	1.50	9.5		
1210.5	36.85	1.75	1.03	1.107	2.22	9.8	0.62	-0.02
1212.0	36.96			1.132	2.93	10.1		
1214.0	37.11	3.01	0.77	1.091	3.12	9.6	1.84	1.22
1217.0	37.34			0.970	3.58	8.0		
1219.0	37.49	2.75	0.80	1.070	3.69	9.3	1.52	0.92
1220.5	37.60	2.96	0.84	1.417	3.23	13.1	2.52	1.93
1222.0	37.71	2.52	0.40	1.185	3.41	10.7	1.58	1.00
1224.0	37.86			1.448	2.58	13.4		
1227.0	38.08	2.66	0.59	1.300	2.97	11.9	1.98	1.42
1229.0	38.23	2.79	0.55	1.344	3.59	12.4	2.20	1.64
1230.5	38.35			1.525	3.78	14.1		
1232.0	38.42	2.51	0.25					
1234.0	38.48	2.30	0.43	1.609	3.77	14.8	2.21	1.66
1237.0	38.57	2.44	0.31	1.672	5.59	15.3	2.47	1.92
1239.0	38.64	2.36	0.34	1.713	3.71	15.7	2.45	1.90
1240.5	38.68	2.39	0.21	1.723	5.71	15.7	2.50	1.95
1242.0	38.73	2.37	0.34	1.587	3.18	14.6	2.25	1.70
1244.0	38.79	2.60	0.44	1.688	4.36	15.5	2.65	2.11
1247.0	38.89	2.77	0.55	1.509	4.73	14.0	2.50	1.96
1249.0	38.95	2.23	0.32	1.340	3.97	12.4	1.63	1.09
1250.5	39.00	2.46	0.27	1.533	6.04	14.2	2.24	1.70
1252.0	39.04	3.16	0.68	1.294	5.16	11.9	2.46	1.93
1254.0	39.11	2.26	0.54	1.800	4.65	16.3	2.50	1.96
1257.0	39.20	2.07	0.28					
1259.0	39.26	2.65	0.67	1.296	3.62	11.9	1.96	1.43
1260.5	39.31	2.07	0.29	1.747	4.90	15.9	2.22	1.69
1262.0	39.36	2.77	0.53	1.670	4.12	15.3	2.79	2.26
1264.0	39.42	2.85	0.67	1.583	4.67	14.6	2.72	2.19
1267.0	39.51	2.99	0.61	1.300	3.75	11.9	2.31	1.79
1269.0	39.57	3.00	0.69	1.217	3.84	11.1	2.13	1.60
1270.5	39.62	2.90	0.63	1.374	3.71	12.7	2.38	1.85
1272.0	39.67	2.78	0.62	1.366	3.88	12.6	2.23	1.70
1274.0	39.73	3.08	0.63	1.630	3.80	15.0	3.04	2.50
1277.0	39.82	3.13	0.84	1.176	3.21	10.6	2.17	1.63
1279.0	39.89	2.47	0.48	0.926	1.44	7.4	0.84	0.30

Table A5.4: *Trace element and results of stable isotope analyses of G. crassaformis down core samples. Test size = 300-400 µm. (continued)*

depth	age	$\delta^{18}O$	$\delta^{13}C$	Mg/Ca	Ba/Ca	T[1]	$\delta^{18}O_{sw}$[2]	$\delta^{18}O_{ivf\ sw}$[3]
cm	kyr	‰ VPDB	‰ VPDB	mmol/mol	µmol/mol	°C	‰ SMOW	‰ SMOW
1282.0	40.08	2.90	0.97	1.084	2.60	9.5	1.71	1.17
1284.0	40.27	3.34	0.83	1.403	3.15	13.0	2.87	2.32
1287.0	40.57	3.05	0.72	1.167	2.02	10.5	2.07	1.51
1289.0	40.77	2.92	0.75	1.255	3.60	11.5	2.14	1.57
1292.0	41.06	2.74	0.50	1.176	5.63	10.6	1.78	1.20
1294.0	41.21	2.90	0.68	1.469	3.41	13.6	2.57	1.98
1297.0	41.36	3.06	0.63	0.951	1.89	7.7	1.50	0.92
1299.0	41.46	3.13	0.68	1.268	4.23	11.6	2.38	1.79
1300.5	41.54	3.04	0.50	1.540	3.53	14.2	2.84	2.24
1302.0	41.62	3.41	0.88	1.250	3.56	11.4	2.62	2.02
1304.0	41.77	2.99	0.84	1.256	3.69	11.5	2.21	1.61
1307.0	41.98	3.04	0.64	0.916	4.48	7.2	1.38	0.77
1309.0	42.12	3.23	0.93	1.314	3.35	12.1	2.58	1.97
1310.5	42.22			1.356	4.30	12.5		
1312.0	42.33	2.96	0.65	1.147	3.00	10.3	1.93	1.31
1314.0	42.47	3.37	0.88	1.201	3.75	10.9	2.47	1.85
1317.0	42.60	3.02	0.67	1.274	4.20	11.7	2.29	1.66
1319.0	42.66	3.03	0.65	1.265	3.94	11.6	2.27	1.65
1322.0	42.74	2.96	0.61	1.210	2.78	11.0	2.08	1.46
1324.0	42.80	3.06	0.67	1.332	2.52	12.3	2.45	1.82
1327.0	42.88	3.13	0.62	1.074	2.65	9.4	1.92	1.29
1329.0	42.93	2.88	0.64	1.206	6.05	10.9	1.99	1.36
1330.5	42.97			1.138	1.42	10.2		
1332.0	43.02	3.00	0.75	1.101	2.93	9.7	1.85	1.22
1334.0	43.07	3.03	0.77	1.178	3.30	10.6	2.07	1.44
1337.0	43.21	3.48	0.77	1.325	3.22	12.2	2.85	2.22
1339.0	43.34	3.36	0.76	1.050	3.29	9.1	2.08	1.45
1340.5	43.43			1.167	1.65	10.5		
1342.0	43.53	3.18	0.74	1.140	1.87	10.2	2.13	1.50
1344.0	43.66	3.35	0.95	1.125	2.24	10.0	2.27	1.63
1347.0	43.85	2.99	0.90	0.993	2.56	8.3	1.55	0.91
1349.0	43.98	3.30	0.74	1.221	3.91	11.1	2.45	1.81
1350.5	44.07			0.785	1.13	5.2		
1352.0	44.17	2.52	0.89	1.063	2.94	9.2	1.27	0.63
1354.0	44.29	3.29	0.93	1.270	1.86	11.6	2.54	1.91
1357.0	44.49	3.12	1.06	0.825	2.24	5.8	1.16	0.53
1359.0	44.61	2.89	0.77	1.152	3.10	10.3	1.87	1.24
1360.5	44.71	3.30	0.84					
1362.0	44.80	3.12	0.86	1.224	2.64	11.1	2.27	1.64

Table A5.4: *Trace element and results of stable isotope analyses of G. crassaformis down core samples. Test size = 300-400 µm. (continued)*

depth	age	$\delta^{18}O$	$\delta^{13}C$	Mg/Ca	Ba/Ca	T[1]	$\delta^{18}O_{sw}$[2]	$\delta^{18}O_{ivf\ sw}$[3]
cm	kyr	‰ VPDB	‰ VPDB	mmol/mol	µmol/mol	°C	‰ SMOW	‰ SMOW
1364.0	44.93	3.02	0.69	0.870	1.38	6.5	1.21	0.58
1367.0	45.12	3.16	0.54	1.115	3.78	9.9	2.05	1.42
1369.0	45.25	2.68	0.64	1.061	2.63	9.2	1.44	0.81
1370.5	45.34	3.13	0.93	1.204	2.79	10.9	2.24	1.61
1372.0	45.43	2.87	0.67	1.289	3.50	11.8	2.17	1.54
1374.0	45.55	2.51	0.58	1.178	3.25	10.6	1.55	0.93
1377.0	45.72	2.82	0.51	1.025	2.16	8.7	1.47	0.85
1379.0	45.84	2.69	0.33	1.079	5.09	9.4	1.49	0.87
1380.5	45.92	2.65	0.64	1.274	2.22	11.7	1.91	1.29
1382.0	46.01	2.81	0.52	1.174	4.05	10.6	1.84	1.22
1384.0	46.12	2.57	0.62	1.198	3.51	10.8	1.66	1.03
1387.0	46.30	2.86	0.65	1.444	4.18	13.4	2.48	1.85
1389.0	46.41	2.65	0.65	1.303	3.47	12.0	1.97	1.35
1390.5	46.51	2.96	0.78	1.296	4.69	11.9	2.27	1.65
1392.0	46.61	2.70	0.81	1.281	6.49	11.7	1.98	1.36
1394.0	46.74	3.03	0.84	1.184	3.37	10.7	2.08	1.46
1397.0	46.94	3.06	0.84	1.337	3.18	12.3	2.46	1.84
1399.0	47.08	2.80	0.73	1.339	5.88	12.3	2.20	1.58
1400.5	47.18	3.47	0.72	1.243	3.69	11.3	2.66	2.04
1402.0	47.28	2.78	0.83	1.627	5.11	15.0	2.73	2.11
1404.0	47.41	3.20	0.92					
1407.0	47.61	2.93	0.86	1.373	4.03	12.7	2.40	1.78
1409.0	47.75	2.94	0.76	1.500	3.25	13.9	2.66	2.03
1410.5	47.85	3.27	0.82	1.165	2.38	10.5	2.29	1.66
1412.0	47.95	3.06	0.84	0.927	2.19	7.4	1.43	0.81
1414.0	48.08	3.06	0.78	1.164	2.60	10.5	2.07	1.44
1417.0	48.28	3.18	0.93	1.419	2.54	13.1	2.74	2.12
1419.0	48.42	3.02	0.93	1.114	4.21	9.9	1.91	1.28
1422.0	48.62	3.08	0.89	1.124	3.46	10.0	2.00	1.37
1424.0	48.75			1.312	4.02	12.1		
1427.0	48.95	3.31	0.77	0.957	2.93	7.8	1.77	1.14
1429.0	49.08	3.17	0.84	1.204	2.83	10.9	2.28	1.66
1430.5	49.19	2.51	0.67	1.348	4.82	12.4	1.93	1.31
1432.0	49.29	3.02	0.92	1.157	4.01	10.4	2.01	1.39
1434.0	49.42	3.25	0.89					
1439.0	49.75			1.014	2.16	8.6		
1442.0	49.95	3.06	0.94	1.220	2.71	11.1	2.20	1.59
1444.0	50.09	3.39	0.98	1.441	3.11	13.3	3.00	2.39
1449.0	50.42	2.90	1.05	0.814	1.49	5.6	0.91	0.31

Table A5.4: *Trace element and results of stable isotope analyses of G. crassaformis down core samples. Test size = 300-400 µm. (continued)*

depth	age	$\delta^{18}O$	$\delta^{13}C$	Mg/Ca	Ba/Ca	T[1]	$\delta^{18}O_{sw}$[2]	$\delta^{18}O_{ivf\ sw}$[3]
cm	kyr	‰ VPDB	‰ VPDB	mmol/mol	µmol/mol	°C	‰ SMOW	‰ SMOW
1452.0	50.62			1.055	1.61	9.1		
1454.0	50.76	3.37	0.88					
1457.0	50.96			0.836	0.96	6.0		
1459.0	51.09	3.21	0.91	1.094	1.81	9.6	2.04	1.45
1462.0	51.29	2.83	0.99	1.512	2.66	14.0	2.57	1.98
1464.0	51.43	2.99	0.89	1.072	1.84	9.4	1.77	1.18
1467.0	51.63	2.79	0.88	1.224	3.30	11.1	1.94	1.37
1469.0	51.76	2.85	0.69	1.135	2.16	10.1	1.79	1.22
1472.0	51.96	2.97	0.74	1.036	2.36	8.9	1.65	1.10
1474.0	52.09	2.78	0.55	1.479	4.68	13.7	2.46	1.92
1477.0	52.25	2.43	0.75	1.562	4.69	14.4	2.27	1.73
1479.0	52.36	2.72	0.70	1.392	5.23	12.9	2.24	1.71
1480.5	52.45	2.99	0.58	1.179	2.50	10.6	2.04	1.51
1482.0	52.53	2.68	0.39	1.458	3.40	13.5	2.32	1.81
1484.0	52.64	2.64	0.53	1.470	3.34	13.6	2.31	1.80
1487.0	52.80	2.75	0.58	1.631	3.90	15.0	2.71	2.21
1489.0	52.91	2.79	0.65	1.395	3.22	12.9	2.30	1.81
1490.5	52.99	3.17	0.77	1.550	2.76	14.3	2.98	2.50
1492.0	53.07	2.75	0.57	1.191	2.38	10.8	1.83	1.34
1494.0	53.18	2.68	0.57	1.203	2.79	10.9	1.78	1.30
1497.0	53.35	2.21	0.51	1.608	3.21	14.8	2.13	1.65
1499.0	53.46	2.56	0.58	1.217	2.96	11.1	1.69	1.22
1500.5	53.54	2.75	0.66	1.575	3.21	14.5	2.61	2.14
1502.0	53.62	2.72	0.51	1.815	3.96	16.4	2.97	2.50
1504.0	53.73	2.65	0.52	1.343	2.93	12.4	2.06	1.59
1507.0	53.86	2.51	0.40	1.452	4.37	13.4	2.14	1.68
1509.0	53.93	2.62	0.41	1.312	3.45	12.1	1.96	1.50
1510.5	53.98	2.53	0.38	1.378	3.03	12.7	2.02	1.56
1512.0	54.03	2.51	0.42	1.331	4.80	12.3	1.90	1.44
1514.0	54.11	2.77	0.42	1.223	2.95	11.1	1.92	1.47
1517.0	54.21	2.72	0.48	1.277	2.99	11.7	1.99	1.54
1519.0	54.29	2.45	0.48	1.502	5.56	13.9	2.18	1.73
1520.5	54.34	3.52	0.72	1.475	3.06	13.6	3.19	2.74
1522.0	54.39	2.82	0.67	1.519	2.61	14.0	2.57	2.13
1524.0	54.47	2.83	0.72	1.079	2.70	9.4	1.63	1.18
1527.0	54.61	3.09	0.61	1.357	2.59	12.5	2.53	2.08
1529.0	54.74	2.76	0.56	1.318	2.40	12.1	2.12	1.68
1530.5	54.83			1.107	2.21	9.8		
1532.0	54.93	3.08	0.76	1.276	2.80	11.7	2.35	1.90

Table A5.4: *Trace element and results of stable isotope analyses of G. crassaformis down core samples. Test size = 300-400 µm. (continued)*

depth	age	$\delta^{18}O$	$\delta^{13}C$	Mg/Ca	Ba/Ca	T[1]	$\delta^{18}O_{sw}$[2]	$\delta^{18}O_{ivf\ sw}$[3]
cm	kyr	‰ VPDB	‰ VPDB	mmol/mol	µmol/mol	°C	‰ SMOW	‰ SMOW
1534.0	55.06	3.18	0.66	0.983	2.30	8.2	1.72	1.26
1537.0	55.25	2.90	0.68	1.201	2.30	10.9	2.00	1.54
1539.0	55.38	2.81	0.59	1.361	2.87	12.6	2.25	1.79
1540.5	55.47	3.04	0.62	1.390	3.38	12.8	2.54	2.08
1542.0	55.57	3.00	0.61	1.161	2.50	10.4	2.00	1.54
1544.0	55.70	2.63	0.44	1.162	3.58	10.4	1.64	1.17
1547.0	55.89	2.94	0.68	1.232	2.70	11.2	2.11	1.63
1549.0	56.02	2.99	0.68	1.534	3.59	14.2	2.77	2.30
1550.5	56.12	2.54	0.48	1.402	3.75	13.0	2.07	1.60
1552.0	56.21	3.05	0.68	1.432	6.46	13.2	2.64	2.16
1554.0	56.34	2.71	0.50	1.340	4.22	12.3	2.11	1.63
1557.0	56.53	2.85	0.38	1.293	3.24	11.9	2.15	1.66
1559.0	56.66	2.64	0.31	1.168	2.93	10.5	1.66	1.17
1560.5	56.76	3.43	0.69	1.230	3.26	11.2	2.59	2.10
1562.0	56.86	2.91	0.48	1.172	3.98	10.6	1.94	1.44
1564.0	56.98	2.71	0.52	1.420	3.38	13.1	2.28	1.78
1567.0	57.18	2.89	0.48	1.219	3.31	11.1	2.02	1.52
1569.0	57.31	2.67	0.36	1.477	3.29	13.7	2.34	1.84
1570.5	57.40	2.95	0.50	1.530	3.92	14.1	2.72	2.21
1572.0	57.50	2.61	0.63	1.412	3.53	13.1	2.16	1.65
1574.0	57.63	3.02	0.43	1.112	4.12	9.8	1.90	1.39
1577.0	57.82	2.66	0.68	1.227	3.85	11.2	1.82	1.31
1579.0	57.95	2.66	0.42	1.230	3.81	11.2	1.82	1.32
1580.5	58.04	2.77	0.27	1.118	3.36	9.9	1.66	1.16
1582.0	58.14	2.77	0.28	1.215	5.07	11.0	1.90	1.40
1584.0	58.27	2.64	0.32	1.522	4.60	14.1	2.41	1.91
1585.5	58.33	2.59	0.13	1.270	4.56	11.6	1.84	1.35
1587.0	58.40	2.89	0.33	1.401	3.11	12.9	2.42	1.93
1589.0	58.48	2.74	0.10	1.205	3.60	10.9	1.85	1.36
1590.5	58.55	2.69	0.05	1.146	3.79	10.2	1.66	1.17
1592.0	58.61	2.60	0.10	1.518	3.82	14.0	2.35	1.87
1594.0	58.69	2.59	0.19	1.384	2.32	12.8	2.08	1.60
1595.5	58.76	2.86	0.21	1.357	2.95	12.5	2.30	1.82
1597.0	58.82	2.65	0.17	1.307	3.72	12.0	1.99	1.51
1599.0	58.91	2.79	0.23	1.246	2.92	11.4	1.99	1.51
1600.5	58.97	2.36	0.39	1.343	3.48	12.4	1.77	1.30
1602.0	59.03	2.83	0.40	1.403	5.20	13.0	2.36	1.88
1604.0	59.12	2.50	0.19	1.379	3.82	12.7	1.98	1.51
1605.5	59.18	3.15	0.30	1.136	2.49	10.1	2.09	1.62

Table A5.4: *Trace element and results of stable isotope analyses of G. crassaformis down core samples. Test size = 300-400 µm. (continued)*

depth	age	$\delta^{18}O$	$\delta^{13}C$	Mg/Ca	Ba/Ca	T[1]	$\delta^{18}O_{sw}$[2]	$\delta^{18}O_{ivf\ sw}$[3]
cm	kyr	‰ VPDB	‰ VPDB	mmol/mol	µmol/mol	°C	‰ SMOW	‰ SMOW
1607.0	59.24	2.87	0.28	0.987	2.28	8.2	1.41	0.95
1609.0	59.33	3.19	0.40	1.176	2.20	10.6	2.22	1.76
1612.0	59.46	2.98	0.37	0.950	4.39	7.7	1.42	0.97
1614.0	59.54	3.20	0.38	1.261	4.24	11.5	2.43	1.98
1615.5	59.60	3.14	0.40	1.222	2.38	11.1	2.28	1.83
1617.0	59.67	2.80	0.24	1.329	3.15	12.2	2.18	1.74
1619.0	59.75	2.80	0.20	1.216	6.33	11.0	1.93	1.49
1620.5	59.81	2.65	0.27	1.218	3.17	11.1	1.78	1.34
1622.0	59.88	2.95	0.35	1.363	3.64	12.6	2.40	1.97
1624.0	59.96	3.23	0.40	1.583	4.38	14.6	3.10	2.67
1625.5	60.03	3.10	0.49	1.254	3.87	11.5	2.32	1.89
1627.0	60.09	2.99	0.27	1.505	3.86	13.9	2.72	2.29
1629.0	60.17	2.71	0.34	1.364	4.41	12.6	2.16	1.74
1630.5	60.24	3.15	0.42	1.487	3.00	13.7	2.85	2.43
1632.0	60.30	3.18	0.42	1.215	4.10	11.0	2.31	1.89
1634.0	60.39	2.93	0.36	1.199	4.93	10.9	2.03	1.61
1637.0	60.51	3.02	0.25	1.349	4.89	12.4	2.45	2.04
1639.0	60.60	3.17	0.34	1.012	2.44	8.6	1.79	1.38
1640.5	60.66	3.35	0.54	1.268	3.36	11.6	2.60	2.19
1642.0	60.72	2.91	0.47	1.321	4.04	12.2	2.27	1.85
1644.0	60.81	2.92	0.35					
1645.5	60.87	3.13	0.42	1.333	3.16	12.3	2.52	2.10

[1] *Mg/Ca-based temperature estimates calculated with Equation 5.10 from Chapter 5*

[2] *calculated after Bemis et al., (1998)*

[3] *corrected for the relative sea level following the approach of Waelbroeck et al. (2002)*

The age model was taken from Weldeab et al. (2007a, b) and Weldeab (2012a, b). For our record the models were overlapped at about 1200.5 cm core depth. We analyzed samples from the same core depth as done in the studies (Weldeab et al., 2007a, b; Weldeab, 2012a, b).

FIGURES

Additional Figures Chapter 3

Additional Figures Chapter 4

Additional Figures Chapter 5

Additional Figures Chapter 3

Figure A3.1 *Foraminiferal element concentrations in the reductive solution of the Flow Through (FT) cleaning method*

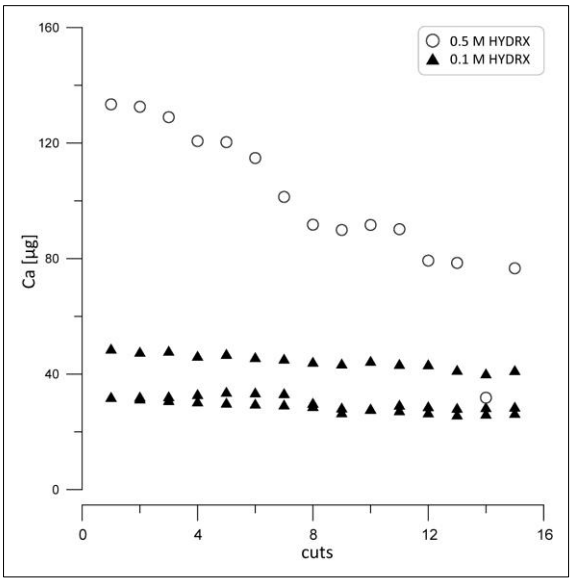

a) Ca concentrations in the reductive cleaning solution (HYDRX) measured in cuts of about 3.5 ml, cleaning included clay removal and oxidative cleaning

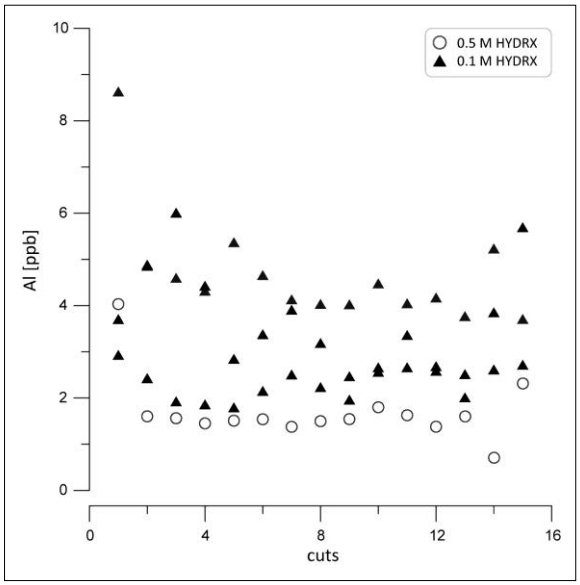

b) Al concentration in 1 ml of the reductive solution (HYDRX) measured in cuts of about 3.5 ml, cleaning included clay removal and oxidative cleaning

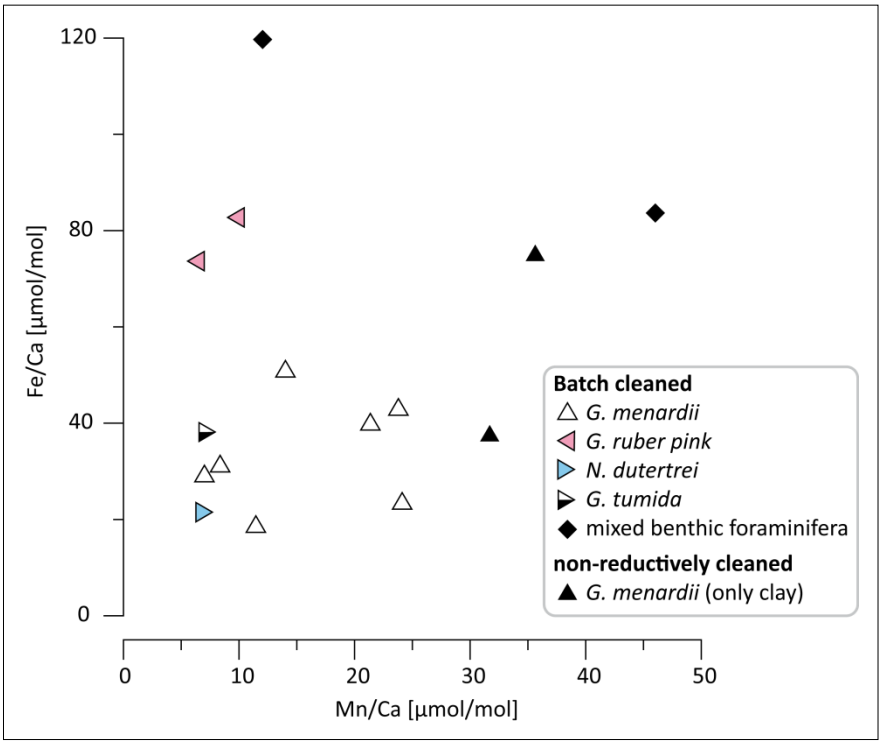

Figure A3.2 *Fe/Ca versus Mn/Ca*

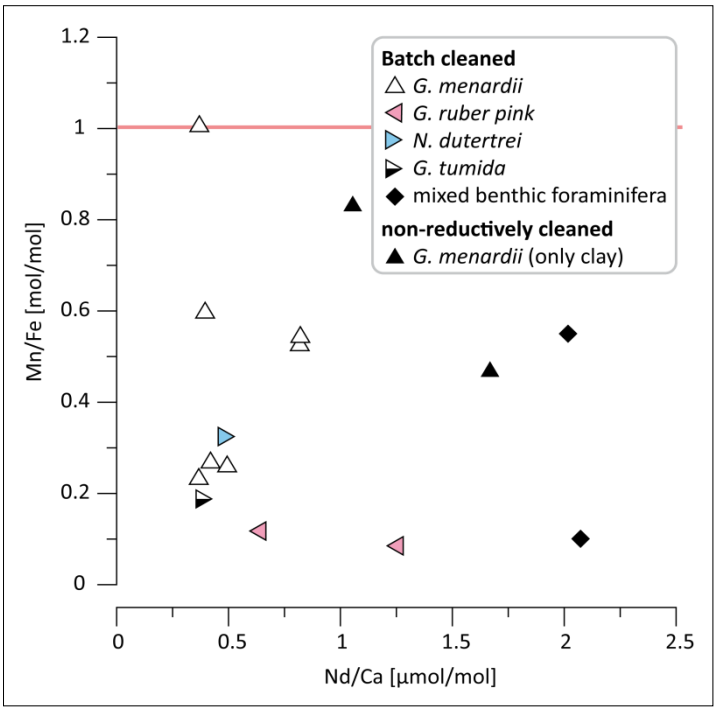

Figure A3.3 *Mn/Fe versus Nd/Ca*

Additional Figures Chapter 4

MREE/MREE*vs. HREE/LREE

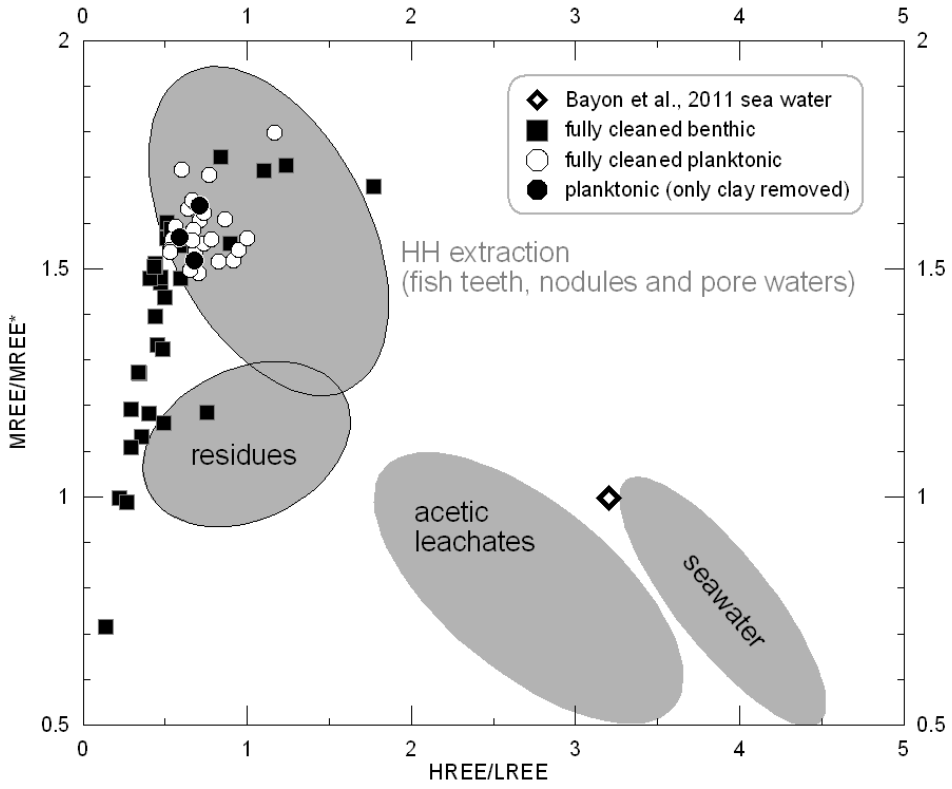

Figure A4.1: *MREE/MREE*=(Gd+Tb+Dy)/((LREE+HREE)/2) versus HREE/LREE = (Tm+Yb+Lu)/(La+Pr+Nd) plot: shaded gray areas from Martin et al. (2010) and references therein.*

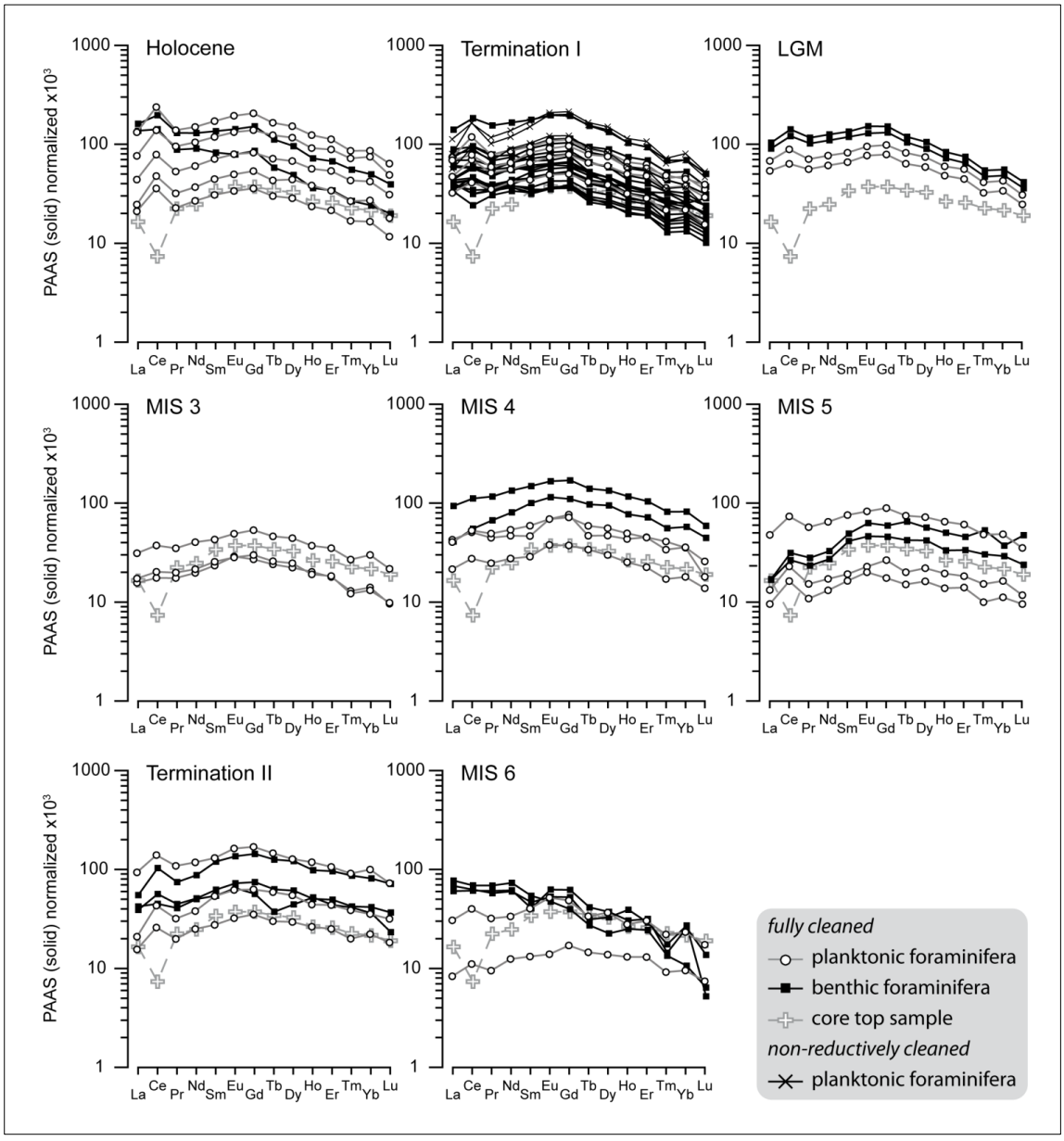

Figure A4.2: *REE patterns of planktonic foraminifera during glacial-interglacial cycles*

Additional Figures Chapter 5

Temperature and alinity profiles from the Gulf of Guinea

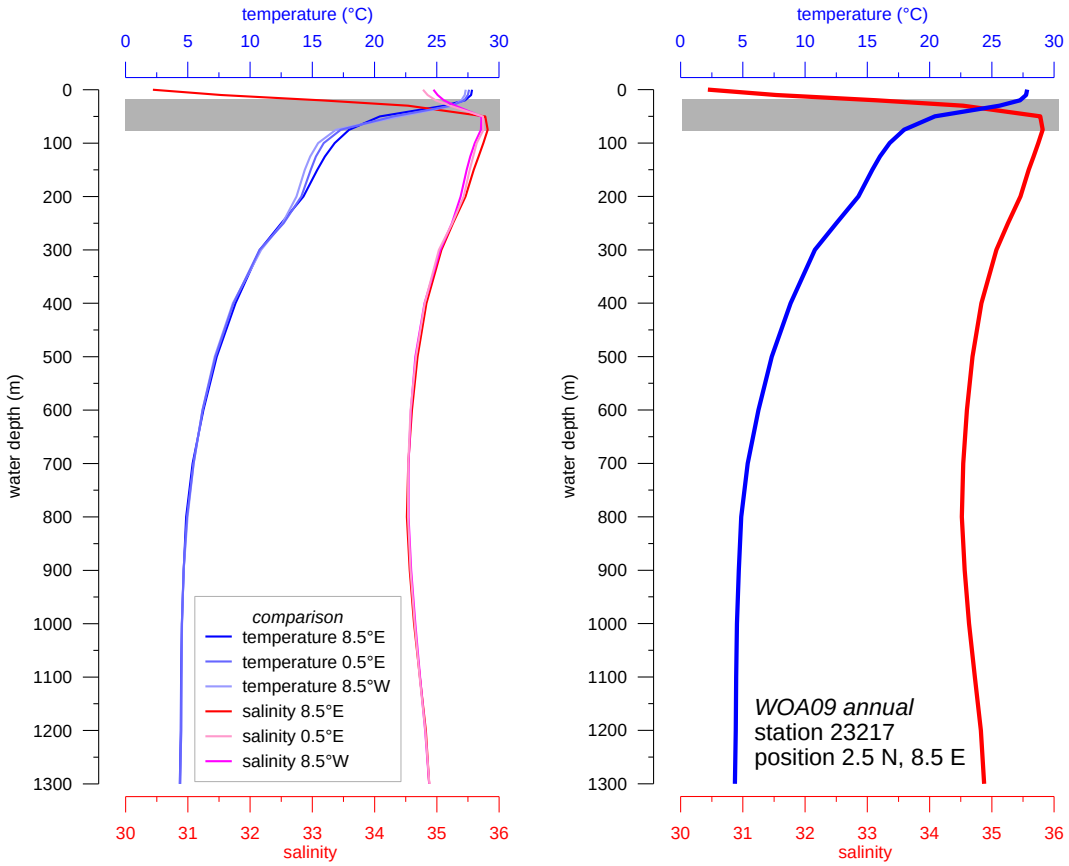

Figure A5.1: ***Left:*** *WOA09 annual water profiles (world ocean atlas 2009) on a transect along 2.5°N;* ***Right:*** *Figure shows the closest profile to the core location MD03-2707; profiles were cut at 1300 m (water depth of MD03-2707 is 1295 m)*

Figure A5.2 *Element/calcium ratios*

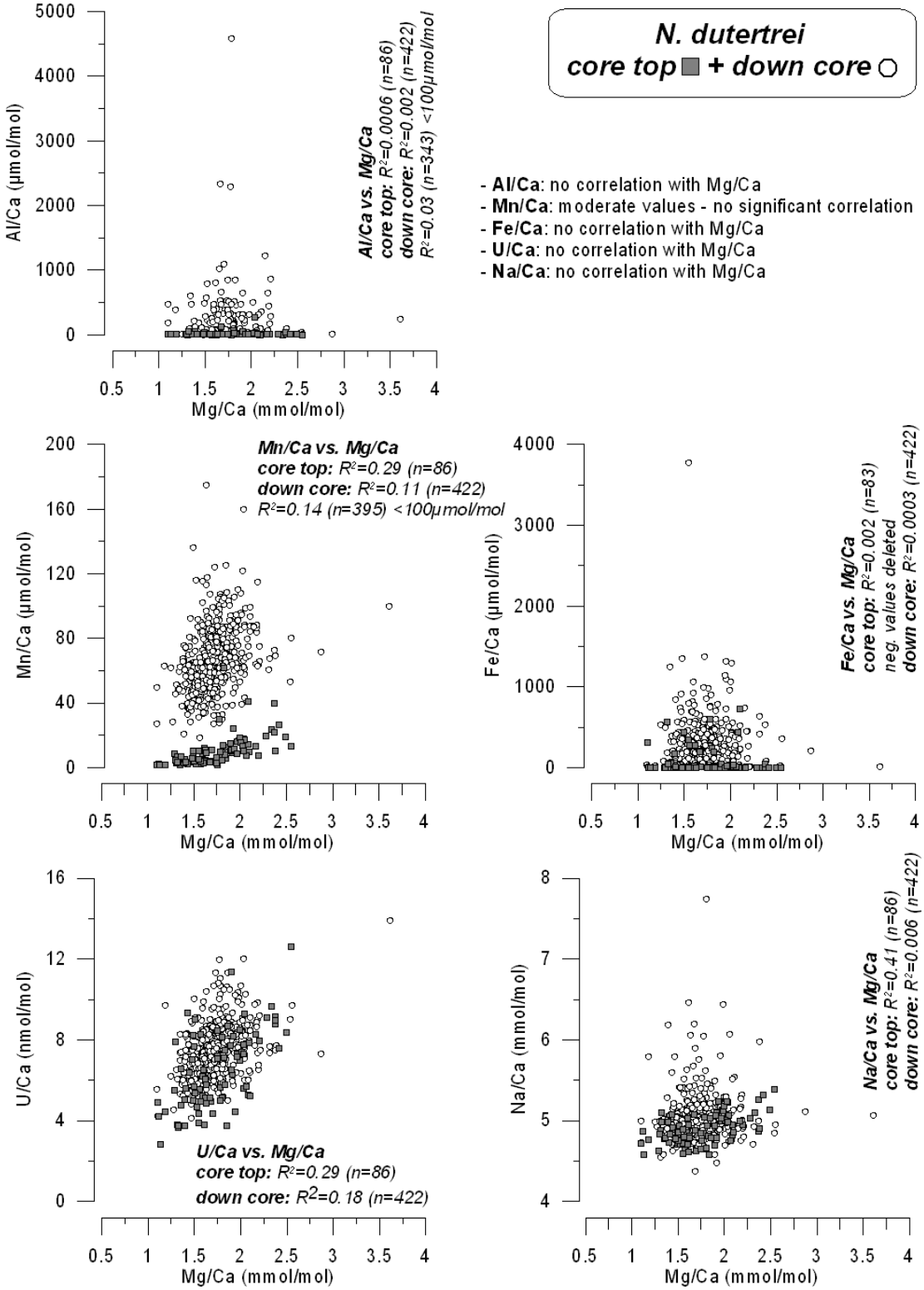

a) *N. dutertrei*

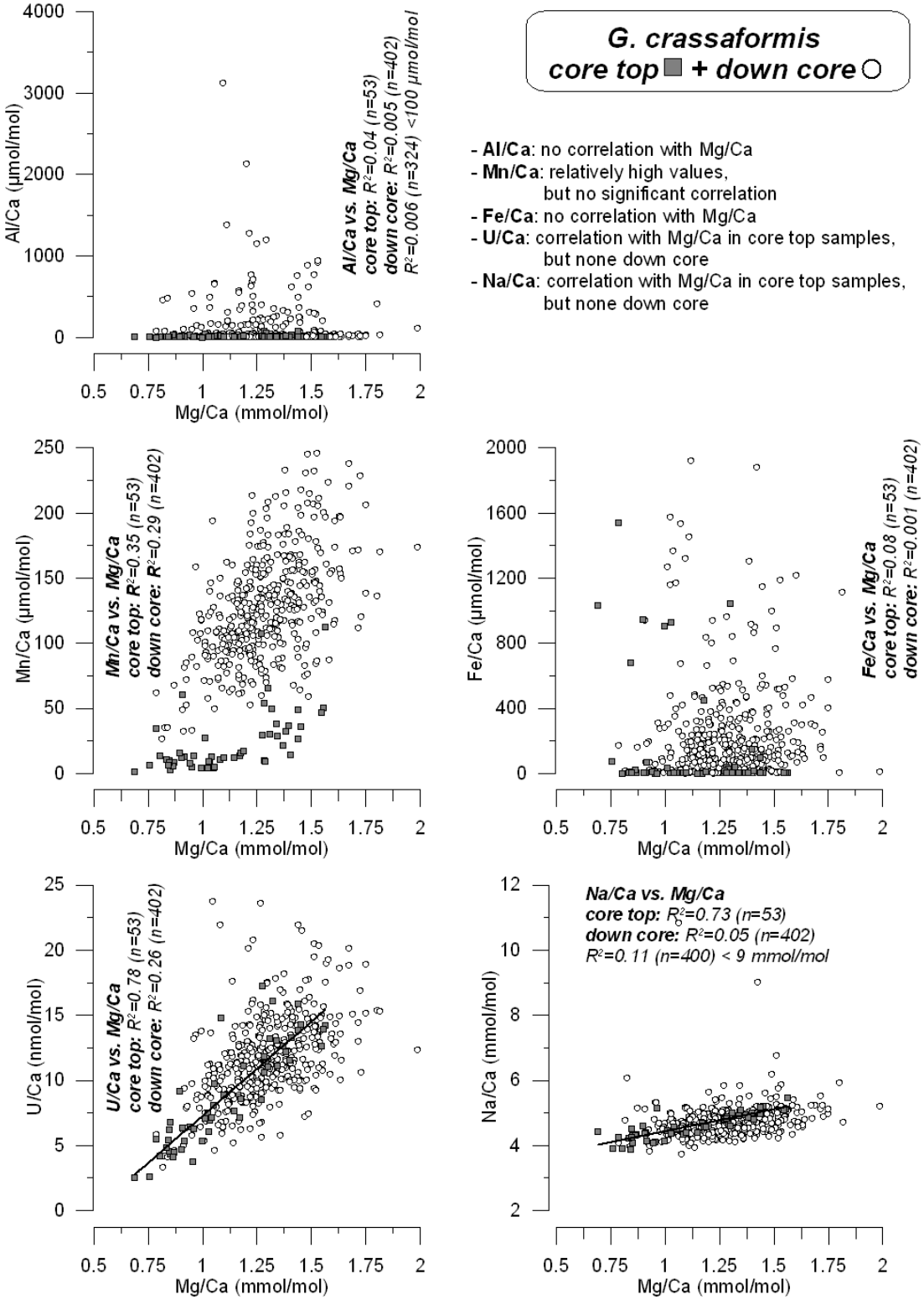

b) *G. crassaformis*

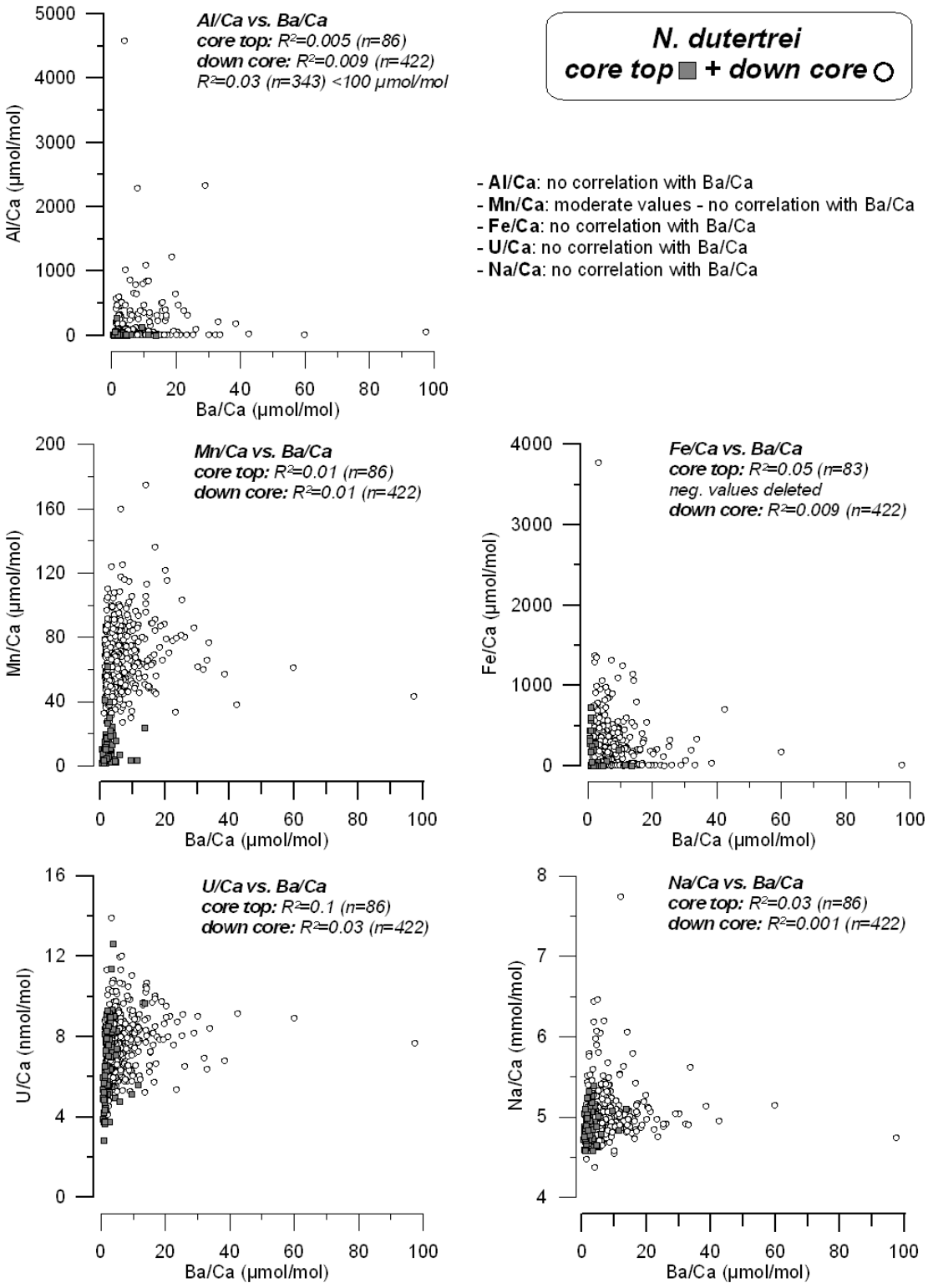

c) *N. dutertrei*

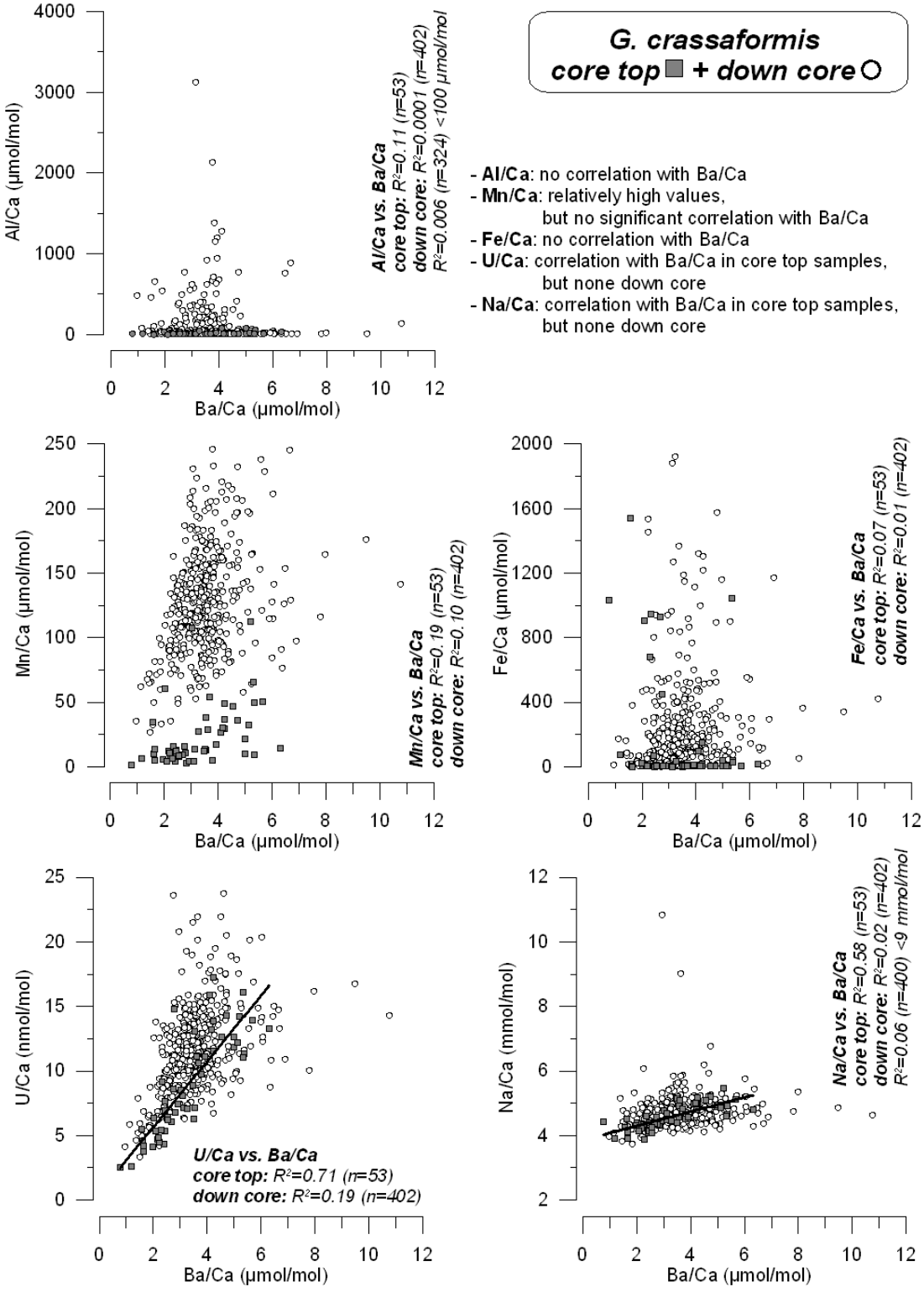

d) *G. crassaformis*

Calcite saturation the Gulf of Guinea

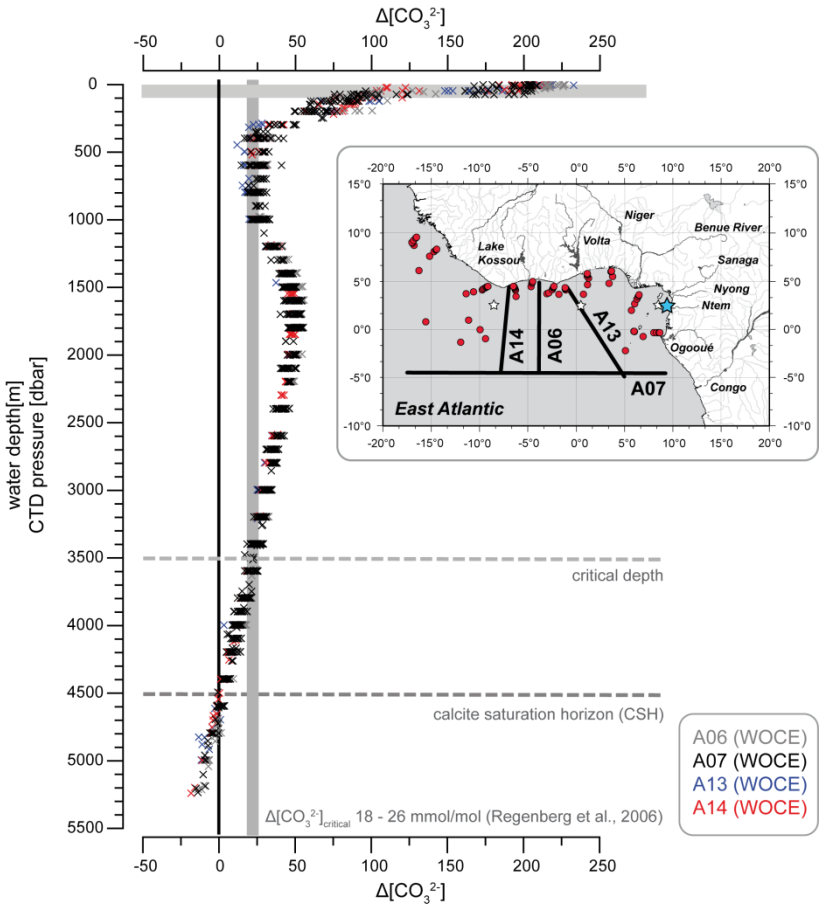

Figure A5.3: *Calcite saturation the Gulf of Guinea*

$\Delta[CO_3^{2-}]$ the difference between the $[CO_3^{2-}]_{insitu}$ (CO2SYS from (Pierrot et al., 2006) using CO_2 constants from Dickson (1990) and Mehrbach et al. (1973) refit by Dickson and Millero (1987) and $[CO_3^{2-}]_{sat}$ (Jansen et al., 2002); critical depth below which Mg^{2+} is expected to be dissolved; CSH (calcite saturation horizon) = top of the lysocline

CTD data (salinity, temperature, pressure, total phosphate and total silicate), Alkalinity and TCO_2 taken from WOCE data (transects A06, A07 taken by Oudot, 1993a and 1993b, A13 and A14 taken by Wallace et al., 1995) to calculate $[CO_3^{2-}]_{insitu}$. Calculation of $[CO_3^{2-}]_{insitu}$ were performed with CO2SYS program (Makro for Excel) (Pierrot et al., 2006) using CO_2 constants from Dickson (1990) and Mehrbach et al. (1973) refit by Dickson and Millero (1987). $[CO_3^{2-}]_{sat}$ at the saturation depth was calculated after Jansen et al. (2002). $\Delta[CO_3^{2-}]$, the difference between the $[CO_3^{2-}]_{insitu}$ and $[CO_3^{2-}]_{sat}$, is used to define the calcite saturation horinzon (CSH). Furthermore, the $\Delta[CO_3^{2-}]$ ranging between 18 and 26 µmol/mol (Regenberg et al., 2006) was used to define the critical depth. Below the critical depth the Mn^{2+} is supposed to be dissolved and thus the dissolution will start. In the Gulf of Guinea the CSH is located around 4500 m water depth and the critical water depth of about 3500 m water depth.

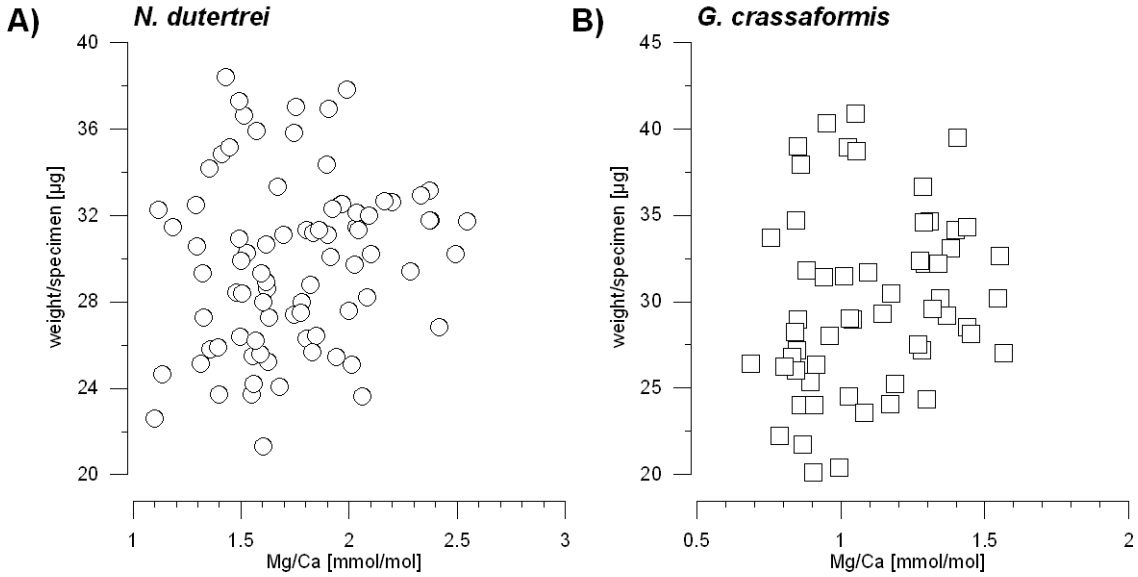

Figure A5.4 *Weight of individual foraminifera vs. Mg/Ca*
A) *N. dutertrei (R^2=0.03),* ***B)*** *G. crassaformis (R^2=0.04)*

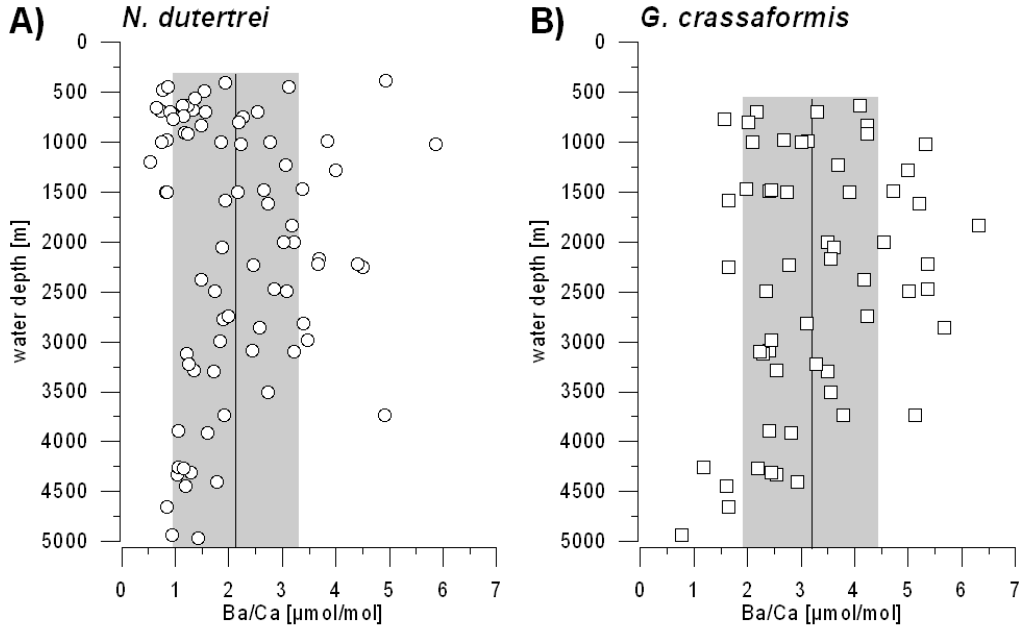

Figure A5.5 *Ba/Ca versus depth of* ***A)*** *N. dutertrei (Ba/Ca > 9 µmol/mol excluded, n = 3) R^2 = 0.001, n = 79 and* ***B)*** *G. crassaformis: R^2 = 0.074, n = 57. The black lines represent the average Ba/Ca ratios and the gray areas mark the standard deviation.*

Danksagung

Diese letzte Seite möchte dafür nutzen, mich von Herzen zu bedanken:

... bei Prof. Dr. Martin Frank: Vielen herzlichen Dank für Deine Betreuung, Deine Unterstützung, Deine wertvollen Ratschläge und Deine Geduld während der letzten Jahre.

... bei Dr. Syee Weldeab für seine Betreuung, die freundliche Aufnahme und Unterstützung in Santa Barbara.

... bei Ed: Vielen Dank für den vielen Input, die Diskussionen, Korrekturen, Kommentare, die Hilfe beim FT-Setup und an der Quadrupol und natürlich die schicken REE-Muster.

... bei Prof. Dr. Dirk Nürnberg für seine Starthilfe bei der Mg/Ca-Auswertung und die Bereitschaft als Zweitgutachter tätig zu sein.

... bei den Mädels, besonders bei Clauschi, Kristin, Anna, Almuth, Christina, Agnes und Kerstin für offene Ohren, Feedback zu wissenschaftlichen Themen und Fragestellungen, aufbauende Worte, herzhaftes Lachen, tiefe Gespräche, Schoki, Spaß und Ermutigungen.

... bei der gesamten Arbeitsgruppe, allen anderen "Science-Lounge-Leuten" und den Stammtischlern für fachliche Hilfe, Anleitungen und Erklärungen im Labor und an der Nu, Antworten und Ratschläge, die gute Laune, die vielen tollen Gespräche und das ein oder andere gemeinsame Bierchen.

... bei Jutta - Einfach für alles! ;-)

... bei Nadine für ihre Hilfe, Ratschläge, das Ausleihen von beheizbaren Ultraschallgeräten und das Versorgen mit diversen Bechern, Proben-Spritzen usw.

... bei Ana für ihre geduldige Hilfe an der Quadrupol.

... bei allen Hiwis, die mir fleißig beim Picken geholfen haben, insbesondere Kristin D.

... bei meinen Freunden und Bekannten: Vielen Dank für Euer Verständnis für fehlende Zeit und sonstige Launen, unsere Ausflüge, Eure Freundschaft, offenen Ohren, Ratschläge und schöne Zeiten.

... bei meiner Familie für die zahllosen und endlosen Telefonate, das Trocknen von Tränen, ihren unerschütterlichen Zuspruch und jegliche Rückendeckung.

& last but not least:

... bei einem ganz besonderen Menschen - Markus: Danke, dass Du immer für mich da bist, auch wenn Du weit weg bist.